Towards the identification and functional characterization of *Verticillium* effectors involved in xylem hyperplasia formation in Arabidopsis

Dissertation

zur Erlangung des mathematisch-naturwissenschaftlichen Doktorgrades

"Doctor rerum naturalium"

der Georg-August-Universität Göttingen

im Promotionsprogramm Biologie

der Georg-August University School of Science (GAUSS)

vorgelegt von

Leonie Weber

aus Ehingen (Donau)

Göttingen 2019

Betreuungsausschuss

1. Betreuer: Prof. Dr. Volker Lipka
Zellbiologie der Pflanze, Albrecht-von-Haller Institut für Pflanzenwissenschaften

2. Betreuer: PD Dr. Thomas Teichmann
Zellbiologie der Pflanze, Albrecht-von-Haller Institut für Pflanzenwissenschaften

Anleiter: Prof. Dr. Volker Lipka
Zellbiologie der Pflanze, Albrecht-von-Haller Institut für Pflanzenwissenschaften

Mitglieder der Prüfungskommission

Referent: Prof. Dr. Volker Lipka
Zellbiologie der Pflanze
Albrecht-von-Haller Institut für Pflanzenwissenschaften

Korreferent: PD Dr. Thomas Teichmann
Zellbiologie der Pflanze
Albrecht-von-Haller Institut für Pflanzenwissenschaften

Weitere Mitglieder der Prüfungskommission

Prof. Dr. Gerhard Braus
Molekulare Mikrobiologie und Genetik
Institut für Mikrobiologie und Genetik

Prof. Dr. Ivo Feußner
Biochemie der Pflanze
Albrecht-von-Haller Institut für Pflanzenwissenschaften

Prof. Dr. Christiane Gatz
Molekularbiologie und Physiologie der Pflanze
Albrecht-von-Haller Institut für Pflanzenwissenschaften

Prof. Dr. Andrea Polle
Forstbotanik und Baumphysiologie
Fakultät für Forstwissenschaften und Waldökologie

Tag der mündlichen Prüfung: 01.07.2019

Promovierenden-Erklärung
der Georg-August-Universität Göttingen

Die Gelegenheit zum vorliegenden Promotionsvorhaben ist mir nicht kommerziell vermittelt worden. Insbesondere habe ich keine Organisation eingeschaltet, die gegen Entgelt Betreuerinnen und Betreuer für die Anfertigung von Dissertationen sucht oder die mir obliegenden Pflichten hinsichtlich der Prüfungsleistungen für mich ganz oder teilweise erledigt.

Hilfe Dritter wurde bis jetzt und wird auch künftig nur in wissenschaftlich vertretbarem und prüfungsrechtlich zulässigem Ausmaß in Anspruch genommen. Insbesondere werden alle Teile der Dissertation selbst angefertigt; unzulässige fremde Hilfe habe ich dazu weder unentgeltlich noch entgeltlich entgegengenommen und werde dies auch zukünftig so halten.

Die Ordnung zur Sicherung der guten wissenschaftlichen Praxis an der Universität Göttingen wird von mir beachtet.

Eine entsprechende Promotion wurde an keiner anderen Hochschule im In- oder Ausland beantragt; die eingereichte Dissertation oder Teile von ihr wurden nicht für ein anderes Promotionsvorhaben verwendet.

Mir ist bekannt, dass unrichtige Angaben die Zulassung zur Promotion ausschließen bzw. später zum Verfahrensabbruch oder zur Rücknahme des erlangten Grades führen.

Leonie Weber

Göttingen, den 4.6.2019

Abstract

Isolates of the vascular plant pathogen *Verticillium spp.* can be categorized according to the disease phenotypes they induce on *Arabidopsis thaliana* Col-0 plants (Thole 2016). While Arabidopsis plants show no obvious disease symptoms in response to inoculation with some *Verticillium* isolates (asymptomatic class), plants infected with wilting-class isolates are characterized by stunted growth and wilting symptoms accompanied by enhanced lignification of xylem elements (Reusche et al. 2014). Chlorosis-class isolates, on the other hand, trigger stunting, chlorosis and developmental reprogramming characterized by transdifferentiation of bundle sheath and xylem parenchyma cells into xylem elements and establishment of xylem hyperplasia (Reusche et al. 2012). The first aim of this thesis was to identify chlorosis-class specific candidate effectors that trigger developmental reprogramming in Arabidopsis. To this end, whole-genome comparison of wilting-class reference isolate *V. dahliae* JR2 and *de novo* sequenced chlorosis-class reference isolate *V. dahliae* V76 was conducted. Comparative genomics revealed V76-specific regions which were subsequently mined for putative effector candidates. Finally, four *LINEAGE-SPECIFIC CANDIDATE EFFECTORs* (*LSCEs*) were identified.

LSCE2 was selected as the primary candidate for further investigation due to its high transcriptional induction *in planta*. Sequence analyses revealed two identical copies of *LSCE2* in the genomes of haploid chlorosis-class reference isolates *V. dahliae* V76 and chlorosis-class allodiploid *V. longisporum* VL43. Furthermore, it was demonstrated that *LSCE2* is located in a ~ 20 kb tandem-inverted LSCE region in both isolates. In total, six genes were predicted to be encoded in the LSCE region, including the transposable element-associated enzymes reverse transcriptase and a transposase. It was therefore hypothesized that transposable elements were involved in the evolution of the LSCE region.

Analyses of a set of 15 *V. dahliae* and 10 *V. longisporum* isolates from all infection classes confirmed that *LSCE2* is present exclusively in chlorosis-class isolates. In addition, it was demonstrated that all *Verticillium spp.* isolates harbor a single-copy homolog of *LSCE2,* here designated *LSCE2-like*, in their core genome. It is likely that *LSCE2* arose from duplication and subsequent neofunctionalization from *LSCE2-like*.

Next, it was investigated if *LSCE2* is involved in the establishment of the chlorosis-class disease phenotype. To this end, *LSCE2* single and double knockout lines in the *V. dahliae* V76 and *V. longisporum* VL43 background were generated. In addition, *LSCE2* was expressed ectopically in the wilting-class reference isolate *V. dahliae* JR2. Deletion of both *LSCE2* copies completely abolished chlorosis-class disease symptoms on Arabidopsis. Concomitantly, transgenic expression conferred the ability to induce chlorosis-class disease symptoms to *V. dahliae* JR2. Consequently, it can be postulated that the effector *LSCE2* mediates developmental reprogramming of Arabidopsis in chlorosis-class *Verticillium spp.* infections.

To further characterize protein properties of LSCE2, a His-tagged version of the protein was expressed and purified using the *Pichia pastoris* expression system and affinity chromatography. Remarkably, transdifferentiation and chlorosis were observed after infiltration of Arabidopsis leaves with the purified protein. In addition, Arabidopsis lines stably expressing the fluorescence-tagged fusion protein LSCE2-GFP were generated. Transgenic lines with different expression levels of LSCE2-GFP showed dosage-dependent induction of stunting, chlorosis and transdifferentiation of bundle sheath cells. Taken together, this work demonstrates that a single lineage-specific *Verticillium* effector molecule, LSCE2, induces the complex cell-type specific developmental reprogramming patterns characteristic for chlorosis-class *Verticillium* infections.

Zusammenfassung

Isolate des vaskulären Pflanzenpathogens *Verticillium spp.* können anhand des Krankheitsphänotyps den sie bei *Arabidopsis thaliana* Col-0 auslösen kategorisiert werden (Thole 2016) . Während Arabidopsis keine offensichtlichen Krankheitssymptome bei Inokulierung mit manchen *Verticillium*-Isolaten zeigt (Asymptomatische Klasse), bilden Pflanzen die mit Welke-Klasse Isolaten infiziert sind verkümmertes Wachstum und Welkesymptome aus, die von verstärkter Lignifizierung von Xylemelementen begleitet werden (Reusche et al. 2014) . Isolate der Chlorose-Klasse, andererseits, lösen verkümmertes Wachstum, Chlorose und entwicklungsorientierte Umprogrammierung charakterisiert durch Transdifferenzierung von Bündelscheiden- und Xylemparenchymzellen zu Xylemelementen sowie die Etablierung von Xylemhyperplasie (Reusche et al. 2012) . Das erste Ziel dieser Dissertation war die Identifizierung von Chlorose-Klasse spezifischen Effektorkandidaten, die die entwicklungsorientierte Umprogrammierung in Arabidopsis auslösen. Dazu wurde ein Genomvergleich von Welke-Referenzisolat *V. dahliae* JR2 und dem *de novo* sequenzierten Chlorose-Isolat *V. dahliae* V76 durchgeführt. Vergleichende Genomanalysen offenbarten V76-spezifische Regionen die daraufhin auf potentielle Effektorkandidaten untersucht wurden. Abschließend wurden vier Effektorkandidaten, „*LINEAGE-SPECIFIC CANDIDATE EFFECTORs*" (*LSCEs*), identifiziert.

LSCE2 wurde wegen seiner hohen transkriptionellen Induktion *in planta* als primärer Kandidat für weitere Untersuchungen ausgewählt. Sequenzanalysen zeigten das Vorhandensein von zwei identischen Kopien in den Genomen des haploiden Chlorose-Isolats *V. dahliae* V76 sowie des allodiploiden Chlorose-Isolats *V. longisporum* VL43. Es wurde zudem gezeigt, dass *LSCE2* in beiden Isolaten in einer ~20 kb tandem-invertierten LSCE-Region lokalisiert ist. Insgesamt wurde die Kodierung von sechs Genen in der LSCE-Region bestimmt, darunter die Transposon-assoziierten Enzyme Reverse Transkriptase und Transposase. Es wurde hierauf die Hypothese aufgestellt, dass Transposons in der Evolution der LSCE-Region beteiligt waren.

Analysen einer Gruppe von 15 *V. dahliae*- und 10 *V. longisporum*-Isolaten aller Infektionsklassen bestätigten, dass *LSCE2* exklusiv in den Genomen von Chlorose-Isolaten vorhanden ist. Zudem wurde gezeigt, dass alle *Verticillium spp.*-Isolate ein Einzelkopie-Homolog zu *LSCE2*, hier *LSCE2-like* benannt, in ihrem Genom besitzen. In aller Wahrscheinlichkeit entstand *LSCE2* durch Duplikation und darauffolgender Neofunktionalisierung aus *LSCE2-like*.

Als nächstes wurde untersucht, ob *LSCE2* in der Etablierung des Chlorose-Klassen spezifischen Krankheitsphänotyps involviert ist. Dazu wurde *LSCE2* einzeln und doppelt in *V. dahliae* V76 und *V. longisporum* VL43 deletiert. Zusätzlich wurde *LSCE2* ektopisch im Welke-Referenzisolat *V. dahliae* JR2 exprimiert. Die Deletion beider *LSCE2*-Kopien führte zu einer kompletten Aufhebung der Chlorose-Klassen spezifischen Krankheitssymptome auf Arabidopsis. Gleichzeitig übertrug die transgene Expression von *LSCE2* die Fähigkeit, Chlorose-Klasse Symptome auszulösen auf *V. dahliae* JR2. In Konsequenz kann postuliert werden, dass der Effektor *LSCE2* die entwicklungsorientierte Umprogrammierung von Arabidopsis bei Infektion mit Chlorose-Klassen *Verticillium spp.* vermittelt.

Um weiterführend die Eigenschaften des LSCE2-Proteins zu charakterisieren, wurde eine His-getaggte Version des Proteins im *Pichia pastoris* Expressionssystem exprimiert und mittels Affinitätschromatographie aufgereiningt. Bemerkenswerterweise wurden Transdifferenzierung und Chlorose nach Infiltration von Arabidopsisblättern mit aufgereinigtem Protein beobachtet. Zusätzlich wurden Arabidopsislinien generiert, die das Fluoreszenz-getaggte Fusionsprotein LSCE2-GFP stabil exprimieren. Transgene Linien mit unterschiedlichen Expressionsleveln von LSCE2-GFP zeigten eine dosierungsbedingte Induktion von verkümmertem Wachstum, Chlorose und Transdifferenzierung von Bündelscheidenzellen. Zusammengefasst zeigt diese Arbeit, dass ein einzelnes Klassen-spezifisches *Verticillium* Effektormolekül, LSCE2, die komplexen, zelltypspezifischen Umprogrammierungsmuster induziert, die für Infektionen mit Chlorose-Klassen *Verticillium* Isolaten charakteristisch sind.

Table of contents

Table of abbreviations

%	percent
Δ	knockout
°C	degree Celcius
A.	Arabidopsis
A.	Agrobacterium
aa	amino acids
At	*Arabidopsis thaliana*
Avr	avirulence
bp	base pair(s)
BLAST	basic local alignment search tool
C-	carboxyl-terminal
CDB	Czapek Dox Broth
cDNA	complementary DNA
CWDE	cell wall degrading enzyme
Da	Daltons
dai	days after infiltration
dH_2O	deionized water
DNA	deoxyribonucleic acid
DNase	deoxyribonuclease
dNTP	deoxynucleosidetriphosphate
dpi	days post infection
ER	endoplasmatic reticulum
EtOH	ethanol
F.	Fusarium
Fig.	figure
g	gram
GAP	glyceraldehyde 3-phosphate
GAPDH	glyceraldehyde 3-phosphate dehydrogenase
gDNA	genomic DNA
GFP	green fluorescent protein
HGT	horizontal gene transfer
k	kilo
kb	kilobase(s)
LD	long day
LS	lineage-specific
LSCE	Lineage-Specific Candidate Effector
m	meter

m	milli
M	molar
Mb	megabases
min	minute(s)
mM	millimolar
mRNA	messenger RNA
N-	amino-terminal
ng	nanogram
nm	nanometer
nt(s)	nucleotide(s)
ORF	open reading frame
p	promoter
P.	Pichia
PCR	polymerase chain reaction
PDB	potato dextrose broth
pH	negative decimal logarithm of the H+ concentration
qRT-PCR	quantitative Real-time PCR
RNA	ribonucleic acid
rpm	rounds per minute
RT	room temperature
scf	scaffold
SD	short day
sec	second(s)
semi qPCR	semi-quantitative PCR
spp.	species pluralis
TD	transdifferentiation
TE	tracheary element
V	Volt
v.	version
V.	Verticillium
v/v	volume per volume
w/v	weight per volume
WT	wild-type
α	anti-
µ	micro

1 Introduction

1.1 The vascular plant pathogen *Verticillium spp.*

Verticillium is a genus of soil-borne ascomycete fungi with a wide range of host plants. Plant pathogenic *Verticillium* species are hemibiotrophs that cause plant diseases generally referred to as 'Verticillium wilt' (Fradin and Thomma 2006; Inderbitzin et al. 2011b) . The disease cycle of plant pathogenic *Verticillium spp.* can be divided into a biotrophic and a necrotrophic phase (Figure 1.1) (Fradin and Thomma 2006) . During the biotrophic phase, *Verticillium* hyphae enter roots through endodermis-free zones and grow inter- and intracellularly until they reach the central cylinder (Huisman 1982; Bishop and Cooper 1983) . Within the vascular bundle, *Verticillium* colonizes xylem vessels and produces conidia which are carried with the xylem stream throughout the vasculature of the plant (Fradin and Thomma 2006) . At this stage, fungal biomass accumulation as well as plant defense responses such as secretion of gels and the formation of tyloses cause xylem vessel occlusion which in most cases causes wilting of the foliage (Street and Cooper 1984; Benhamou 1995) . Effectors as well as phytotoxins secreted by the fungus then induce macroscopic disease symptoms such as wilting, necrosis and chlorosis of the leaves (Pegg 1965; Pemberton and Salmond 2004; Buchner et al. 1982) . This marks the transition from the biotrophic to the necrotrophic phase of the pathogen (Fradin and Thomma 2006) . During the necrotrophic phase, the fungus leaves the vasculature and uses nutrients released from senescing plant tissues to produce melanized resting structures called microsclerotia (Fradin and Thomma 2006) . Microsclerotia then return to the soil through decomposing plant material where they can rest for years until a new disease cycle is started (Figure 1.1) (Wilhelm 1955).

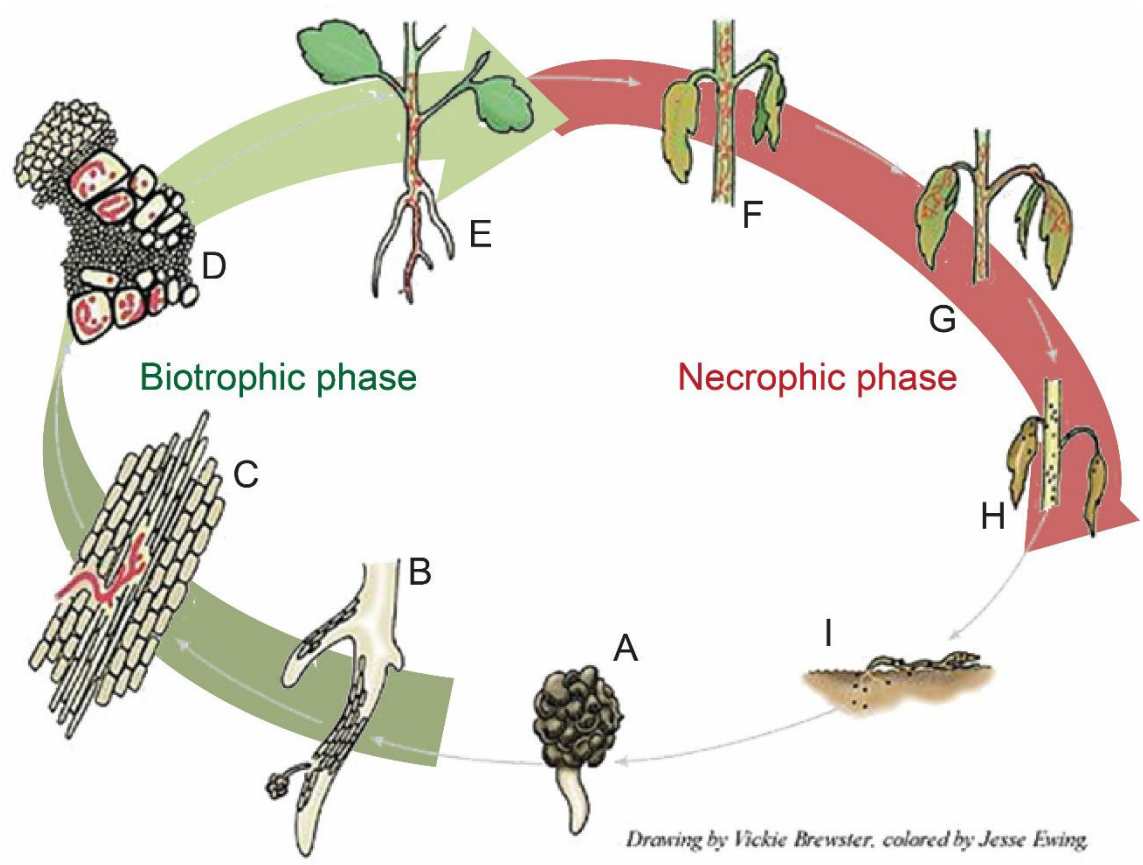

Figure 1.1 The *Verticillium* disease cycle. *Verticillium* is a hemibiotrophic, vascular pathogen with a biotrophic (green) and a necrotrophic (red) phase during plant infection. (A) Root exudates stimulate germination of microsclerotia in the soil. (B) Fungal hyphae (red) enter roots at endodermis-free zones. (C) Invasive hyphae enter the central cylinder. (D) Hyphae colonize xylem vessels and produce conidia. (E) The fungus colonizes the vascular tissue systemically. (F) Chlorosis, necrosis and wilting of foliage is induced. (G) Senescing tissues are colonized. (H) Microsclerotia are formed. (I) Microsclerotia return to the soil through decomposing plant material. Figure adopted and modified from apsnet.org./edcenter/intropp/lessons/fungi/ascomycetes/Pages/VerticilliumWilt.

Using modern phylogenetic and taxonomic methods, Inderbitzin et al. (2011a) defined and characterized nine haploid and one hybrid *Verticillium* species (Figure 1.2). While all *Verticillium* species have a plant-associated lifestyle, only *Verticillium alfalfae*, *V. nonalfalfae*, *V. albo-atrum*, *V. dahliae* and *V. longisporum* are known as plant pathogens (Inderbitzin et al. 2011a). *V. alfalfae* and *V. nonalfalfae,* which had previously been identified as *V. albo-atrum,* were introduced as two new species, leading to some taxonomic confusions in the field (Inderbitzin et al. 2011a; Inderbitzin and Subbarao 2014). *Verticillium longisporum* has first been described as a subspecies of *V. dahliae* but gained species rank in 1997 when Karapapa et al. discovered that *Verticillium* strains isolated from Brassica hosts share unique morphological and genomic traits. It has since then been shown that *V.*

longisporum is a near-diploid (allodiploid) hybrid species that arose several times independently from at least four different ancestors (Inderbitzin et al. 2011b; Depotter et al. 2016). The parental line shared by all *V. longisporum* lineages has been named 'species A1' and forms a phylogenetic sister clade to the clade containing *V. alfalfae*, *V. nonalfalfae* and *V. dahliae* (Figure 1.2). The three parental lines that gave rise to the three distinct lineages (A1/D1, A1/D2 and A1/D3) are either closely related to (D1) or contained within (D2, D3) the *Verticillium dahliae* clade (Figure 1.2) (Inderbitzin et al. 2011a; Inderbitzin et al. 2011b). Although they are closely related, no *V. dahliae* isolate has been found that can be phylogenetically grouped with the *V. longisporum* parental lines.

While the infection strategies of the five aforementioned pathogenic species are similar, they differ significantly in host range. Indeed, *V. alfalfae* has only been isolated from one host, alfalfa (*Medicago sativa*), though successful interaction has also been shown with the closely related model plant *Medicago truncatula* (Inderbitzin et al. 2011a; Molinéro-Demilly et al. 2006). *Verticillium nonalfalfae* has a more extensive host range and infects, amongst others, hops (*Humulus lupulus*), potato (*Solanum tuberosum*), tree-of-heaven (*Alianthus altissima*) and *Pelargonium* (Inderbitzin et al. 2011a; Rebbeck et al. 2013; Kasson et al. 2014; Garibaldi et al. 2016). Although *V. albo-atrum* was mentioned in studies before 2011 as agents of Verticillium wilt on various plants, the recent taxonomical developments described above suggest a more restricted host range. To this day, potato is the only clearly identified host plant of *V. albo-atrum* (Inderbitzin et al. 2011a). *Verticillium dahliae* is the species with the most extensive host range of the genus. Its more than 200 hosts include economically important crop plants such as cotton (*Gossypium hirsutum*), tomato (*Solanum lycopersicum*) and olive (*Olea europaea*) (Fradin and Thomma 2006) but notably (almost) no brassicaceous hosts (Depotter et al. 2016). *Verticillium dahliae* outbreaks have been occurring around the globe from South Africa (Ferreira 1990) over Europe (García-Ruiz et al. 2014) to China (Zhang et al. 2009), Australia (Ramsay, JR et al. 1996) and America (Johnson and Dung 2010). While no exact numbers of the economic damage caused by *V. dahliae* exist, Verticillium wilt has been recognized as a serious threat to crop production worldwide (Cirulli et al. 2010; Jiménez-Díaz et al. 2012; Land et al. 2016). *V. longisporum*, although also recognized as a threat to crops (Depotter et al. 2016), has a more restricted host range. It has almost exclusively been isolated from brassicaceous hosts including oilseed rape (*Brassica napus*), cauliflower (*Brassica oleracea* var. *botrytis*) and sugar beet (*Beta vulgaris*) (Inderbitzin et al. 2011a; Depotter et al. 2016).

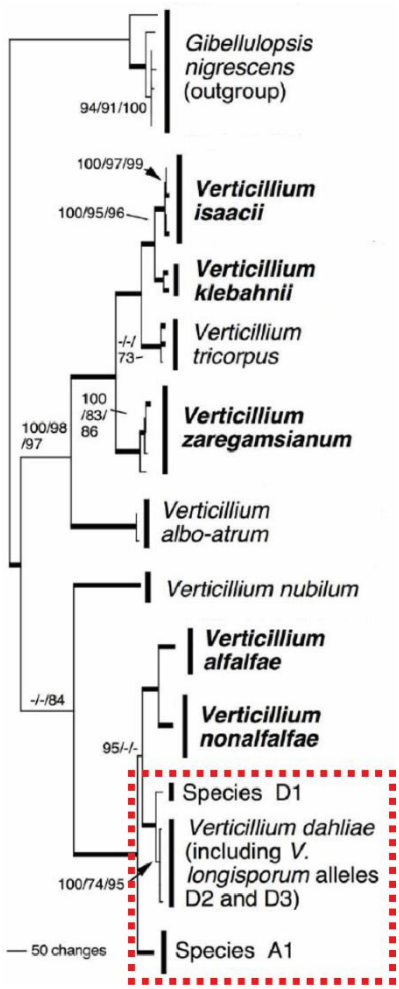

Figure 1.2 Phylogenetic relationship of the ten *Verticillium* species based on the combined actin, elongation factor 1-alpha, glyceraldehyde-3-phosphate dehydrogenase and tryptophan synthase dataset of 2658 characters and 77 taxa, with *Gibellulopsis nigrescens* as outgroup. The Bayesian consensus tree is shown. Species are marked by vertical bars followed by species names, species in bold were described in the study by Inderbitzin et al. (2011a). The two main clades recovered are indicated on the right. Numbers at the branches are Bayesian, likelihood and parsimony support values above 70 in that order, branches in bold had maximal support in all analyses. Each isolate of *V. longisporum* has two alleles that are present in two different clades in the tree, in hypothetical Species A1, and either in hypothetical Species D1 or in *V. dahliae*, reflecting the hybrid origin of this species. Figure and figure legend were adopted from Inderbitzin et al. (2011a) and modified. *Verticillium* species used here are marked by a red rectangle.

1.2 *Verticillium spp.* disease classes

Verticillium spp. isolates can differ significantly in regards to their pathogenicity on different host plants. For example, *V. dahliae* isolate VdLs17 causes severe disease symptoms on lettuce (Short et al. 2014) but not on tomato (deJonge et al. 2012). The cause of this disparity was discovered by deJonge et al. (2012) who showed that *V. dahliae* pathogenicity on tomato depends on the recognition of the fungal effector *Ave1* (*Avirulence on Ve1 tomato*) by the tomato immune receptor *Ve1*. In consequence, a single gene, *Ave1*, determines if a *V. dahliae* isolate is categorized as race 1 (*Avr1* present, avirulent on tomato) or race 2 (*Avr1* absent, virulent on tomato). Differences in pathogenicity have also been found in infections of *V. nonalfalfae* isolates on hops. Based on the progression of hop wilt disease, isolates are categorized as mild-strains or lethal-strains (Radišek et al. 2003; Talboys 1958) . The genetic bases of the pathotype have been investigated but are not fully understood yet (Marton et al. 2018). Another well-studied tandem of *Verticillium spp.* pathotypes are defoliating and non-defoliating strains. The two disease classes have been described based on the symptoms observed upon cotton infection (Schnathorst T and Mathre 1966). Defoliating strains cause the abscission of diseased leaves from the plant whereas leaves from plants infected with nondefoliating strains show wilting symptoms but stay attached to the stem (Schnathorst T and Mathre 1966; Jiménez-Díaz et al. 2017) . While genetic markers for discerning between defoliating and nondefoliating strains exist (Pérez-Artés et al. 2000), the bases for the establishment of the defoliating disease phenotype remain to be elucidated.

The *V. dahliae* disease classes investigated here were established after careful observation of the *V. longisporum*-Arabidopsis pathosystem. Infection of Arabidopsis with virulent *V. longisporum* causes stunted growth and chlorosis of older rosette leaves due to early senescence (Johansson et al. 2006; Reusche et al. 2012; Reusche et al. 2013). Notably, *V. longisporum* infection does not induce wilting symptoms on Arabidopsis. Instead, Reusche et al. (2012) demonstrated that *V. longisporum* isolate VL43 triggers substantial developmental reprogramming of the host including transdifferentiation of bundle sheath cells that surround the vascular bundles into *de novo* formed, functional xylem vessels (Reusche et al. 2012) . In addition, reactivated cambial activity and transdifferentiation of xylem parenchyma into xylem vessels massively increase the amount of xylem elements in the vascular bundle (Figure 1.3). The resulting hyperplastic xylem increases the water storage capabilities of the

infected plants and thus enhances their drought stress tolerance (Reusche et al. 2012; Reusche et al. 2014).

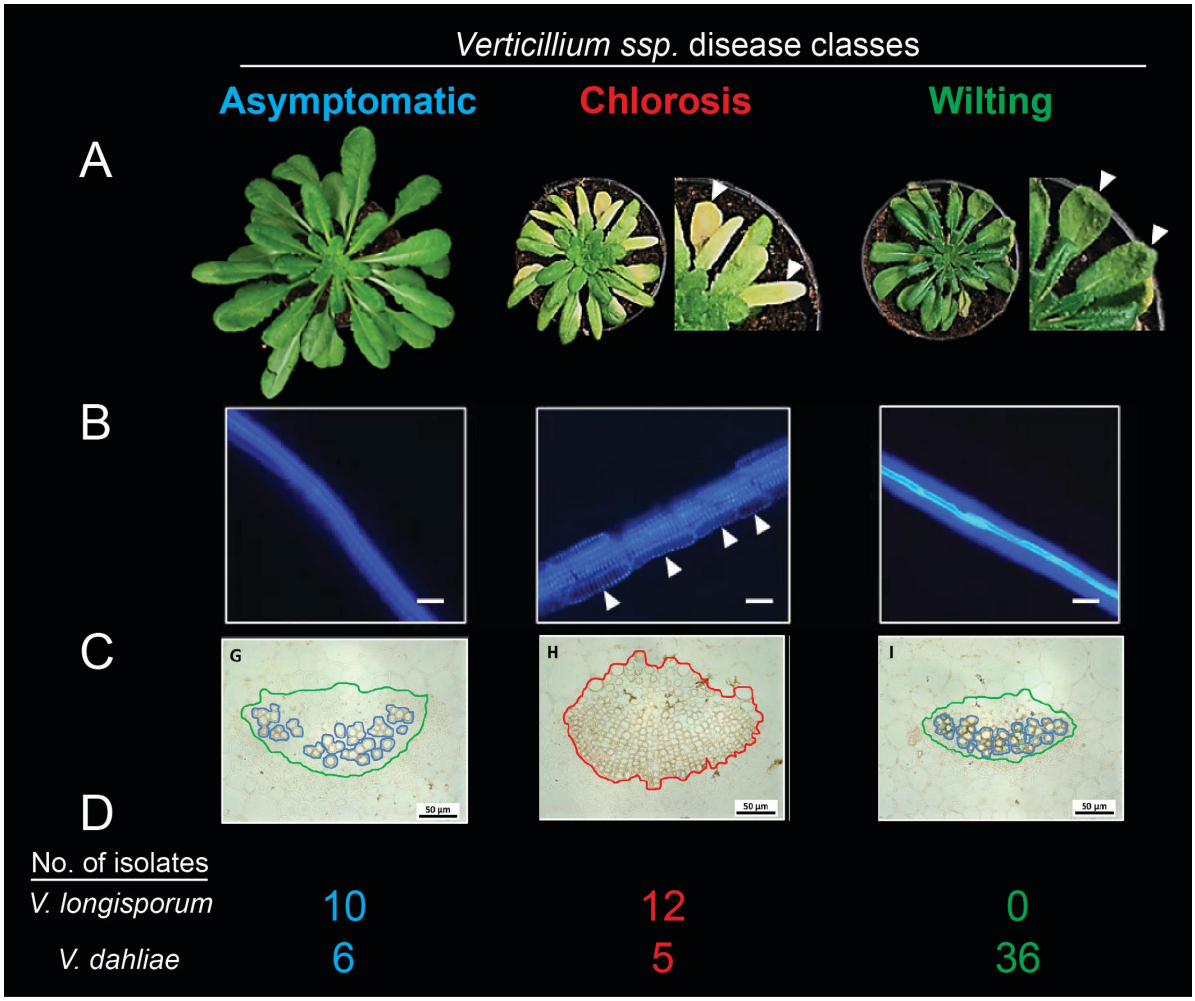

Figure 1.3 Distinct disease symptoms on Arabidopsis caused by *Verticillium spp.* disease classes. (A) Macroscopic disease symptoms in Arabidopsis after infection with *Verticillium spp.* isolates from the three Arabidopsis disease classes established by Thole (2016). Representative Arabidopsis plants 28 days past infection (dpi) with asymptomatic, chlorosis-class or wilting-class *Verticillium spp.* isolates. White arrowheads mark chlorotic rosette leaves after chlorosis-class infection and wilting rosette leaves after wilting-class infection. (B) Epifluorescence microscopic pictures of Arabidopsis leaf veins. White arrowheads mark *de novo* formed xylem elements formed through transdifferentiation from bundle sheath cells. An enhanced fluorescent signal from leaf veins of Arabidopsis infected with wilting-class isolates indicates enhanced xylem lignification. (C) Bright field microscopy of leaf midrib transections stained with potassium permanganate to visualize the extent of lignification (stained in brown). Details of leaf midrib xylem anatomy: xylem cells (blue), xylem parenchyma (green) and hyperplastic xylem (red) are encircled. Figure was adopted and modified from Reusche *et al.*, 2012 and Reusche *et al.*, 2014.

Arabidopsis as a member of the Brassicaceae is not a natural host of *V. dahliae*. However, infection of Arabidopsis with *V. dahliae* can be achieved in the laboratory (Steventon et al. 2001). Arabidopsis plants infected with virulent *V. dahliae* isolates usually develop disease symptoms distinctly different from *V. longisporum* infections and show stunting, wilting of older rosette leaves and enhanced lignification of xylem elements (Reusche et al. 2014). This is interesting due to the fact that, as previously described, one of the parental lines giving rise to the hybrid species *V. longisporum* is closely related to *V. dahliae* (Inderbitzin et al. 2011b). The genetic background of *V. longisporum* indicates that some *V. dahliae* isolates may also cause disease symptoms so far exclusively reported for *V. longisporum*. To test this hypothesis, a selection of 47 *V. dahliae* and 22 *V. longisporum* isolates from various geographical locations and host plants was investigated and categorized according to the disease symptoms induced upon Arabidopsis infection (Thole 2016). According to these results, the analyzed *V. dahliae* isolates were assigned to three disease classes (Thole 2016). Asymptomatic *V. dahliae* isolates do not induce any disease symptoms on their host. Wilting-class isolates cause stunting, wilting and enhanced lignification of xylem vessels while chlorosis-class (also referred to as 'early-senescence'-class by Thole (2016)) isolates induce symptoms identical to *V. longisporum* VL43 (Figure 1.3). While most *V. dahliae* isolates belonged to either the asymptomatic or wilting class, five *V. dahliae* chlorosis-class isolates were discovered. Interestingly, out of 22 investigated *V. longisporum* isolates, none induce wilting-class disease symptoms on Arabidopsis (Figure 1.3). It was subsequently hypothesized that the ability to induce either chlorosis- or wilting-class symptoms is determined either by differentially expressed effectors or an entirely different, disease-class specific effector repertoire (Thole 2016). Additionally, the observations suggest that the effector repertoire required for the induction of chlorosis-class disease symptoms has to be shared by both *V. dahliae* and *V. longisporum* chlorosis-class isolates. On the basis of this hypothesis, candidate effectors were identified (Thole 2016).

Notably, chlorosis-class infection symptoms are not restricted to Arabidopsis or the Brassicaceae. Transdifferentiation of bundle sheath cells has also been shown during *V. longisporum* VL43 infection of rapeseed (*Brassica napus*) (Reusche et al. 2012) and during chlorosis-class *Verticillium spp.* infection of *Nicotiana benthamiana* (Thole 2016). In addition, xylem hyperplasia was reported to be induced in hop plants during *V. nonalfalfae* infection (Talboys 1958). In general, studies on Verticillium wilt have been focusing on macroscopic disease symptoms such as wilting, defoliation or vascular

discoloration and cytological studies are rare. It is therefore very well possible that transdifferentiation of bundle sheath cells and/or xylem hyperplasia as well as other yet undescribed processes are triggered during *Verticillium spp.* infections on host plants other than Arabidopsis.

1.3 Chlorosis-class disease symptoms on Arabidopsis

1.3.1 Transdifferentiation in plants

Transdifferentiation, a process occurring in both plants and animals, is universally defined as 'the irreversible switch of one differentiated cell type into another' (Okada 1991; Nguyen and Mccurdy 2016). Transdifferentiation has been best studied in animal systems. In this field, a set of criteria has emerged to distinguish transdifferentiation from other forms of cell differentiation. Most importantly, clearly identifiable cell types must be observed before and after transdifferentiation and secondly, the cell lineage relationship between the original and transdifferentiated cell type must be established (Nguyen and Mccurdy 2016). However, since plant cells in comparison to animal cells have considerably more developmental plasticity, the term 'transdifferentiation' has been applied more loosely in plant systems (Jong and Leyser 2012; Nguyen and Mccurdy 2016). From the mid twentieth century, (trans)differentiation has mainly been investigated during the wound- and hormone-induced xylem regeneration from parenchyma cells (Jacobs 1952; Torrey 1975). The term 'transdifferentiation', however, has not been used until 1990 in an article reviewing the *in vitro* conversion of *Zinnia elegans* mesophyll cells into tracheary elements (Sugiyama and Komamine 1990). The *Zinnia elegans* system, established in 1980, has to this day been used in numerous studies and is besides Arabidopsis the best studied system for transdifferentiation (Fukuda and Komamine 1980; Nguyen and Mccurdy 2016). The *in vitro* system uses Zinnia mesophyll cells isolated by maceration of leaf material. The cells are then incubated in culture medium containing the phytohormones cytokinin and auxin for three to four days during which the cells transdifferentiate into xylem parenchyma cells and tracheary elements (Fukuda and Komamine 1980). In 2004, Fukuda summarized and categorized the stages of transdifferentiation from mesophyll cells to tracheary elements (TEs) (Fukuda 2004). In Stage I, mesophyll cells undergo dedifferentiation. Not much emphasis has been given to this early stage of

transdifferentiation but studies suggest that wounding, e.g. the process of generating cell suspensions, is sufficient to induce dedifferentiation (Fukuda and Komamine 1980; Milioni et al. 2001). The presence of auxin and cytokinin is required for the initiation of Stages II and III which are mechanistically similar to stages which occur during xylogenesis *in planta* (Fukuda 2004). Stage II marks the differentiation of dedifferentiated cells into xylem precursor-like cells and Stage III the final differentiation into tracheary elements. The entire transdifferentiation process requires not more than 48 h and, interestingly, auxin and cytokinin are only required in a short time frame of 10 min in order to induce transdifferentiation (Milioni et al. 2001). Numerous genes are differentially expressed during *Z. elegans* mesophyll transdifferentiation. However, which endogenous factors determine the potential of these cells to transdifferentiate *in vitro* remains largely unknown (Iakimova and Woltering 2017). Overall, it has been shown that two processes are crucial for tracheary element formation: programmed cell death (Groover and Jones 1999; Iakimova and Woltering 2017) and secondary cell wall formation (Fukuda 2004) which are both tightly regulated during *Z. elegans* mesophyll transdifferentiation.

The endogenous interaction networks governing xylogenesis have been more extensively studied and are best understood in the model plant *Arabidopsis thaliana*. *A. thaliana* cell cultures undergo transdifferentiation into TEs in the presence of auxin, cytokinin and brassinolide (Kubo et al. 2005). Microarray analyses of this system revealed a group of seven *VASCULAR-RELATED NAC-DOMAIN* (*VND*) transcription factors which were then demonstrated to be master regulators for xylem vessel formation (Kubo et al. 2005; Zhou et al. 2014; Tan et al. 2018). *VND1* to *VND7* encode members of the large NAC (for NAM, ATAF1/2 and CUC2) -domain transcription factor family which is involved in numerous pathways including responses to abiotic and biotic stress and regulation of developmental processes (Kim et al. 2007; Nuruzzaman et al. 2013). Kubo et al. (2005) discovered that expression of either *VND6* or *VND7* under control of the constitutive 35S promoter triggers ectopic TE formation in Arabidopsis roots and hypocotyls (Kubo et al. 2005). However, phytohormone-induced ectopic TE formation in Arabidopsis still functions in *vnd6 vnd7* knockout lines whereas it is abolished in the triple knockout line *vnd1 vnd2 vnd3* (Tan et al. 2018). Ectopic overexpression of *VND1-VND5* does not induce ectopic TE formation but trigger ectopic xylem element-like secondary cell wall (Zhou et al. 2014). This underlines that while *VND6* and *VND7* are master switches for TE formation, all *VND* transcription factors are part of a complex network regulating xylogenesis in Arabidopsis. Reusche et

al. (2012) investigated *VND6* and *VND7* expression in Arabidopsis plants infected with chlorosis-class *V. longisporum* isolate VL43 and found that both genes are upregulated during infection. Concomitantly, they demonstrated that transdifferentiation of bundle sheath cells during *V. longisporum* VL43 infection is reduced in *VND7-SRDX* suppressor lines (Reusche et al. 2012). It was consequently hypothesized that transdifferentiation in the *V. longisporum*-Arabidopsis pathosystem is induced by a mobile systemic signal that directly or indirectly triggers *VND6*/*VND7*-depending developmental reprogramming in their host.

1.3.2 Hyperplasia formation in response to pathogen attack

Xylem hyperplasia, i.e. the increase of xylem elements due to (trans)differentiation of xylem parenchyma cells and/or reactivation of cambial activity, has been described as a response of plants to vascular pathogens. In 1958, P.W. Talboys observed xylem hyperplasia in hops infected with *Verticillium nonalfalfae* (there referred to as *V. albo-atrum*). They suggested that low amounts of fungal mycelium in the vascular tissue trigger compensatory xylem formation responses in their host. This leads to a less severe disease phenotype when compared to the interaction of susceptible hop with more virulent *V. nonalfalfae* isolates (Talboys 1958). Xylem hyperplasia formation in response to vessel occlusion was also reported after infection of carnations with the vascular plant pathogen *Fusarium oxysporum* (Baayen 1986). In addition, Baayen et al. (1986) observed that xylem hyperplasia induced regeneration of vascular tissue (neovascularization) in resistant plants to maintain their water status.

In recent years, xylem hyperplasia has mainly been studied as a symptom of gall formation caused by bacteria, insects or root-knot nematodes (Cook 1923; Tooker and Moraes 2008; Favery et al. 2016). Galls are masses of tumor-like tissue that often serve as feeding sites of the pathogen. Although galls seem disorganized, functional vascular tissue is required in order to sustain them (Ullrich and Aloni 2000). In galls caused by the proteobacterium *Agrobacterium tumefaciens*, for example, distinct three-dimensional patterns of phloem and xylem vessels are formed which are connected to the host's vasculature. The vasculature in the gall, however, is morphologically different from vascular tissues formed during normal development (Aloni et al. 1995). *A. tumefaciens* integrates transfer (T)-DNA into

the host's genome which encodes, amongst other factors, enzymes of auxin (SCHRODER et al. 1984) and cytokinin biosynthesis (Akiyoshi et al. 1984) . As described above, both phytohormones are required for xylem formation but it has not been described yet how *Agrobacterium* controls vascular formation within galls. A special case of gall development is leafy gall formation caused by the actinobacterium *Rhodococcus fascians*. In contrast to *A. tumefaciens*, *R. fascians* induces galls with fully differentiated vasculature derived from meristems but also transdifferentiated parenchyma cells (neovascularization) (O Manes et al. 2001; Dolzblasz et al. 2018). Auxin and cytokinin secreted by *R. fascians* have been reported to control leafy gall formation and neovascularization (Stes et al. 2011; Dolzblasz et al. 2018) . The question how phytohormones could be involved in *Verticillium spp.*-induced xylem hyperplasia and transdifferentiation has not been addressed in detail. In a study conducted by Reusche et al. (2013), it was shown that cytokinin levels are negatively regulated by chlorosis-class *V. longisporum* VL43 during infection of *A. thaliana* by inducing transcription of cytokinin oxidases/dehydrogenases. They also observed that exogenous application of cytokinin during infection significantly inhibited fungal proliferation and leaf senescence (Reusche et al. 2013). The influence of auxin and/or cytokinin treatment on *de novo* xylem formation remains to be elucidated.

1.3.3 Chlorosis and senescence are tightly regulated developmental processes

Chlorosis-class *Verticillium spp.* isolates induce chlorosis on mature Arabidopsis rosette leaves (Figure 1.3). Chlorosis (Greek: *khloros* meaning 'greenish-yellow') occurs when chlorophyll is degraded due to endogenous or exogenous factors. Chlorosis is a natural part of developmental processes, e.g. leaf senescence or fruit ripening (Hörtensteiner 2006; Hörtensteiner and Kräutler 2011) but can also be induced, amongst others, by phytotoxin activity (Bender 1999) and nutrient deficiency (Abadía et al. 2002; Tanoi and Kobayashi 2015) . Leaf senescence, the most common instigator of leaf chlorosis, is a developmental process usually regulated by ageing and is employed to recover resources from older leaves that are no longer efficient in photosynthesis (Lim et al. 2007; Woo et al. 2013) . Chloroplast and chlorophyll degradation are in fact the first cellular events in senescing tissues during which nutrients are released from chloroplasts and free chlorophyll is detoxified (Lim et al. 2007). Senescence is triggered by abiotic and biotic stresses including drought,

nutrient limitation and pathogen attacks (Bell 1993; Munné-Bosch and Alegre 2004; Lim et al. 2007). Reusche et al. (2013) investigated the cause for chlorosis triggered by *V. longisporum* VL43 infection and found that senescence marker genes *SENESCENCE-ASSOCIATED GENE12*, *SENESCENCE-ASSOCIATED GENE13*, and *WRKY53* are significantly upregulated in infected plants. In addition, treatment with the senescence-inhibiting phytohormone cytokinin significantly reduces the number of chlorotic leaves on VL43 infected plants (Reusche et al. 2013). It can therefore be assumed that chlorosis-class *Verticillium spp.* isolates trigger chlorosis through the induction of early senescence in Arabidopsis. Chloroplast and chlorophyll degradation are in fact the first cellular events during senescence during which nutrients are released from chloroplasts free chlorophyll is detoxified (Lim et al. 2007).

Some organs such as fruit, petals and leaves in perennial plants are abscised at the final stage of senescence. However, leaf abscission has not been observed after chlorosis-class *Verticillium spp.* infection of Arabidopsis. This is most likely because Arabidopsis in general does not have the ability to shed its rosette leaves due to the fact that the rosette lacks functional abscission zones (Stenvik et al. 2006). However, defoliation as a consequence of leaf abscission has been reported from infections with *V. dahliae* defoliating isolates on cotton, olive and other woody plants (Wiese and Devay 1970; Keykhasaber et al. 2018). Organ abscission takes place in the abscission zone at the juncture of the organ and the main body of the plant and consists of several layers of small cells (Jensen and Valdovinos 1967). Recently, the mechanism of flower organ abscission in Arabidopsis has been uncovered. Lee et al. (2018) demonstrated that cells in the abscission zone form a honeycomb structure from lignin. This mechanical 'brace' spatially separates and stabilizes the layers of separating cells. Interestingly, this process is accompanied by transdifferentiation of non-epidermal cells at the site of organ detachment into epidermal cells (Lee et al. 2018). If transdifferentiation processes are also responsible for defoliation in cotton upon infection with chlorosis-class/defoliating isolates has not been studied yet.

1.4 The functions of effector proteins in plant-pathogen interactions

1.4.1 The plant innate immune system

Plants have evolved elaborate strategies to defend themselves against pathogen attack. The first, constitutive layers of plant defense include physical barriers such as the plant leaf cuticle, cell walls and suberization of the root endodermis (Miedes et al. 2014). For the soil-borne root pathogen, for example, *Verticillium*, the root endodermis forms an insurmountable barrier (Schnathorst and Sibbett 1971; Fradin and Thomma 2006). Consequently, the fungus must rely on endodermis-free zones at the root tip or mechanically induced wounding sites. Other pathogens have evolved mechanisms to breach constitutive barriers such as the formation of appressoria or secretion of cell wall-degrading enzymes (Hématy et al. 2009). When constitutive barriers are circumvented or breached, the second layer of defense is triggered. Pathogen associated molecular patterns (PAMPs) such as fungal chitin or bacterial flagellin are recognized by plant pattern recognition receptor (PRR) molecules which then elicit signaling cascades resulting in numerous defense reactions including, amongst others the production of reactive oxygen species (ROS) and programmed cell death (Figure 1.4) (Jones and Dangl 2006). ROS, in turn, can also function as signaling molecules and trigger, for example, cell wall lignification, a symptom commonly observed during wilting-class *Verticillium dahliae* infections (Barros et al. 2015; Reusche et al. 2014; Thole 2016). There are two ways for pathogens to avoid or overcome PAMP triggered immunity (PTI). Either pathogens avoid PAMP detection or they interfere with the plant immune response. Both can be achieved by deploying so-called effectors. The successful infection of plants through the release of effector molecules is called effector triggered susceptibility (ETS) (Figure 1.4) (Kazan and Lyons 2014; Jones and Dangl 2006).

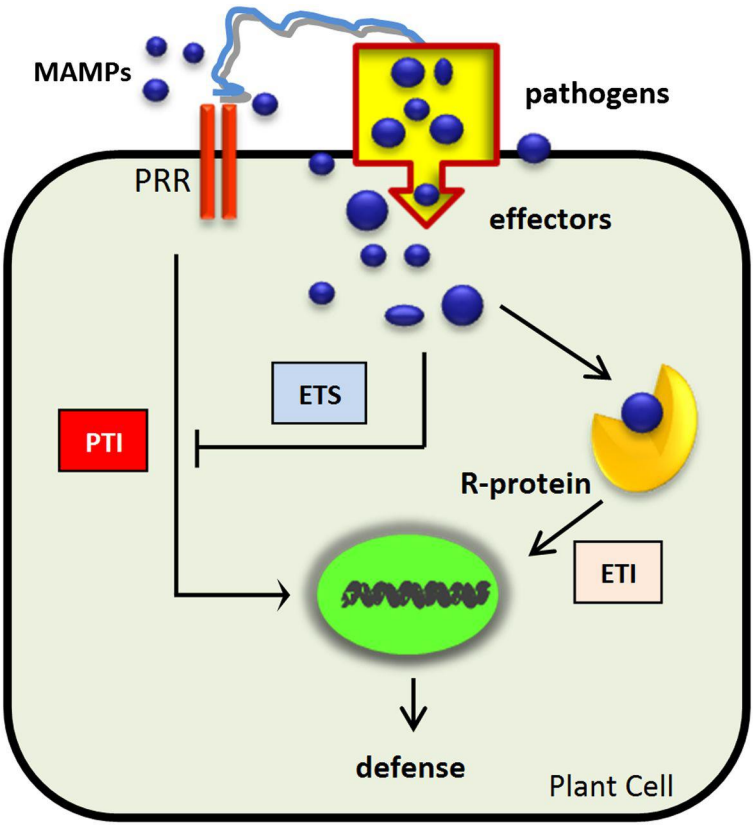

Figure 1.4 A simplified view of plant–pathogen interactions. Pathogen-derived conserved molecules known as microbe-associated molecular patterns (MAMPs) are detected by plasma membrane–located pattern recognition receptors (PRRs), and this recognition initiates PAMP-triggered immunity PTI. Pathogens interfere with immune signaling through effectors to induce susceptibility. This is known as effector-triggered susceptibility (ETS). In return, plants have evolved effector recognition proteins (R proteins) that trigger an immune reaction following effector recognition to stop pathogen growth. This phenomenon is known as effector-triggered immunity (ETI). Figure and figure legend are adopted from Kazan and Lyons (2014).

Effectors can be broadly defined as 'molecules that alter host cell structure and function, facilitating infection and/or triggering defense responses' (Selin et al. 2016). Some bacterial pathogens are able to deliver effectors directly into plant cells by employing the type III secretion machinery (Chatterjee et al. 2013) but usually effectors are secreted into the apoplast where they remain (apoplastic effector) or are taken up into the plant cell cytoplasm (cytoplasmic effector) (Figure 1.4) (Kamoun 2006). Effectors are structurally and functionally extremely diverse and only a small overview can be given here. Cell wall degrading enzymes (CWDEs), for example, degrade plant cell wall barriers and liberate nutrients for pathogen uptake (Kubicek et al. 2014) . Glucanase inhibitors, on the other hand, protect the pathogen's cell wall from degradation by enzymes deployed by the plant (Rose et al. 2002) .

Pathogens also protect themselves from recognition with, for example, LysM effectors that interfere with chitin (PAMP) perception (Kombrink and Thomma 2013). Another example are transcription activator-like effectors (TALEs) that are secreted directly into the cytoplasm by bacterial type III secretion systems and activate host susceptibility genes (Boch and Bonas 2010; Bogdanove et al. 2010). Plants, on the other hand, are able to counter ETS with mechanisms that recognize effectors and subsequently trigger immune responses (effector triggered immunity, ETI). Effectors that activate ETI and thus cause a pathogen to become avirulent are called avirulence (Avr) factors. Pathogens then either evolve versions of the Avr effectors that are no longer recognized or loose the effector through, for example, pseudogenization (Stergiopoulos et al. 2007; Boller and He 2009). Due to the fact that plant-pathogen systems are never stable and evolve constantly, considerable selective pressure is placed on both pathogens and plants. The resulting 'arms race' between plants and pathogens produces thus ever changing forms of ETS and ETI (Jones and Dangl 2006; Boller and He 2009).

1.4.2 The *Verticillium spp.* two-speed genome gives rise to lineage-specific effectors

Verticillium species are, with the exception of *V. longisporum*, haploid organisms that are hypothesized to reproduce exclusively asexually (Usami et al. 2008; Inderbitzin et al. 2011a). The first *Verticillium* genomes were published by Klosterman et al. (2011) who compared in their study the genomes of *V. dahliae* VdLs17 and *V. alfalfae* VaMs102 (there referred to as *V. albo-atrum*) to gain insights into niche adaptation of the pathogen. This is an interesting topic especially for asexual, haploid organisms since they cannot rely on meiosis as a driving force for genome evolution and adaptation (Stukenbrock 2013). The comparison of the two *Verticillium* genomes revealed that extensive chromosomal rearrangements exist between the two species and that the main source of genetic variability are sequences only present in one of the genomes. Klosterman et al. (2011) also observed that these so-called lineage-specific (LS) regions are enriched in transposable elements (TE). A whole-genome comparison between the two *V. dahliae* isolates JR2 and VdLs17 by deJonge et al. (2013) corroborated extensive chromosomal rearrangements as well as lineage-specific regions in the genus *Verticillium*. In addition to an enrichment of TEs, deJonge et al. (2013) identified a high number of

genes encoding putative effectors in LS regions. Based on this and subsequent studies, the hypothesis was proposed that *Verticillium* has a 'two-speed' genome consisting of a stable, highly conserved core genome and more variable LS genome where transposons mediate plasticity through structural rearrangements. (deJonge et al. 2013; Klimes et al. 2015; Faino et al. 2016; Shi-Kunne et al. 2018). Exemplary for an effector located in a LS region is *Ave1* which mediates virulence on tomato and is encoded in a ~ 50 kb region found only in *V. dahliae* race 1 isolates (deJonge et al. 2012). Combining whole-genome comparisons with RNA sequencing (RNAseq) analyses proved a powerful tool to uncover putative effector genes as new *Verticillium* effectors have been identified by this methodology. DeJonge et al. (2013) found in their initial whole-genome comparison a VdLs17-specific LysM effector which was later designated *Vd2LysM* (Kombrink et al. 2017). *Vd2LsyM* was reported to bind chitin and was, therefore, hypothesized to inhibit PTI in tomato (Kombrink et al. 2017). Recently, a ~20 kb region was identified that is present exclusively in *V. dahliae* cotton-defoliating isolates (Zhang et al. 2019). Encoded in this region is a cluster of genes involved in N-acyl-ethanolamine (NAE) biosynthesis, a compound that was hypothesized by Zhang et al. (2019) to mediate defoliation in cotton.

1.5 Thesis aims

Verticillium spp. isolates are categorized into three distinct disease classes regarding their disease phenotype on the model plant *Arabidopsis thaliana* (Thole 2016). Asymptomatic isolates do not induce any disease symptoms on Arabidopsis while plants infected with wilting- and chlorosis-class isolates develop distinct disease phenotypes. The chlorosis-class disease phenotype is characterized by substantial developmental reprogramming that induces transdifferentiation of bundle sheath cells as well as xylem parenchyma cells into *de novo* formed xylem elements and the reactivation of the vascular cambium. Previous studies have shown that lineage-specific regions present in the genomes of *Verticillium spp.* isolates with distinct disease phenotypes harbor candidate effector genes which may be essential for specific adaptations to plant hosts (deJonge et al. 2012; deJonge et al. 2013; Faino et al. 2016). The aim of this thesis was to discover and eventually characterize putative effectors involved in the establishment of chlorosis-class disease symptoms. For this purpose, the genome of

chlorosis-class isolate *V. dahliae* V76 was sequenced and aligned to the genome of wilting-class reference isolate *V. dahliae* JR2. *V. dahliae* was chosen for comparative genomics in favor of *V. longisporum* due to the fact that chromosome-level assemblies were already publicly available for wilting-class isolate *V. dahliae* JR2. In addition, genomic analyses in the haploid species *V. dahliae* were expected to be less complicated than in the allodiploid species *V. longisporum*. Moreover, deletions of candidate genes can be more easily obtained in a haploid fungal species.

After comparative genomics, chlorosis-class LS regions were mined for lineage-specific candidate effectors (*LSCE*s). Bioinformatic analyses revealed that one gene, *LSCE2*, was highly induced in all *V. dahliae* chlorosis-class isolates upon host plant infection. The next aim was to examine the influence of *LSCE2* on the establishment of the chlorosis-class disease phenotype on Arabidopsis. To this end, *LSCE2* knockout lines were generated in the *V. dahliae* V76 as well as *V. longisporum* VL43 background and used for infection experiments on Arabidopsis. Furthermore, it was investigated whether transgenic expression of *LSCE2* in wilting-class isolate *V. dahliae* JR2 isolate is sufficient to induce chlorosis-class disease symptoms on Arabidopsis. In addition, fungal proliferation of wild-type isolates as well as mutant lines was monitored *in planta* to investigate whether deletion and/or transgenic expression of *LSCE2* has an influence on fungal virulence. Finally, protein biochemical analyses on LSCE2 were conducted. The effect of purified LSCE2 was monitored after infiltration into Arabidopsis leaves and the phenotype of Arabidopsis mutants constitutively expressing *LSCE2* was characterized. In addition, potential targets of LSCE2 were uncovered with yeast-two-hybrid analyses.

2 Materials and Methods

2.1 Materials

2.1.1 Arabidopsis plant material

In this study, wild-type *Arabidopsis thaliana* Columbia-0 (N1092; NASC[1]) was used for infection and transformation experiments. In addition, one transgenic Arabidopsis line was generated (Table 2.1).

[1] Nottingham Arabidopsis Stock Centre (NASC), University of Nottingham, Loughborough, United Kingdom

Table 2.1 Arabidopsis transgenic line generated in this study

Name	Transformed organism	Plasmid	Description	Selection marker
LSCE2-GFP	*A. thaliana* Col-0	pLW27	constitutive expression of *LSCE2* in Arabidopsis	BASTA

2.1.2 Fungi

2.1.2.1 *Verticillium spp.*

Verticillium dahliae and *Verticillium longisporum* wild-type isolates (Table 2.2) as well as genetically modified lines (Table 2.3) were used in this study.

Table 2.2 *Verticillium* isolates used in this study

Isolate	Species	Isolated from	Geographical origin	Reference
DVD-31	*V. dahliae*	*Solanum lycorpersicum*	Essex county (Canada)	B. Thomma[1]
DVD-S29	*V. dahliae*	*soil*	Essex county (Canada)	B. Thomma[1]
JR2	*V. dahliae*	*Solanum lycorpersicum*	Ontario (Canada)	B. Thomma[1]
ST100	*V. dahliae*	*soil*	Belgium	B. Thomma[1]
T9	*V. dahliae*	*Gossypium spec.*	California (USA)	A. v. Tiedemann[2]
V138I	*V. dahliae*	*Gossypium spec.*	Cordoba (Spain)	R. Jiménez-Díaz[3]
V192I	*V. dahliae*	*Gossypium spec.*	Seville (Spain)	R. Jiménez-Díaz[3]
V76	*V. dahliae*	*Gossypium spec.*	Mexico	A. v. Tiedemann[2]

V781I	*V. dahliae*	*Olea europaea*	Cordoba (Spain)	R. Jiménez-Díaz[3]
VdLs17	*V. dahliae*	*Lactuca sativa*	California (USA)	B. Thomma[1]
Vd39	*V. dahliae*	*Helianthus annuus*	Hessen (Germany)	A. v. Tiedemann[2]
Vd42	*V. dahliae*	*Brassica rapa*	Krasnodar (Russia)	A. v. Tiedemann[2]
Vd52	*V. dahliae*	*Capsicum annuum*	Burgenland (Austria)	A. v. Tiedemann[2]
Vd54	*V. dahliae*	*Capsicum annuum*	Burgenland (Austria)	A. v. Tiedemann[2]
Vd152	*V. dahliae*	*Quercus spec.*	Hungary	A. v. Tiedemann[2]
VL43 (A1/D1)*	*V. longisporum*	*Brassica napus*	Mecklenburg (Germany)	G. Braus[4]
VL10 (A1/D1)	*V. longisporum*	*Brassica napus*	Rostock (Germany)	A. v. Tiedemann[2]
VL35 (A1/D1)	*V. longisporum*	*Pisum sativum*	Rostock (Germany)	A. v. Tiedemann[2]
VL60 (A1/D1)	*V. longisporum*	*Brassica oleracea*	California (USA)	G. Braus[4]
VL83 (A1/D1)	*V. longisporum*	*Brassica napus*	Mecklenburg (Germany)	G. Braus[4]
VL334 (A1/D1)	*V. longisporum*	*Brassica napus*	France	A. v. Tiedemann[2]
VL13 (A1/D1)	*V. longisporum*	*Gossypium spec.*	Spain	A. v. Tiedemann[2]
VL18 (A1/D1)	*V. longisporum*	*Brassica napus*	Lebckendorf (Germany)	A. v. Tiedemann[2]
VL24 (A1/D1)	*V. longisporum*	*Brassica napus*	Bandlesdorf (Germany)	A. v. Tiedemann[2]
VL32 (A1/D3)	*V. longisporum*	*Brassica napus*	Mecklenburg (Germany)	B. Thomma[1]

[1] Laboratory of Phytopathology, University of Wageningen, The Netherlands
[2] Division of Plant Pathology and Crop Protection, University of Göttingen, Germany
[3] Department of Plant Pathology, University of Córdoba and Institute of Sustainable Agriculture, Cordoba, Spain
[4] Department of Molecular Microbiology & Genetics, University of Göttingen, Germany
**V. longisporum* lineage according to (van Tran et al. 2013)

Table 2.3 Genetically modified *Verticillium* lines generated and used in this study

Name	Transformed organism	Plasmid	Description	Selection marker
V76Δ*LSCE2*#1	*V. dahliae* V76	pLW14	*LSCE2* single knockout line	Hygromycin
V76Δ*LSCE2*#2	*V. dahliae* V76	pLW19	*LSCE2* single knockout line	Nourseothricin
V76Δ*LSCE2*#3	*V. dahliae* V76	pLW19	*LSCE2* single knockout line	Nourseothricin
V76ΔΔ*LSCE2* #1	V76ΔLSCE2#1	pLW14+19	*LSCE2* double knockout line	Hygromycin Nourseothricin
V76ΔΔ*LSCE2* #2	V76ΔLSCE2#1	pLW14+19	*LSCE2* double knockout line	Hygromycin Nourseothricin
V76ΔΔ*LSCE2* #3	V76ΔLSCE2#1	pLW14+19	*LSCE2* double knockout line	Hygromycin Nourseothricin
VL43Δ*LSCE2* #1	*V. longisporum* VL43	pLW19	*LSCE2* single knockout line	Hygromycin
VL43Δ*LSCE2* #2	*V. longisporum* VL43	pLW19	*LSCE2* single knockout line	Hygromycin
VL43Δ*LSCE2* #3	*V. longisporum* VL43	pLW19	*LSCE2* single knockout line	Hygromycin
VL43ΔΔ*LSCE2* #1	VL43Δ*LSCE2*#1	pLW14+19	*LSCE2* single knockout line	Hygromycin Nourseothricin

VL43ΔΔ*LSCE2* #2	VL43Δ*LSCE2*#1	pLW14+19	*LSCE2* single knockout line	Hygromycin Nourseothricin
VL43ΔΔ*LSCE2* #3	VL43Δ*LSCE2*#1	pLW14+19	*LSCE2* single knockout line	Hygromycin Nourseothricin
JR2 [pLSCE2:*LSCE2*]#1	*V. dahliae* JR2	pLW11	transgene expression of *LSCE2* under native promoter	Hygromycin
JR2 [pLSCE2:*LSCE2*]#2	*V. dahliae* JR2	pLW11	transgene expression of *LSCE2* under native promoter	Hygromycin
JR2 [pLSCE2:*LSCE2*]#3	*V. dahliae* JR2	pLW11	transgene expression of *LSCE2* under native promoter	Hygromycin

2.1.2.2 Yeast

For Yeast-two-Hybrid experiments (2.2.5), *Saccharomyces cerevisiae* strain AH109 (MAT a, trp1, leu2, ura3, his3, gal4Δ, gal80Δ, LYS2::GAL1UAS-GAL1TATA-HIS3, GAL2UAS-GAL2TATA-ADE2, ura3::MEL1UAS-MEL1TATA-lacZ) was used. *Pichia pastoris* strain X-33 was used for expression of LSCE2 and LSCE2-like.

2.1.3 Bacteria

2.1.3.1 *Escherichia coli*

One Shot® TOP10 Chemically Competent *E. coli* cells (Thermo Fisher Scientific (Waltham, Massachusetts, USA) were used for amplification of vector plasmids.

2.1.3.2 *Agrobacterium tumefaciens*

For Agrobacterium-mediated transformation of *Verticillium* spores, *A. tumefaciens* strain AGL1 (C58 RecA (rif R/carbR) Ti pTiBo542DT-DNA (strepR) Succinamopine) was used (Lazo et al. 1991). Floral-dip transformation of *A. thaliana* was done with *A. tumefaciens* strain GV3101 (C58 (RIF R) Ti pMP90 (pTiC58DT-DNA) (gentR/strepR) Nopaline) (Koncz and Schell 1986).

2.1.4 Plasmids

Table 2.4 Plasmids generated in this study

Name	Construct	Selection marker	Assembly method	Used for
pLW11	pk01-prom*LSCE2*$_{V76}$: g*LSCE2*$_{V76}$:term *LSCE2*$_{V76}$	Kanamycin	NEBuilder	Transgene expression of *LSCE2* in *Verticillium*
pLW14	pk01[1]-765 bp *LSCE2*$_{V76}$ 5' flanking region: Hygromycin resistance cassette: 970 bp *LSCE2*$_{V76}$ 3' flanking region	Kanamycin	NEBuilder[2]	Generation of *Verticillium LSCE2* knockout lines
pLW19	pk01-765 bp *LSCE2*$_{V76}$ 5' flanking region: Nourseothricin resistance cassette: 970 bp *LSCE2*$_{V76}$ 3' flanking region	Kanamycin	NEBuilder	Generation of *Verticillium LSCE2* knockout lines
pLW27	pGreenII0229-prom*AtUBQ10*:*LSCE2*$_{V76}$ CDS aa 19-273:4xAla:*GFP*	Ampicillin/ BASTA	NEBuilder	Transgene expression of *LSCE2* in *Arabidopsis*
pLW36	pPICZαA[3]-LSCE2$_{V76}$ aa 19-273	Zeocin	Restriction enzyme cloning	Expression of *LSCE2* in *P. pastoris*
pLW38	pPICZαA[3]-LSCE2-like$_{JR2}$ aa 19-273	Zeocin	Restriction enzyme cloning	Expression of LSCE2-like in P. pastoris
pLW40	pDONR207[4]:*LSCE2*$_{V76}$ CDS aa 19-273	Gentamicin	Gateway	Donor plasmid
pLW41	pDEST[4]-GBKT7: *LSCE2*$_{V76}$ CDS aa 19-273	Ampicillin	Gateway	Expression of *LSCE2* in *S. cerevisiae* for interaction assay
	pDONR207[4]: *A. thaliana* interaction candidates CDS	Gentamicin	Gateway	Donor plasmid
	pDEST-GAD[4]:*A. thaliana* interaction candidates CDS	Ampicillin	Gateway	Expression of *A. thaliana* interaction candidates *in S. cerevisiae* for interaction assay

[1] Obtained from AG Braus, Department of Molecular Microbiology & Genetics, University of Göttingen, Germany
[2] (Hellens et al. 2000)
[3] EasySelect Pichia Expression Kit (Thermo Fisher Scientific; Waltham, USA)
[4] Obtained from AG Gatz, Department of Plant Molecular Biology and Physiology, University of Göttingen, Germany

2.1.5 Oligonucleotides

Oligonucleotides were designed with the Geneious® software (v. 8.1.8, https://www.geneious.com (Kearse et al. 2012)) and produced as ordered by Thermo Fisher Scientific (Waltham, USA) (Table 2.5). Oligonucleotide stock solutions were prepared to a concentration of 100 µM with ddH_2O. 10 µM working solutions were used in polymerase-chain-reactions (PCRs) and sequencing reactions. All oligonucleotide solutions were stored at -20 °C.

Table 2.5 Oligonucleotides used in this study

Name_orientation	Sequence (5'→ 3')	Description	Reference
KT1_for	TCACTCATTAGGCACCCCAG	Sequencing of inserts in pk01 upstream of resistance cassette	K. Thole[1]
KT2_rev	CTCCAGCCAAGCCCAAAA		
KT3_for	TGTGTAGAAGTACTCGCCGA	Sequencing of inserts in pk01 downstream of resistance cassette	K. Thole[1]
KT4_rev	GTTGTAAAACGACGGCCAGT		
MR37_for	GACGCTTCATCTCGTCC	Amplification of At*UBQ5*, AT3G62250 for qRT-PCR	M. Reusche[1]
MR38_rev	GTAAACGTAGGTGAGTCCA		
LW4_for	ATGCAGATAACGTCCCTCTC	Amplification of *LSCE1*	this study
LW5_ref	CAGCTTCGCAAAGTCGGTGC		
LW8_for	GGTACCCGGGGATCTTTCG	Amplification of Hygromycin resistance cassette	this study
LW9_rev	AAAGAAGGATTACCTCTAAACAA		
LW10_rev	TTCCACACAACATACGAGCC	Amplification of pk01 vector backbone	this study
LW11_for	TCCTCGTGTACTGTGTAAGC		
LW30_for	CCCAGTCACGAAACCCTACG	Amplification of Vd ß-tubulin VDAG_10074 for qPCR	this study
LW31_rev	CCAGAGGCCTGCAAAGAAAG		
LW46_for	CGCTTCAAATCTTCTCGCAC	Amplification of VDAG_02705	this study
LW47_rev	TTCGTGAAGGAATGGACGGA		
LW49_rev	GAAGTACAGATGCATGACGG	Sequencing of inserts in pk01 upstream of Hygromycin resistance cassette	this study
LW102_for	TCGCGTTAACGCTAGCATGGATCTC	Sequencing of pDONR207	this study
LW103_rev	GTAACATCAGAGATTTTGAGACAC		
LW104_for	TCATCGGAAGAGAGTAGTAAC	Sequencing of pDEST_GBKT7	this study
LW105_rev	ATCATAAATCATAAGAAATTCGCCCG		
JU244_AD5XXL_for	GGACGGACCAAACTGCGTATAACGCGTT TGGAATCACTACAGGGATG	Colony PCR, Yeast-two-Hybrid screen	J. Uhrig[2]
JU245_AD3XL_rev	GCGACCTCATGCTATACCTGAGAAAGCA ACCTGACCTACAGGAAAGAG		
JU_upperGAD_for	TTCGATGATGAAGATACCCCACCAAACC C	Sequencing of Yeast-two-Hybrid colony PCR	J. Uhrig[2]
LW118_for	GGGGACAAGTTTGTACAAAAAAGCAGGC TCCATTGCCATCCCGCAATCCG	Amplification of *LSCE2* for assembly of pLWy01	this study
LW119_rev	GGGGACCACTTTGTACAAGAAAGCTGGG TTCAAAGCTGGCCTGCGTCA		
LW120_for	TTCCGCCAGCCACAATGAAG	Amplification and sequencing of *LSCE2*	this study
LW121_rev	TCAAAGCTGGCCTGCGTCA		
LW125_for	GGCTCGTATGTTGTGTGGAAAATCCCAT AAAAGCGCTGAA	Amplification of insert for pLW11 assembly (NEBuilder)	this study
LW126_rev	TCGAAAGATCCCCGGGTACCGCACCATG CATAAAACGATG		
LW129_for	TGTACAGTGACCGGTGACTC	Amplification of Nourseothricin (Nat) resistance cassette, used with LW9	this study
LW133_for	GCTCCGTAACACCCAATACG	Sequencing of inserts in pk01 with Nat resistance cassette, used with KT4	this study
LW134_rev	CATCCACTGCACCTCAGAGC	Sequencing of inserts in pk01 with Nat resistance cassette, used with KT1	this study
LW139_rev	TCGAAAGATCCCCGGGTACCGTGGCTG GCGGAATATATTG	Amplification of 5' insert for pLW14 assembly (NEBuilder), used with LW125	this study
LW140_for	TTTAGAGGTAATCCTTCTTTTCAGTTGAT CCAACCCGCTG	Amplification of 3' insert for pLW14 assembly (NEBuilder), used with LW125	this study
LW141_rev	GCTTACACAGTACACGAGGAGCACCATG CATAAAACGATG		
LW150_for	GAGTTTTTCTGATTAACAGAATGAAGTTC TCAAGAATCGT	Amplification of insert for pLW17 assembly (NEBuilder)	this study
LW151_rev	TCCCCCGGGCTGCAGGAATTTCAAAGCT GGCCTGCGTCAA		
LW152_for	GAGTTTTTCTGATTAACAGAATGATTGCC ATCCCGCAAT	Amplification of insert for pLW18 assembly (NEBuilder), used with LW151	this study

LW161_for	GGGGACAAGTTTGTACAAAAAAGCAGGC TCCATGGCCTCGAAGTATGGTTC	Amplification of AT4G26610 for assembly of pLWy02 (Gateway)	this study
LW162_rev	GGGGACCACTTTGTACAAGAAAGCTGGG TTCAAAAGAAATCGAACTCCAG		
LW163_for	GGGGACAAGTTTGTACAAAAAAGCAGGC TCCATGGCTCAGGCTGTAGAAGA	Amplification of AT4G04860 for assembly of pLWy03 (Gateway)	this study
LW164_rev	GGGGACCACTTTGTACAAGAAAGCTGGG TTCAGTCTTGGTGGATTTCATC		
LW165_for	GGGGACAAGTTTGTACAAAAAAGCAGGC TCCATGTCGAATAATAATAATTCT	Amplification of AT5G52020 for assembly of pLWy04 (Gateway)	this study
LW166_rev	GGGGACCACTTTGTACAAGAAAGCTGGG TTCATTTATAACTCCAAAGAT		
LW167_for	GGGGACAAGTTTGTACAAAAAAGCAGGC TCCATGCGGATGAGCTGTAATGG	Amplification of AT3G02550 for assembly of pLWy05 (Gateway)	this study
LW168_rev	GGGGACCACTTTGTACAAGAAAGCTGGG TTTAGAGCATAAGCTCAGTCT		
LW169_for	GGGGACAAGTTTGTACAAAAAAGCAGGC TCCATGTCTTGCTGTGGAGGAAA	Amplification of AT3G09390 for assembly of pLWy06 (Gateway)	this study
LW170_rev	GGGGACCACTTTGTACAAGAAAGCTGGG TTCACTTGCAGGTGCAAGGAT		
LW171_for	GGGGACAAGTTTGTACAAAAAAGCAGGC TCCATGGGAAGGTCACCGTGC	Amplification of AT4G38620 for assembly of pLWy07 (Gateway)	this study
LW172_rev	GGGGACCACTTTGTACAAGAAAGCTGGG TTTATTTCATCTCCAAGCTTCG		
LW173_for	GGGGACAAGTTTGTACAAAAAAGCAGGC TCCATGGGAAGATCTCCTTGTTG	Amplification of AT4G09460 for assembly of pLWy08 (Gateway)	this study
LW174_rev	GGGGACCACTTTGTACAAGAAAGCTGGG TTTACAACAGTGACAAACGCG		
LW175_for	GGGGACAAGTTTGTACAAAAAAGCAGGC TCCATGGATAAGACAGCGACATT	Amplification of AT5G06860 for assembly of pLWy09 (Gateway), used with LW176	this study
LW176_for	GGGGACAAGTTTGTACAAAAAAGCAGGC TCCAAAGATCTCTGTAACCAAAATG	Amplification of AT5G06860 without SP for assembly of pLWy10 (Gateway)	this study
LW177_rev	GGGGACCACTTTGTACAAGAAAGCTGGG TTTACTTGCAAATTTCAAGAGG		
LW178_for	GGGGACAAGTTTGTACAAAAAAGCAGGC TCCATGGGAGGCAAAGGTGTGAT	Amplification of AT4G21960 for assembly of pLWy11 (Gateway), used with LW180	this study
LW179_for	GGGGACAAGTTTGTACAAAAAAGCAGGC TCCGTAACAGAGGCTGAGCCAGG	Amplification of AT4G21960 without SP for assembly of pLWy12 (Gateway)	this study
LW180_rev	GGGGACCACTTTGTACAAGAAAGCTGGG TTCAATGGTTCTTGTTTGCGAG		
LW181_for	GGGGACAAGTTTGTACAAAAAAGCAGGC TCCATGTCGCCGTTTGTGAAGTT	Amplification of AT5G59770 for assembly of pLWy13 (Gateway)	this study
LW182_rev	GGGGACCACTTTGTACAAGAAAGCTGGG TTCACATTCTCTTTCTCTTGCC		
LW183_for	GGGGACAAGTTTGTACAAAAAAGCAGGC TCCATGCAATTTTTTGCAGTTGC	Amplification of AT3G19460 for assembly of pLWy14 (Gateway)	this study
LW184_rev	GGGGACCACTTTGTACAAGAAAGCTGGG TCTACTGATGTTTCTTCTCTTT		
LW185_for	GGGGACAAGTTTGTACAAAAAAGCAGGC TCCATGGGCCAAGCGCCGTC	Amplification of AT5G67250 for assembly of pLWy15 (Gateway)	this study
LW186_rev	GGGGACCACTTTGTACAAGAAAGCTGGG TTCAAGTAGAACTACTAGCATT		
LW187_for	GGGGACAAGTTTGTACAAAAAAGCAGGC TCCATGTTTAACGGGTTAATGGA	Amplification of AT5G21990 for assembly of pLWy16 (Gateway)	this study
LW188_rev	GGGGACCACTTTGTACAAGAAAGCTGGG TCTAGTTTCCAATATAGCCGA		
LW189_rev	GAGTCACCGGTCACTGTACAGTGGCTGG CGGAATATATTG	Amplification of 5' insert for pLW19, used with LW125	this study
LW194_for	GAATGATCTAGAGTTATTTT	Amplification/ sequencing of *LSCE2-like*	this study
LW195_rev	AGATCCTCAGAACTTATTTA		
LW196_for	GGGGACAAGTTTGTACAAAAAAGCAGGC TCCATGAAGTTCTCAAGAATCGT	Amplification of *LSCE2* for assembly of pLW22 and pLW23 (with LW118) (Gateway)	this study
LW201_rev	GGGGACCACTTTGTACAAGAAAGCTGGG TAAAGCTGGCCTGCGTCAAAAG		
LW199_for	ATGGTGAGCAAGGGCGA	Amplification of pHG113	H. Ghareeb[1]
LW200_rev	CTGTTAATCAGAAAAACTCAG		
LW216_for	TGAGTTTTTCTGATTAACAGATGATTGCC ATCCCGCAAT	Amplification of insert for assembly pLW27 (NEBuilder)	this study
LW198_rev	TCCTCGCCCTTGCTCACCATGGCCGCTG CAGCAAGCTGGCCTGCGTCAAAAG		
LW205_for	CTCCACTGACGTAAGGGATG	Sequencing of plasmids with 35S promoter	this study

LW206_rev	CCCTTATCTGGGAACTACTC	Sequencing of plasmids with 35S terminator	this study
LW217_for	GAGGGGCGCCTCACACGCAA	Amplification/ sequencing of LSCE region spacer	this study
LW218_rev	GGGCGCCTGGGGCTACTGTT		
LW221	GCTGTCGAGATTGCTCATGC	Amplification/ sequencing of LSCE region	this study
LW18	CTAACACACTGCGTCGACCT		
LW222	AATCCCTGCATGGCGGAAGT	Amplification/ sequencing of LSCE region	this study
LW224	CCCAATCCAATACCGAAGGC		
LW226	TAGGATGGCTCCGACCTATC	Amplification/ sequencing of LSCE region	this study
LW227_rev	TACGGCTCTGGTCCTCATCT		
LW228_for	CATGTTCGCAGTCGTTGTCG		
LW230	GAACGAAGTGGAGGAGCTTA	Amplification/ sequencing of LSCE region	this study
LW231	TTCCAGCACCACTGACATGA		
LW232	CCCAGAACCGACCTCTATTC	Amplification/ sequencing of LSCE region	this study
LW233	TTGGACACGACTGATGGCTG		
LW234	GTGGATTATGCCTCGAACGT	Amplification/ sequencing of LSCE region	this study
LW108	GCATGGGTAGACTTAGAGCA		
LW107	ACACTCGAGAACTGTACGAC	Amplification/ sequencing of LSCE region	this study
LW64	GAACTTGAGCGGGGCCAAA		
LW153	GCCGGGAAATGACATGTTGC	Amplification/ sequencing of LSCE region with LW121	this study
LW215	CACTTGGCATGTAGTTCGGC	Amplification/ sequencing of LSCE region with LW120	this study
LW235	TGGAGTAGCTACAGTGTCGG	Amplification/ sequencing of LSCE region	this study
LW236	ACCCTTATGCCTCCAAGACA		
LW237	ACCATGGCGTCTTCTCTTTC	Amplification/ sequencing of LSCE region	this study
LW238	GTAGCGAACAATCTGCCTCG		
LW239	CATCATGAGCCTCCACGACA	Amplification/ sequencing of LSCE region	this study
LW240	GGCCTCTTTGTATCTTGGCA		
LW241	AATCACGGAACCCACCAACT	Amplification/ sequencing of LSCE region with LW217	this study
VActF	TAATTCACAATGGAGGGTAGG	Amplification/ sequencing of *Verticillium spp. actin*	Inderbitzin et al. 2011
VActR	GTAAGGATACCACGCTTGG		
VEFf	AACGTCGTCGTCATCGGCCACG	Amplification/ sequencing of *Verticillium spp.* elongation factor 1-a	Inderbitzin et al. 2011
VEFr	CCACGCTCACGCTCGGCCTT		
VGPDf2	GGCATCAACGGTTTCGGCC	Amplification/ sequencing of *Verticillium spp.* GAP dehydrogenase	Inderbitzin et al. 2011
VGPDr	GTAGGAGTGGACGGTGGTCATGAG		
VTs3f	GCGCTGCAAGGCCGAGAAC	Amplification/ sequencing of Verticillium spp.Tryptophan synthase	Inderbitzin et al. 2011
VTs3r	GCGGAACGAGACGGCCTCC		
LW281_for	AAAGAATTCATTGCCATCCCGCAATCCG	Amplification of *LSCE2* for pLW36 assembly	this study
LW278_rev	GTCTCTAGACCAAGCTGGCCTGCGTCAAAAG		
LW282_rev	GTCTCTAGACCAAGCTGGCCTGCATCAAAAG	Amplification of *LSCE2* for pLW38 assembly, with LW281	this study
5'AOX1	GACTGGTTCCAATTGACAAGC	Amplification/ sequencing of pLW36 and pLW38	Easy Select Pichia Expres-sion Kit
3'AOX1	GCAAATGGCATTCTGACATCC		

2.1.6 Antibodies

Antibodies used in this study for detection of proteins on Western Blots (2.2.9.1) are shown in Table 2.6. Antibodies were stored at 4 °C.

Table 2.6 Primary and secondary antibodies used in this study

Primary antibody	Source (organism)	Dilution factor	Purchased from
α-GFP 3H9	Rat	1:5000	ChromoTek (München, Germany)
Secondary antibody	**Source (organism)**	**Dilution factor**	**Purchased from**
goat-anti-rat AP conjugate	Goat	1:5000	Sigma-Aldrich (St. Louis, MO, USA)

2.1.7 Enzymes

2.1.7.1 Restriction endonucleases

Restriction endonucleases were utilized in test digests to verify vector size and correct integration of inserts as well as in restriction enzyme-mediated plasmid assembly and gDNA digest for Southern Blot analyses. Enzymes were purchased from Thermo Fisher Scientific (Waltham, USA) and reactions were set up according to the manufacturer's user guide.

2.1.7.2 DNA polymerases and nucleic acid modifying enzymes

DNA polymerases as well as nucleic acid modifying enzymes are listed in Table 2.7. All enzymes were used as recommended by the manufacturer.

Table 2.7 DNA polymerases and nucleic acid modifying enzymes used in this study

Enzyme	Used in Method	Manufacturer
Taq DNA polymerase	Standard PCR	homemade
Phusion High-Fidelity DNA Polymerase	PCR for cloning purposes	Thermo Fisher Scientific (Waltham, USA)
NEBuilder HiFi DNA Assembly Master Mix	Seamless assembly of vectors	New England Biolabs (Ipswich, USA)
SsoFast™ EvaGreen® supermix	qRT-PCR	Bio-Rad (Munich, Germany)
DNAse I	Treatment of RNA before cDNA synthesis	Thermo Fisher Scientific (Waltham, USA)
RevertAid Reverse Transcriptase	cDNA synthesis from RNA	Thermo Fisher Scientific (Waltham, USA)
RNase A	Treatment of DNA	Thermo Fisher Scientific (Waltham, USA)

2.1.8 Kits

Kits were used for several applications in this study as described in Table 2.8.

Table 2.8 Kits used in this study

Name	Application	Manufacturer
E.Z.N.A.® Fungal DNA Mini Kit	Purification of *Verticillium dahliae* V76 DNA for PacBio sequencing	Omega Bio-Tek (Norcross, GA, USA)
EasySelect™ *Pichia* Expression Kit	Expression of *LSCE2* and *LSCE2-like* in *Pichia*	Thermo Fisher Scientific (Waltham, USA)
GeneJET® Plasmid Miniprep Kit	Isolation of plasmid DNA from *E. coli* cultures	Thermo Fisher Scientific (Waltham, USA)
NucleoSpin®Gel and PCR Clean-up Kit	Purification of DNA fragments from PCR reactions and agarose gels	Machery-Nagel (Düren, Germany)

2.1.9 Chemicals

Chemicals used in this study for were purchased from Analytic Jena (Jena, Germany), Roth (Karlsruhe, Germany), VWR (Darmstadt, Germany), Merck (Darmstadt, Germany), Sigma-Aldrich (Deisenhofen, Germany), Serva (Heidelberg, Germany), Invitrogen (Karlsruhe, Germany), New England Biolabs (Frankfurt, Germany), Difco (Heidelberg, Germany), Duchefa Biochemie (Haarlem, the Netherlands), Qiagen (Venlo, the Netherlands), Becton Dickinson (Franklin Lakes, NJ, USA), Thermo Fisher Scientific (Waltham, USA) and Bio-Rad (Hercules, CA, USA).

2.1.10 Antibiotics

Media for fungi and bacteria were supplemented with antibiotics to avoid contamination and/or select for transgene organisms. Antibiotics were prepared as stock solutions, sterile filtrated (0.2 µm pore filter) and added to media after autoclaving as described in Table 2.2.

Table 2.9 Antibiotics used in this study

Antibiotic	Stock solution	Final concentration in media
Ampicillin	100 mg/ml diluted in dH_2O	100 µg/ml
Carbenicillin	100 mg/ml diluted in dH_2O	50 µg/ml
Cefotaxim	250 mg/ml diluted in dH_2O	250 µg/ml
Hygromycin B	50 mg/ml diluted in PBS (phosphate-buffered saline) as provided by supplier	50 µg/ml
Kanamycin	50 mg/ml diluted in dH_2O	50 µg/ml
Nourseothricin	200 mg/ml diluted in dH_2O	80 µg/ml
Rifampicin	50 mg/ml diluted in DMSO (dimethyl sulfoxide)	25 µg/ml
Zeocin	100 mg/ml, provided by supplier	25 µg/ml (*E. coli*)/ 100 or 500 µg/ml (*P. pastoris*)

2.1.11 Media

Media were prepared with ultrapure, distilled water (ddH_2O). For sterilization, media were autoclaved (121 °C, 100 kPa, 20 min), heat sensitive components and antibiotics were filter sterilized and added after autoclaving to cooled-down media.

2.1.11.1 Media for bacteria

LB (Lysogeny Broth) - cultivation of *E. coli* and *A. tumefaciens*

Ingredient	Concentration
Peptone	16 g/l
Yeast extract	5 g/l
NaCl	10 g/l
pH 7.0	
Agar (for solid media)	15 g/l

DYT (Double Yeast Tryptone) - cultivation of *A. tumefaciens*

Ingredient	Concentration
Peptone	16 g/l
Yeast extract	10 g/l
NaCl	10 g/l
pH 7.0	
Agar (for solid media)	15 g/l

2.1.11.2 Media for *Verticillium*

Potato Dextrose Broth (PDB), used for fungal biomass accumulation and **Czapek Dox Broth (CDB)**, a minimal medium used for colony growth assays, were prepared as recommended by the manufacturer (Duchefa Biochemie, Haarlem, Netherlands). For solid media, solutions were supplemented with 15 g/l agar.

SXM (Simulated Xylem sap Medium) - generation of *Verticillium* spores

Component	Concentration
Casein hydrolysate	4 g/l
Pectin (from apple)	2 g/l
$MgSO_4$ [1M]	2 ml/l
Trace element solution [1000x]	1 ml/l
AspA [50x]	20 ml/l

Trace element solution [1000x]

Solution A

Component	Concentration
$FeSO_4$ *$7H_2O$	5 g/l
EDTA	50 g/l
pH 5.5 (KOH)	

Solution B

Component	Concentration
$ZnSO_4 * 7H_2O$	22 g/l
H_3BO_3	22 g/l
$MnCl_2 * 4H_2O$	5 g/l
$CoCl_2 * 6H_2O$	1.6 g/l
$CuSO_4 * 5H_2O$	1.6 g/l
$(NH_4)_6Mo_7O_{24} * 4H_20$	1.1 g/l

Solutions A and B were combined and pH adjusted to 6.5 with KOH. Solution was sterile filtrated and stored at 4 °C.

AspA [50x]

Component	Concentration
$NaNO_3$	3.5 M
KCl	350 mM
KH_2PO_4	550 mM
pH 5.5 (KOH)	

2.1.11.3 Media for *Agrobacterium*-mediated transformation of *Verticillium*

Induction Medium

Component	Concentration
MM salts [2.5 x]	1 x
Glucose	10 mM
Glycerol	0.5 %
for solid medium, add 15 g/l agar	
MES*[1]	40 mM
Acetosyringone[1]	0.2 mM

*(2-(N-morpholino)ethanesulfonic acid), pH 5.3, 1 M stock solution

[1] Added after autoclaving

MM salts [2.5 x]

Component	Concentration
KH_2PO_4	3.625 g/l
K_2HPO_4 x3 H_2O	6.714 g/l
NaCl	0.375 g/l
$MgSO_4$ x7 H_2O	1.25 g/l
$CaCl_2$ x2 H_2O	0.165 g/l
$FeSO_4$ x7 H_2O	0.006 g/l
$(NH_4)_2SO_4$	1.25 g/l

2.1.11.4 Media for *S. cerevisiae*

Yeast Extract Peptone Dextrose Medium with Adenine (YPAD)

Component	Concentration
Peptone	20 g/l
Yeast extract	10 g/l
Adenine	0.1 g/l
Glucose	20 g/l
pH 6.0 (with HCl)	

for solid medium, add 12 g/l Agar-Agar Kobe I

Synthetic Complete dropout medium (SD) (-Leu, -His, -Trp)

Component	Concentration
Yeast nitrogen base w/o AA	6.7 g/l
Glucose	20 g/l
Adenine	40 g/l
CSM (-Leu, -His, -Trp)	0.61 g/l
pH 5.6 (with NaOH)	

SD (-Leu, -Trp): SD (-Leu, -His, -Trp) + 20 mg/l Histidine

SD (-Leu): SD (-Leu, -His, -Trp) + 20 mg/l Histidine, + 50 mg/l Tryptophane

Semi-solid SD -Leu, -His, -Trp + 3 mM 3-AT

Component	Concentration
Yeast nitrogen base w/o AA	6.7 g/l
Glucose	20 g/l
Adenine	40 g/l
CSM (-Leu, -His, -Trp)	0.61 g/l
Gelrite	0.05 % (w/v)
3-amino-1,2,4-triazole (3-AT)	3 mM
Ampicillin	100 µg/ml
adjust pH 5.6 (with NaOH)	

Semi-solid medium was prepared by first autoclaving 25 ml 1 % (w/v) Gelrite (Duchefa, Haarlem, Netherlands) for 10 min. Immediately after autoclaving, the liquid Gelrite was mixed with 475 ml SD -Leu, -His, -Trp, pre-heated to 60 °C. The mixture is then cooled quickly in a chilled water bath. 3-AT and ampicillin are added directly prior to use.

2.1.11.5 Media for *P. pastoris*

Yeast Extract Peptone Dextrose Medium (YPD)

Component	Concentration
Peptone	20 g/l
Yeast extract	10 g/l
add after autoclaving	
Glucose	20 g/l
adjust pH 6.0 (with HCl)	

Minimal Dextrose Medium (MDM)

Component	Concentration	Stock solution
add as sterile stock solutions to autoclaved dH_2O +15 g/l agarose		
Yeast nitrogen base (YNB)	1.34 %	10 X
Biotin	$4*10^5$ %	500 X
Glucose	20 %	10 X

Minimal Methanol Medium (MM)

Component	Concentration	Stock solution
add as sterile stock solutions to autoclaved dH_2O+15 g/l agarose		
Yeast nitrogen base (YNB)	1.34 %	10 X
Biotin	$4*10^{-5}$ %	500 X
Methanol	0.5 %	10 X

Buffered Glycerol-complex Medium (BMGY)

Component	Concentration	Stock solution
Yeast extract	1 %	
Peptone	2 %	
add as sterile stock solutions after autoclaving		
Potassium phosphate pH 6.0	100 mM	1 M
YNB	1.34 %	10 X
Biotin	$4*10^{5}$ %	500 X
Glycerol	1 %	10 X

Buffered Methanol-complex Medium (BMMY)

Component	Concentration	Stock solution
Yeast extract	1 %	
Peptone	2 %	
add as sterile stock solutions after autoclaving		
Potassium phosphate pH 6.0	100 mM	1 M
YNB	1.34 %	10 X
Biotin	$4*10^{5}$ %	500 X
Methanol	1 or 3 %	10 X

2.1.12 Buffers and solutions

In the following, general solutions and buffers are listed under the method they were used for.

Preparation of chemically competent *E. coli* cells

RF I solution	RbCl	100 mM
	$MnCl_2$ x 4 H_2O	50 mM
	Potassium acetate (1 M stock pH 7.5)	30 mM
	$CaCl_2$ x 2 H_2O	10 mM
	Glycerol	15 % (w/v)
	pH 5.8 with glacial acetic acid	
RF II solution	MOPS (1 M stock pH 6.8)	10 mM
	RbCl	10 mM
	$CaCl_2$ x 2 H_2O	75 mM
	Glycerol	15 % (w/v)
	pH 6.8 with NaOH	

Agarose gel electrophoresis

Agarose gel	Agarose	0.4 – 2 % (w/v)
	TAE buffer	1 x
TAE buffer [50 x]	Tris	2 M
	Glacial acetic acid	57.1 ml/l
	EDTA (pH 8.0)	50 mM
Loading Dye [6x]	Orange G	0.25 % (w/v)
	Xylencyanol FF	0.25 % (w/v)
	Glycerol	30 % (v/v)

Polymerase-chain-reaction (PCR)

***Taq* buffer [10 x]**	Tris	100 mM
	KCl	500 mM
	$MgCl_2$	15 mM
	Triton X-100	1 % (w/v)
	pH 9.0 (KOH)	

Fungal DNA extraction

Lysis buffer	Tris (pH 7.5)	50 mM
	EDTA (pH 8.0)	50 mM
	SDS	3 % (w/v)
	ß-Mercaptoethanol	1 % (v/v)
TE buffer	Tris (pH 8.0)	10 mM
	EDTA (pH 8.0)	1 mM

Plant DNA extraction

CTAB extraction buffer (CEB)	Tris (pH 8.0)	100 mM
	EDTA (pH 8.0)	20 mM
	NaCl	1.4 M
	CTAB	2 % (w/v)
	PVP 40.000	1 % (w/v)
TE buffer	Tris (pH 8.0)	10 mM
	EDTA (pH 8.0)	1 mM

	RNA extraction	
Precipitation buffer	NaCl	1.2 M
	Trisodium citrate	0.8 M
	Southern Blot	
(Pre-)Hybridization buffer	NaCl	0.5 M
	Blocking Reagent*	4 % (w/v)
	Prepare with hybridization buffer solution* instead of water	
	*included in Amersham AlkPhos Direct Labeling Module (GE Healthcare, Chicago, IL, USA)	
Wash Buffer 1	Urea	2 M
	SDS	50 mM
	$NaPO_4$ x$2H_2O$	50 mM
	NaCl	150 mM
	$MgCl_2$ (1 M)	1 mM
	Blocking reagent*	0.2 % w/v
	*included in Amersham AlkPhos Direct Labeling Module (GE Healthcare, Chicago, IL, USA)	
Wash Buffer 2 (20 x stock)	Tris Base	1 M
	NaCl	2 M
	pH 10	
Wash Buffer 2		for 200 ml total volume
	20 x stock	10 ml
	$MgCl_2$ (1 M)	400 µl
	ddH_2O	190 ml
	Western Blot	
		for 250 ml total volume
12 % gel buffer	Tris (1M, pH 8.8)	160.2 ml
	SDS (10 %)	4.24 ml
		for 250 ml total volume
Stacking gel buffer	Tris (1M, pH 6.8)	38.58
	SDS (10 %)	3.06
10 X SDS running buffer	Glycine	144.2 g/l
	Tris-base	30.4 g/l
	SDS	1 %
4 X SDS loading dye	Tris (pH 6.8)	200 mM
	DTT	400 mM
	SDS	8 %
	Glycerol	40 %
	Bromphenol blue	~ 0.1 %
Transfer buffer	Tris-base	1 M
	Boric acid	1 M
	pH 8.3	
Tris-buffered saline –Tween (TBS-T)		20 X stock solution
	NaCl	3 M
	Tris (pH 8.0)	200 mM
	Tween-20	1 %
Blocking solution	Milk powder	4 %
	TBS-T	1 %
AP buffer	Tris (pH 9.5)	100 mM
	NaCl	100 mM
	$MgCl_2$	50 mM

Histochemical staining for microscopy

Trypan blue solution	Lactic acid	12.5 % (v/v)
	Glycerol	12.5 % (v/v)
	Phenol	12.5 % (v/v)
	Ethanol (96 %)	50 % (v/v)
	Trypan blue	0.125 g/l
Chloral hydrate solution	Chloral hydrate	2.5 kg/l

2.1.13 Consumables

Consumables used in this study were purchased from Biozym (Hessisch Oldendorf, Germany), Carl-Roth (Karlsruhe, Germany), Eppendorf (Hamburg, Germany), Hawita Gruppe GmbH (Vechta, Germany), Heinemann (Duderstadt, Germany), Hera (Blaufelden, Germany), Hereaus Holding GmbH (Hanau, Germany), Greiner Bio-One (Frickenhausen, Germany), Kulzer Heraeus (Hanau, Germany), Macherey-Nagel (Düren, Germany), Mars (Viersen, Verden, Germany), Meditrade (Kiefersfelden, Germany), Merck Millipore (Darmstadt, Germany), Nette Papier (Göttingen, Germany), Pack Pack (Jever, Germany), Pechinery Plastic Packaging (Chicago, IL, USA), Sarstedt (Nümbrecht, Germany), Sigma-Aldrich (Steinheim, Germany), Sartorius (Göttingen, Germany), Schott (Mainz, Germany), Th. Geyer (Renningen, Germany), Tölle (Göttingen, Germany), Vitakraft (Bremen, Germany) and VWR (Radnor, PA, USA).

2.1.14 Devices

Device	Model	Manufacturer
Bunsen burner	Phoenix eco	Schuett biotec (Göttingen, Germany)
Cart	-	Blanco (Leipzig, Germany)
Centrifuge	Pico 21	Thermo Fisher Scientific (Langenselbold, Germany)
Clean bench	Hera safe	Thermo Fisher Scientific (Langenselbold, Germany)
Climate chambers	-	Johnson Controls (Milwaukee, WI, USA)
Computer	Optiplex 760	Dell (Halle (Saale), Germany)
Counting chamber	Thoma	Optik Labor (Lancing, UK)
Dewer	-	Nalgene (Rochester, NY, USA) / Isotherm KGW (Karlsruhe, Germany)
Digital camera	Lumix FZ150	Panasonic (Hamburg, Germany)
Fluorescence microscope	DM 5000B / CTR HS	Leica (Wetzlar, Germany)
Freezer (-20 °C)	Mediline	Liebherr (Kirchdorf an der Iller, Germany)

Freezer (-80 °C)	Hera freeze	Thermo Fisher Scientific (Langenselbold, Germany)
Gel documentation system	GenoPlex	VWR (Hannover, Germany)
Hybridization oven	Hybaid Micro-4	MWG Biotech, Ebersberg, Germany
Epi-illuminator	B-BOX	SMOBiO, Hsinchu City, Taiwan
Blot imaging system	ChemiDoc Touch	Bio-Rad (Hercules, CA, USA)
Gel electrophoresis equipment	-	Bio-Rad (Hercules, CA, USA)
Gel running chamber	Sub cell® GT	Bio-Rad (Hercules, CA, USA)
Histoform	S	Kulzer Heraeus (Hanau, Germany)
Ice machine	-	Ziegra (Isernhagen, Germany)
Incubation shakers	Certomat BS-1	Sartorius (Göttingen, Germany)
Magnetic stirer	RH basic 2 IKAMAG	IKA (Staufen, Germany)
Microwave	R-26ST	Sharp (Osaka, Japane)
Microtome	Hyrax M55	Zeiss (Göttingen, Germany)
Multifuge	3SR+	Thermo Fisher Scientific (Langenselbold, Germany)
Orbital shaker	GFL 3017	GFL (Burgwedel, Germany)
PCR Cycler	MyCycler	Biorad (Hercules, CA, USA)
pH meter	Inolab®	WTW (Weilheim, Germany)
Photometer spektrometer of600	NanoDrop	
Pipet	Research	Eppendorf (Hamburg, Germany)
Printer I	UP-D897	Sony (Surrey, UK)
Printer		
qRT-PCR Cycler	C100 Touch with CFX96 system	Bio-Rad (Hercules, CA, USA)
Quantum meter	MQ-200	Apogee (Logan, UT, USA)
Refrigerator	Mediline	Liebherr (Kirchdorf an der Iller, Germany)
Rotator	-	Heinemann (Duderstadt, Germany)
Steam sterilizer	Varioklav 75S / 135S	Thermo Fisher Scientific (Langenselbold, Germany)
Stereomicroscope	M165FC	Leica (Wetzlar, Germany)
Thermomixer	Compact / Comfort	Eppendorf (Hamburg, Germany)
Vortexer	VF2	IKA (Staufen, Germany)
Water filter system	Arium® 611 DI	Sartorius (Göttingen, Germany)

2.1.15 Software

Software	Source
Acrobat Reader	http://get.adobe.com/uk/reader/ (Adobe Systems Inc., San José, CA; USA)
Adobe Illustrator CS5 v 15.0.0	(Adobe Systems Inc., San José, CA; USA)
Adobe Photoshop CS5 v 12.0	(Adobe Systems Inc., San José, CA; USA)
Bio-Rad CFX Manager 3.0	http://bio-rad.com/pcrsoftware (Bio-Rad Laboratories, Hercules, CA, USA)
BlattFlaeche v. 1.0.4.6	http://datinf.de/home (Datinf® GmbH, Tübingen, Germany)
CLC Genomics Workbench v 7.0.1	https://www.qiagenbioinformatics.com/products/clc-genomics-workbench/ (Qiagen, Venlo, Netherlands)
Clone Manager Professional Suite v 8	http://www.scied.com/pr_cmpro.htm (Sci-Ed Software, Denver, CO, USA)
Geneious™ Pro v. 8.1.6	http://www.geneious.com/ (Biomatters Ltd., Auckland, New Zealand)
ImageJ 1.51d	http://rsbweb.nih.gov/ij/ (W. Rasband, National Institutes of Health, USA)
KaKs_Calculator 2.0	https://sourceforge.net/projects/kakscalculator2/ (Wang et al. 2010)
LAS AF v.2.6.7266.0	Leica Application Suite (Leica GmbH, Wetzlar, Deutschland)
MEGA7 v7.0.14	https://www.megasoftware.net/ (Kumar et al. 2016)
NCBI BLAST	http://blast.ncbi.nlm.nih.gov/Blast.cgi
Office 2010	(Microsoft, redmont, WA, USA)
PhyDE –Phylogenetic Data Editor v 0.9971	http://www.phyde.de/ Müller, J., Müller, K., Neinhuis, C., and Quandt, D. (2015).
SecretomeP 2.0	http://www.cbs.dtu.dk/services/SecretomeP/; (Bendtsen et al., 2004a)
SignalP 3.1	http://www.cbs.dtu.dk/services/SignalP/; (Bendtsen et al., 2004b)
SnapGene Viewer v 4.3.7	https://www.snapgene.com/?referrer=SnapGene%20Viewer (GSL Biotech LLC, Chicago, IL, USA)
TreeGraph 2 v 2.14.0-771	http://treegraph.bioinfweb.info/ (Stöver and Müller 2010)
VertiBase	http://biofung.gobics.de:1555/; coordinated by Prof. Dr. G. Braus, Georg-August-University of Göttingen

2.2 Methods

If not specified otherwise, all methods were performed at room temperature (RT).

2.2.1 Cultivation and maintenance of plant material

2.2.1.1 Cultivation of *A. thaliana* plants for seed production

A. thaliana seeds were sown on steam sterilized (30 min, 90 °C) soil (Frühstorfer Erde, Type T, Archut) with five seeds per square (8x8 cm) plastic pot. ds were stratified at 4 °C in the dark for two days before being transferred to a climate chamber (Johnson Controls, Milwaukee, WI, USA) under short day (SD) conditions (8 hours light at 22 °C; 16 hours dark at 18 °C; 65 % relative humidity; light intensity: ~ 120 µEinsteins m^{-2} sec^{-1}). After one week, pots with germinated seedlings were moved to long day (LD) conditions (16 hours light at 22 °C; 8 hours dark at 20 °C; 65 % relative humidity; light intensity: ~ 120 µEinsteins m^{-2} sec^{-1}). Plants were cultivated with regular watering for ~6 weeks until siliques formed. Watering was then ceased and plants were left to ripen and dry out. To collect ds from opening siliques, upper plant parts were tucked into paper bags. Seeds were harvested by manual destruction of siliques and subsequent sieving to separate ds from residual plant parts before being collected in paper bags. Seeds were cold-treated for 24 h at -21 °C in order to avoid contamination with insects.

2.2.1.2 Cultivation of *A. thaliana* for infection experiments

Arabidopsis seedlings for *Verticillium* infection experiments were grown in plastic dishes (17.5 cm*13 cm*5.5 cm) in an 8 x 6 pattern. Dishes were used double-layered with a separation layer of 2 ml tubes in between in order to allow aeriation. The upper dish was perforated to allow excess water to escape and filled with 200 ml granulated clay (Seramis, Mars GmbH, Mogendorf, Germany), covered by 800 ml of a 1:1 steam sterilized soil/sand mixture. The substrate was watered with ~300 ml tab water, supplemented with 0.1 % fertilizer (Wuxal, Manna, Düsseldorf, Germany). Stratification was achieved after 2 days at 4 °C in the dark. Seed dishes were then transferred to short day conditions, but left covered with a clear plastic hood for 2 weeks. For the last 1 – 1.5 weeks, plants were watered if needed.

2.2.1.3 BASTA-selection of transformed Arabidopsis seeds

Seeds from transformed Arabidopsis plants were sown on square (8x8 cm) plastic pots and transferred to short day conditions. After germination, seedlings were sprayed every two to three days with 0.1 % BASTA® (Bayer CropScience AG, Monheim, Germany) solution for two weeks. Surviving seedlings were transferred to round pots and grown at short day conditions.

2.2.2 Cultivation and maintenance of *Verticillium spp.*

2.2.2.1 Cultivation of *Verticillium spp.* for biomass production

Fungal biomass was needed for DNA and RNA extraction. Baffled Erlenmeyer flasks containing 180 ml potato dextrose broth (PDB) supplemented with cefotaxime and ampicillin were inoculated with either 1 cm^3 agar plugs or spores from a spore stock (2.2.2.4) and incubated shaking at 90 rpm, at 22 °C in the dark for 1 week.

2.2.2.2 Generation of *Verticillium spp.* spores

Verticillium spp. was grown in simulated xylem medium (SXM) in order to promote spore production. 180 ml liquid SXM medium in baffled Erlenmeyer flasks (Schott, Mainz, Germany), supplemented with cefotaxime and ampicillin, were inoculated with either 1 cm^3 agar plugs or spores from a spore stock (2.2.2.4) and incubated shaking at 90 rpm for one week in short day conditions. Spores were isolated as described in 2.2.2.3.

2.2.2.3 Harvest of *Verticillium spp.* spores

Fungal spores were harvested by filtering liquid cultures (2.2.2.2) through sterile filter paper (MN 615 ¼; ⌀ 240 mm; Macherey-Nagel, Düren, Germany). The resulting filtrate was collected in 50 ml screw cap tubes (Sarstedt, Nümbrecht, Germany) and subsequently centrifuged at 4000 rpm, 4 °C for 15 min. The supernatant was removed and spores were resuspended in 35 ml ice-cooled, sterile dH_2O. The suspension was then again centrifuged at 4000 rpm, 4 °C for 10 min.

Pelleted spores were resuspended in 5 – 20 ml ice-cooled, sterile dH_2O, depending on the amount of recovered spores. Spore concentration was determined by first counting spores in a counting chamber (Thoma, Optik Labor, Lancing, UK) and subsequent calculation with the formula

$$Spore\ concentration = Volume * n * dilution\ factor$$

where the *volume* of the counting chamber used here is 10 000 µm³ and *n* the average of spores counted in two chambers.

2.2.2.4 Preparation of *Verticillium spp.* spore stocks

Spore stocks were prepared by mixing 750 µl undiluted spore solution (2.2.2.3) with 250 µl sterile 60 % glycerol in 2 ml cryogenic vials (Corning Inc., Corning, NY, USA). Suspensions were then frozen in liquid nitrogen and stored at -80 °C.

2.2.2.5 *Verticillium spp.* growth assay on solid medium

In vitro growth dynamics of *Verticillium* isolates and mutant lines were determined by dripping 5 µl of a $1x10^6$ spores/ml suspension onto the center of a petri dish (Ø 10 cm) containing solid Czapek Dox agar, supplemented with ampicillin and cefotaxime. Plates were incubated upside-down in a climate chamber at short day conditions. Photographs of the colonies were taken 7, 14 and 21 days after plating. Surface area was calculated from the colony diameter, measured using ImageJ (v.1.51d, http://imagej.nih.gov).

2.2.3 Infection of *A. thaliana* seedlings with *Verticillium spp.*

3 – 3.5 week old *A. thaliana* seedlings, grown as described in 2.2.1.2, were inoculated with *Verticillium spp.* applying the previously described root-dip method (Veronese et al. 2003). After careful uprooting, excess soil and sand was removed before roots were mechanically damaged by twirling. 23 plants per infection were treated thus and placed into petri dishes where their roots were covered with ice-cooled $1x10^6$ spores/ml suspensions (2.2.2.2). Roots were incubated in spore suspensions for 45 min at room temperature (RT). Control plants were mock-inoculated in dH_2O without spores. After inoculation, seedlings were planted into round pots (Ø 8 cm) filled with steam-sterilized soil. Pots were arranged on trays and covered with clear plastic hoods. To reduce stress, trays were kept in the laboratory for

one day before being transferred to SD conditions. Hoods were removed after 4 days and plants were watered as required. Plant development was documented 7, 14 and 21 days past inoculation (dpi).

2.2.3.1 Determination of *A. thaliana* rosette leaf area

Development of plants infected as described in 2.2.3 was documented 7, 14 and 21 dpi. 4 plants per treatment were selected and photographed from above, then the surface area of visible rosette leaves was calculated using the software BlattFlaeche (v. 1.0.4.6, http://datinf.de).

2.2.4 Working with bacteria

2.2.4.1 Cultivation and maintenance of *E. coli* cultures

E. coli was grown either on solid LB medium (2.1.11.1) at 37 °C or in liquid LB medium at 37 °C shaking at 180 rpm. Media were supplemented, if required with the appropriate antibiotics (2.1.10).

2.2.4.2 Cultivation and maintenance of *A. tumefaciens* cultures

A. tumefaciens colonies were cultivated either on solid LB medium (2.1.11.1) at 28 °C or in liquid LB medium at 28 °C shaking at 180 rpm. Media were supplemented, if required with the appropriate antibiotics (2.1.10). Glycerol stocks were prepared from colonies grown overnight in liquid medium. Cell suspensions were mixed 1 : 1 with sterile, 60 % (v/v) glycerol before being frozen in liquid N_2. Glycerol stock were stored at -80 °C. LB or DYT medium was used for *A. tumefaciens* cultures.

2.2.4.3 Preparation of chemically competent *E. coli* cells

Chemically competent *E. coli* cells for transformation experiments were prepared with the RbCl/$CaCl_2$ method. 4 x 200 ml LB medium in 1 l baffled Erlenmeyer flasks were inoculated with 2 ml of an overnight liquid culture, prepared with one colony of freshly grown One Shot® TOP10 chemically competent *E. coli* cells (Thermo Fisher Scientific (Waltham, Massachusetts, USA). After adding 2 ml $MgCl_2$ as well as $MgSO_4$ solution (both 1 M), cultures were incubated at 37 °C shaking at 260 rpm for 2 – 2.5 h until and OD_{600} of 0.4 – 0.6 was reached. Cell suspensions were then cooled down on ice for 20 min and subsequently centrifuged at 3000 rpm and 4 °C for 15 min. After centrifugation, the supernatant was removed and cells were resuspended in 100 ml 4 °C RF I solution (2.1.11.4), using

pre-cooled pipettes. Following resuspension, cells were kept on ice for 40 min before being centrifuged at 3000 rpm and 4 °C for 15 min. Cells were then resuspended in 5 ml 4 °C RF II solution (2.1.11.4) and kept on ice afterwards for 15 min. In the final step, 50 µl aliquots in 1.5 ml tubes were taken from the cell suspension and frozen in liquid N_2. Cell suspensions were stored at -80 °C.

2.2.4.4 Preparation of chemically competent *A. tumefaciens* cells

Chemically competent *A. tumefaciens* cells for transformation were prepared by first inoculating 50 ml LB medium with a single *A. tumefaciens* AGL1 (2.1.3.2) colony. The inoculated liquid culture was grown overnight at 28 °C, shaking at 160 rpm until an OD_{600} of 0.8 was reached. Cell suspensions were chilled on ice for 15 min and then centrifuged at 4000 rpm for 10 min at 4 °C. The supernatant was removed afterwards and pelleted cells were resuspended in 20 ml sterile, ice cold $MgCl_2$ solution (100 mM). Cell suspensions were kept on ice for 1 h before being centrifuged again at 4000 rpm for 10 min at 4 °C. Following centrifugation, the supernatant was taken off and cells were resuspended in 20 ml sterile, ice cold $CaCl_2$ solution (20 mM). Cell suspensions were then incubated on ice for 4 – 5 hours. Aliquots of competent cells were prepared by first adding glycerol to a final concentration of 20 % and then freezing volumes of 200 µl in 1.5 ml tubes in liquid N_2. Cell suspensions were stored at -80 °C.

2.2.4.5 Preparation of electro-competent *A. tumefaciens* cells

For electroporation of *A. tumefacien*s strain GV3101, electro-competent cells were prepared. First, 50 ml DYT, containing the appropriate antibiotics, were inoculated with one freshly grown colony from solid DYT medium and then incubated overnight at 28 °C, shaking at 180 rpm. This pre-culture was used to inoculate 250 ml DYT to an OD_{600} of 0.3 which was then grown at 28 °C and 180 rpm until the culture reached an OD_{600} of 1.2. Cells were then pelleted via centrifugation for 30 min at 4500 g and 4 °C and resuspended in 30 ml ice-cold HEPES (1mM, pH 0.7). This was repeated twice. After the last centrifugation step, cells were resuspended in 30 ml ice-cold 10 % glycerol (v/v). Again, cells were centrifuged as described above but resuspended in 2 ml ice-cold 10 % glycerol (v/v). From this suspension, 50 µl aliquots were pipetted into 1.5 ml tubes and subsequently frozen in liquid N_2. Aliquots were stored at -80 °C.

2.2.4.6 Transformation of chemically competent *E. coli* cells

E. coli was used to amplify plasmids generated by ligations. For transformation, the heat shock method was used. First, 50 µl aliquots of chemically competent cell suspensions (2.2.4.3) were carefully thawed on ice. Then, 1 – 5 µl ligation product, depending on the expected efficiency of ligation, were pipetted carefully into the suspension. After incubation, cells were heat-shocked for 45 s at 42 °C in a thermomixer (Eppendorf; Hamburg, Germany). Immediately after the heat shock, 800 µl liquid LB medium were added to the suspensions which were subsequently incubated for 1 h at 37 °C, shaking at 700 rpm in the thermomixer. Following incubation, cells were pelleted via centrifugation for 4 min at 4000 g, the supernatant was taken off by decanting and cells were resuspended in ~ 200 µl backflow. This cell suspension was then plated onto solid LB medium, supplied with the appropriate antibiotics. The plates were incubated overnight at 37 °C.

2.2.4.7 Transformation of chemically competent *A. tumefaciens* cells

A. tumefaciens AGL1 was used to transform *Verticillium spp*.. 200 µl aliquots of chemically competent cells (2.2.4.4) were used per transformation. The aliquots were carefully thawed on ice before 1 µg plasmid DNA was added. The suspensions were first incubated on ice for 10 min and then in liquid N_2 for another 10 min. From the liquid N_2, cells were directly transferred to a thermomixer set to 37 °C and kept there for 5 min. Afterwards, samples were incubated at 28 °C for 1 h, shaking in a thermomixer at 500 rpm. Following incubation, cells were pelleted via centrifugation for 4 min at 4000 g, the supernatant was taken off by decanting and cells were resuspended in ~ 200 µl backflow. This cell suspension was then plated onto solid LB or medium, supplied with the appropriate antibiotics. The plates were incubated for 3 days at 28 °C.

2.2.4.8 Transformation of electro-competent *A. tumefaciens* cells

A. tumefaciens strain GV3101 was transformed via electroporation. After thawing 50 µl aliquots (2.2.4.5) on ice, 150 – 200 ng plasmid DNA were carefully mixed into the suspension. The mixture was then transferred to sterile, ice-cooled electroporation cuvettes (1 mm cuvette gap width, Biozym; Hessisch Oldendorf, Germany) and kept on ice afterwards. Electroporation was performed with the Micro Pulser™ (BioRad, Munich, Germany), set to 25 µF, 2.5 kV and 400 Ω. Directly after electroporation, 500 µl ice-cooled LB medium was pipetted into the cuvettes, mixed with the cells and

transferred to new, 1.5 ml tubes. This was followed by incubation at 28 °C for 1 h, shaking in a thermomixer at 500 rpm. Following incubation, cells were pelleted via centrifugation for 4 min at 4000 g, the supernatant was taken off by decanting and cells were resuspended in ~ 200 µl backflow. The cell suspension was then plated onto solid LB medium, supplied with the appropriate antibiotics. The plates were incubated for 3 days at 28 °C.

2.2.5 *Agrobacterium*-mediated *A. thaliana* transformation

A. thaliana was transformed using the floral-dip method (Clough and Bent 1998) . 5 ml LB *A. tumefaciens* pre-culture, supplied with appropriate antibiotics were incubated 2 days at 28 °C, 180 rpm. The pre-culture was used to inoculate 500 ml LB, supplied with appropriate antibiotics. The main culture was incubated overnight at 28 °C, 180 rpm. After incubation, cultures were centrifuged at 5000 rpm, 10 min. The supernatant was then discarded and the pellet resuspended in 500 ml infiltration medium (5 % sucrose, 0.05 % Silvet-77). A. thaliana Col-0 flowers were dipped for ~30 sec into the solution and gently moved. After dipping, trays containing plants were covered with clear plastic hoods and dark plastic bags. Plastic bags were removed after one day incubation in the lab. Then, plants were moved to long day conditions.

2.2.6 Agrobacterium-mediated *Verticillium spp.* transformation

Agrobacterium-mediated transformation of *Verticillium* follows the method established for transformation of ascomycete spores (Eckert et al. 2005) . First, an *Agrobacterium* pre-culture was prepared by inoculating 2 ml LB medium, supplemented with the appropriate antibiotics, with one freshly grown *Agrobacterium tumefaciens* AGL1 colony containing the desired plasmid from solid medium and incubating 20 h at 28 °C and 180 rpm. 1 ml of the pre-culture was used to inoculate 20 ml Induction Medium (2.1.11.3) in a 50 ml tube which was then incubated 5 h at 28 °C and 180 rpm. Afterwards, 500 µl Induction Medium containing agrobacteria were mixed with 500 µl $1x10^6$ spores/ml *Verticillium spp.* spore suspension (2.2.2.2). From this suspension, 200 µl were pipetted onto solid Induction Medium plates (Ø 10 cm, 2.1.11.3), covered with filter discs (Ø 85 mm, grade 3 hw, 65 g/m²; Sartorius, Göttingen, Germany). In order to allow even distribution of the suspension droplets, plates were rotated continuously on an inoculating turntable during pipetting. The resulting five plates were incubated at 25 °C upside down in the dark for 3 days after which filter discs were transferred to PDA plates (2.1.11.2) supplemented with cefotaxime to kill the agrobacteria as well as hygromycin or

nourseothricin to allow only colony formation from transformed *Verticillium spp.* spores. When colonies were visible after 7 to 14 day incubation at 25 °C, some colonies were singled out twice on solid PDB containing appropriate antibiotics in order to avoid mixed cultures. Correct insertion of knockout constructs was verified via PCR (2.2.8.3.2) and Southern Blot (2.2.8.7) using DNA isolated from fungal mycelia (2.2.8.2).

2.2.7 Working with yeast

2.2.7.1 Yeast-two-Hybrid methods

All methods in the following section were adapted from methods previously described by Uhrig and McFarlane (Uhrig and MacFarlane 2008).

2.2.7.1.1 Cultivation and maintenance of yeast (Saccharomyces cerevisiae)

Yeast colonies were grown for proliferation either on solid YPAD medium (2.1.11.4) at 30 °C or in liquid YPAD at 30 °C and 250 rpm.

2.2.7.1.2 Yeast (double) transformation

Transformation of yeast with both Yeast-two-Hybrid prey and bait plasmids was used to first test auto-activation of constructs and later confirm interaction with interaction candidates found in the Yeast-two-Hybrid screen. 10 ml liquid YPAD medium were inoculated with a freshly grown yeast AH109 colony and incubated overnight at 30 °C and 250 rpm. After incubation the OD_{600} of the cell suspension was measured and then used to inoculate 60 ml YPAD main culture to an OD_{600} of 0.5. The main culture was afterwards incubated at 30 °C and 250 rpm until the cell suspension reached an OD_{600} of 2.0. The cells were subsequently harvested by centrifugation for 5 min at 4000 rpm. Following centrifugation, the supernatant was removed and the pelleted cells were resuspended in sterile 25 ml ddH_2O. After centrifuging again for 5 min at 4000 rpm and discarding the supernatant, cells were resuspended in sterile 1 ml 100 mM lithium acetate and then transferred to 1.5 ml tubes. By centrifuging the tubes for 15 sec at 13 000 rpm, cells were once more pelleted. After discarding the supernatant, cells were resuspended in 100 µl 100 mM lithium acetate and subsequently aliquoted to 50 µl volumes. The aliquots were centrifuged in 1.5 ml tubes for 15 sec at 13 000 rpm, the supernatant

was discarded and 350 µl sterile transformation mix, containing 240 µl 50 % (w/v) PEG_{3350M}, 36 µl 1M lithium acetate, 50 µl 2 mg/ml herring sperm DNA (heated to 96 °C for 10 min and then kept on ice prior to use) and 24 µl ddH_2O, were added together with 12 µl plasmid mix containing 300 ng of each plasmid. This mixture was vortexed until the pelleted cells were resuspended and afterwards incubated for 30 min at 30 °C, followed by incubation at 42 °C for another 30 min. Prior to plating onto SD dropout plates, cells were pelleted via centrifugation for 15 sec at 6000 rpm and resuspended in 200 µl sterile ddH_2O. Plates were incubated for 3 days at 30 °C.

2.2.7.1.3 Amplification of cDNA libraries for Yeast-two-Hybrid screen

Yeast-two-Hybrid screens are employed to discover potential interaction partners of proteins of interest. For this, the protein of interest is fused as bait to the Gal4 binding domain while cDNA libraries coding for potential interaction partners fused to the Gal4 activating domain act as prey. In this study, potential LSCE2-target proteins in Arabidopsis were searched for, so in order to get a preferably complete pool of Arabidopsis targets, two libraries, a standard Arabidopsis library from Arabidopsis cell suspension culture (Nemeth et al. 1998) as well as a root library (Klopffleisch et al. 2011) , were screened. Both libraries were obtained from J. Uhrig (Department of Plant Molecular Biology and Physiology, Göttingen University). Libraries consist of aliquots containing yeast cell suspensions where each cell carries one plasmid containing a prey construct. These aliquots are prepared by first resuspending cells from an already existing aliquot in 20 ml sterile ddH_2O and plating 100 x 200 µl of this suspension onto SD -Leu plates (10 x 10 cm, 2.1.11.4) using sterile glass beads for spreading the cells evenly. In order to test viability and cell content, the cell titer of the suspension was determined by plating 10, 1 and 0.1 µl of it onto SD -Leu plates. After two days incubation at 30 °C, the colonies were washed off the SD -Leu plates with 10 ml YPAD each. The resulting cell suspension was collected in a 1 l Erlenmeyer flask and its OD_{600} measured before it was incubated on ice for 1 h. After chilling, the suspension was transferred to 50 ml tubes and centrifuged at 4000 rpm for 5 min at 4 °C. After discarding the supernatant, cells were resuspended in 30 ml ice-cold YPAD and united in a 1 l Erlenmeyer flask. The OD_{600} of this suspension was then measured and ice-cold YPAD was added accordingly to reach an OD_{600} of 40. 500 ml of the resulting suspension were mixed with 500 ml ice-cold, 50 % (v/v) glycerol, aliquoted and incubated at -20 °C for 30 min before being transferred to -80 °C.

2.2.7.1.4 Yeast-two-Hybrid screen: interaction mating and selection

Yeast AH109 colonies transformed with bait constructs (2.2.7.1.2) and grown on YPAD plates were used to inoculate 50 ml SD (-Trp, 4 % Glucose, 2.1.11.4). The liquid culture was incubated overnight at 30 °C, shaking at 200 rpm. The next day, prey libraries (2.2.7.1.3) were quickly thawed by applying body heat and used to inoculate 200 ml YPAD (2.1.11.4) in 1 l Erlenmeyer flasks. The suspension was incubated 1 h at 30 °C and 200 rpm before the OD_{600} of both prey and bait cultures were measured. The volume equivalent of 10 OD from both bait and prey culture were mixed and subsequently centrifuged for 4 min at 4000 rpm (RT). After discarding the supernatant cells were resuspended in 10 ml YPAD containing 20 % PEG6000 and transferred to 100 ml flasks. The cell suspensions were then incubated for 4.5 h at 30 °C and 80 rpm during which mating between yeast cells containing prey and bait constructs took place. The suspensions were then centrifuged for 4 min at 4000 rpm, the supernatant was discarded and cells were resuspended in 2 ml SD (-Leu, -His, -Trp). In order to determine mating efficiency, 10, 20 and 50 µl of the 2 ml cell suspension were spread onto SD (-Leu, -His) plates and incubated 2 days at 30 °C. The suspension was then mixed with 500 ml semi-solid SD medium (-Leu, -His, -Trp, 2.1.11.4) by vigorous shaking. This selection mix was afterwards poured into 10 – 15 Ø 10 cm petri dishes and left to incubate for 5 – 10 days until colonies had grown.

2.2.7.2 Expression of LSCE2 and LSCE2-like in *Pichia pastoris*

The following methods are based on the protocol included in the Easy Select Pichia Expression Kit (Thermo Fisher Scientific, Waltham, MA, USA).

2.2.7.2.1 Cultivation and maintenance of P. pastoris

Pichia was grown for proliferation either in liquid YPD (2.1.11.5) at 30 °C shaking at 200 rpm or on solid YPD plates at 28 °C.

2.2.7.2.2 Preparing P. pastoris cells for electroporation

Cells for electroporation were prepared by first inoculating 2 x 2.5 ml YPD with freshly grown *P. pastoris* X-33 colonies. This pre-culture was incubated at 30 °C and 160 rpm. After around 8 hours, 500 µl of the pre-culture were used to inoculate 2 x 250 ml YPD which were incubated overnight at 30

°C and 160 rpm. The next day, the OD_{600} of the liquid culture was measured and subsequently adjusted to 0.3 before it was again incubated as described above until an OD_{600} of 1.2 – 1.5 was reached. Then, the liquid cultures were centrifuged in 2 x 500 ml centrifuge bottles at 2 000 g and 4 °C for 5 min. After discarding the supernatant, pellets were resuspended and combined in 100 ml YPD, mixed with 20 ml 1 M HEPES pH 8 ((4-(2-hydroxyethyl)-1-piperazineethanesulfonic acid)). Following resuspension, 2.5 ml 1 M DTT (dithiothreitol) were mixed gently into the suspension which was then incubated for 15 min at 30 °C. After incubation, the suspension volume was adjusted to 400 ml with ice-cold ddH_2O. The suspension was then centrifuged at 2 000 g and 4 °C for 5 min and the cell pellet resuspended in 250 ml ice-cold ddH_2O. Following another centrifugation step (2 000 g, 4 °C, 5 min), cells were resuspended first in 20 ml 1 M ice-cold sorbitol and then after repeating the centrifugation in 500 µl 1 M ice-cold sorbitol. From this suspension, 80 µl aliquots were taken and used directly for electroporation (see below).

2.2.7.2.3 Electroporation of P. pastoris cells

80 µl *P. pastoris* cells (see above) were mixed with 10 µl linearized (digested with restriction enzyme PmeI) plasmid DNA. The mixture was transferred to a pre-cooled electroporation cuvette (2 mm cuvette gap width, Biozym; Hessisch Oldendorf, Germany) and kept on ice for 5 min. Electroporation was performed with the Micro Pulser™ (BioRad, Munich, Germany), with a pulse strength of 2 kV. Immediately after electroporation, 1 ml ice-cold 1 M sorbitol was added to the cell suspension which was subsequently transferred to a 15 ml tube and incubated 1 – 2 h at 30 °C. Cells were then spread in 80, 100 and 150 µl aliquots onto YPD plates containing 100 or 500 µg/ml zeocin. Plates were incubated 3 days at 28 °C.

2.2.7.2.4 Determination of Mut-phenotype of P. pastoris transformants

P. pastoris strain X-33 is Mut^+, meaning that, due to the fact that the *AOX1* gene is not disrupted (which is the case in Mut^S strains), X-33 is able to grow effectively on medium containing methanol. This was tested by picking 20 individual transformants and transferring a small amount of colony material with a sterile pipette tip to plates consisting of rich YPD medium containing 100 µg/ml zeocin, Minimal Dextrose Medium or Minimal Methanol Medium (2.1.11.5). Colonies were grown 3 days at 28 °C.

2.2.7.2.5 Small-scale expression of recombinant proteins in Pichia

Growth conditions for optimal protein expression and secretion by *Pichia* transformants vary for individual proteins. It is therefore necessary to determine the best temperature and medium methanol content at which transformants are grown. In a small-scale approach, five colonies were selected from YPD plates grown as described in 2.2.7.2.4 and added to 3 ml YPD containing 500 µg/ml zeocin. The liquid cultures were grown for around 7 hours at 30 °C, shaking at 210 rpm. 600 µl of these pre-cultures were used to inoculate 10 ml BMGY (2.1.11.5) which were then incubated at 30 °C and 210 rpm. After one and a half days (~ 32 h) of growth, cells were pelleted via centrifugation at 3 000 g for 15 min at room temperature and afterwards resuspended in BMMY containing 3 % methanol (2.1.11.5). The cell suspensions were incubated at either 16 or 25 °C, shaking at 210 rpm for two days. Then, cell cultures were fed with 100 % methanol to a concentration in the culture of either 1 or 3 % each day for 5 days, resulting in a total 7 days of growth after inducing *LSCE2/-like* expression via methanol in *Pichia*.

2.2.8 Molecular biological methods – nucleic acids

2.2.8.1 Genomic DNA isolation from plant material

Prior to DNA extraction, plant material was ground in a mortar to a fine powder with liquid nitrogen. The material was stored at -80 °C. 200 mg plant material were mixed with 700 µl CTAB extraction buffer containing 0.1 mg/ml RNaseA. The mixture was incubated 5 min at 65 °C. Then, 700 µl chloroform:isoamyl alcohol solution (24:1) were added before the sample was mixed and centrifuged at 13 000 rpm for 5 min at RT. After centrifugation, the upper, aqueous phase of the suspension was transferred to a new 1.5 ml tube. For DNA precipitation, 700 µl isopropanol were added, the solution was mixed by inverting the tubes and then incubated for 5 – 10 min at RT. Precipitated DNA was pelleted by centrifugation (5 min, 13 000 rpm). Following this, supernatant was removed and pellet was washed in 80 % EtOH. After washing, samples were again centrifuged (13 000 rpm, 5 min) and the supernatant removed. Pellet was left to dry for 10 – 20 min at RT and then resuspended in 50 µl TE buffer before adding 1 µl RNaseA. Samples were subsequently incubated 20 min at 60 °C. DNA

concentration and pureness were measured photometrically (NanoDrop One, Thermo Fisher Scientific, Waltham, MA, USA).

2.2.8.2 Genomic DNA isolation from fungal material

Mycelia grown in PDB (2.2.2.1) was harvested by filtering of the liquid culture through filter paper (MN 615 ¼; ⌀ 240 mm; Macherey-Nagel, Düren, Germany), separating medium and spores from the mycelia retained in the filter. Excess medium was removed from the material by slightly squishing the mycelia between paper towels. In order to facilitate grinding, mycelia was put onto an aluminum sheet which was then folded and frozen in liquid N_2. The now flattened mycelia was ground to a fine powder in liquid N_2, then stored at -80 °C in 2 ml tubes. For DNA extraction, 1 ml mycelia was mixed with 700 µl lysis buffer (2.1.11.4) and subsequently incubated at 65 °C for 1 h. Samples were mixed in regular intervals. After incubation, 700 µl phenol were added and samples were mixed before centrifugation for 15 min at 13 000 rpm. Following centrifugation, the aqueous upper phase was transferred to a new 2 ml tube and mixed with 800 µl chloroform. Samples were then centrifuged again at 13 000 rpm for 10 min. Again, the aqueous phase was removed and transferred to a new tube. DNA was precipitated by the addition of 500 µl isopropanol and subsequent centrifugation at 13 000 rpm for 1 min. The supernatant was discarded after centrifugation and the DNA pellet was washed in 300 µl 70 % EtOH, followed by centrifugation at 13 000 rpm for 1 min. Following this, EtOH was removed and the pellet dried in order to allow residual EtOH to evaporate. Afterwards, the DNA pellet was resolved in 75 – 100 µl TE buffer. To facilitate DNA solution and remove RNA, samples were treated with 1 µl RNaseA and incubated at 65 °C for 20 min. Due to the fact that the isolated DNA was highly concentrated and residual fungal carbohydrates interfered with photometric measurements, DNA concentration was estimated via gel electrophoresis (0) by loading 1 µl extracted DNA onto an agarose gel.

2.2.8.2.1 Treatment of Verticillium dahliae V76 gDNA for PacBio Sequencing

Verticillium dahliae V76 gDNA meant for *de novo* sequencing was required to contain no traces of RNA as well as being free of any nucleases. Therefore, DNA extracted as described in 2.2.8.2, but with a second EtOH washing step, was treated with 1 µl RNaseA and incubated ~20 min until analytical gel electrophoresis showed no residual RNA contamination. Following this, three samples were combined to eventually increase DNA concentration and the sample volume was filled up to 300

µl with nuclease-free ddH_2O. DNA was then purified using the E.Z.N.A.® Fungal DNA Mini Kit (Omega Bio-Tek, Norcross, GA, USA), following the protocol for fresh and frozen specimens from step 14 which starts the column based purification process. DNA was eluted 3 x with 50 µl elution buffer from the columns. After elution, DNA integrity was confirmed via gel electrophoresis and concentration determined photometrically.

2.2.8.3 RNA extraction from plant and fungal material

RNA was extracted from either 200 mg frozen, ground plant material or 200 mg frozen, ground *Verticillium spp.* hyphal material. The material was mixed with 1.4 ml QIAzol Lysis Reagent (Qiagen, Hilden, Germany) and then incubated for 10 min on a vortex shaker. After adding 260 µl chloroform to the mixture, it was incubated again 10 min on a vortex shaker. Following incubation, the samples were centrifuged for 45 min at 13000 rpm and 4 °C. The aqueous phase that had formed was transferred to a new 2 ml tube containing 400 µl isopropanol and 400 µl precipitation buffer (2.1.11.4). The samples were mixed by inverting the tubes and incubated 10 min at room temperature. RNA was precipitated and pelleted by centrifuging the samples for 30 min at 13 000 rpm and 4 °C. After discarding the supernatant, the pellet was washed with 250 µl 70 % EtOH, then centrifuged 15 min at 13 000 rpm and 4 °C. The washing step was repeated once before the RNA pellet was air-dried at RT for ~5 min. Depending on pellet size, RNA was resuspended in 30 – 80 µl RNase-free ddH_2O. Following extraction, RNA concentration and purity was measured with a photospectrometer and RNA integrity was determined via gel electrophoresis. RNA samples were stored at -80 °C.

2.2.8.3.1 DNA digest and cDNA synthesis from RNA

CDNA synthesized from RNA was used to confirm gene expression, determine levels of expression and amplify gene coding sequences for plasmid assembly. In order to avoid DNA contamination, RNA samples, extracted as described in 0, were subjected to DNaseI (Thermo Fisher Scientific; Waltham, MA, USA) digest. The digest was performed with 1 µg RNA as recommended by the producer with the addition of 0.5 µl RiboLock RNase Inhibitor (Thermo Fisher Scientific; Waltham, MA, USA) per sample. The DNA-free RNA was then used as template for reverse transcription using Reverd Aid H Minus Reverse Transcriptase (Thermo Fisher Scientific; Waltham, MA, USA). The reaction was carried out

with 1 µl 100 µM oligo $d(T)_{18}$ primer, following the protocol supplied by the manufacturer. CDNA samples were stored at -20 °C.

2.2.8.3.2 RNAseq

In planta RNAseq data from plants infected with *V. dahliae* V76, ST100, T9, V138I and V781I at 4, 8, 12 and 16 dpi were previously generated (Thole 2016). *In vitro* RNAseq data was sequenced from *V. dahliae* V76 grown in 7 days in liquid PDB using Illumina sequencing with 125 bp paired-end reads.

2.2.8.4 Polymerase chain reaction (PCR)

Polymerase chain reaction (PCR) was used to amplify DNA fragments for analyses or cloning purposes. Fragments for cloning were amplified with proof-reading Phusion High-Fidelity DNA Polymerase (Thermo Fisher Scientific, Waltham, MA, USA) in order to avoid amplification artifacts in the amplicon. Reactions were set up as specified below.

Component	Volume per 20 µl reaction [µl]
Taq buffer (10 x)	2
dNTPs (10 mM)	0.5
Forward primer (10 mM)	0.75
Reverse primer (10 mM)	0.75
Taq polymerase	0.5
ddH_2O	14.5
Template DNA (0.1 ng – 50 ng)	1

Component	Volume per 50 µl reaction [µl]
HF buffer (5 x)	10
dNTPs (10 mM)	0.4
Forward primer (10 mM)	1
Reverse primer (10 mM)	1
Phusion polymerase	0.25
ddH_2O	35.75
Template DNA (10 ng – 100 ng)	1

Reactions were carried out in thermocyclers (MyCycler: BioRad, Hercules, CA, USA) under the conditions described in the following.

***Taq* polymerase thermocycler protocol**

Step	Temperature	Time	
Initial denaturation	94 °C	3 min	
Denaturation	94 °C	30 sec	35 x
Annealing	50 – 62* °C	30 sec	
Extension	72 °C	1 min per 1 kb	
Final extension	72 °C	3 min	

*depending on predicted melting temperature of primer pairs

Phusion thermocycler protocol

Step	Temperature	Time	
Initial denaturation	98 °C	40 sec	
Denaturation	98 °C	15 sec	33 x
Annealing	60 – 62* °C	20 sec	
Extension	72 °C	30 sec per 1 kb	
Final extension	72 °C	10 min	

*depending on predicted melting temperature of primer pairs

2.2.8.4.1 Quantitative real-time polymerase chain reaction (qRT-PCR)

In order to estimate *Verticillium spp.* biomass content within infected *A. thaliana* plants, fungal DNA content relative to plant DNA content was determined via qRT-PCR. *Verticillium spp. ß-tubulin* (VDAG_10074) was selected as the target that was compared in terms of the amount of generated amplicons to the Arabidopsis reference *UBQ5* (AT3G62250) sequence. Reactions were set up as described below with the SsoFast EvaGreen supermix (BioRad, Munich, Germany). One sample contained pooled DNA from four plants, harvested at the same time point after infection.

Component	Volume per 20 µl reaction [µl]
SsoFast EvaGreen supermix	10
Forward primer (10 mM)	0.4
Reverse primer (10 mM)	0.4
ddH_2O	8.2
Sample DNA (20 ng/µl)	1

The reactions were pipetted into clear 96 well plates (BioRad, Munich, Germany) with three technical replicates per sample. The experiments were repeated once with the locations of the wells containing *Vdß-tubulin* and *AtUBQ5* exchanged. The following protocol was used for the amplification and real-time fluorescence detection of DNA fragments in thermocycler C100 Touch with CFX96 system (Biorad, Hercules CA, USA).

Step	Temperature	Time	
Initial denaturation	95 °C	2 min	
Denaturation Annealing Extension	95 °C 60 °C 72 °C	5 sec 25 sec 15 sec	40 x
Melting curve	55 - 95 °C	10 sec	80 x + 0.5 °C each cycle

After qRT-PCR, the data were analyzed using the BioRad CFX Manager software (v 3.1; BioRad, Munich, Germany). Before the quantification data were used further, the quality of the detected melt curves was controlled. Samples with melt curves that differed highly from the other technical replicates and therefore were most likely due to reaction artifacts were taken out of the analyses. The quantity of *Verticillium spp* DNA relative to Arabidopsis DNA based on the amount of amplicons of *Vß-tubulin* as well as *AtUBQ5* was calculated from the relative quantities (RQ) by the $\Delta\Delta C_q$ method (Pfaffl 2001) using cycle quantification (Cq) values. The Cq value is defined as the number of the PCR cycle in which the detected fluorescence curve of the sample crosses the threshold line of background fluorescence signal (Pfaffl 2001).

$$Relative\ quantity\ (RQ) = E^{\left(C_{q(MIN)} - C_{q(sample)}\right)}$$

$$Relative\ amount\ of\ fungal\ DNA\ (\Delta\Delta Cq) = \frac{RQ_{V\beta-tubulin}}{RQ_{AtUBQ5}}$$

Here, ‘E’ is the efficiency of primer and probe set. Generally this efficiency is assumed to be 100 %, which gives an E value of 2. Cq (MIN) signifies the average Cq for the sample with the lowest average Cq for the target sequence. Data from at least four biological replicates, meaning independent infection experiments, was averaged and standard deviation calculated to generate diagrams.

2.2.8.5 Agarose gel electrophoresis

DNA fragments were separated by size via agarose gel electrophoresis. Gels were prepared with an agarose (UltraPure™ Agarose; Biozym, Hessisch Oldendorf, Germany) concentration of 0.4 to 2 % (w/v), depending on the DNA fragment size, in 1 x TAE buffer (2.1.11.4). Agarose was dissolved by boiling the solution in a microwave. After cooling of the agarose solution to ~ 60 °C, HDGreen Plus DNA Stain (Intas, Göttingen, Germany) was added to a concentration of 5 µl stain per 100 ml agarose gel. The liquid gel was poured into a gel caster (Sub-Cell GT Cell; Biorad, Hercules CA, USA) including a comb in order to prepare gel pockets for sample loading. Gels were placed into electrophoresis tanks (Biorad, Hercules CA, USA) containing 1 x TAE buffer. Prior to loading, DNA samples were mixed with 6 x loading dye (2.1.11.4) and in order to compare fragment sizes a size marker (1 kb or 100 bp GeneRuler™ DNA ladder; Thermo Fisher Scientific, Waltham, MA, USA) was loaded in addition. Electrophoresis was performed by applying an electrical current (80 – 120 V), creating an electrical field that pulls negatively charged DNA molecules toward the anode. For analysis and documentation, bands were made visible under UV light (312 nm wavelength) with a transilluminator (GenoPlex; VWR, Darmstadt, Germany) and pictures ware taken with the help of the GeneSnap software (version 7.07; Synoptics, Cambridge, UK). In order to avoid damaging DNA with UV light, bands that were used for further applications were cut out from the gel with a scalpel on an epi-illuminator (B -BOX™; SMOBiO, Hsinchu City, Taiwan), emitting blue light (470 nm wavelength) which does not act as a mutagen on DNA.

2.2.8.6 Purification and gel elution of PCR products

For sequencing and generating components for plasmid assembly, DNA amplicons were either purified from PCR reaction mixtures (2.2.8.3.2) or eluted from agarose gels after electrophoresis (0) using the NucleoSpin® Gel and PCR Clean-up kit (Macherey-Nagel; Düren, Germany). Reactions were performed following the protocol provided by the manufacturer. For amplicons larger than 1500 bp, DNA elution from the columns was performed with NE buffer heated to 70 °C followed by incubation of the columns at 70 °C for 5 min.

2.2.8.7 Isolation of bacterial plasmid DNA

Plasmids were isolated from liquid bacteria cultures using the GeneJET Plasmid Miniprep kit (Thermo Fisher Scientific, Waltham, CA, USA) according to the manufacturer's protocol.

2.2.8.8 Cloning

2.2.8.8.1 Restriction enzyme cloning

Restriction enzyme cloning is based on the ligation of sticky ends created by restriction enzymes. Inserts were amplified by PCR (2.2.8.4) using primers with overhangs containing appropriate cleavage sites for restriction enzymes. Inserts and vector plasmids were then digested with two restriction enzymes simultaneously following the manufacturer's manual. The digested fragments were then loaded onto an agarose gel and cut out after gel electrophoresis (2.2.8.5). After elution using the NucleoSpin Gel and PCR Clean-up Kit (Macherey Nagel, Düren, Germany), inserts were ligated with the vector backbone using the Rapid DNA Ligation Kit (Thermo Fisher Scientific, Waltham, CA, USA) according to the manufacturer's protocol. The ligation product was afterwards cloned into *E. coli* (2.2.4.6).

2.2.8.8.2 Gateway™ cloning

Gateway™ cloning is a method based on site-specific recombination properties of bacteriophage lambda. First, the desired insert was amplified via PCR (2.2.8.4) with primers containing *attB* recombination sites. The PCR products were purified (2.2.8.6) and added together with the donor vector to the BP Clonase II enzyme mix (Thermo Fisher Scientific, Waltham, CA, USA). The reaction was set up and carried out according to the manufacturer's protocol. The BP reaction was then transformed into *E. coli* cells (2.2.4.6) from which recombined donor vectors were isolated (2.2.8.7). In a second reaction, this donor vector recombines the insert with the desired destination vector. For this, the LR Clonase II enzyme mix (Thermo Fisher Scientific, Waltham, CA, USA) was used, following to the manufacturer's instructions. The LR reaction was then transformed into *E. coli* cells (2.2.4.6).

2.2.8.8.3 NEBuilder seamless DNA assembly

With the NEBuilder (New England Biolabs, Ipswich, MA, USA) DNA assembly method, one or more DNA fragments can be seamlessly assembled. For this, the desired inserts were amplified via PCR (2.2.8.4) with primers including 20 bp overhangs overlapping with the adjacent sequence in the desired finished plasmid. The vector was also PCR-amplified with primers lacking overhangs in order to create a linearized backbone. The reaction was set up with the NEBuilder HiFi DNA Assembly Master Mix (New England Biolabs, Ipswich, MA, USA), following the manufacturer's manual. Reactions were incubated for 1 h at 50 °C and then transformed into *E. coli* (2.2.4.6).

2.2.8.9 Southern blot with *Verticillium spp.* genomic DNA

The Southern blot method was used to confirm knock-out mutants in *Verticillium* as well as prove the existence of the tandem-inverted LSCE region. Blots were made with the Amersham Gene Images AlkPhos Direct Labelling and Detection System (GE Healthcare, Chicago, IL, USA). In short, Southern blots make DNA bands visible that are generated by digesting genomic DNA with a specific restriction enzyme. The bands are then hybridized with a probe containing a sequence also found in the desired DNA band, labelled with a fluorescent tag. Restriction enzymes are selected in a way that produces bands with different sized for samples with different attributes. Restriction digest was planned *in silico* with the Clone Manager Professional Suite software (v. 8; Scientific & Educational Software).

2.2.8.9.1 Digest of gDNA with restriction enzymes

30 – 50 µg *Verticillium spp.* DNA (> 1.5 µg/µl) were digested at the optimal temperature given for each restriction enzyme overnight in reactions as described below. Restriction enzymes were purchased from Thermo Fisher Scientific (Waltham, CA, USA).

Component	Volume per 40 µl reaction [µl]
Restriction enzyme buffer 10 x	4
Restriction enzyme	2
DNA	6 – 12 µl
ddH_2O	x

The digested DNA was mixed with 6 x DNA loading dye (Thermo Fisher Scientific) and then loaded onto a 10 x 15 cm agarose gel with 7 µl DNA ladder on both sides. The concentration of agarose was 1 % for fragments ranging from 500 to 6000 bp and 0.4 % for larger fragments. The gel was run for at least 90 min at 90 V. After gel electrophoresis a picture under UV light was taken to confirm complete digest of the DNA.

2.2.8.9.2 Blotting of agarose gels

The area where DNA was found on the gel was cut out with a scalpel and transferred into a container. It was then covered with 0.25 M HCl and incubated on an orbital shaker (GFL 3017; GFL, Burgwedel, Germany) set to 55 rpm for 10 min. The solution was taken off and incubation was repeated with 0.5 NaOH/ 1 M NaCl for 25 min and finally 1.5 M NaCl/ 0.5 M Tris pH 7.4 for 30 min. The gel was then placed upside down on a glass plate covered with clear plastic wrap. Onto the gel, a DNA- binding membrane (Amersham Hybond-N RPN203N; GE Healthcare, Chicago, IL, USA) was placed. The membrane was covered with 3 consecutive pieces of blotting paper (GB 58/ B002; Whatman, Dassel, Germany) followed by a 10 cm stack of paper towels. The capillary force of the blotting paper and paper towels was increased by weighting the installation down using heavy books (~ 3 kg). During the blotting process, the watery solution containing DNA is pulled from the agarose gel into the blotting paper and paper towels. When passing through the membrane, however, DNA is retained and bound. After two hours, the membrane was removed and dried for 10 min at 75 °C, then irradiated with UV light on both sides for three minutes to strengthen adhesion of DNA.

2.2.8.9.3 Preparation of labelled probe

DNA probes were generated with PCR (2.2.8.3.2) and labelled using the Alkphos labelling module (RPN3680; GE Healthcare, Chicago, IL, USA), following the protocol provided by the manufacturer. In addition to DNA amplicons specific to the targeted DNA bands, 0.5 ng DNA ladder were included in the probes. For bands between 500 to 6000 bp, a 1 kb DNA ladder (GeneRuler; Thermo Fisher Scientific) was used while for larger fragments up to 21 000 bp, the GeneRuler High Range DNA Ladder (Thermo Fisher Scientific, Waltham, CA,USA) was needed.

2.2.8.9.4 Hybridization

The following steps were performed following the protocol provided for the Amersham Gene Images AlkPhos Direct Labelling and Detection System (GE Healthcare, Chicago, IL, USA). For hybridization with a labelled probe (2.2.8.9.3), blotted membranes were put into hybridization tubes (Ø 40 mm, 200 mm; Glasgerätebau Ochs, Bovenden, Germany) containing 10 ml Prehybridization Buffer (2.1.11.5) and then incubated at least 30 min at 55 °C rotating in a hybridization oven (Hybaid Micro-4; MWG Biotech, Ebersberg, Germany). Subsequently, the probe was added directly to the hybridization buffer and the membrane was incubated under continuous rotation at 55 °C overnight. Hybridization buffer as well as hybridization buffer containing probes were collected after use and stored at -20 °C. Probes were re-used up to 5 times. Following overnight hybridization, probe was exchanged for 50 ml pre-warmed (55 °C) Wash Buffer 1 (2.1.11.5). The membranes were washed twice in Wash Buffer 1 by incubating them in the hybridization oven for 10 min. Afterwards, membranes were transferred to containers and washed twice for 5 min with Wash Buffer 2 (2.1.11.5) on an orbital shaker (GFL 3017; GFL, Burgwedel, Germany) set to 55 rpm.

2.2.8.9.5 Detection

Membranes were removed from the wash buffer (2.2.8.9.4), relieved of excess buffer by touching the edge of the membrane with a paper towel and then placed onto a plastic foil. Subsequently, 500 µl CDP-Star Detection Reagent (GE Healthcare, Chicago, IL, USA) were pipetted on the upper edge of a membrane, which was then covered with plastic foil. The detection reagent was spread carefully over the entire membrane by stroking over the plastic-covered surface. The still covered membrane was then incubated inside a dark film cassette (Angewandte Gentechnologie Systeme, Heidelberg, Germany) for 5 min. Superfluous reagent was carefully taken off the membrane with a paper towel, then the membrane was placed on a new piece of plastic foil and moved into the detection device (ChemiDoc Touch; BioRad, Munich, Germany) where the bioluminescence signals of the labelled probe were visualized.

2.2.9 Molecular biological methods – proteins

2.2.9.1 Purification of recombinant protein from *P. pastoris* cultures

LSCE2 and LSCE2-like was purified from recombinant P. pastoris cultures (2.2.7.2). 50 ml liquid culture were loaded onto His GraviTrap™ columns (GE Healthcare, Chicago, Il, USA). Proteins were then purified following the manufacturer's protocol. Protein was eluted with 3 ml elution buffer containing 100 mM imidazole. Protein was stored at 4 °C before infiltration.

2.2.9.2 Western Blot

2.2.9.2.1 Sodium dodecyl sulfate (SDS) polyacrylamide gels

SDS gels were handcast between glass plates with 1.5 mm casting gaps (BioRad, Munich, Germany) that were held by casting stands (BioRad, Munich, Germany). Around 8 ml SDS resolving gel, mixed as described below, were poured into the gap, overlaid with ~ 1 ml isopropanol and left to polymerize for 30 to 60 min. After polymerization, isopropanol was removed and stacking gel, prepared as described below, was poured onto the running gel, filling up the glass chamber. Afterwards, a comb for generating gel pockets (BioRad, Munich, Germany) was inserted into the stacking gel which was then left to polymerize for 30 to 60 min. Gels were either used immediately or stored at 4 °C.

SDS resolving gel

Compound	Volume (for 100 ml 12 % SDS gel) [ml]
12 % gel buffer (2.1.12)	59
Acrylamide (30 %)	40
Ammonium persulfate (APS) (10 %)	1
Tetramethylethylendiamin (TEMED)	0.4

SDS stacking gel

Compound	Volume (for 10 ml stacking gel) [ml]
Stacking gel buffer (2.1.12)	8.16
Acrylamide (30 %)	1.66
APS (10 %)	0.05
TEMED	0.005

2.2.9.2.2 SDS polyacrylamide gel electrophoresis (SDS-PAGE)

SDS gels, prepared as described above, were inserted into electrophoresis chambers (BioRad, Munich, Germany) and covered with 10 x SDS running buffer (2.1.12). After removing the comb, gels were loaded with protein samples in 4 % SDS loading dye (2.1.12) as well as a protein size marker (PageRuler Prestained Marker; Thermo Fisher, Waltham, CA, USA). Electrophoresis was run at 30 mA per gel for ~ 1.5 hours, until the loading dye left the resolving gel.

2.2.9.2.3 Blotting of SDS polyacrylamide gels

After gel electrophoresis, proteins were blotted from SDS gels onto a membrane. For this, blotting sandwiches were assembled consisting of, from cathode to anode, a sponge, 3 pieces of blotting paper (GB 58/ B002; Whatman, Dassel, Germany), SDS acrylamide gel, membrane (Roti-PVDF, pore size 0.45 µm; Carl Roth, Karlsruhe, Germany), 3 pieces of blotting paper and another sponge. The sandwich was inserted into a blotting cassette (BioRad, Munich, Germany) which was in turn submerged in a buffer tank (BioRad, Munich, Germany) and covered with transfer buffer (2.1.12). Blotting was done by applying an 80 V current for 2 hours while the blotting apparatus was cooled continuously.

2.2.9.2.4 Protein detection

Blotted membranes (see above) were removed from the blotting sandwich, transferred to a container and covered with blocking solution (2.1.12) for at least 1 h while shaking at 55 rpm. The blocking solution was then removed from the membranes which were afterwards covered with blocking solution containing the primary antibody (2.1.6) and incubated overnight at 4 °C, shaking at 55 rpm. The next day, after removing the primary antibody, membranes were washed by incubating them 6 x 12 min in

blocking solution, shaking at 55 rpm. After removing the blocking solution, membranes were incubated for 2 h (55 rpm) with the secondary antibody (2.1.6), diluted in blocking solution. The membranes were rinsed afterwards with 1 % TBS-T (2.1.12) and subsequently washed 6 x 12 min with 1 % TBS-T (55 rpm). Detection with alkaline phosphatase (AP) requires buffered conditions, therefore membranes were incubated in AP buffer (2.1.12)

2.2.10 Histological Methods

2.2.10.1 Staining of leaves with Trypan Blue

For assessing transdifferentiation of bundle sheath cells into xylem vessels in leaves of infected plants, these tissues were stained with trypan blue. From infected Arabidopsis, the 5th rosette leaf from each harvested plant was removed at 21 dpi. The leaves were put into a 50 ml tube, and covered with trypan blue staining solution (2.1.11.5) which was then directly transferred to a boiling water bath. After 5 min, the staining solution was removed and the leaves were covered with chloral hydrate solution (2.5 g/ml). The chloral hydrate solution was exchanged after 3 days and then again until the solution stayed clear. Samples were stored in 60 % glycerol.

2.2.10.2 Fixation, embedding and processing of Arabidopsis leaf transections

In order to generate microtome cuts from leaf tissue for microscopy, samples were embedded in cold curing resin based on hydroxyethylmethacrylate. For this, the Technovit 7100/Technovit 3040 (Kulzer, Hanau, Germany) system was used.

2.2.10.2.1 Sample fixation and dehydration

Leaves from infected Arabidopsis plants were used to cut out ~ 1 mm wide strips transecting the leaf midrib. These cuts were placed into brown 2 ml tubes and fixated overnight in formic acetic acid, shaking in a thermoblock at 1000 rpm at RT. After fixation, samples were dehydrated in an ethanol series consisting of 50, 60, 70, 85, 95 and 100 % ethanol. Samples were incubated in 1 ml of each solution for 90 min under light agitation shaking in a thermoblock at 1000 rpm at RT. Samples were kept in 100 % EtOH under light agitation overnight and in fresh 100 % EtOH for two more hours the next day.

2.2.10.2.2 Infiltration

After removing the ethanol, samples were incubated under light agitation for 4 h in 1 ml 50 % pre-infiltration solution, which was prepared by mixing Technovit 7100 Base Liquid with ethanol. This step was repeated with 1 ml 75 % pre-infiltration solution, samples were kept in the solution overnight. The next day, the pre-infiltration solution was exchanged for 1 ml infiltration solution which was prepared by solving 1 g Technovit 7100 Hardener I in 100 ml Technovit 7100 Base Liquid. Infiltration of the samples with the infiltration solution was facilitated by applying a vacuum for 10 min inside an exsiccator, which was then slowly alleviated. This process was repeated four times and the samples were afterwards kept in the infiltration solution for 3 days under light agitation.

2.2.10.2.3 Embedding

Directly prior to embedding, polymerization solution was prepared by mixing 1.5 ml infiltration solution with 100 µl Technovit 7100 Hardener II for 4 min. This amount is sufficient for preparing three sample blocks. Sample blocks were generated by first filling Histoform S (Kulzer, Hanau, Germany) molds half way with polymerization solution and then placing up to three leaf transections into one mold which was then filled entirely with polymerization solution. The polymerization process was completed after 2 hours at RT. Then, Histoblocks (Kulzer, Hanau, Germany) were placed into the recess of the Histoform S mold and subsequently combined with the sample blocks by pouring activated Technovit 3040 into the recess of the back of the Histoblock. Activated Technovit 3040 was prepared by mixing one part Technovit 3040 liquid with one part Technovit 3040 powder and vortexing for 30 s, then adding another part powder and vortexing another 30 s. After 10 min, Histoblocks together with sample blocks were removed from the Histoform S and stored at 4 °C.

2.2.10.2.4 Microtome sectioning

Sample blocks were fastened into the holding device of the microtome (Hyrax M55; Zeiss, Oberkochen, Germany) and cut with a carbide blade to 5 mm thick sections. Sections were placed onto water-covered 76 x 26 mm microscope slides (Roth, Karlsruhe, Germany) and subsequently dried on a heating plate at 70 °C (OTS40, Medite, Burgdorf, Germany). Thus treated sections were used for microscopy and staining and did not require any other form of fixation.

2.2.10.2.5 Staining of microtome sections

For bright field microscopy, leaf transections were stained with toluidine blue which is a basic dye that stains, amongst others, acidic components of the cell wall. Microscope slides with fixed sections (2.2.10.2.4) were immersed in toluidine blue (0.05 % w/v) staining solution for 1 min, then rinsed with water and dried on a heating plate at 70 °C.

2.2.11 Bioinformatic methods

2.2.11.1 Genomics

2.2.11.1.1 De novo sequencing

De novo sequencing of *V. dahliae* strain V76 was performed by BaseClear (Leiden, Netherlands). Sequence data generated with PacBio (Menlo Park, CA, USA) sequencing using a Sequel SMRT cell was combined in a hybrid approach with Illumina (San Diego, CA, USA) HiSeq 2500 data. By this approach the quality of long sequences generated by PacBio technology was ameliorated by shorter but more accurate 300 bp paired-end sequence reads generated by Illumina HiSeq 2500 sequencing with the MiSeq Reagent Kit v3. This resulted in a final assembly of 61 scaffolds.

2.2.11.1.2 Whole genome alignment

In order to identify lineage-specific (LS) regions, meaning regions that are present in the V76 genome but not in the reference genome of wilting isolate JR2, all 61 scaffolds of the V76 assembly (2.2.11.1) were aligned with the *V. dahliae* JR2 genome, which has previously been sequenced and assembled to the chromosome level (deJonge et al. 2013) and deposited at NCBI (GCA_000400815.2). The alignment was computed using MAUVE 2.4.0 (Darling et al. 2004) in progressive mode with default parameters. The resulting alignments were then parsed with custom scripts generated by S. Dietrich and A. Poehlein to extract lineage specific regions and to obtain the input for Circos version 0.69-6 (Krzywinski et al. 2009) which was used to create the visualization in Figure 3.1. Only LS regions ≥ 1 kb were used for further analyses.

2.2.11.1.3 Determination of potential lineage-specific candidate effectors (LSCEs)

Potential lineage-specific candidate effectors (LSCEs) were previously generated RNAseq data from *V. dahliae* 'early senescence' isolates during infection of *A. thaliana*. A candidate was defined as a region of transcriptional activity during infection that is situated within a lineage-specific region. Therefore, RNAseq reads were mapped to LS regions using the 'map to reference' tool included in the CLC Genomics Workbench software (v.10.1.1; Qiagen, Hilden, Germany). Default mapping parameters were applied, allowing read mapping above 75 % read coverage and 80 % read sequence similarity. To reduce noise, candidate search was limited a transcript size of a minimum 150 bp. These analyses yielded a list of 273 potential candidates which were first BLAST-searched (Altschul et al. 1990) to identify sequence homologs and subsequently manually curated to account for potential inaccuracies in the assembly or genome alignment methods to remove false positives. The resulting curated list of 115 potential candidates was then mined for promising LSCEs which met the several criteria. Candidates were required to either possess a secretion signal predicted by SignalP-4.1 (Nielsen 2017) or predicted to be non-conventionally secreted by SecretomeP 2.0 (Bendtsen et al. 2004) . Nucleotide sequences of candidates were furthermore not allowed to be more than 95 % similar to *V. dahliae* JR2 or VdLs17 homologs while presence of >90 % similar homologs in the *V. longisporum* VL43 genome was mandatory. Finally, only candidates that were transcriptionally induced upon host infection in comparison to growth in liquid PDB medium were included. Expression analyses using RNAseq data were conducted with the CLC Genomics Workbench software (v.10.1.1; Qiagen, Hilden, Germany).

2.2.11.2 Phylogenetics

2.2.11.2.1 Sequence data analysis

PCR amplicons (2.2.8.4) destined for phylogenetic analyses were sent for sequencing to SeqLab (Microsynth AG, Balgach, Switzerland). Sequence quality was determined by evaluating pherograms of the provided sequencing reactions using PhyDE v. 0.9971 (PhyDE® - Phylogenetic Data Editor 2014). Sequences were then aligned manually in PhyDE.

2.2.11.2.2 Phylogenetic inference

Phylogenetic trees were computed using MEGA v.7.0.14 (Kumar et al. 2016) . The Maximum Likelihood algorithm was used as statistical method and the phylogeny was tested with 1 000 bootstrap replicates. As a model for nucleotide substitution, the General Time Reversible model with gamma distributed and invariant sites (GTR+G+I) was selected. Maximum Likelihood needs to be paired with a heuristic method for statistically determining the best supported tree topology. For this, 'Subtree Pruning and Regrafting' was selected. The resulting bootstrap consensus trees were exported and edited in TreeGraph2 (Stöver and Müller 2010).

3 Results

3.1 *De novo* sequencing and assembly of the *V. dahliae* V76 genome and subsequent alignment with *V. dahliae* JR2 reveal potential chlorosis lineage-specific candidate effectors

3.1.1 *De novo* sequencing and genome assembly of chlorosis-class isolate *V. dahliae* V76

High quality sequence data is a requirement for discovering effector candidates in *Verticillium* genomes, since numerous potential effectors have been found to be located in lineage-specific regions (LS) (deJonge et al. 2013) . These regions have been reported to be associated with transposons as well as chromosomal breakpoints (deJonge et al. 2013) and are therefore not easily sequencable. As of yet, no genome assembly for a *V. dahliae* chlorosis-class isolate has been published in a public database in contrast to wilting-class isolates which are represented by chromosome-level assemblies of VdLs17 and JR2 (Klosterman et al. 2011; deJonge et al. 2013). *V. dahliae* chlorosis-class isolate V76, isolated from cotton in Mexico, was chosen as the chlorosis-class reference isolate to be sequenced due to its capacity to robustly and strongly induce the chlorosis-class disease phenotype on Arabidopsis (Thole 2016). PacBio sequencing produces large (<10 kb) sequence reads which are, however, prone to errors in the nucleotide sequence (error rate 13 - 15 %) (Ardui et al. 2018). In contrast to this, Illumina-based sequencing reads are short (~100 bp) but highly accurate (error rate ~ 0.1 %) (Ardui et al. 2018). A hybrid sequencing strategy combining PacBio long read and Illumina short read data has the potential to provide long, accurate genomic sequence information (Albrecht et al. 2017) and was employed here for the generation of a V76 chlorosis-class reference genome. The genome was sequenced using PacBio Sequel Single Molecule Real-Time (SMRT) technology and Illumina HiSeq 2500 sequencing with the MiSeq Reagent Kit v3 producing 300 bp paired-end reads. The final V76 genome assembly consisted of 61 scaffolds with a combined

length of 36.1 million base pairs (Mb) (Table 3.1). This is comparable to the size of the *V. dahliae* JR2 reference genome 36.2 Mb which is, however, assembled to the level of eight chromosomes (deJonge et al. 2013). On average, V76 scaffolds were 0.6 Mb long with the shortest scaffold at 8 000 base pairs and the largest at 4.87 Mb (Table 3.1; Supplement Table 6.1), which corresponds to the size range of *V. dahliae* chromosomes (deJonge et al. 2013).

Table 3.1 Summary of *V. dahliae* isolate V76 *de novo* genome assembly. Sequencing and assembly was performed with PacBio Sequel Single Molecule Real-Time (SMRT) technology and Illumina HiSeq 2500 sequencing with the MiSeq Reagent Kit v3 producing 300 bp paired-end reads.

	Scaffolds (scf)	Total genome size [Mb]*	Average scf length [Mb]	Longest scf [Mb]	Shortest scf [kb]
V76 *de novo* genome assembly	61	36.1	0.6	4.87	8

3.1.2 Whole genome alignment of *V. dahliae* isolates V76 and JR2 reveals lineage-specific (LS) regions

The aim of this study was to uncover *Verticillium* effector(s) involved in the establishment of chlorosis-class specific disease symptoms. As mentioned before (1.4.2), disease class-specific effectors may be located in lineage-specific (LS) regions that are only shared by chlorosis-class isolates. In order to identify these regions, the *de novo* sequenced genome of chlorosis-class isolate *V. dahliae* V76 was aligned with the genome of wilting-class isolate JR2. Whole-genome alignments were generated with the MAUVE v. 2.4.0 software in progressive mode (Darling et al. 2010) and subsequently parsed with custom scripts in order to identify lineage-specific regions. This data were used in a Circos diagram to illustrate collinear blocks between the V76 scaffolds and JR2 chromosomes (Figure 3.1). While some V76 scaffolds were made up entirely of sequences homologous to one JR2 chromosome (e.g. scf #35), most V76 scaffolds shared homologous sequences with two or more JR2 chromosomes. Our data analysis confirms earlier studies in which *V. dahliae* genomes were demonstrated to be prone to extensive chromosomal rearrangements (deJonge et al. 2013) . LS-regions were found in both genomes. While large V76 scaffolds have relatively few LS-regions, short scaffolds (e.g. scf #33)

tended to include a higher percentage of LS sequences, especially when they were comprised of sequences aligning to various JR2 chromosomes. Entire scaffolds that could not be aligned to the JR2 genome were called 'unplaced scaffolds'. In order to determine the origin of these scaffolds, they were subjected to BLAST homology searches. Four scaffolds were identified to be of mitochondrial origin while the other twelve scaffolds consist of sequences that were present in multiple copies in both genomes, e.g. rRNAs (Supplement Table 6.1), and pose therefore an unsolvable problem for the MAUVE algorithm which is limited in this regard (Darling et al. 2010).

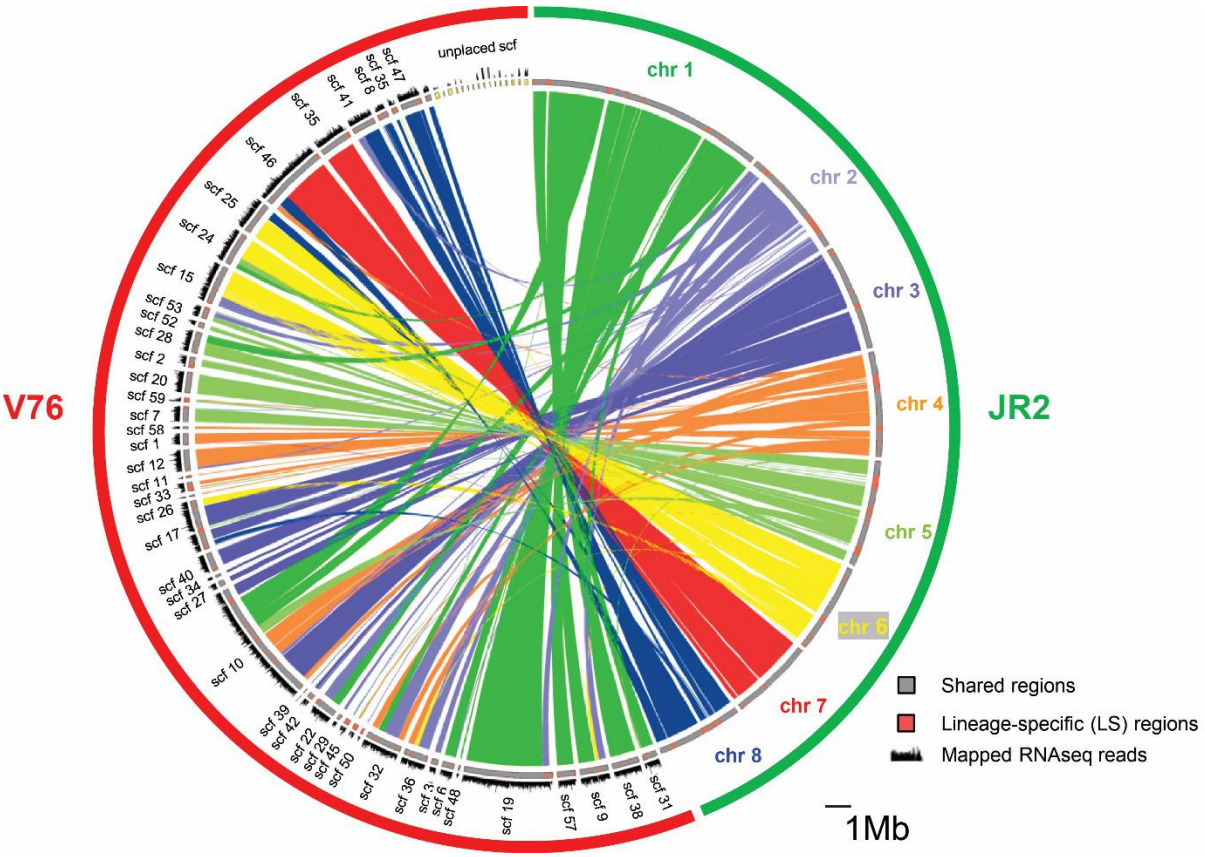

Figure 3.1 Whole-genome alignment of *de novo* sequenced *V. dahliae* chlorosis-class isolate V76 and reference wilting-class isolate JR2. Circos alignment diagram depicts collinear regions between V76 and JR2 by connecting V76 scaffolds with corresponding JR2 chromosomes in their respective color. Also shown are the locations of V76 and JR2-specific regions (red on grey) as well as mapped RNAseq from V76 during infection *in planta* from 4 to 16 dpi. Scaffolds which could not be aligned with the JR2 genome are gathered as 'unplaced scaffolds' at the top of the scheme.

3.1.3 Bioinformatic analyses identify chlorosis lineage-specific candidate effectors

The aim of this study was to identify *Verticillium* effector(s) involved in the establishment of chlorosis-class specific disease symptoms. To this end, we sequenced the genome of the reference isolate *V. dahliae* V76 and identified LS regions. Recent studies suggested that lineage-specific effector repertoires are responsible for specific disease symptoms in host plants (deJonge et al. 2012; Chen et al. 2018). Therefore, it was decided to mine V76-specific (LS) regions for potential effectors. Following the cutoff suggested by deJonge et al. (2013), LS regions considered in this study were required to exceed 1 kb. In the V76 genome, 242 LS regions with a total size of 1.39 Mb (3.8 % of the total genome) were recovered. In order to identify expressed gene models expressed upon host infection, *in planta* RNAseq reads from five *V. dahliae* chlorosis-class isolates (V76, T9, ST100, V138I and V781I) and four time points (4, 8 12 and 16 dpi) were combined and mapped to the LS regions. This ensured that potential effectors with diverse expression dynamics were included and that potential effectors were expressed in all chlorosis-class isolates. A length cut-off for sequences with mapped RNAseq reads to be counted as expressed gene models was set at 150 bp to exclusively include potential gene sequences. In total, 115 *in planta* expressed gene models were discovered in the LS regions. To interact with plant targets, effectors must be secreted by the fungus and therefore need to either include a N-terminal signal peptide for ER-mediated secretion or a signal for an unconventional secretion pathway (Selin et al. 2016). Thus, all 115 candidate genes were analyzed using the publicly accessible servers SignalP (http://www.cbs.dtu.dk/services/SignalP/) for prediction of traditional N-terminal secretion signals and SecretomeP (http://www.cbs.dtu.dk/services/SecretomeP/) for unconventional secretion. 31 gene model products were predicted to include either one of the secretion signals. To further reduce the number of potential effectors, a set of criteria was devised. Potential effectors were required to be found with high similarity (>90 %) in the genome of chlorosis-class *V. longisporum* isolate VL43 while the similarity with *V. dahliae* wilting-isolate homologs did not exceed 95 %. In addition, only gene models with induced *in planta* expression levels, determined by RNAseq analyses, were included. Finally, a protein size cutoff was set at 400 amino acids as it has been demonstrated that effectors are usually small proteins (Klosterman et al. 2011; Selin et al. 2016). A total of four *LINEAGE-SPECIFIC CANDIDATE EFFECTORs* (*LSCEs*) met all selection criteria (Table 3.2).

After identifying four *LSCE*s, these potential effectors were analyzed in more detail (Table 3.2). The peptide length of the effectors ranged from 63 aa (*LSCE1*) to 391 aa (*LSCE3*). A canonical N-terminal signal peptide was predicted for *LSCE2*, *LSCE3* and *LSCE4* whereas *LSCE1* was predicted to be non-conventionally secreted. For a first functional characterization, all *LSCE*s were searched for functional domains using the publicly available services Motif Scan (https://myhits.isb-sib.ch/cgi-bin/motif_scan) and blastx (https://blast.ncbi.nlm.nih.gov/Blast.cgi). No functional motifs were predicted for *LSCE1*, *LSCE2* and *LSCE4*. *LSCE3*, on the other hand, shared homologies with the Polysaccharide Lyase Family 6. Polysaccharide lyases cleave certain activated glycosidic linkages present in acidic polysaccharides and are usually not associated with pathogenicity. Next, expression of the gene models was investigated. Transcriptional activity of a gene can be evaluated by calculating the reads per kilobase (of the gene model) per million (RPKM) total mapped reads from an RNAseq mapping. The RPKM values were calculated for all *LSCE* candidates with *in vitro* and *in planta* RNAseq data. Except for *LSCE1*, all *LSCE*s were expressed only marginally or not at all *in vitro.* From the *in planta* expression data, *LSCE2* stood out with an RPKM value of 1112 (Table 3.2), indicating massive induction of this gene upon host infection.

Table 3.2 Properties of lineage-specific candidate effectors (*LSCEs)*

LSCE	Location in V76 genome	Secretion	Size [aa]	Copies in V76	Copies in VL43	RPKM[2] in vitro	RPKM in planta[3]	Predicted motifs
1	scf #33	Non-classical	63	2	2 (100%)[1]	25	35	none
2	scf #33	Signal petide	237	2	2 (99.7%)	3	1112	none
3	scf #41	Signal petide	391	1	1 (95%)	0	13	Polysaccharide lyase PL-6
4	scf #59	Non-classical	330	1	1 (95%)	0	6	none

[1] Nucleotide sequence similarity
[2] Reads per kilobase gene model per million mapped reads
[3] Combined data from 4, 8, 12 and 16 dpi and infections with *V. dahliae* V76, T9, ST100, V138I and V781I

Notably, RPKM values in the initial analyses were calculated and subsequently combined from different time points and infections. This could potentially mask expression peaks at some point during the infection if the gene is otherwise expressed to low degrees. Therefore, the *in planta* expression of all five *LSCE*s in the reference line V76 at distinct time points during host infection (4, 8, 12 and 16 dpi) was investigated. The data confirm the highest induction of *LSCE2* at all time points except 16 dpi (Table 3.3). Considering the properties of all *LSCE*s, *LSCE2* was selected as the primary candidate for further investigation. The protein is small (237 aa), has a predicted signal peptide, has otherwise no domains with a known function and is massively induced during host infection in all investigated *V. dahliae* chlorosis-class isolates.

Table 3.3 Expression of *LSCE 1 – 4 in planta* based on RNAseq data from *V. dahliae* V76 during host plant infection. RNA was extracted from plants at 4, 8, 12 and 16 dpi. Reads were mapped to V76 scaffolds and Reads per kilobase gene model per million mapped reads (RPKM) was calculated for each candidate effector.

	RPKM in planta			
LSCE	**4 dpi**	**8 dpi**	**12 dpi**	**16 dpi**
1	81	3	31	89
2	107	56	550	57
3	28	3	3	91
4	3	19	189	110

Intriguingly, *LSCE2* was found to be located on the same scaffold (scf #33) as *LSCE1,* separated by merely ~8200 bp (Figure 3.2). While both genes were induced upon host infection in all chlorosis-class isolates, *LSCE2* was expressed to significantly higher levels (Figure 3.2). Furthermore, sequence analyses revealed that *LSCE1* and *LSCE2* are present in two copies on scf #33 whereas *LSCE3* and *LSCE4* are single-copy genes. The same was found in the genome of chlorosis-class *V. longisporum* VL43 (Braus et al., unpublished; available at http://www.vertibase.org). Very interestingly, after subsequent careful sequence comparisons it was discovered that *LSCE2* is located in a ~ 20 kb, tandem-inverted region on V76 scf #33.

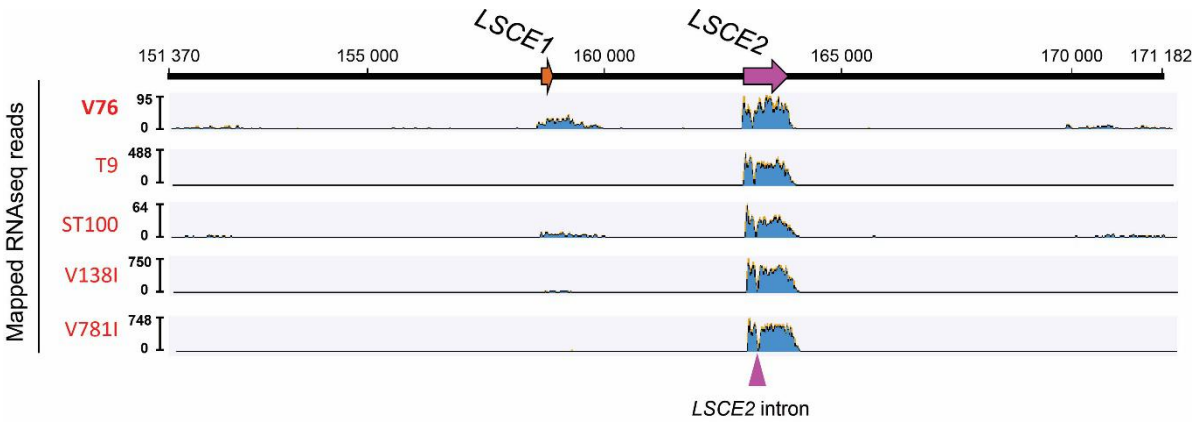

Figure 3.2 ***In planta*** **RNAseq reads from** ***V. dahliae*** **chlorosis isolates V76, T9, ST100, V138I and V781I mapped to a ~20 kb region including** ***LSCE1*** **and** ***LSCE2*** **on V76 genome assembly scaffold #33.** Graphs in blue illustrate total amount of RNAseq reads mapped to the sequence. Scale bars show maximum amount of RNAseq reads mapped to the sequence.

3.2 Bioinformatic analyses of *LSCE2* and phylogenetic considerations

3.2.1 *LSCE1* and *LSCE2* are located in a tandem-inverted, lineage-specific region in chlorosis-inducing *V. dahliae* and *V. longisporum* isolates

The ~ 20 kb tandem-inverted lineage-specific candidate effector-containing (LSCE) region was further characterized using bioinformatic and experimental tools. In addition to the two effector candidates *LSCE1* and *LSCE2*, four gene models where identified in the LSCE region via homology searches in the databases (Figure 3.3C). The first of these gene models was predicted to encode a reverse transcriptase, a gene which is usually contained in retrotransposons (Supplement Figure 6.1) (Kazazian 2004) . The second gene model was named 'Hypothetical protein1' and encoded for a protein of 135 aa. It shared homologies with another hypothetical protein found in *V. longisporum* (BN1708_013154) but does not contain any predicted domains that point towards possible functions of the protein (Supplement Figure 6.2). The third gene in the LSCE region is *LSCE1* which had a homolog in V. longisporum but otherwise only one other homologous sequence from *Stachybotrys chartarum* with low (44 %) similarity to *LSCE1* was found (Supplement Figure 6.3). *LSCE1* was followed by a gene model that shared 61 % sequence homologies with an annotated transposase

found in *Aspergillus kawachii* IFO 4308 (Supplement Figure 6.4). Transposases, in contrast to reverse transcriptases, are usually found in DNA transposons (Kazazian 2004). Transposable elements are reported to contribute to the plasticity of *Verticillium* genomes and have been associated with the emergence of LS regions (Klimes et al. 2015). Whether the LSCE region is part of a functional transposon has not been determined yet. The fourth gene model found besides the *LSCE*s in the LSCE region was named 'Hypothetical protein2'. The predicted 103 aa protein shares homologies with a FabD/lysophospholipase-like protein from *Purpureocillium lilacinum* and includes a predicted partial patatin-like phospholipase domain (Supplement Figure 6.5). Patatin-like phospholipases are able to hydrolyze phosypholipids as well as galactolipids and have a role in the synthesis of phytohormones jasmonic acid and oxilipin (Canonne et al. 2011). *LSCE2* was the sixth gene model predicted to be encoded on the LSCE region. In the publicly available databases, only one homolog in *Fusarium oxysporum* was discovered (Supplement Figure 6.6).

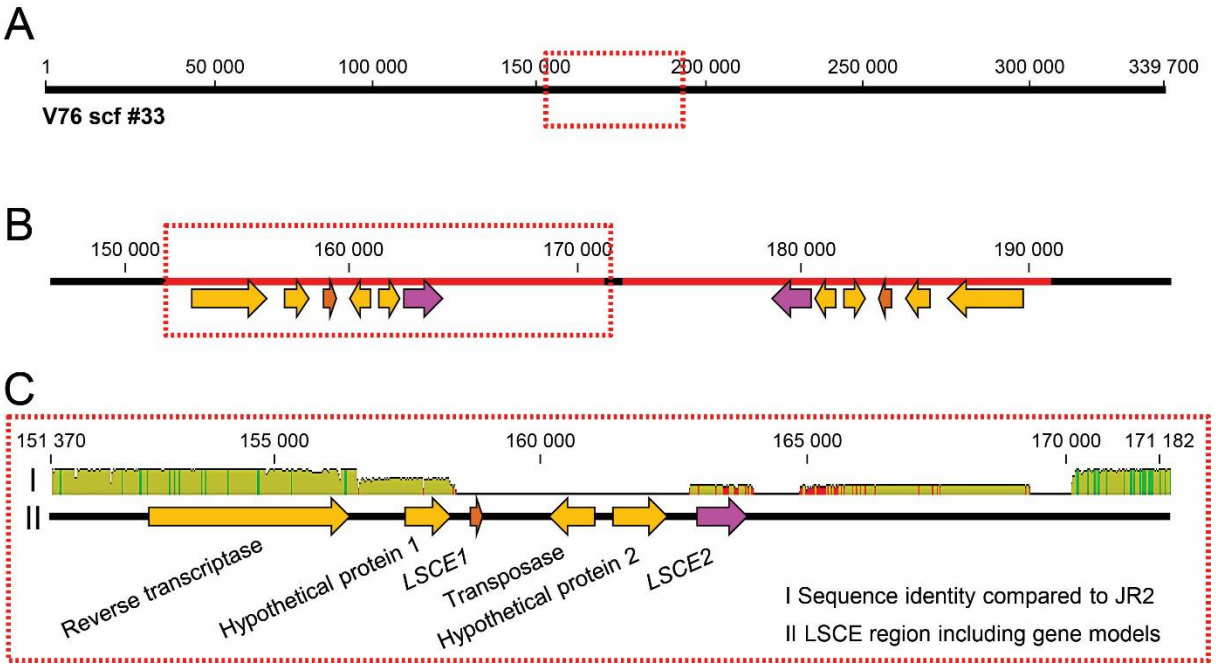

Figure 3.3 Schematic overview of the tandem-inverted, lineage-specific region containing candidate effectors *LSCE1* and *LSCE2* (LSCE region). (A) Overview of the entire V76 genome assembly scaffold 33. Location of the LSCE region is marked with a red rectangle. (B) Tandem-inverted LSCE regions (red) with gene models (arrows) in their respective orientation. The two LSCE region copies are separated by a 'spacer' sequence of 343 bp. Gene models were determined by RNAseq mappings and blastx homology searches. (C) Detailed depiction of the ~20 kb LSCE region. Gene models in lane II were annotated according to homologies found in blastx searches. Lane I shows a graphic representation of the mean pairwise identity over all pairs in the column computed with Geneious 8.1.8 software (Kearse et al. 2012) (Green: 100% identity, Greeny-brown: at least 30% and under 100% identity, Red: below 30% identity).

Duplicated regions and transposable elements are difficult to sequence and therefore prone to sequencing as well as assembly errors (Treangen and Salzberg 2011) . In order to exclude an erroneous scaffold assembly, sequence as well as tandem-inversion of the LSCE region was experimentally confirmed. First, the entire LSCE region was amplified via PCR and sequenced using overlapping amplicons (Supplement Figure 6.7). The sequencing results aligned perfectly with the LSCE region, confirming the nucleotide sequence of the LSCE region. Ambiguities in the sequencing results were retraced to homologous sequences in the core genome of V76. Then, the presence of the two inverted copies of the LSCE region was investigated experimentally. Assembly data suggested that identical copies of the tandem-inverted LSCE region were not directly adjacent to each other but separated by a short 'spacer' sequence of 343 bp which was not copied (Figure 3.4). To confirm the presence of the spacer region, V76 gDNA was amplified via PCR with primers that aligned to the border between spacer and LSCE region. The sequenced amplicon was in most positions identical to the spacer sequence. Ambiguities were traced back to a homologous sequence on scaffold #46 of the *V. dahliae* V76 genome assembly (Figure 3.4).

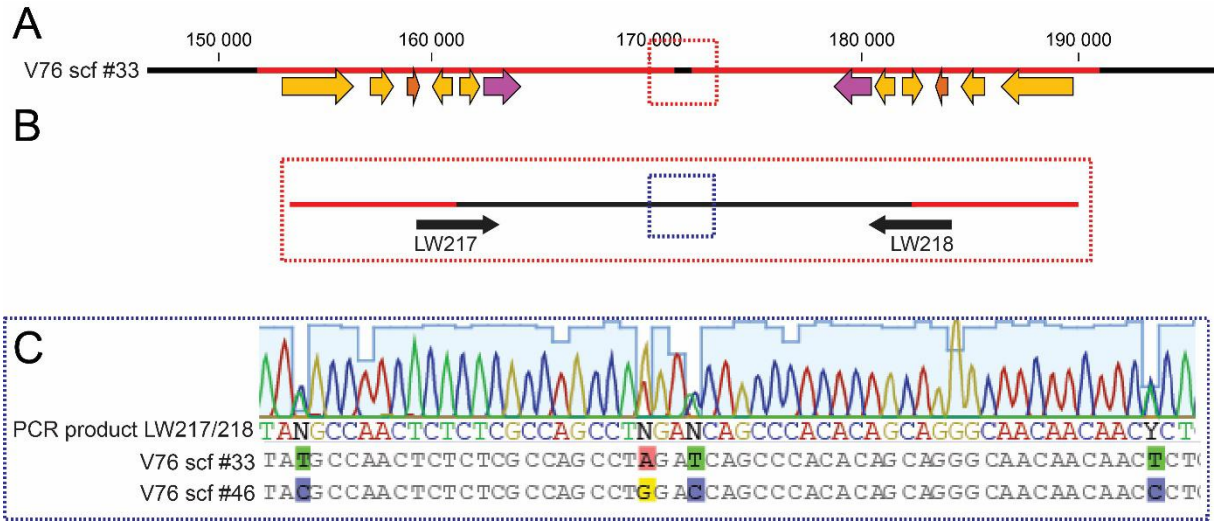

Figure 3.4 A 343 bp ‚spacer' separates the tandem-inverted copies of the LSCE regions. (A) Schematic overview of the tandem-inverted LSCE regions (red) on *V. dahliae* V76 scaffold 33. (B) Primer binding sites (black arrows) for amplification and sequencing of the spacer (black line). (C) Section of the alignment of spacer sequencing product (LW217/218) with the spacer sequence (scf #33) and a spacer-homologous sequence (scf #46). Sequencing chromatogram is shown on top. Ambiguous sequencing results are highlighted in color.

Detecting both copies of the LSCE region in their entire length via PCR was experimentally not feasible. Therefore, Southern blot hybridization was utilized for detecting defined parts of the LSCE region in the V76 genome. Simultaneously the presence of the tandem-inverted region in *Verticillium spp.* chlorosis- as well as wilting-class isolates was investigated. To this end, the genomic DNA of six chlorosis-class and five wilting-class isolates was digested with SacI and subsequently hybridized with a probe consisting of the 343 bp spacer region (Figure 3.5A). In all chlorosis-class isolates, two signals of approximately 1.6 kb and 1.1 kb were detected (Figure 3.5B). The upper band corresponded to the expected size of the LSCE region fragment (1589 bp) while the lower band corresponded to a region on V76 scf #46 which was homologous to the terminal ~7000 bp of the LSCE region. While the latter region was also detected in the genomes of all wilting-class isolates, the LSCE region was exclusively found in the chlorosis-class isolates. Next, the presence of two *LSCE2* copies in the chlorosis-class isolates was investigated. Genomic DNA of six *Verticillium spp.* chlorosis class isolates and wilting-class *V. dahliae* JR2 was digested with SalI, which was predicted to cut within the *LSCE2* copies. The resulting fragment was hybridized with a 1316 bp probe consisting of the 254 3' terminal bases of *LSCE2* and 1062 bp of its 3' downstream region (Figure 3.5A). A ~ 15 kb signal was detected in all chlorosis-class isolates but not in wilting-class isolate JR2 (Figure 3.5C). The location of the band corresponded to the size of the expected 15 519 bp DNA fragment (Figure 3.5A). Taken together, experimental analyses of the LSCE region confirmed its tandem-inverted orientation and the presence of two copies of *LSCE2*. Furthermore, it was shown that the LSCE region and consequently two copies of *LSCE2* were exclusively present in the genomes of *Verticillium spp.* chlorosis-class isolates V76, ST100, T9, V781I, V138I and VL43.

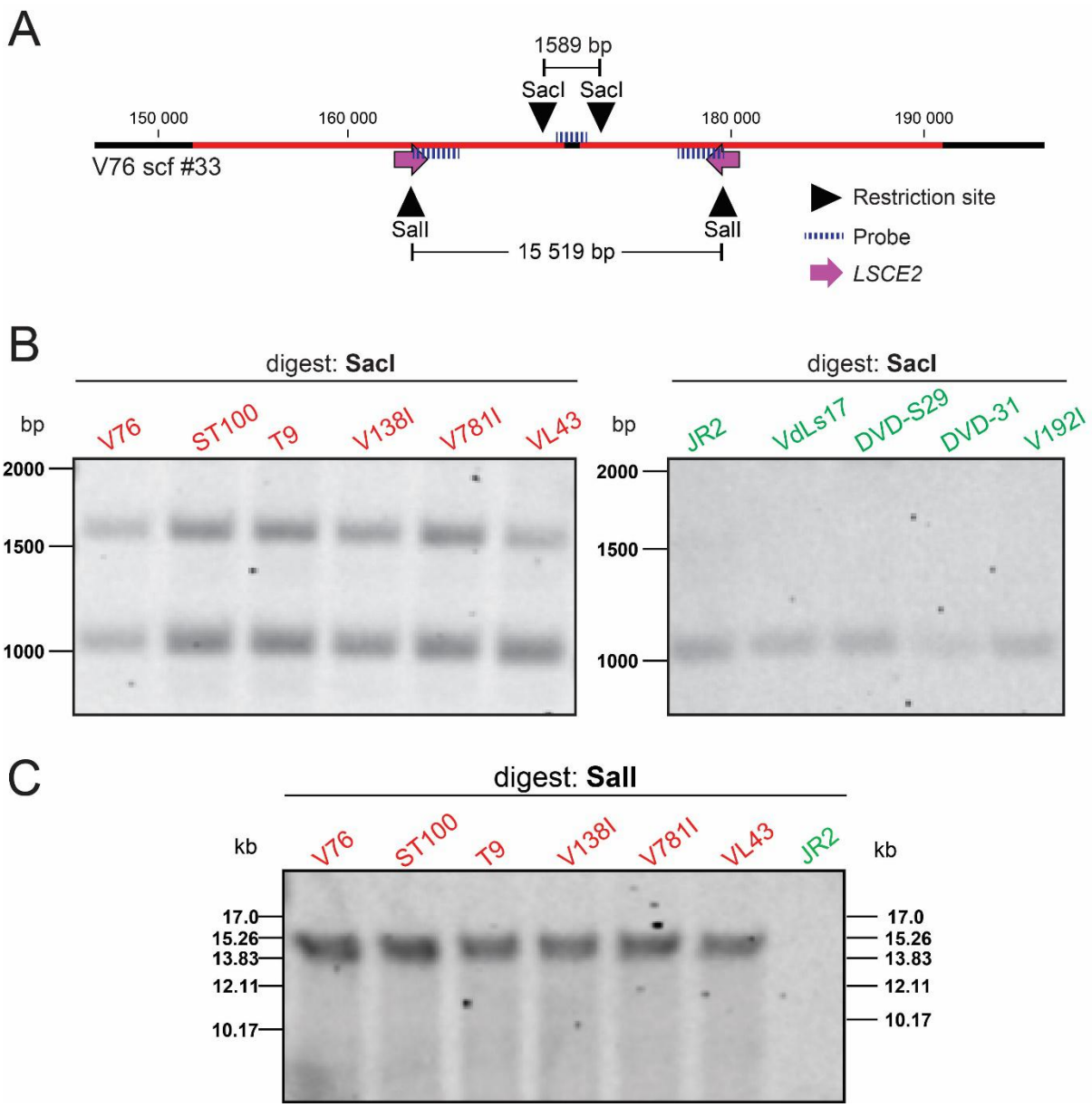

Figure 3.5 Southern Blot confirms presence of tandem-inverted LSCE region in five *V. dahliae* chlorosis isolates and *V. longisporum* VL43. (A) Scheme showing SalI and SacI restriction sites. LSCE regions are shown in red, *LSCE2* is marked by pink arrows and the 343 bp spacer region is shown in black between the LSCE regions. DNA fragments detected in the blots are marked and their sizes, 15 519 bp (SalI) and 1589 bp (SacI), are noted. Probes are marked in blue dashed lines. (B) Detection of Southern hybridization probes. gDNA from six chlorosis class isolates (red) and five wilting-class isolates (green) was digested with SacI and hybridized using a the 343 bp spacer sequence as probe. (C) Detection of Southern hybridization probes. SalI-digested, genomic DNA from *Verticillium spp*. was hybridized with a 1316 bp probe consisting of *LSCE2* (partial) and 3 ‘ downstream sequence.

3.2.2 *LSCE2-like* is a homolog of *LSCE2* and present in the core genome of all *Verticillium spp.* isolates

Sequence alignments of the V76 LSCE region with the JR2 genome showed that parts of the region are found as homologous sequences also in the wilting-class isolate (Supplement Figure 6.8). Interestingly, a ~ 1 500 bp region including *LSCE2* had a sequence homolog in the JR2 genome (Figure 3.6). The *LSCE2* homologous gene in this region was designated as *LSCE2-like*. A comparative protein sequence analysis of V76 LSCE2 and JR2 LSCE2-like revealed overall high sequence conservation (Figure 3.7A) between the two proteins. Interestingly, the predicted N-terminal secretion signal (aa 1 – 18) and the subsequent 46 aa harbored only a single amino acid exchange. There were, in fact, only two regions of ~ 20 aa with a high rate of sequence dissimilarities. The first starting at position 141 and ending at position 161 and the second from position 188 to 210 (Figure 3.7). The positioning of amino acids and the resulting interaction between the residues in a peptide determine its secondary structure.

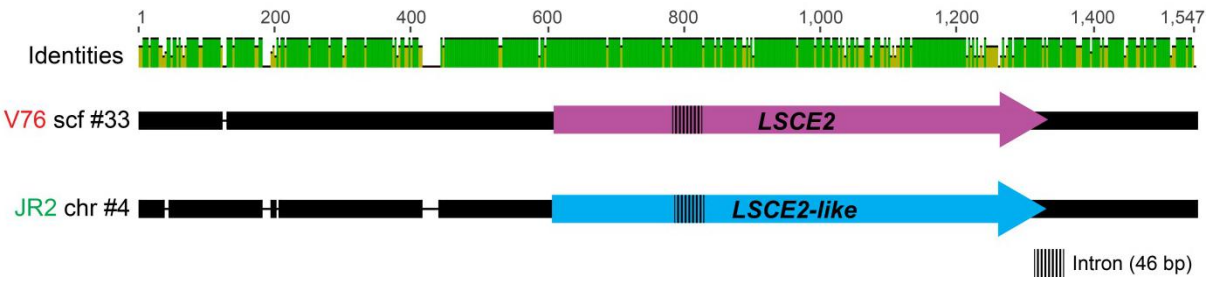

Figure 3.6 A ~ 1500 bp region including *LSCE2* is homologous to a region in the core genome of V76 including *LSCE2-like*. Alignment of a 1538 bp sequence from the LSCE region located on the *V. dahliae* V76 genome assembly scaffold 33 with a homologous region on scaffold 58. Location of *LSCE2* (pink) and *LSCE2-like* (blue) genomic sequences are shown as arrows, the intron is shown in grey. Sequence identities are depicted in the diagram above from high (green) to low (yellow). Indels (Insertion or Deletion) in the alignment are shown as gaps.

To determine whether and how amino acid exchanges may influence the secondary structures of the protein, an *in silico* analysis of the sequences was conducted using the publicly available Chou and Fasman Secondary Structure Prediction server (http://www.biogem.org/tool/chou-fasman/). The resulting prediction suggested that especially amino acid exchanges in the center of the protein sequence (~aa 100 – 160) might have an impact on protein folding (Figure 3.7B). Notably, a coil domain predicted at position 120 in LSCE2 as well as turn and helix motifs in the same area were missing in LSCE2-like. Possibly, this may suggest distinct functions of LSCE2 and LSCE2-like due to an entirely different structural organization patterns.

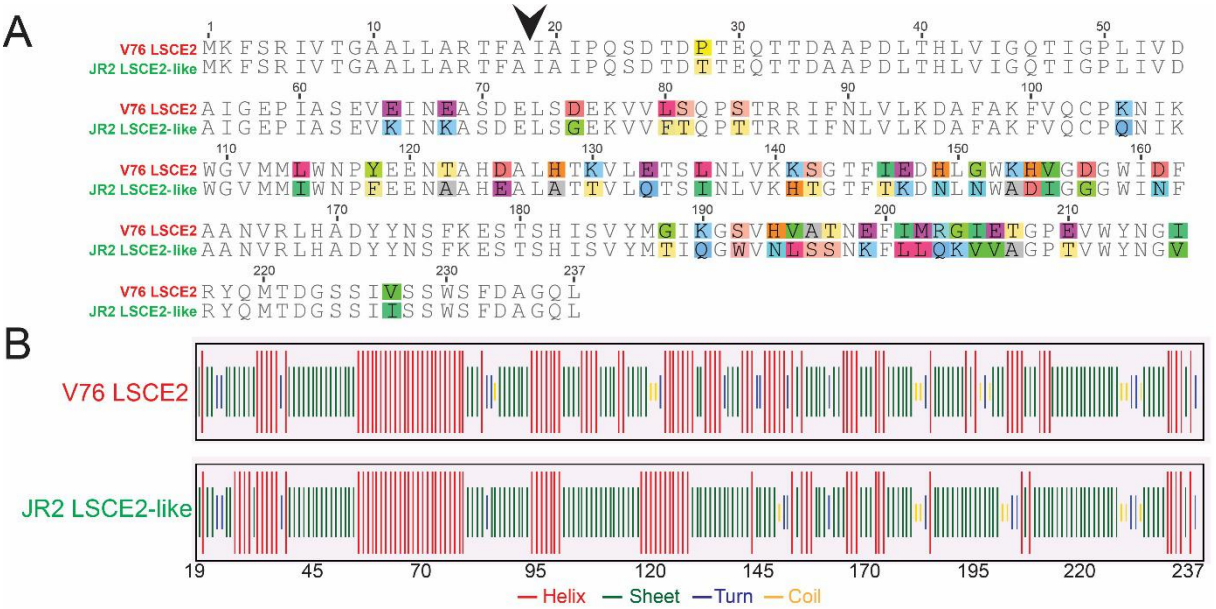

Figure 3.7 Sequence and predicted structural comparisons between V76 LSCE2 and JR2 LSCE2-like. (A) Amino acid sequence alignment of *V. dahliae* V76 LSCE2 and *V. dahliae* JR2 LSCE2-like. Highlighted in color are amino acid exchanges between the sequences. Black arrowhead marks predicted signal peptide cleavage site. (B) Secondary structure prediction of LSCE2 and LSCE2-like without the predicted signal peptide. Structures were predicted using the Chou and Fasman Secondary Structure Prediction server (CFSSP) (Ashok Kumar 2013).

Next, the presence and sequence of *LSCE2* as well as *LSCE2-like* in other *Verticillium spp.* genomes was investigated. To this end, PCR amplification and subsequent sequencing of PCR products was conducted with genomic DNA from 15 *V. dahliae* isolates as well as 10 *V. longisporum* isolates from the chlorosis, wilting and asymptomatic disease class. All *Verticillium spp.* isolates used in this study have been characterized in an earlier study by K. Thole (2016). Using the sequence data, alignments

including the gene sequences of *LSCE2* and *LSCE2-like* were built (Supplement Figure 6.9; Figure 6.10). These analyses confirmed the presence of *LSCE2* exclusively in chlorosis-class *Verticillium spp.* isolates. *LSCE2-like*, on the other hand was found as a single-copy gene in the genomes of all isolates (Table 3.4). In addition, a BLAST homology search in the publicly available NCBI databases (https://blast.ncbi.nlm.nih.gov/Blast.cgi) revealed a *LSCE2* homolog in the genome of *Fusarium oxysporum f. sp. radicis-cucumerinum* Forc016 with sequence similarities of 90.5 and 90 % on the nucleotide and protein level, respectively (Table 3.4). As of yet, no study has characterized this gene in *Fusarium*.

A high level of sequence conservation was observed in *LSCE2* sequences. *LSCE2* was identical in all *V. dahliae* and also in *V. longisporum* chlorosis-class isolates (Supplement Figure 6.9). Furthermore, sequence comparison between the two species revealed similarities of 99.3 % on nucleotide and 98.5 % on the protein level. Interestingly, while assessing the sequencing chromatograms, no nucleotide ambiguities were detected. This suggested that the *LSCE2* copies were identical not only in V76 but also in the other chlorosis-class isolates.

Sequence alignment revealed that *LSCE2-like* encoded a potentially functional gene in asymptomatic and wilting-class *V. dahliae* isolates and in *V. longisporum* VL32 (Supplement Figure 6.10). In the *LSCE2-like* sequences of the *V. dahliae* chlorosis-class isolates, on the other hand, the initial start codon ‘ATG’ was mutated to ‘ATA’ and the spliceosome recognition site ‘GT’ at the beginning of the intron in *LSCE2* was changed to ‘AT’ (Supplement Figure 6.10). Furthermore, in all except one *V. longisporum LSCE2-like* sequences, the fifth (VL35, VL60, VL334) and/or the 16th nucleotide was deleted (Supplement Figure 6.10). The frame shifts very early in the sequences generated completely different amino acid sequences and premature stop codons. Due to the loss of function in these *LSCE2-like* genes, they were designated as pseudogenes. Pseudogenes are defined as genes that are homologous to functional genes but contain disruptive mutations that cause the gene to lose its functionality (Vanin 1985). A loss of functionality is also achieved when a gene is no longer expressed. To assess whether the potentially functional *LSCE2-like* was expressed; semi-quantitative PCR analyses were conducted with fungal material grown *in vitro*. No transcriptional activity of *LSCE2-like* was detected in any *Verticillium spp.* isolate (Figure 3.8).

Table 3.4 Sequence identities of *LSCE2* and *LSCE2-like* gene and protein sequences from 15 *V. dahliae* and 10 *V. longisporum* isolates in comparison to V76 *LSCE.* Genomic and translated protein sequences were aligned in Geneious. Distance matrixes with percent (%) identities were calculated with Geneious v. 8.1.8 from nucleotide and amino acid alignments. Translation of pseudogenes into proteins was not applicable (N/A).

		% Sequence identity with V76 *LSCE2*		
	Isolate	**Nucleotides**	**Amino acids**	
V. dahliae	**T9**	100	100	*LSCE2*
	ST100	100	100	
	V138I	100	100	
	V781I	100	100	
V. longisporum	**VL10**	99.3	98.5	
	VL35	99.3	98.5	
	VL43	99.3	98.5	
	VL60	99.3	98.5	
	VL83	99.3	98.5	
	VL334	99.3	98.5	
V. dahliae	V76*	81.6	N/A	*LSCE2-like*
	T9*	81.6	N/A	
	ST100*	81.6	N/A	
	V138I*	81.6	N/A	
	V781I*	81.6	N/A	
	JR2	90.7	82.1	
	VdLs17	90.7	82.1	
	DVD-S29	90.5	81.6	
	DVD-31	90.5	81.6	
	V192I	90.5	81.6	
	Vd39	90.9	82.4	
	Vd42	90.7	81.9	
	Vd52	90.7	81.9	
	Vd54	90.2	81.9	
	Vd152	90.6	81.9	
V. longisporum	VL10*	92.5	N/A	
	VL35*	90.5	N/A	
	VL43*	92.5	N/A	
	VL60*	92.4	N/A	
	VL83*	92.5	N/A	
	VL334*	92.4	N/A	
	VL13*	92.5	N/A	
	VL18*	92.5	N/A	
	VL24*	92.5	N/A	
	VL32	90.7	82.1	
	Fusarium oxysporum	90.5	90	

Chlorosis

Wilting

Asymptomatic

* Pseudogene

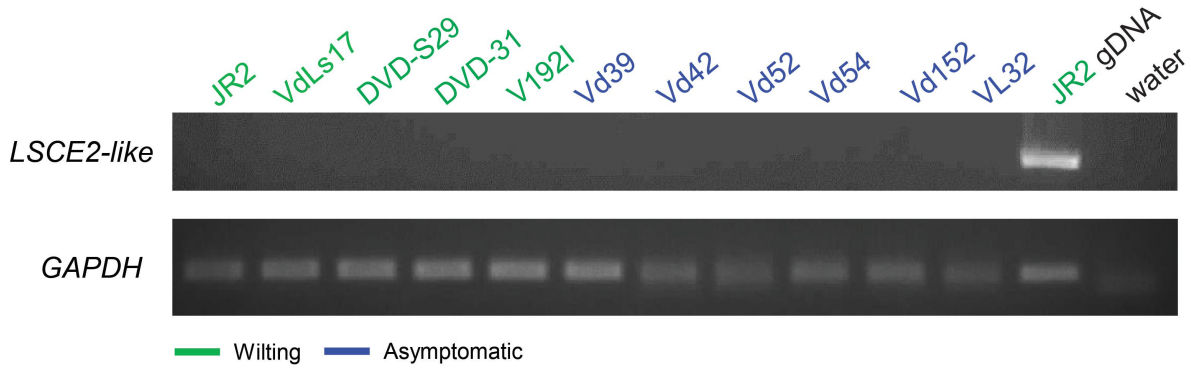

Figure 3.8 Functional *LSCE2-like* is not expressed *in vitro*. Semi-quantitative PCR with cDNA from fungal mycel grown in liquid PDB. The housekeeping gene GAP dehydrogenase was chosen as reference. PCR conditions included 35 cycles. Genomic DNA from *V. dahliae* JR2 was used as positive control and water as negative control. The experiment was repeated twice with identical results.

Overall, *LSCE2-like* genomic sequences were ~ 91 % identical to *LSCE2* on the nucleotide level (Table 3.4). The exception was *LSCE2-like* from chlorosis-class *V. dahliae* isolates which shared only 81.6 % sequence identities with *LSCE2*. To further assess whether a selective pressure influences *LSCE2-like* evolution, the ratio of nonsynonymous substitutions per nonsynonymous site (K_a) to the number of synonymous substitutions per synonymous site (K_s) was calculated within the coding regions for *LSCE2* and *LSCE2-like*. In a pairwise analysis, V76 *LSCE2* was compared to *LSCE2-like* from V76, JR2 and VL43 and *LSCE2* from VL43. None of the K_a/K_s values were significantly ($P < 0.05$) higher or lower than 1, suggesting that neither of the sequences were subject to positive ($K_a/K_s > 1$) or purifying selection ($K_a/K_s > 1$) (Table 3.5).

Table 3.5 Assessment of the selective pressure on *LSCE2* and *LSCE2-like*. 711 bp *LSCE2* and *LSCE2-like* coding sequences from reference isolates *V. dahliae* V76, *V. dahliae* JR2 and *V. longisporum* VL43 were used. Values were calculated with the Nei Gojobori method (Nei and Gojobori 1986) using the Ka_Ks Calculator software (Wang et al. 2010) . Significance ($P < 0.05$) was tested with Fisher's exact test. No significance was detected.

V76 *LSCE2* vs	Nucleotide substitutions (Deletions)	Synonymous substitutions	Non-synonymous substitutions	K_a/K_s
VL43 *LSCE2*	5	1	4	1.18
V76 *LSCE2-like**	134	39	83 (12 stop codons)	0.78
JR2 *LSCE2-like*	69	15	54	1.04
VL43 *LSCE2-like**	55 (1)	12	43	1.03

*Pseudogene

With phylogenetic inference, the evolutionary relationships between *Verticillium spp. LSCE2* and *LSCE2-like* were analyzed. A maximum likelihood phylogenetic tree was calculated from an alignment including 734 bp *LSCE2* and *LSCE2-like* gene sequences from 25 *Verticillium spp.* isolates (Figure 3.9A). The *F. oxysporum f. sp. radicis-cucumerinum LSCE2* homolog was chosen as outgroup. *LSCE2* sequences from *V. dahliae* and *V. longisporum* formed two distinct, highly supported clades which were separated from the *LSCE2-like* clade and the outgroup (Figure 3.9A). Phylogenetic inference did not resolve which one of the *LSCE2* clades was more closely related to *LSCE2-like* and the *F. oxysporum LSCE2* homolog. *LSCE2-like* sequences, on the other hand, formed a single clade with maximal bootstrap support. Within the clade, *LSCE2-like* sequences from *V. longisporum* A1/D1 lineage were grouped together with significant support as were sequences form *V. dahliae* and *V. longisporum* VL32 of the A1/D3 lineage. Within the *V. dahliae LSCE2-like* clade, chlorosis-class isolates formed a separate group whereas asymptomatic and wilting-class isolates were not distinct.

Next, it was assessed whether the topology of the *V. dahliae LSCE2-like* phylogenetic tree matched the topology of a tree inferred with general phylogenetic markers *actin* (*ACT*), *elongation factor 1-alpha* (*EF*), *glyceraldehyde-3-phosphate dehydrogenase* (*GPD*) and *tryptophan synthase* (*TS*) as proposed by Inderbitzin et al. (2011). To this end, a maximum likelihood phylogenetic tree was calculated based on a combined *ACT*, *EF*, *GPD* and *TS* dataset of 2658 characters from all *V. dahliae* isolates and *V. alfalfae* VaMs102 as outgroup (Figure 3.9B). Chlorosis-class isolates formed a distinct, highly supported clade but in contrast to the *LSCE2-like* tree, the asymptomatic isolate Vd39 was grouped together with chlorosis-class isolates. Simultaneously, the bootstrap support of the asymptomatic/wilting-class clade decreased from high (93 %) in the *LSCE2-like* tree to low (66 %) in the general tree. Again, asymptomatic and wilting-class *V. dahliae* isolates did not form distinct phylogenetic clades. Taken together, the similarities between the two phylogenetic trees suggest that in *V. dahliae LSCE2-like* evolved at rates similar to those of the phylogenetic marker genes used here. This would be expected of genes in the core genome. The data did not allow a similar analysis with *LSCE2* due the fact that *LSCE2* gene sequences as well as phylogenetic marker sequences were identical in all *V. dahliae* chlorosis-class isolates.

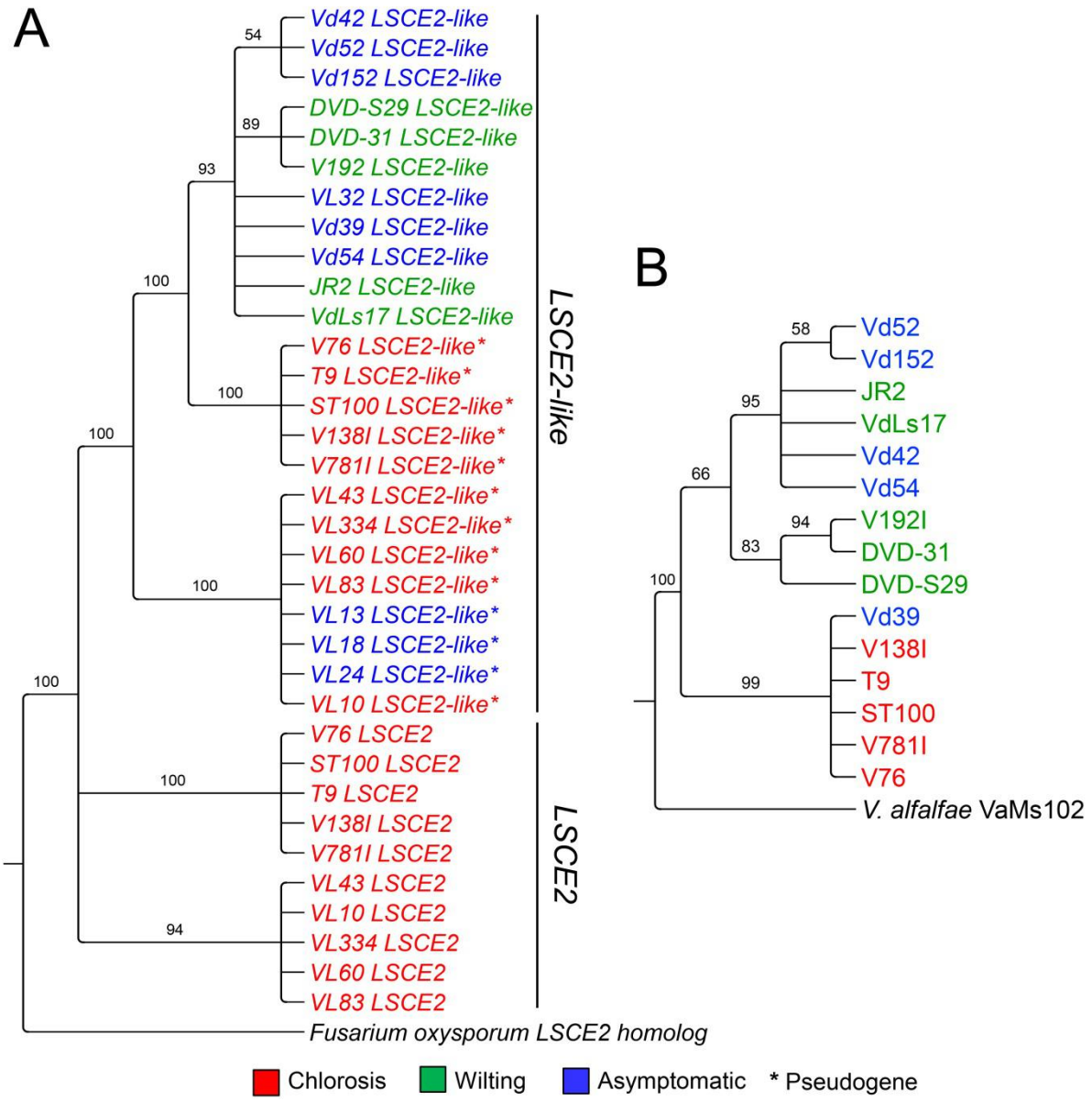

Figure 3.9 *Verticillium spp. LSCE2* and *LSCE2-like* sequences form distinct groups in a phylogenetic tree. (A) Maximum likelihood phylogenetic tree based on gene sequences (734 bp) of *LSCE2* and/or *LSCE2-like* from *Verticillium spp.* chlorosis (red), wilting (green) and asymptomatic (blue) isolates. Pseudogenes are marked with asterisks. A *LSCE2* homologous sequence from *Fusarium oxysporum f. sp. radicis-cucumerinum* Forc016 was chosen as outgroup. Note that only one *LSCE2* copy is shown per isolate as these copies were identical in all isolates. (B) Maximum likelihood phylogenetic tree of 14 *V. dahliae* isolates based on a combined dataset of four marker genes (*actin, elongation factor 1-alpha, glyceraldehyde-3-phosphate dehydrogenase and tryptophan synthase*). Verticillium alfalfae VaMs102 was chosen as outgroup. Bootstrap consensus trees based on 1000 bootstrap replicates are shown. Nodes were included when bootstrap support values were ≥ 50.

3.3 Characterization of *Verticillium spp. LSCE2* knockout and transgene lines regarding their disease phenotype on *A. thaliana*

3.3.1 Deletion of one or both *LSCE2* copies in chlorosis-class isolates *V. dahliae* V76 and *V. longisporum* VL43 has no effect on fungal morphology

Verticillium genes can be deleted via site-directed homologous recombination (Amey et al. 2003). This method is based on an endogenous DNA repair mechanism where identical sequences are swapped between two DNA strands (Folger et al. 1982) . Accordingly, *LSCE2* knockout constructs were designed to contain antibiotic resistance cassettes flanked by up- and downstream *LSCE2* sequences. Homologous recombination was triggered by the two flanking sequences, resulting in the integration of the resistance cassette and loss of *LSCE2*. Due to the fact that *LSCE2* was present in two identical copies in the genomes of *V. dahliae* V76 and *V. longisporum* VL43 (Figure 3.3), single knockout lines had to be transformed a second time with a construct containing a different antibiotic resistance cassette. The correct integration and resulting replacement of the wild-type *LSCE2* gene with the resistance cassette was tested via Southern blot analyses. With this method it is not only possible to confirm the correct insertion of the construct but also discover possible ectopic insertions of the construct. Ectopic, random integration of inserts into the target genome is mediated by non-homologous end joining, a fungal repair mechanism for DNA double strand breaks (Moore and Haber 1996) . Random insertions can cause the disruption of genes anywhere in the genome and are therefore to be avoided. The signals detected after Southern hybridization for *Verticillium spp.* wild-type (WT), single (Δ) and double (ΔΔ) *LSCE2* knockout lines corresponded in general to the expected fragment sizes (Figure 3.10A). V76ΔΔ*LSCE2* line #1 lacked the expected signal for the Nourseothricin cassette in both blots and showed an additional signal in the BbsI blot (Figure 3.5B and C). However, no signal corresponding to wild-type *LSCE2* was detected, suggesting that V76ΔΔ*LSCE2* line #1 was a true double knockout. Here, the Nourseothricin cassette was inserted either ectopically or in a way different than expected. A weak additional signal was observed in the Bme1390I blot corresponding to the *LSCE2-like* region (Figure 3.5A). The *LSCE2-like* region was detected due to sequence homologies between the 3' flanking region of *LSCE2* and *LSCE2-like*.

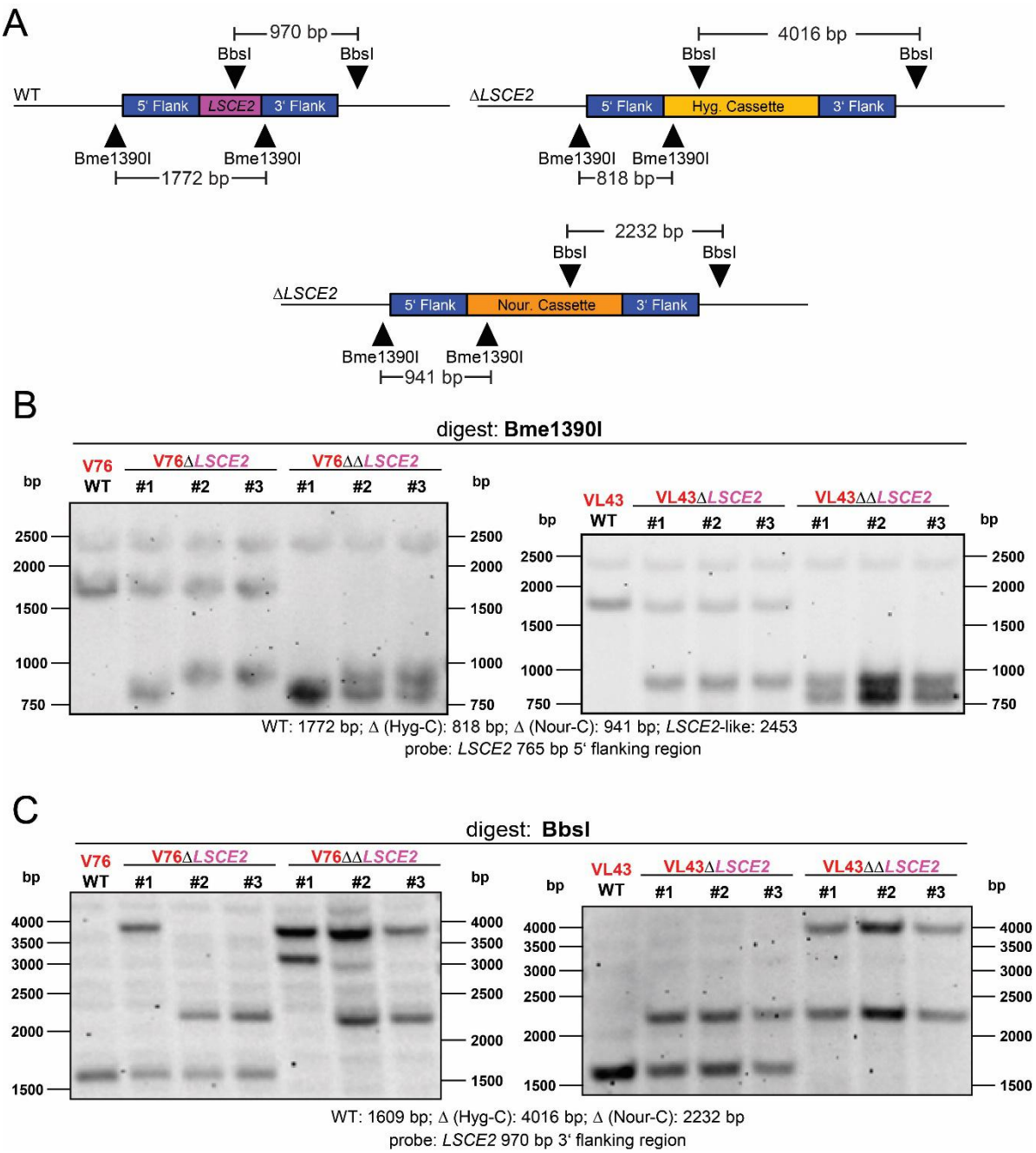

Figure 3.10 Confirmation of *Verticillium spp. LSCE2* single- and double knockout lines via Southern Blot hybridization. (A) Schematic illustration of *LSCE2* region in the genomes of wild-type (WT) isolates and knockout lines. 765 bp 5' flanking region and 970 bp 3' flanking regions used as probes are shown as blue boxes. LSCE2 is shown as a pink box. Hygromycin (Hyg) and Nourseothricin (Nou) resistance cassettes are shown as yellow and orange boxes, respectively. Restriction sites are represented as black triangles. Sizes of the expected fragments are shown above and below restriction sites. (B) gDNA of WT *V. dahliae* V76, *V. longisporum* VL43 and single (Δ) as well as double (ΔΔ) *LSCE2* knockout lines was digested with Bme1390I. Hybridization and signal detection with 765 bp *LSCE2* 5' flanking region. Three individual lines are shown for each knockout construct. (C) gDNA of WT *V. dahliae* V76, *V. longisporum* VL43 and single (Δ) as well as double (ΔΔ) *LSCE2* knockout lines was digested with BbsI. Hybridization and signal detection with 970 bp *LSCE2* 3' flanking region. Three individual lines are shown for each knockout construct.

In order to address the question whether or not a loss of one or both copies of *LSCE2* resulted in pleiotropic growth and fitness effects outside the plant host a comparative fungal growth assay on nutrient-poor Czapec-Dox agar plates was performed. To this end, spore solutions from wild-type isolates and knockout lines were pipetted onto nutrient-poor CDB agar plates and incubated at short day conditions for three weeks. These experiments showed that neither morphology (Figure 3.11A, Figure 3.12A) nor overall colony growth (Figure 3.11B; Figure 3.12B) was affected in *Verticillium spp. LSCE2* knockout lines. Overall, *in vitro* growth of *V. longisporum* VL43 was slower compared to *V. dahliae* V76, which may be the consequence of the near-diploid VL43 genome. Similar results were observed earlier by K. Thole who found that although growth rates of V76 and VL43 were different, both isolates induced strong disease symptoms (Thole 2016).

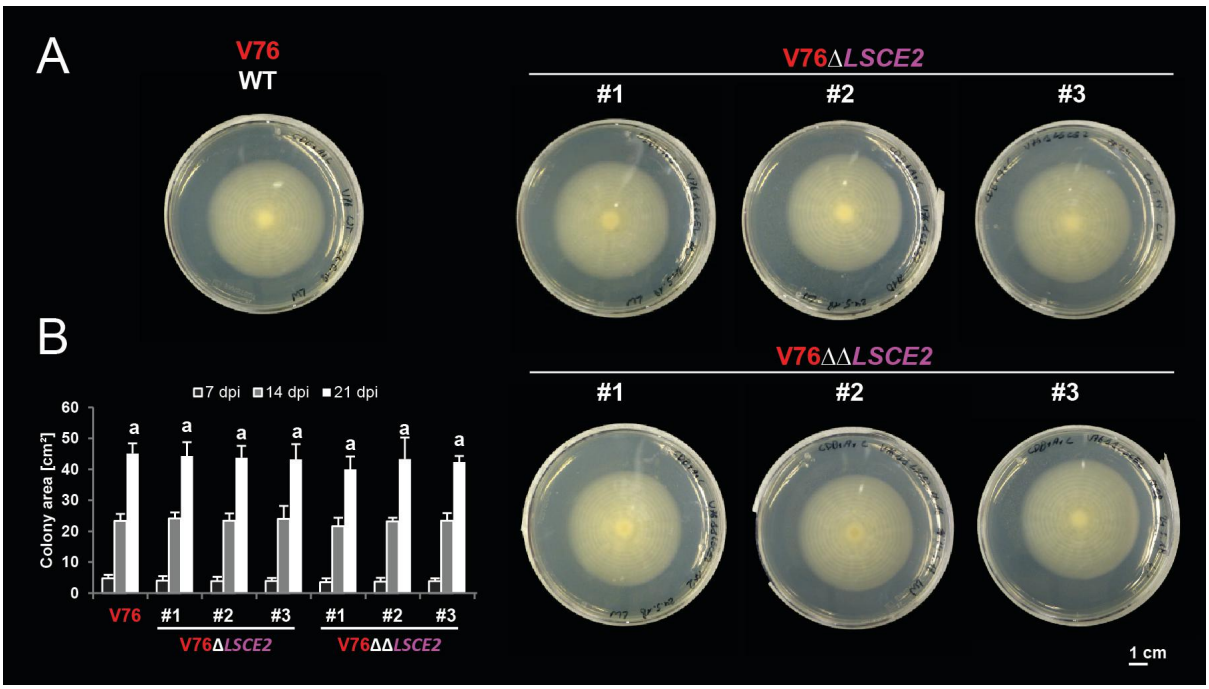

Figure 3.11 Deletion of one or both *LSCE2* copies in *V. dahliae* V76 did not affect fungal *in vitro* growth. (A) Growth phenotypes of V76 wild-type (WT), *LSCE2* single (Δ) and double (ΔΔ) knockout lines. 5 µl of a 10^6 spores/ml suspension were pipetted onto Czapec Dox agar plates (CDA) and incubated upside down at short day conditions for three weeks. Photographic pictures were taken after 14 days of growth. (B) Colony area 7, 14 and 21 days post inoculation (dpi). Error bars represent standard deviation and different letters indicate significant differences at 21 dpi according to Student's t-test ($P \leq 0.05$). Two plates were used per biological replicate (n), n = 3.

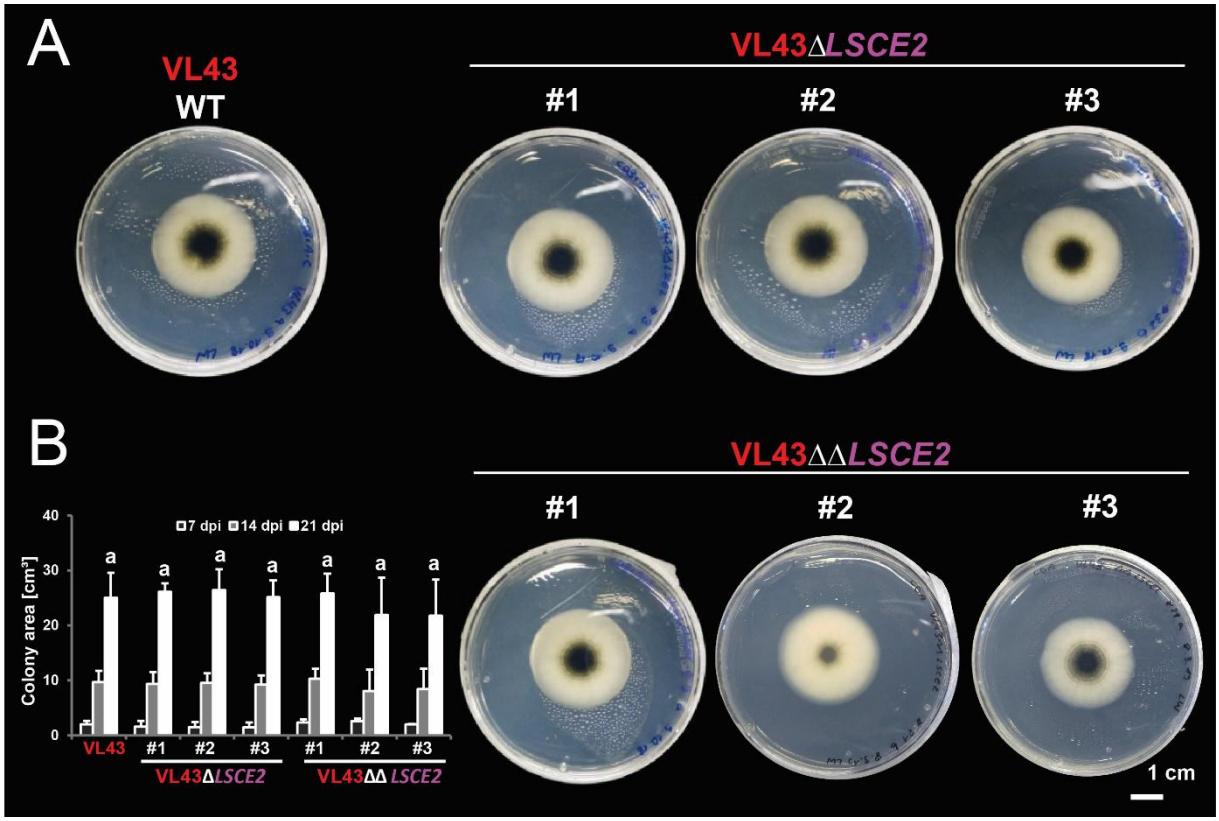

Figure 3.12 Deletion of one or both *LSCE2* copies in *V. longisporum* VL43 did not affect fungal *in vitro* growth. (A) Growth phenotypes of VL43 wild-type (WT), *LSCE2* single (Δ) and double (ΔΔ) knockout lines. 5 µl of a 10^6 spores/ml suspension were pipetted onto Czapec Dox agar plates (CDA) and incubated upside down at short day conditions for three weeks. Photographic pictures were taken after 14 days of growth. (B) Colony area 7, 14 and 21 days post inoculation (dpi). Error bars represent standard deviation and different letters indicate significant differences at 21 dpi according to Student's t-test (P≤0.05). Two plates were used per biological replicate (n), n = 3.

3.3.2 *LSCE2* is required for the establishment of chlorosis-class specific disease symptoms induced by *V. dahliae* and *V. longisporum*

3.3.2.1 *Verticillium spp.* ΔΔ*LSCE2* lines are unable to induce stunting or chlorosis on Arabidopsis

Deletion of *Verticillium spp.* effectors has in previous studies been shown to reduce pathogen virulence and consequently disease symptoms on host plants (Zhang et al. 2016; Kombrink et al. 2017; Marton et al. 2018). Plants infected with the chlorosis-class isolates *V. dahliae* V76 or *V. longisporum* VL43 were monitored for three weeks post infection. Photographs were taken weekly to monitor disease symptom development and plant growth. The severity of stunting induced by *Verticillium spp.* infection was determined by measuring the total surface of the rosette leaves. Plants infected with *Verticillium spp.* displayed strong macroscopic disease symptoms 21 days post infection (dpi) (Figure 3.13; Figure 3.14). Chlorosis of older rosette leaves and overall stunting of the plants after infection with *V. dahliae* V76 and *V. longisporum* VL3 was observed and corresponded to chlorosis-class symptoms described in earlier studies (Reusche et al. 2012; Thole 2016). *Verticillium spp. LSCE2* single knockout (Δ*LSCE2*) lines induced chlorosis on older Arabidopsis rosette leaves to an extent qualitatively indiscernible from chlorosis induced by the wild-type isolates. Stunting of plants infected with wild-type chlorosis-class *Verticillium spp.* was not significantly different from stunting of plants infected with Δ*LSCE2* lines (Figure 3.13B; Figure 3.14B). Deletion of both *LSCE2* copies, on the other hand, had a strong effect on the disease phenotype. Plants infected with ΔΔ*LSCE2* were not stunted in comparison to mock-treated plants and plants infected with the asymptomatic *V. longisporum* isolate VL32 (Figure 3.13B, Figure 3.14B). Concomitantly, no chlorosis was observed on rosette leaves (Figure 3.13A, Figure 3.14A). This was consistent in both *V. dahliae* V76 and *V. longisporum* VL43 ΔΔ*LSCE2* lines. Interestingly, during infection with V76 ΔΔ*LSCE2* lines, wilting of one or two leaves per infected plant was observed (Figure 3.13A). This was unexpected since deletion of an effector usually results in a decrease in virulence but not a change in disease symptoms. Wilting was not observed in plants infected with VL43 ΔΔ*LSCE2* lines.

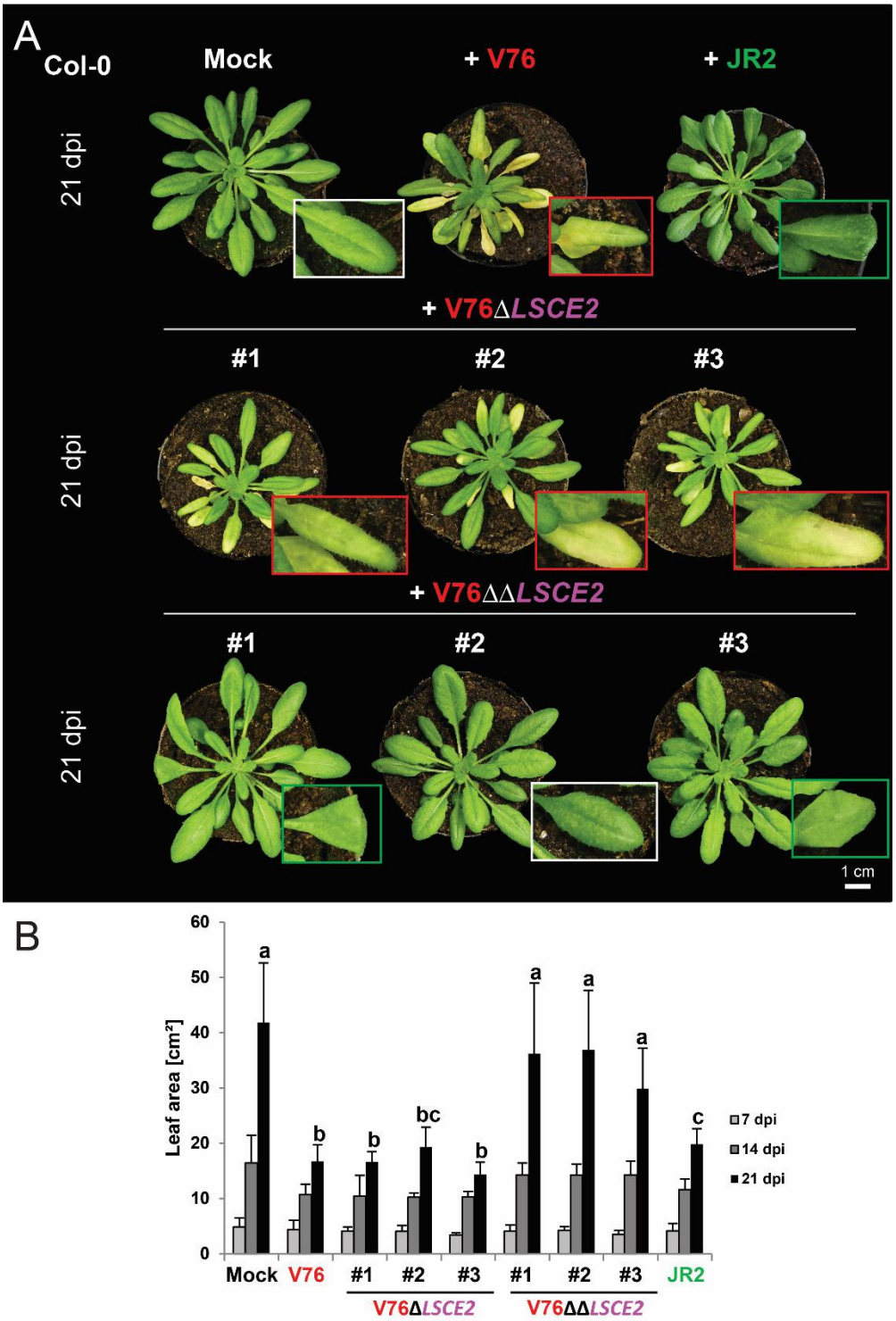

Figure 3.13 Disease phenotype of *A. thaliana* Col-0 infected with *V. dahliae* WT isolates V76, JR2 and V76 *LSCE2* single (Δ) and double (ΔΔ) knockout lines. (A) Plants were photographed 21 days post infection (dpi). Red boxes show examples for chlorotic leaves, green boxes show wilted leaves and white boxes show leaves without disease symptoms (B) Total leaf area 7, 14 and 21 dpi. Error bars represent standard deviation and different letters indicate significant differences at 21 dpi according to Student's t-test ($P \leq 0.05$). Four plants were used per biological replicate (n), n = 3.

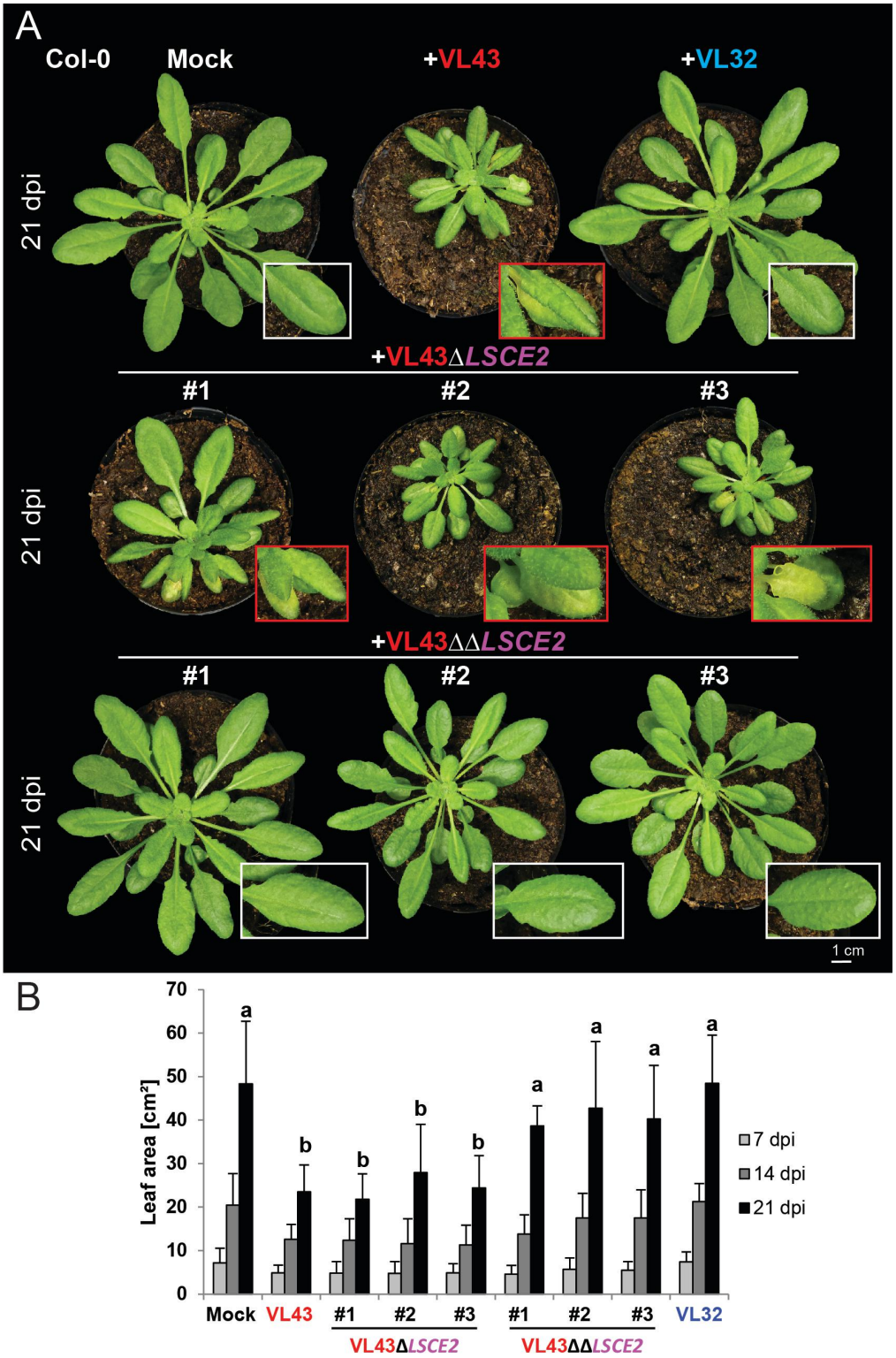

Figure 3.14 Disease phenotype of *A. thaliana* Col-0 infected with *V. longisporum* WT isolates VL43, VL32 and VL43 *LSCE2* single (Δ) and double (ΔΔ) knockout lines. (A) Plants were photographed 21 days post infection (dpi). Red boxes show examples for chlorotic leaves and white boxes show leaves without disease symptoms (B) Total leaf area 7, 14 and 21 dpi. Error bars represent standard deviation and different letters indicate significant differences at 21 dpi according to Student's t-test (P≤0.05). Four plants were used per biological replicate (n), n = 3.

3.3.2.2 *Verticillium spp.* ΔΔ*LSCE2* lines are unable to induce transdifferentiation of bundle sheath cells into xylem elements in Arabidopsis leaves

In earlier studies it has been demonstrated that *Verticillium spp.* chlorosis-class isolates trigger transdifferentiation of bundle sheath cells into functional xylem elements (Reusche et al. 2012; Thole 2016). It was therefore investigated in this study whether deletion of *LSCE2* had an effect on the ability to induce transdifferentiation in Arabidopsis leaves. In order to generate comparable, quantitative data, a defined region on the 5th leaf from infected Arabidopsis plants was evaluated at 21 dpi. To this end, the number of bundle sheath cells and *de novo* formed xylem elements was counted in the section of the third secondary leaf vein between the first and third tertiary leaf vein (Figure 3.15). From these data, the transdifferentiation (TD) ratio was calculated by dividing the number of bundle sheath cells counted on both sides of the vascular bundle by the number of transdifferentiated bundle sheath cells.

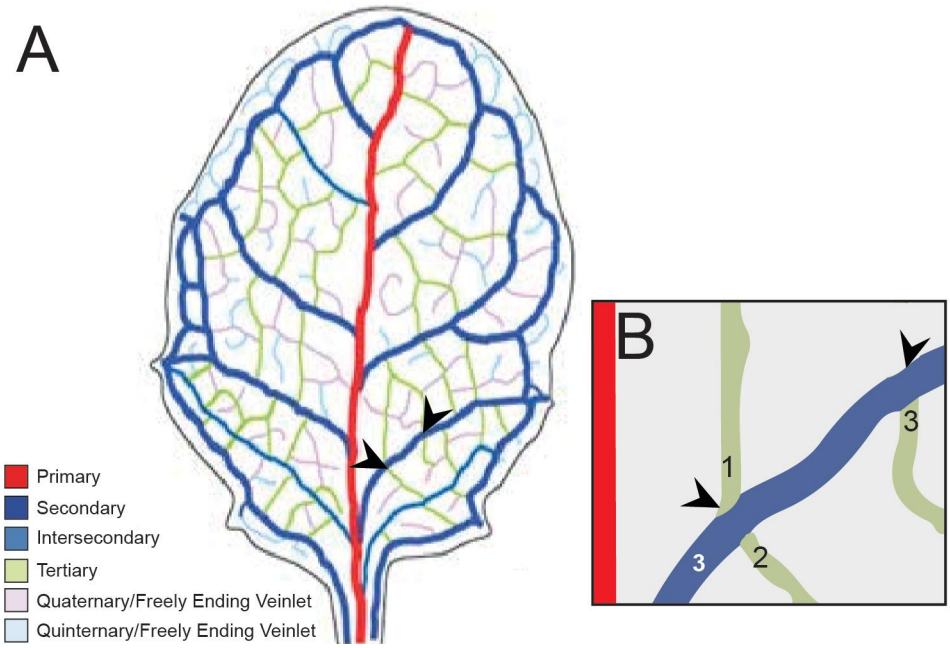

Figure 3.15 Evaluation site for the evaluation of bundle sheath cell transdifferentiation. (A) Longitudinal pinnate vein pattern showing vein order hierarchy of mature Arabidopsis leaf. View represents the abaxial side of the leaf. Colors represent: Red = Primary (mid) vein (1st order); dark blue = secondary vein (2nd order); medium blue = intersecondary vein (2nd order); green = tertiary (3rd order); purple = quaternary (4th order); light blue = quinternary (5th order). Figure and figure legend adopted and modified from (Kang et al. 2007). (B) Section vein of the third secondary leaf vein between first and third tertiary leaf vein of the third secondary leaf vein. Black arrowheads mark beginning and end of evaluation site.

As expected, no transdifferentiation was detected in mock-treated plants and plants infected with wilting-class isolate *V. dahliae* JR2 (Figure 3.16A). Notably, TD was also not observed in plants infected with V76 ΔΔ*LSCE2* lines. Wild-type isolate V76 and Δ*LSCE2* lines, on the other hand, were able to trigger TD. Furthermore, the TD ratios calculated for V76 Δ*LSCE2* lines (0.59; 0.51; 0.53) were not significantly different from wild-type V76 (0.59) (Figure 3.16B). Similar observations were made with *V. longisporum* wild-type isolates and *LSCE2* knockout lines. Asymptomatic *V. longisporum* isolate VL32 as well as VL43 ΔΔ*LSCE2* lines did not induce transdifferentiation whereas TD was observed in plants infected with wild-type VL43 and VL43 Δ*LSCE2* lines (Figure 3.17A). Again, the TD ratios calculated after infection with VL43 Δ*LSCE2* lines (0.41; 0.37; 0.38) did not differ significantly from wild-type VL43 (0.49) (Figure 3.17B). Taken together, the data suggested that deletion of one *LSCE2* copy had no effect on the ability of the lines to induce TD. A double deletion of *LSCE2*, however, completely abolished transdifferentiation of bundle sheath cells in Arabidopsis

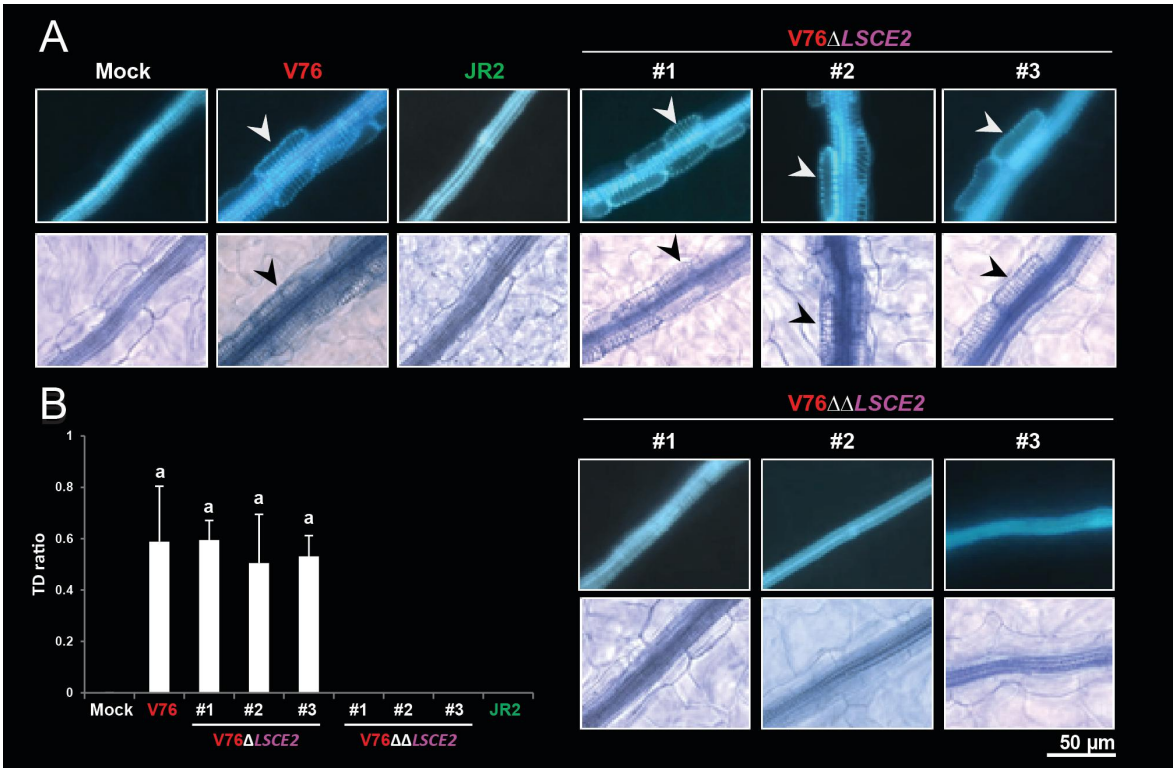

Figure 3.16 Transdifferentiation of bundle sheath cells in leaves of infected *A. thaliana*. (A) Microscopic images of Arabidopsis leaf veins 21 days after mock treatment or infection with wild-type *V. dahliae* V76 and JR2 as well as three V76 single (Δ)- and double (ΔΔ) *LSCE2* knockout lines, respectively. Leaves were stained with trypan blue. Top row: epifluorescence microscopy, bottom row: bright field microscopy. White and black arrowheads mark transdifferentiated bundle sheath cells. (B) Transdifferentiation (TD) ratio, calculated from the fifth leaf of infected *A. thaliana* leaves 21 dpi. Error bars represent standard deviation and different letters indicate significant differences according to Student's t-test (P≤0.05). Four plants were used per biological replicate (n), n = 3.

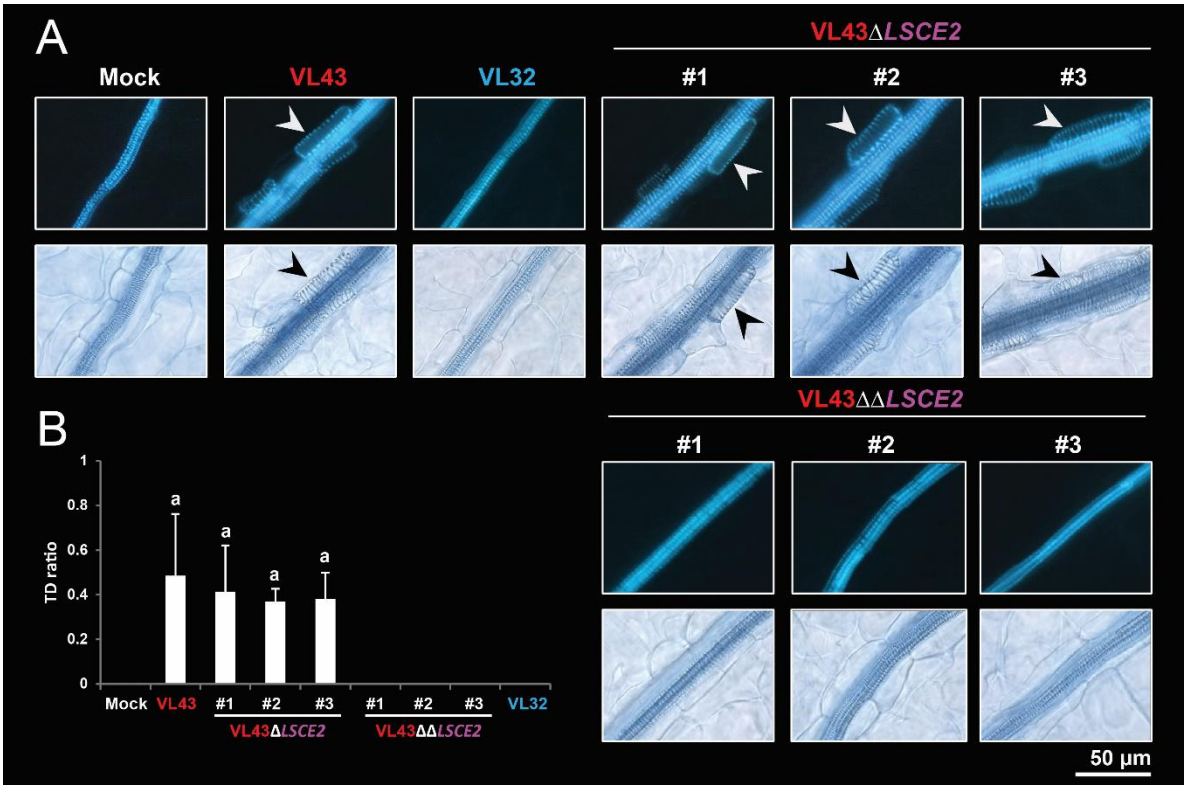

Figure 3.17 Transdifferentiation of bundle sheath cells in leaves of infected *A. thaliana*. (A) Microscopic pictures of Arabidopsis leaf veins 21 days after mock treatment or infection with wild-type *V. longisporum* VL43 and VL32 as well as three VL43 single (Δ)- and double (ΔΔ) *LSCE2* knockout lines, respectively. Leaves were stained with trypan blue. Top row: epifluorescence microscopy, bottom row: bright field microscopy. White and black arrowheads mark transdifferentiated bundle sheath cells. (B) Transdifferentiation (TD) ratio, calculated from the fifth leaf of infected *A. thaliana* leaves 21 dpi. Error bars represent standard deviation and different letters indicate significant differences according to Student's t-test (P≤0.05). Four plants were used per biological replicate (n), n = 3.

3.3.2.3 *Verticillium spp.* ΔΔ*LSCE2* lines are unable to induce xylem hyperplasia in vascular bundles of Arabidopsis leaves

Bundle sheath cells in plants infected with chlorosis-class *Verticillium spp.* isolates are not the only targets of developmental reprogramming induced by the pathogen. It has previously been demonstrated that xylem hyperplasia of the vascular bundle is induced during chlorosis-class infections (Reusche et al. 2012) . Xylem hyperplasia is defined by the significant increase in xylem elements within the vascular bundle. The number of xylem elements is increased by transdifferentiation of xylem parenchyma cells and the reactivation of cambial activity (Figure 3.19).

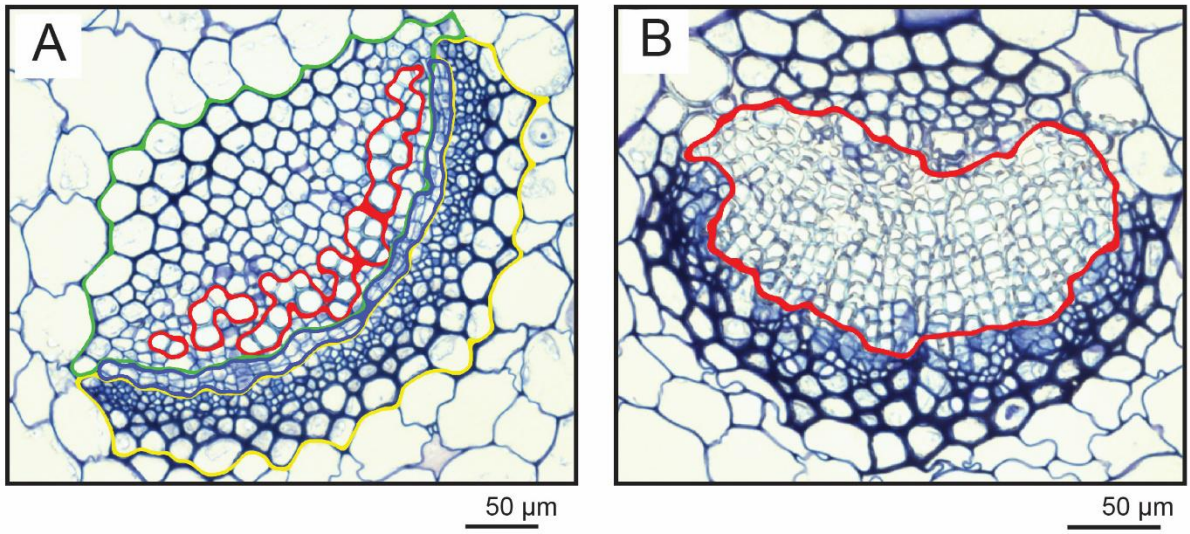

Figure 3.18 Xylem hyperplasia induced by chlorosis-class *Verticillium spp.* isolates. Bright field microscopy images of 5 µm microtome sections stained with toluidine blue. (A) Enlarged midrib transection from mock-treated plant. Xylem parenchyma (green), xylem elements (red), cambium (dark blue) and phloem (yellow) are encircled. (B) Enlarged midrib transection showing hyperplasia after infection with chlorosis-class *V. dahliae* V76. Hyperplastic xylem is encircled in red.

In order to test the effect of deleting one or both *LSCE2* copies on hyperplasia formation, leaf midrib transections were evaluated. Representative leaves from infected and mock-treated plants were harvested at 21 and 28 dpi. Transections from these leaves were embedded and cut into 5 µm microtome sections. These microtome sections were evaluated under epifluorescent light to detect lignin autofluorescence from plant cell walls. Subsequently, cell walls were histochemically stained with toluidine blue and sections were viewed in the bright field. In mock-treated plants, mature xylem vessels, which were discernable by the blue autofluorescence of lignin, were present in files of ~ 2 – 3

cells, surrounded by xylem parenchyma and separated from the phloem by cambium cells (Figure 3.19A). Midrib transections of plants infected with wilting-class isolate JR2 had similar cell distributions. However, xylem element cell walls appeared thicker in the bright field and a stronger autofluorescence signal was detected compared to both mock-treated plants and plants infected with chlorosis-class isolate V76 (Figure 3.19A). An increase in xylem autofluorescence has been associated in earlier studies with enhanced lignification as a plant response to pathogen attack (Reusche et al. 2014; Thole 2016) . Leaf midrib transections from plants infected with the wild-type chlorosis-class isolate V76 displayed symptoms typical for the chlorosis-class disease phenotype, including transdifferentiation of xylem parenchyma cells and disappearance of cambium cells in favor of additional xylem element files (Reusche et al. 2012). Consistent with observations of other disease symptoms, no difference in xylem hyperplasia induction was observed in plants infected with Δ*LSCE2* lines when compared to wild-type infections. No signs of developmental reprogramming were detected in midrib transections of plants infected with ΔΔ*LSCE2* lines (Figure 3.19, Figure 3.20). However, wilting of leaves induced by V76 ΔΔ*LSCE2* lines was accompanied by enhanced lignification of xylem elements (Figure 3.19A). This indicated that the plant immune system reacted to V76 ΔΔ*LSCE2* lines with an immune response similar to wilting-class infections.

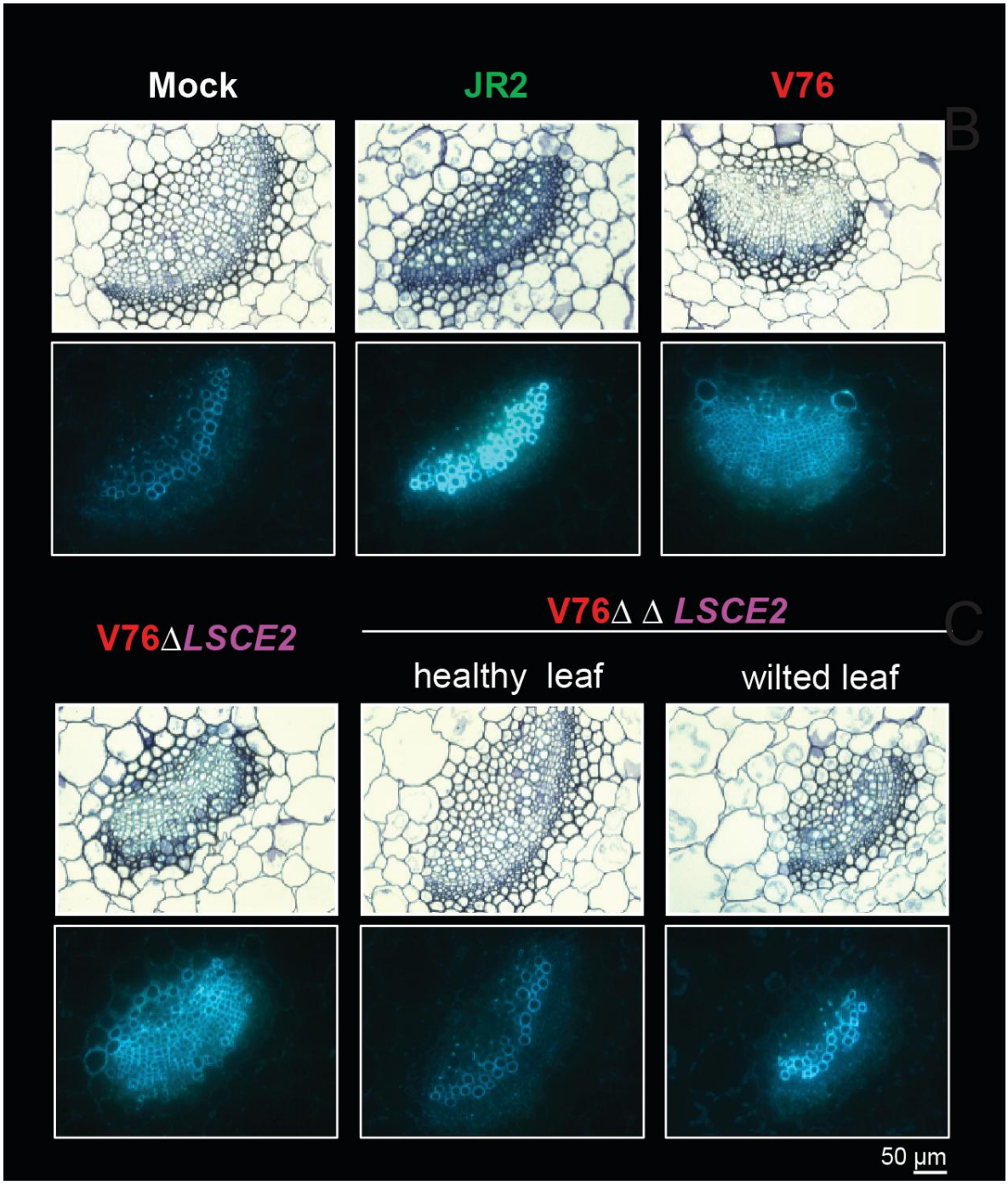

Figure 3.19 Leaf midrib transections show xylem hyperplasia formation in Arabidopsis plants infected with chlorosis-class isolate *V. dahliae* V76 and V76 Δ*LSCE2* lines. Microscopic images of leaf midrib transections from plants infected with WT *V. dahliae* JR2, *V. dahliae* V76, V76 Δ*LSCE2* and V76 ΔΔ*LSCE2,* respectively. Representative leaves with distinct disease symptoms and healthy leaves from mock-treated and V76 ΔΔ*LSCE2* infected plants were harvested at 28 dpi. Leaf transections were embedded before sectioning. 5 µm microtome sections were used for subsequent microscopic analyses. Top row: Bright field microscopy images of sections stained with toluidine blue. Bottom row: Epifluorescence microscopy images of unstained sections.

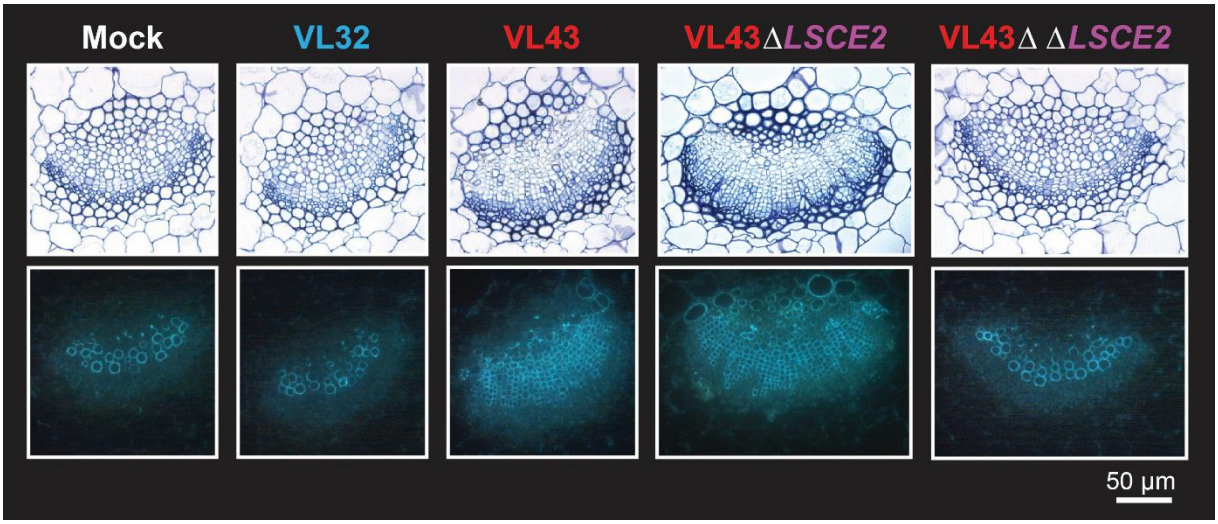

Figure 3.20 Leaf midrib transections show xylem hyperplasia formation in Arabidopsis plants infected with chlorosis-class isolate *V. longisporum* VL43 and VL43 Δ*LSCE2* lines. Microscopic images of leaf midrib transections from plants infected with WT *V. longisporum* VL43, WT *V. longisporum* VL32, VL43 Δ*LSCE2* and VL43 ΔΔ*LSCE2,* respectively. Representative leaves with distinct disease symptoms and healthy leaves from mock-treated and VL43 ΔΔ*LSCE2* infected plants were harvested at 21 dpi. Leaf transections were embedded before sectioning. 5 µm microtome sections were used for subsequent microscopic analyses. Top row: Bright field microscopy images of sections stained with toluidine blue. Bottom row: Epifluorescence microscopy images of unstained sections.

3.3.2.4 Deletion of *LSCE2* decreases virulence only in *V. dahliae* ΔΔ*LSCE2* lines

Verticillium spp. infect host plants through their roots and colonize xylem vessels within the plant vasculature (Fradin and Thomma 2006) . After successful colonization of the root vasculature, the fungus proceeds to colonize aerial tissues though the physical presence of fungal mycelia is not required for the establishment of chlorosis-class disease symptoms (Reusche et al. 2014). It has been shown, however, that disease severity can correlate with the amount of fungal biomass detected within the host plant (Jiménez-Díaz et al. 2017). In past studies, various methods have been implemented to quantify fungal proliferation *in planta*. Here, quantitative real-time PCR (qRT-PCR) was chosen to approximate fungal biomass accumulation within the aerial tissues of the plant by comparing amplification of the Arabidopsis reference gene *AtUBQ5* (AT3G62250) with the *Verticillium spp.* reference gene *Vsp.ß-tubulin* (VDAG_10074).

At 21 dpi, differences in host plant colonization were most pronounced (Figure 3.21). As reported in earlier studies, chlorosis-class isolate V76 colonized Arabidopsis to a significantly higher degree compared to wilting-class isolate JR2 (Thole 2016; Stepanets 2018). Fungal proliferation did not differ significantly between infections with the V76 wild-type and V76 Δ*LSCE2* lines. This corresponded to the earlier observation that Δ*LSCE2* lines also induced disease symptoms identical to wild-type V76 (Figure 3.13; Figure 3.16 and Figure 3.19). ΔΔ*LSCE2* lines, on the other hand, colonized Arabidopsis to a significantly lower degree. Notably, colonization of aerial tissues by *V. dahliae* ΔΔ*LSCE2* lines was not completely abolished but reduced in comparison to the wild-type isolate. Moreover, fungal biomass accumulation of V76 ΔΔ*LSCE2* line #3 was not significantly different from wilting-type isolate JR2.

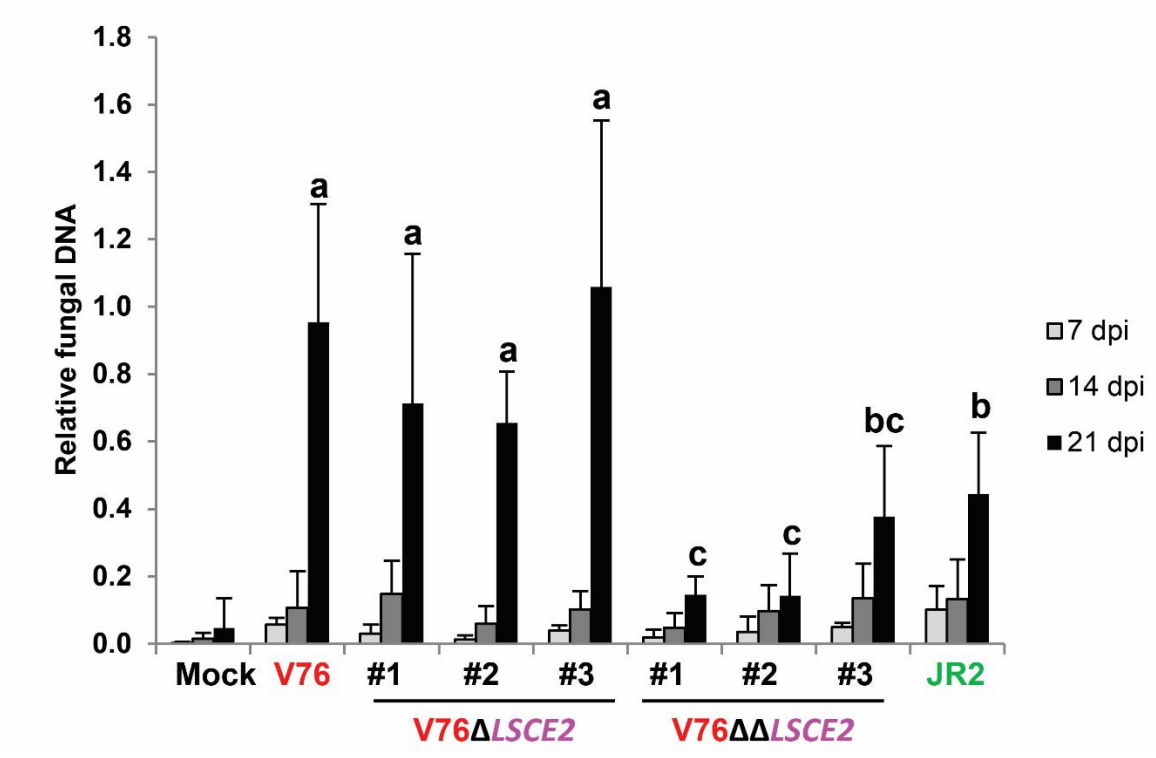

Figure 3.21 Quantification of fungal *in planta* proliferation. QRT-PCR was performed with DNA extracted at 7, 14 and 21 dpi from leaf rosettes of plants mock-treated or infected with *V. dahliae* wild-type V76 and JR2 as well as three V76 single (Δ)- and double (ΔΔ) *LSCE2* knockout lines, respectively. Data are based on ΔΔCq values, using *AtUBQ5* as reference and *Vsp.ß-tubulin* as target sequences. Error bars represent standard deviation and different letters indicate significant differences at 21 dpi according to Student's t-test (P≤0.05). Four plants were used per biological replicate (n), n = 3.

The relative amount of fungal DNA detected at 7 and 14 dpi in plants infected with *V. longisporum* wild-type and deletion lines was higher compared to what was detected after corresponding *V. dahliae* infections (Figure 3.23). Similar results were shown in a previous study (Thole 2016) . This demonstrated that *V. longisporum*, a pathogen adapted to brassicaceous hosts, infects Arabidopsis at earlier time points more successfully than *V. dahliae*. Furthermore, no changes in *in planta* DNA accumulation were observed between both single- and double *LSCE2* knockout lines and wild-type VL43. In addition, VL43-like levels of fungal DNA were detected in plants infected with asymptomatic isolate VL32 (Figure 3.22). Taken together these data suggest that in *V. longisporum* infections, fungal proliferation rates did not correlate with disease severity and that the absence of *LSCE2* did not impair the ability of VL43 ΔΔ*LSCE2* lines to colonize aerial plant tissues.

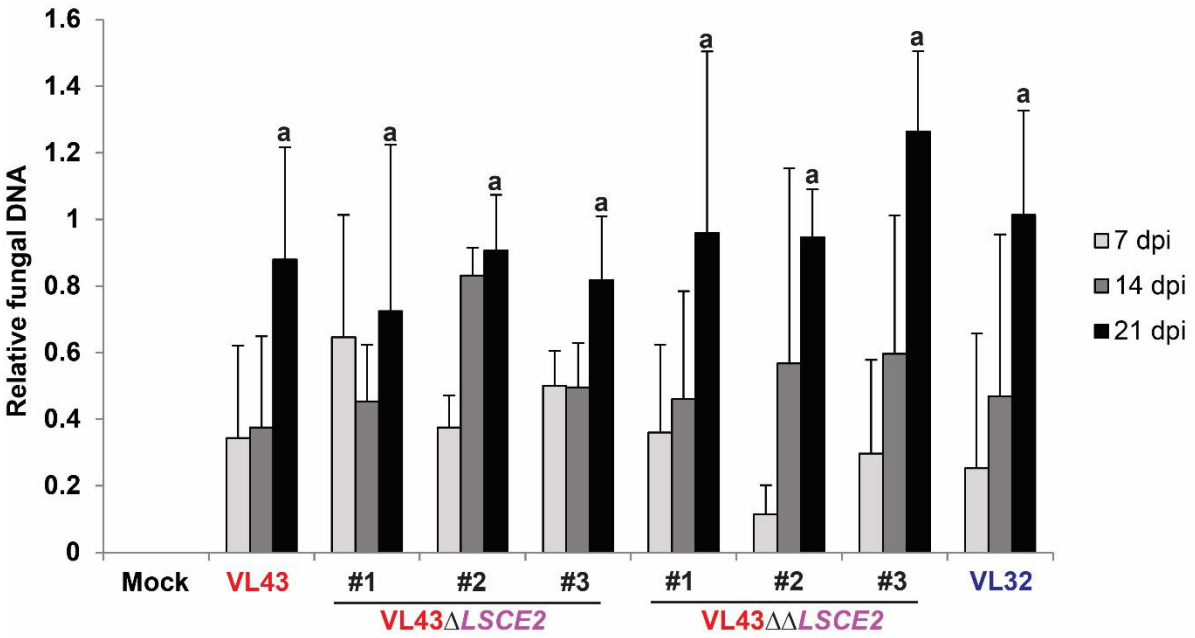

Figure 3.22 Quantification of fungal *in planta* proliferation. QRT-PCR was performed with DNA extracted at 7, 14 and 21 dpi from leaf rosettes of plants mock-treated or infected with *V. longisporum* wild-type VL43 and VL32 as well as three VL43 single (Δ)- and double (ΔΔ) *LSCE2* knockout lines, respectively. Data are based on ΔΔCq values, using *AtUBQ5* as reference and *Vsp.ß-tubulin* as target sequences. Error bars represent standard deviation and different letters indicate significant differences at 21 dpi according to Student's t-test (P≤0.05). Four plants were used per biological replicate (n), n = 3.

In summary, while deletion of one or both *LSCE2* copies in *V. dahliae* or *V. longisporum* had no effect on fungal *in vitro* growth (3.3.1), complete deletion of *LSCE2* had a drastic impact on the chlorosis-class disease phenotype (3.3.2), as V76 and VL43 ΔΔ*LSCE2* lines were unable to induce stunting, chlorosis, transdifferentiation of bundle sheath cells or xylem hyperplasia. Furthermore, fungal biomass quantification demonstrated that virulence was reduced in V76 ΔΔ*LSCE2* lines whereas virulence of *Verticillium spp.* Δ*LSCE2* as well as VL43 ΔΔ*LSCE2* lines was unaffected. Taken together, the data suggested that the presence of a single copy of *LSCE2* enables chlorosis-class *Verticillium spp.* isolates to trigger chlorosis, stunted growth and developmental reprogramming in Arabidopsis.

3.3.3 Transgenic expression of *LSCE2* in wilting-class *V. dahliae* JR2 has no effect on fungal morphology

In order to provide supporting evidence for our working hypothesis that *LSCE2* mediates the complex developmental host plant reprogramming patterns representative for chlorosis-class *Verticillium spp.* isolate, we decided to generate transgenic *LSCE2* expressor lines of the wilting-class reference isolate *V. dahliae* JR2. The construct for transgene expression of *LSCE2* consisted of the $LSCE2_{V76}$ gene sequence under the control of the native promoter and terminator regions and was introduced into the *V. dahliae* JR2 genome via *Agrobacterium*-mediated transformation. The presence of the construct in the genomes of transformed lines (JR2 [*pLSCE2:LSCE2*]*)* was confirmed via PCR (Figure 3.23A). In order to ascertain that transgenic JR2 lines were not contaminated with material from chlorosis-class isolates, additional PCR analyses were conducted. First, gDNA was amplified with primers targeting chlorosis-class specific gene *LSCE1*. As expected, no signal was detected in wild-type JR2 and transgenic lines (Figure 3.23A). Second, primers targeting a gene present in both isolates (VDAG_02705) were used. The shift observed between the signals from V76 and JR2 as well as JR2 transgenic lines corresponded to a 60 nucleotide deletion in $VDAG\_02705_{V76}$ (Figure 3.23B). The results confirmed that the transgenic lines selected for further analyses were not contaminated.

Integration of the *pLSCE2:LSCE2* construct into the genome of *V. dahliae* JR2 occurred at random sites which may have an influence on transgenic expression. Therefore, it was necessary to test *pLSCE2:LSCE2* lines for their ability to express *LSCE2* before time-consuming infection experiments

were conducted. To this end, semi-quantitative PCR analyses were conducted using fungal material from JR2 [*pLSCE2:LSCE2*] lines and wild-type V76 grown *in vitro*. A signal was detected for three independent transgenic lines and wild-type V76 (Figure 3.23C). This demonstrated that transgenic lines were able to express *LSCE2* under its native promoter *in vitro*.

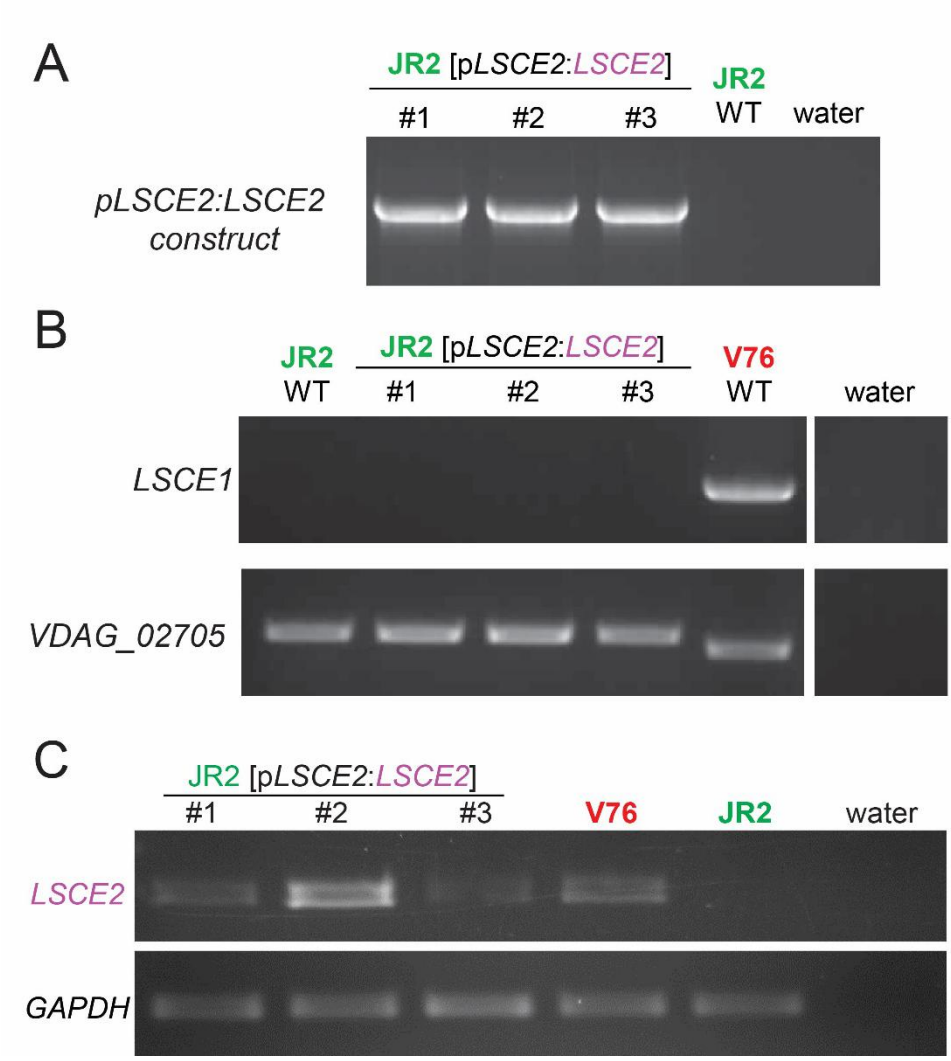

Figure 3.23 PCR confirms presence and expression of the *LSCE2* construct in transgenic wilting-class *V. dahliae* JR2 lines. Agarose gels loaded with PCR products are shown after gel electrophoresis. (A) PCR was performed with primers binding in *LSCE2* (LW120) and inside the TrpC promoter of the Hygromycin resistance cassette (LW49). Three independent lines of each transgene are shown in addition to wild-type *V. dahliae* JR2. (B) Transgene lines were tested for contamination with chlorosis-class isolates. PCR was performed on chlorosis-class specific gene *LSCE1* (LW4/5). PCR on VDAG_02705 (LW46/47) was used as a reference. Water was used as negative control. (C) Expression of *LSCE2* in transgene *Verticillium spp.* lines *in vitro*. RNA from three independent lines was extracted from fungal mycel grown in liquid PDB. Expression levels were tested via semi-quantitative PCR using expression of housekeeping gene glyceraldehyde 3-phosphate dehydrogenase (GAPDH) as reference. 35 amplification cycles were used in each PCR. Water was used as negative control. Experiment was repeated three times with similar results.

In order to exclude pleiotropic growth effects caused by transgenic expression of *LSCE2*, growth morphology and colony area of three independent JR2 [*pLSCE2*:*LSCE2*] lines after 7, 14 and 21 days of growth on solid CDA were monitored. No significant differences between wild-type JR2 and transgenic lines were observed when qualitatively comparing colony morphology and microsclerotia formation at the center of growing colonies (Figure 3.24A). Correspondingly, growth rates did not differ significantly between transgenic lines and wild-type *V. dahliae* isolates (Figure 3.25B). These results were expected since deletion of *LSCE2* in *V. dahliae* also had no effect on *in vitro* growth (Figure 3.11).

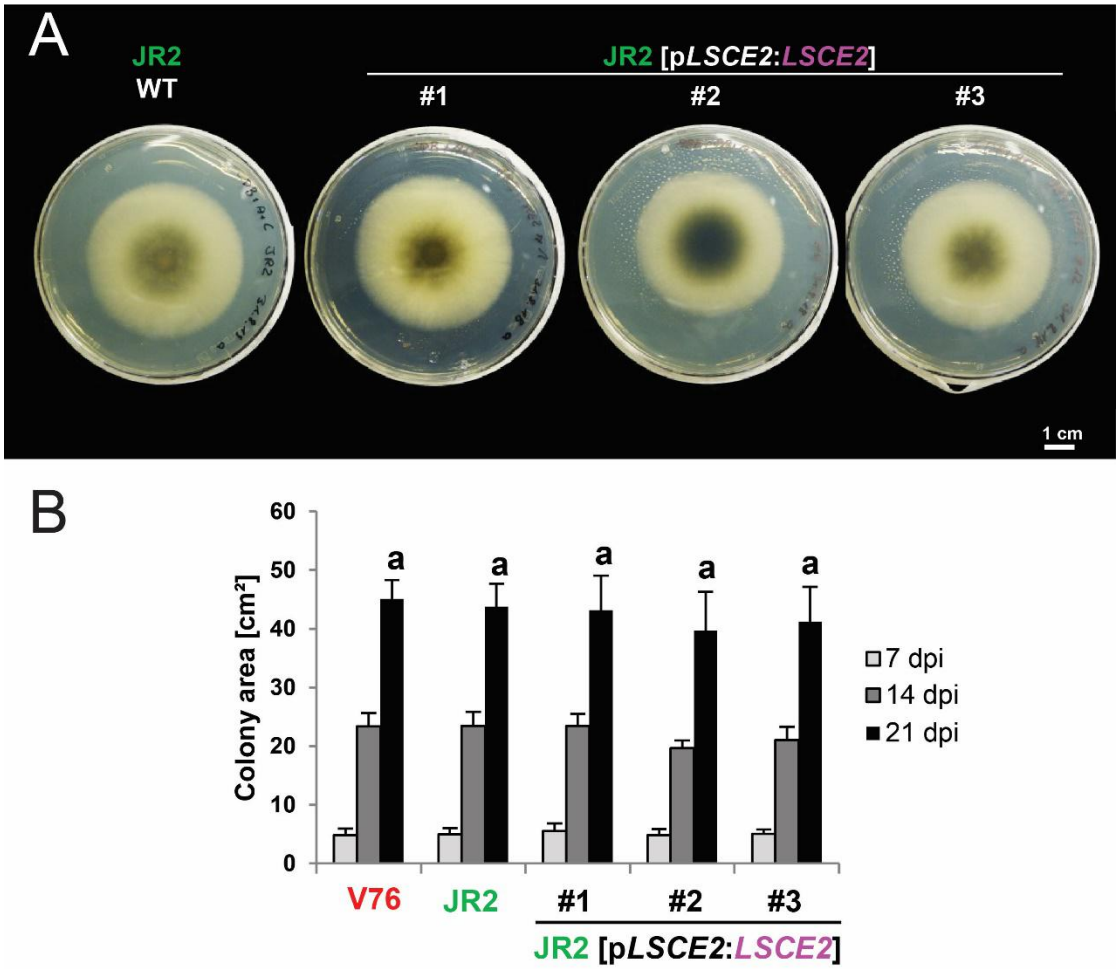

Figure 3.24 Transgene expression of *LSCE2* in *V. dahliae* JR2 does not affect fungal *in vitro* growth. (A) Growth phenotypes of JR2 wild-type (WT) and transgene lines (JR2 [p*LSCE2*:*LSCE2*]). Pictures were taken after 14 days growth on CDA at short day conditions. (B) Colony area 7, 14 and 21 days post inoculation (dpi). Error bars represent standard deviation and different letters indicate significant differences at 21 dpi according to Student's t-test (P≤0.05). Two plates were used per biological replicate (n), n = 3.

3.3.4 Infection assays reveal that transgene expression of *LSCE2* in wilting-class isolate *V. dahliae* JR2 triggers chlorosis-class disease symptom development in Arabidopsis

3.3.4.1 Transgene expression of *LSCE2* enables wilting-class isolate *V. dahliae* JR2 to induce chlorosis on Arabidopsis

After generating transgenic JR2 [*pLSCE2:LSCE2*] lines, it was investigated whether transgenic expression of *LSCE2* in wilting-class isolate *V. dahliae* JR2 affected macroscopic disease symptom development upon host infection. To this end, Arabidopsis plants were infected with wild-type reference isolates and transgenic lines, respectively. Disease symptom development was monitored for three consecutive weeks. Intriguingly, Arabidopsis plants infected with JR2 [*pLSCE2:LSCE2*] lines developed chlorosis-class specific disease symptoms on older rosette leaves at 21 dpi (Figure 3.25A). Concomitantly, wilting of leaves, typical for infections with wild-type *V. dahliae* JR2, was not observed. In addition to the qualitative observation of disease symptoms, the severity of induced host plant stunting was quantitatively assessed by measuring the total rosette leaf area. After 21 dpi, the total rosette leaf area from plants infected with JR2 [*pLSCE2:LSCE2*] lines was not significantly different from total rosette leaf areas of V76- and JR2-infected plants, respectively (Figure 3.25B). These data suggested that the expression of a single effector, *LSCE2*, was sufficient to enable wilting-class isolate JR2 to induce macroscopic chlorosis-class specific disease symptoms on Arabidopsis.

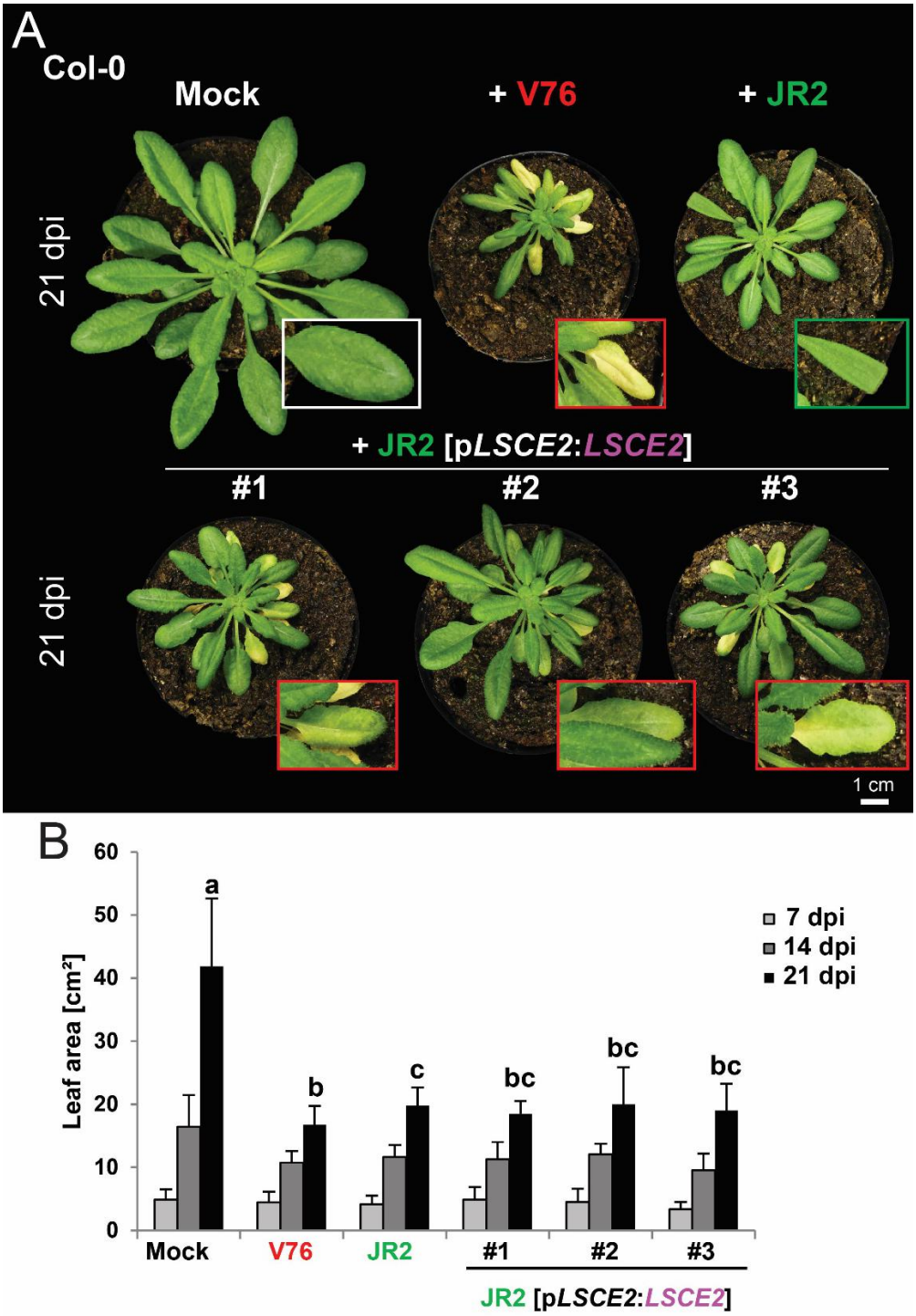

Figure 3.25 Disease phenotype of *A. thaliana* Col-0 infected with *V. dahliae* WT isolates V76, JR2 and *LSCE2* transgene JR2 lines (JR2 [p*LSCE2*:*LSCE2*]). (A) Plants were photographed 21 days post infection (dpi). (B) Total leaf area 7, 14 and 21 dpi. Error bars represent standard deviation and different letters indicate significant differences at 21 dpi according to Student's t-test (P≤0.05). Four plants were used per biological replicate (n), n = 3

3.3.4.2 Transgene expression of *LSCE2* enables wilting-class isolate *V. dahliae* JR2 to induce transdifferentiation of bundle sheath cells in Arabidopsis leaves

Next, the question was addressed whether chlorosis class-specific disease symptoms triggered by transgenic expression of *LSCE2* in the JR2 background correlates with *de novo* xylem formation. Indeed, microscopic analyses of leaves from plants infected with JR2 [p*LSCE2*:*LSCE2*] lines revealed transdifferentiation of bundle sheath cells into new xylem elements (Figure 3.27A). As described earlier in this study, the transdifferentiation (TD) ratio was calculated in order to quantitatively assess the induction of bundle sheath transdifferentiation (3.3.2.2). The TD ratio observed for JR2 [p*LSCE2*:*LSCE2*] line #2 was lower but not significantly different from wild-type V76 (Figure 3.26B). JR2 [p*LSCE2*:*LSCE2*] lines #1 and #3, on the other hand, induced TD to a significantly lower extent when compared to wild-type V76. Consequently, it can be postulated that transgenic expression of *LSCE2* in wilting-class isolate JR2 conferred the ability to trigger developmental reprogramming in Arabidopsis.

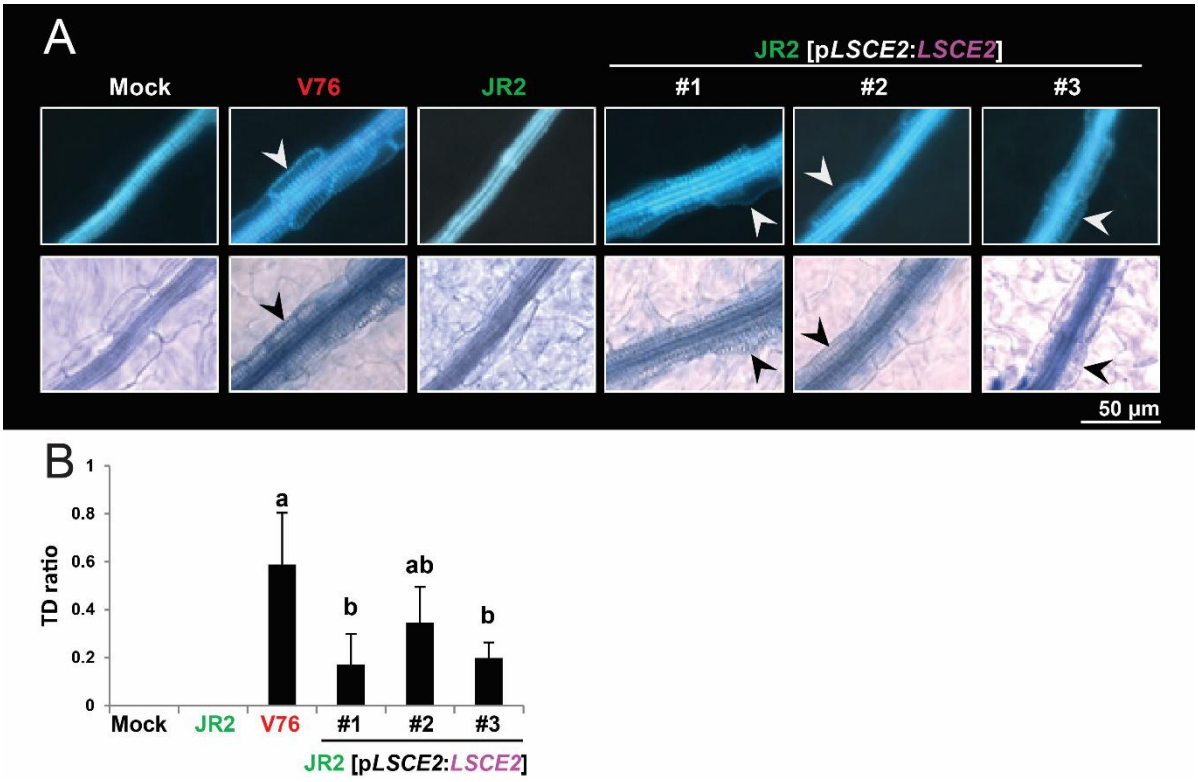

Figure 3.26 Transdifferentiation of bundle sheath cells in leaves of infected *A. thaliana*. (A) Microscopic images of Arabidopsis leaf veins 21 days after mock treatment or infection with wild-type *V. dahliae* V76 and JR2 as well as three transgenic JR2-lines expressing transgenic *LSCE2* (JR2 [p*LSCE2*:*LSCE2*]). Top row: epifluorescence microscopy detecting lignin autofluorescence of xylem secondary cell walls. Bottom row: bright field microscopy; xylem elements were stained with trypan blue. White and black arrowheads mark transdifferentiated bundle sheath cells. (B) Transdifferentiation (TD) ratio, calculated from the fifth leaf of infected *A. thaliana* leaves 21 dpi. Error bars represent standard deviation and different letters indicate significant differences according to Student's t-test (P≤0.05). Four plants were used per biological replicate (n), n = 3.

3.3.4.3 Transgene expression of *LSCE2* enables wilting-class isolate *V. dahliae* JR2 to induce xylem hyperplasia in vascular bundles of Arabidopsis leaves

To verify that developmental reprogramming induced by transgenic expression of *LSCE2* also encompasses transdifferentiation of xylem parenchyma cells and reactivation of cambial activity, leaf midrib transections of infected plants were investigated. A noticeable increase in xylem elements was observed in plants infected with JR2 [p*LSCE2*:*LSCE2*] lines (Figure 3.27). However, xylem hyperplasia induced by JR2 [p*LSCE2*:*LSCE2*] lines was not as dramatic as in plants infected with chlorosis-class isolate V76 (Figure 3.27). At the same time, an increased autofluorescence of xylem vessels suggesting enhanced lignification was detected in plants infected with JR2 [p*LSCE2*:*LSCE2*] line #1. Enhanced lignification is a disease symptom usually observed in plants infected with wilting-class isolates and has been associated with plant defense reactions (Reusche et al. 2012). The fact that enhanced lignification occurred in hyperplastic tissue suggested that both wilting- and chlorosis-class disease symptoms were induced in JR2 [p*LSCE2*:*LSCE2*] lines.

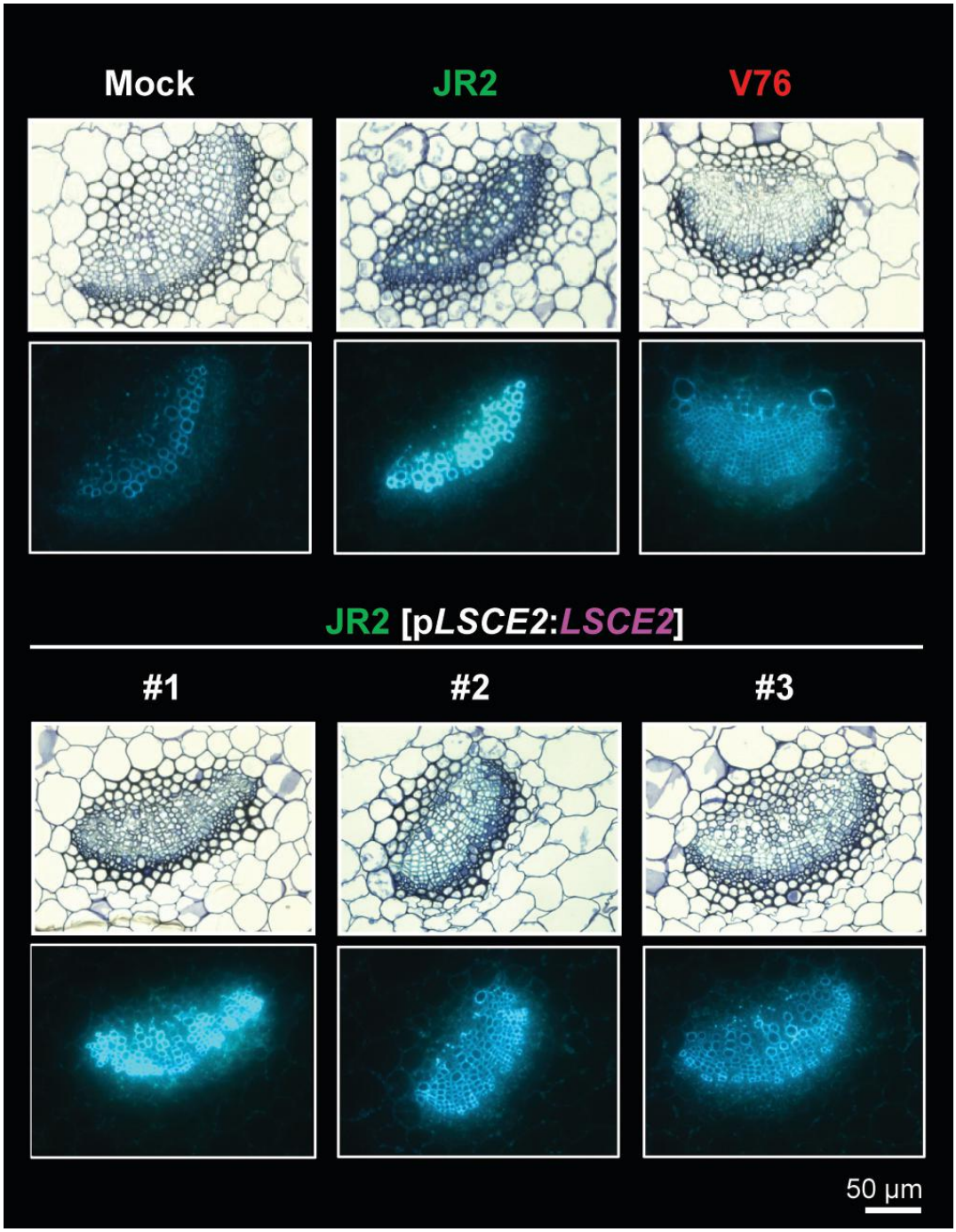

Figure 3.27 Leaf midrib transections show xylem hyperplasia formation in Arabidopsis plants infected with chlorosis-class isolate *V. dahliae* V76 and transgenic JR2 lines (JR2 [p*LSCE2*:*LSCE2*]). Leaves with distinct disease symptoms from plants infected with *V. dahliae* JR2, *V. dahliae* V76 and JR2 [p*LSCE2*:*LSCE2*], respectively, as well as and healthy leaves from mock-treated plants were harvested at 28 dpi. Leaf transections were embedded before sectioning. 5 µm microtome sections were used for subsequent microscopic analyses. Top row: Bright field microscopic images of 5 µm microtome sections stained with toluidine blue. Bottom row: Images from epifluorescence microscopy of unstained microtome sections.

3.3.4.4 Transgenic expression of *LSCE2* in wilting-class isolate *V. dahliae* JR2 does not increase virulence

DeJonge et al. (2012) demonstrated that the deletion of a single effector, *Ave1*, is sufficient to alleviate disease symptoms on tomato while transgene expression of *Ave1* in asymptomatic isolates results in increased virulence and disease symptoms on the same host (deJonge et al. 2012). Correspondingly, deletion of *LSCE2* in V76 resulted in a significant decrease in virulence (Figure 3.21). It was therefore unexpected to find no significant differences of fungal biomass accumulation in plants infected with JR2 [p*LSCE2*:*LSCE2*] lines compared to wild-type JR2 (Figure 3.28). The data suggested that virulence was not increased by transgenic expression of *LSCE2* in wilting-class isolate JR2.

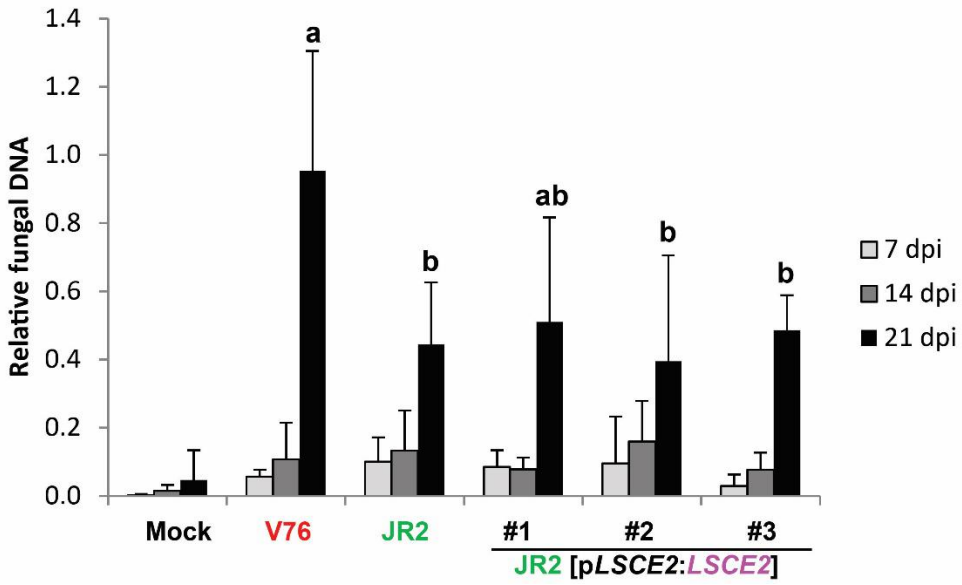

Figure 3.28 Quantification of fungal proliferation *in planta.* To quantify fungal DNA in planta, qRT-PCR was performed with DNA extracted at 7, 14 and 21 dpi from plants mock-treated or infected with *V. dahliae* wild-type V76 and JR2 as well as three transgene JR2 lines expressing *LSCE2* (JR2 [p*LSCE2*:*LSCE2*]). Data are based on ΔΔCq values, using *AtUBQ5* as reference and *Vsp.ß-tubulin* as target sequences. Error bars represent standard deviation and different letters indicate significant differences at 21 dpi according to Student's t-test (P≤0.05). Four plants were used per biological replicate (n), n = 3.

In summary, infection experiments with transgenic JR2 [p*LSCE2*:*LSCE2*] lines supported our working hypothesis that *LSCE2* mediates the complex developmental host plant reprogramming patterns representative for chlorosis-class *Verticillium spp.* infections. Furthermore, the results demonstrated that no chlorosis-class specific gene apart from *LSCE2* was required for the induction of chlorosis-class disease symptoms. The fact that transgenic expression of LSCE2 did not increase virulence in JR2 stood in contrast to the observation that virulence was decreased in V76 ΔΔ*LSCE2* lines (Figure 3.21). However, virulence was not decreased in VL43 ΔΔ*LSCE2* lines (Figure 3.22). This implied that increasing virulence might not be the foremost function of *LSCE2*.

3.4 Protein biochemical characterization of LSCE2

3.4.1 Infiltration of purified LSCE2 into Arabidopsis leaves induces transdifferentiation of bundle sheath cells into xylem elements

The next aim of the study was to characterize the protein biochemical properties of LSCE2. To this end, an expression system was chosen that allowed for the expression of high amounts of LSCE2 protein and in addition provided adequate eukaryotic posttranslational modifications. The *P. pastoris* system for heterologous protein expression was in previous studies successfully applied to *Verticillium* effectors (Kombrink et al. 2017; Zhang et al. 2019) and was thus selected for LSCE2 expression. In parallel, LSCE2-like as a sequence homolog to LSCE2 with a potentially divergent functionality was expressed and analyzed. *P. pastoris* cells were transformed with constructs including the myc- and histidine (His) - tagged coding sequences of $LSCE2_{V76}$ and $LSCE2\text{-}like_{JR2}$. Coding sequences were expressed without the native N-terminal secretion signal peptide. Instead, the α-factor mating signal sequence (SS) was used as recommended by the manufacturer of the EasySelect™ *Pichia* Expression Kit used here (Figure 3.29A). Due to the fact that *P. pastoris* has been shown to secrete very low levels of native proteins (Romanos 1995), LSCE2/-like was directly purified from liquid culture supernatant using gravitational His-trap columns. LSCE2/-like protein was detected in the supernatant and after elution from the columns whereas no significant protein signal was detected for wild-type *P. pastoris* which was used as a negative control (Figure 3.29B-D). Interestingly, although *LSCE2* and *LSCE2-like* constructs were predicted to encode heterologous proteins of identical size and mass (~27

kDa), the proteins migrated to different positions in SDS-PAGE analyses (~27 kDa) (Figure 3.29B and C). While LSCE2-like protein was detected below the marker corresponding to 35 kDa, LSCE2 was detected at a position above 35 kDa. In addition, smears were observed above the proteins, suggesting degradation and/or posttranslational modification of the protein.

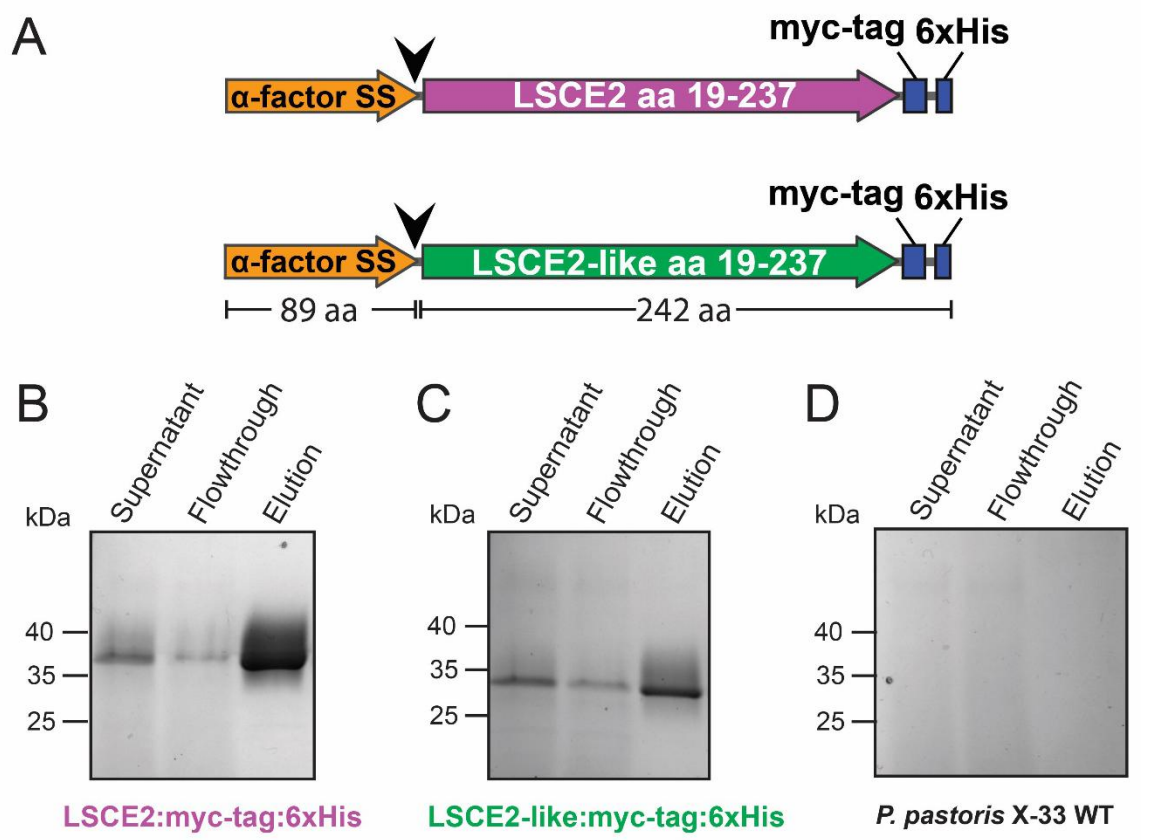

Figure 3.29 Expression of heterologous LSCE2/LSCE2-like constructs in the *P. pastoris* system and subsequent purification. (A) Constructs expressed by transformed *P. pastoris*. *LSCE2*$_{V76}$ and *LSCE2-like*$_{JR2}$ coding sequences without the native N-terminal secretion signal were fused to *P. pastoris* α-factor mating signal sequence (SS) and C-terminal myc-/ His-tags. SS cleavage site after secretion is marked with a black arrowhead. Molecular weight of protein constructs were predicted at 27 kDa (https://web.expasy.org/compute_pi/). (B-D) Acrylamide gels stained after SDS-PAGE with colloidal Coomassie blue before and after purification of heterologous LSCE2 (A), LSCE2-like (B) and protein from wild-type *P. pastoris* strain X-33 (D). Samples loaded were supernatant from *P. pastoris* liquid cultures, flow-through after loading of His GraviTrap™ columns (GE Healthcare, Chicago, IL, USA) and protein eluted from His GraviTrap™ columns.

Next, the isolated proteins were used to address the question if and how LSCE2 and LSCE2-like affect plant cells in absence of *Verticillium* infection. To this end, Arabidopsis leaves were infiltrated with purified protein. Macroscopic inspection of the leaves at 7 days after infiltration (dai) revealed chlorotic regions on leaves infiltrated with LSCE2 whereas no chlorosis was observed after infiltration with

LSCE2-like and wild-type negative control, respectively (Figure 3.30A). Subsequent bright field and fluorescence microscopy of leaves stained with trypan blue showed that in addition to chlorosis, LSCE2 infiltration triggered transdifferentiation of bundle sheath cells (Figure 3.30B). No transdifferentiation was detected in leaves infiltrated with LSCE2-like or the negative control. Notably, transdifferentiation into xylem elements was restricted to bundle sheath cells and not observed for other cell types such as mesophyll and epidermal pavement cells. It is remarkable that LSCE2 was sufficient to induce chlorosis-class disease symptoms in absence of *Verticillium*. In addition, the findings demonstrated a cell-type specific transdifferentiation capacity of bundle sheath cells in Arabidopsis.

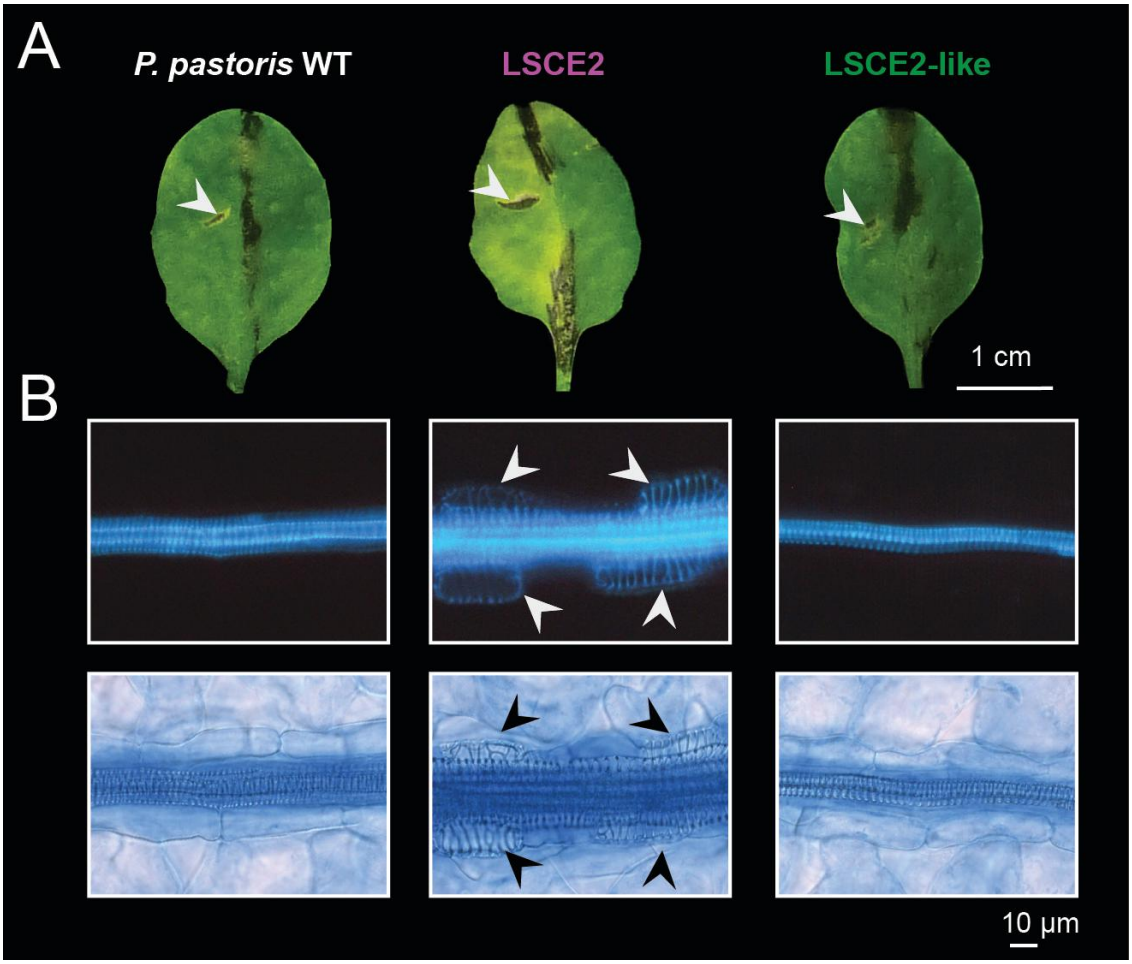

Figure 3.30 LSCE2 induces chlorosis and transdifferentiation in infiltrated Arabidopsis leaves. Leaves from 4.5 week-old plants were infiltrated with protein purified from *P. pastoris* wild-type (WT) isolate X-33 (negative control) or 0.5 mg/ml heterologous LSCE2 and LSCE2-like, respectively. (A) Macroscopic symptom development at 7 days after infiltration (dai). White arrowheads mark infiltration site. (B) Microscopic images of Arabidopsis leaf veins 7 dai. Leaves were stained with trypan blue. Top row: epifluorescence microscopy detects autofluorescence of lignin in xylem element secondary cell walls; Bottom row: bright field microscopy. White and black arrowheads mark transdifferentiated bundle sheath cells.

3.4.2 Transgenic expression of *LSCE2* in Arabidopsis induces developmental reprogramming

Transgenic expression of effector constructs in Arabidopsis can be used as a valuable tool for in-depth functional characterization of proteins. Expression of LSCE2 fused to GFP in Arabidopsis will allow analyzation of subcellular localization and in addition, affinity chromatography of the fusion protein can be used to identify LSCE2 targets Arabidopsis. The fusion construct used in this study consisted of the *LSCE2*$_{V76}$ coding sequence lacking the N-terminal signal peptide fused with four consecutive alanines (Ala) to the coding sequence of *GFP* (Figure 3.31A). For constitutive, transgenic expression of the fusion construct, the Arabidopsis *ubiquitin-10* (At*UBQ10*) promoter was selected in this study. The At*UBQ10* promoter (pAt*UBQ10*) mediates moderate expression of constructs in all tissues and during all developmental stages of Arabidopsis (Norris et al. 1993; Geldner et al. 2009) . In addition, pAt*UBQ10*-driven constructs are not subject to gene silencing or suppression, an effect which is known from the widely used viral 35S promoter (Mishiba et al. 2005).

Following floral-dip transformation of Arabidopsis plants, transgenic seedlings were identified via BASTA selection. Interestingly, after three to six weeks of growth, a subset of these transgenic seedlings developed a vein-clearing phenotype that was accompanied by the onset of early senescence in older rosette leaves (Figure 3.31B). In total, 30 transgenic lines exhibiting the vein clearing phenotype were selected and characterized. Macroscopic assessment of transgenic plants revealed that the vein-clearing phenotype was accompanied by stunted plant growth. Furthermore, the severity of stunting differed between the selected transgenic lines (Figure 3.32A). Moreover, vein clearing and chlorosis was observed exclusively in mature Arabidopsis leaves and never in developing leaves (Figure 3.32B). Intriguingly, the amount of vein clearing and chlorotic leaves was observed to correlate qualitatively with stunting severity (Figure 3.32A and B). Next, it was investigated whether vein clearing was caused by transdifferentiation of bundle sheath cells as reported by Reusche et al. (2012). To this end, microscopic analyses of leaf material stained with trypan blue were conducted. Indeed, transdifferentiation of bundle sheath cells was observed in leaves with vein clearing symptoms (Figure 3.32C). In addition, it was found that neither mesophyll nor epidermal pavement cells were transdifferentiated into xylem elements. This corresponded to the findings of the previously conducted infiltration experiments (Figure 3.30).

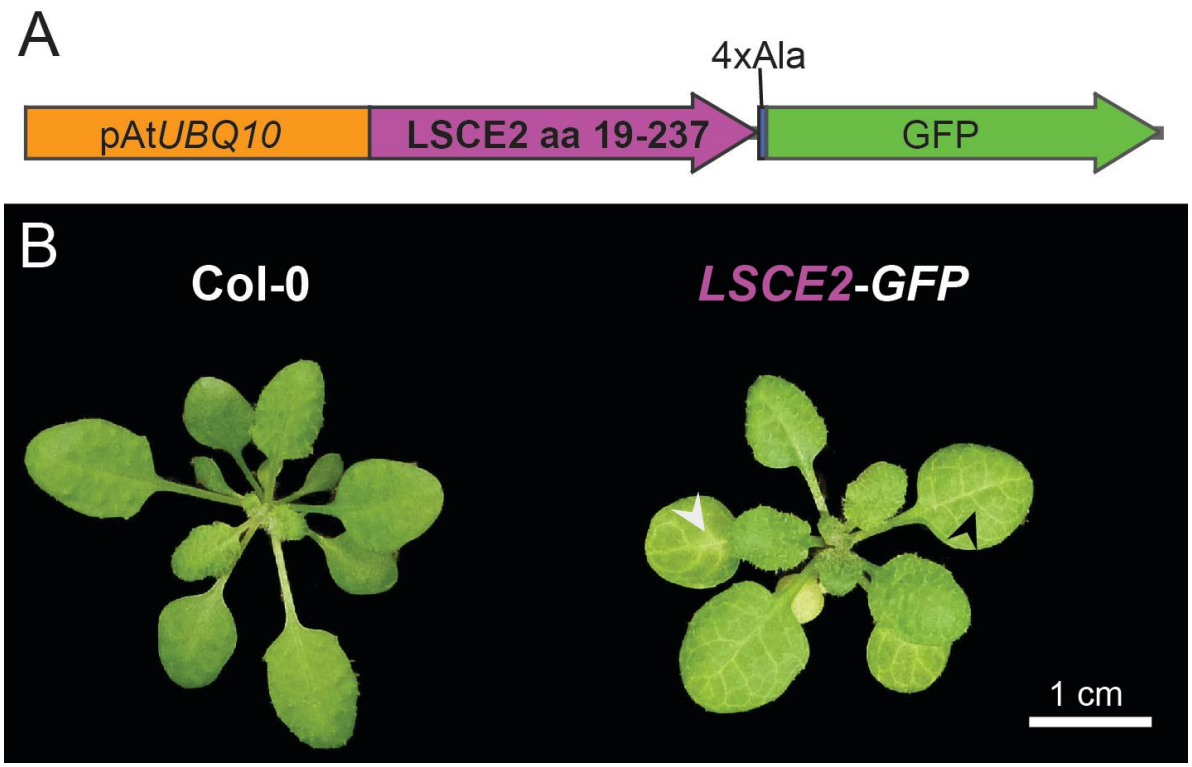

Figure 3.31 Arabidopsis plants expressing *LSCE2* have a distinct vein-clearing phenotype. (A) Schematic representation of the construct used for transgene expression of *LSCE2* in Arabidopsis. LSCE2 lacking the predicted signal peptide was fused with 4 alanins (Ala) as linker to the green fluorescent protein (GFP). Expression is driven by the Arabidopsis ubiquitin-10 promoter (pAT*UBQ10*). (B) Wild-type *Arabidopsis thaliana* Col-0 reference plant and 6 week-old *LSCE2-GFP* transgene plant. Black arrowhead marks exemplary site showing vein clearing. White arrowhead marks onset of chlorosis. Transgene plants were BASTA-selected and subsequently investigated for phenotype development.

In a subsequent experiment, it was investigated whether the expression of the LSCE2-GFP fusion construct correlated with the severity of the observed phenotype. Western blot analyses of total Arabidopsis protein extracts revealed that the signal corresponding to LSCE2-GFP was only barely detectable in plants without a phenotype whereas a strong signal was detected in plants with strong chlorosis-class disease symptoms (Figure 3.32D). These results demonstrated that it was possible to express transgenic LSCE2-GFP constitutively in Arabidopsis. These lines can in future analyses be used for subcellular localization studies and pull-down experiments. Notably, transdifferentiation was again restricted to vascular tissues and bundle sheath cells despite ubiquitous *UBQ10*-promoter driven expression, reinforcing the earlier conclusion of a cell type-specific reprogramming capacity.

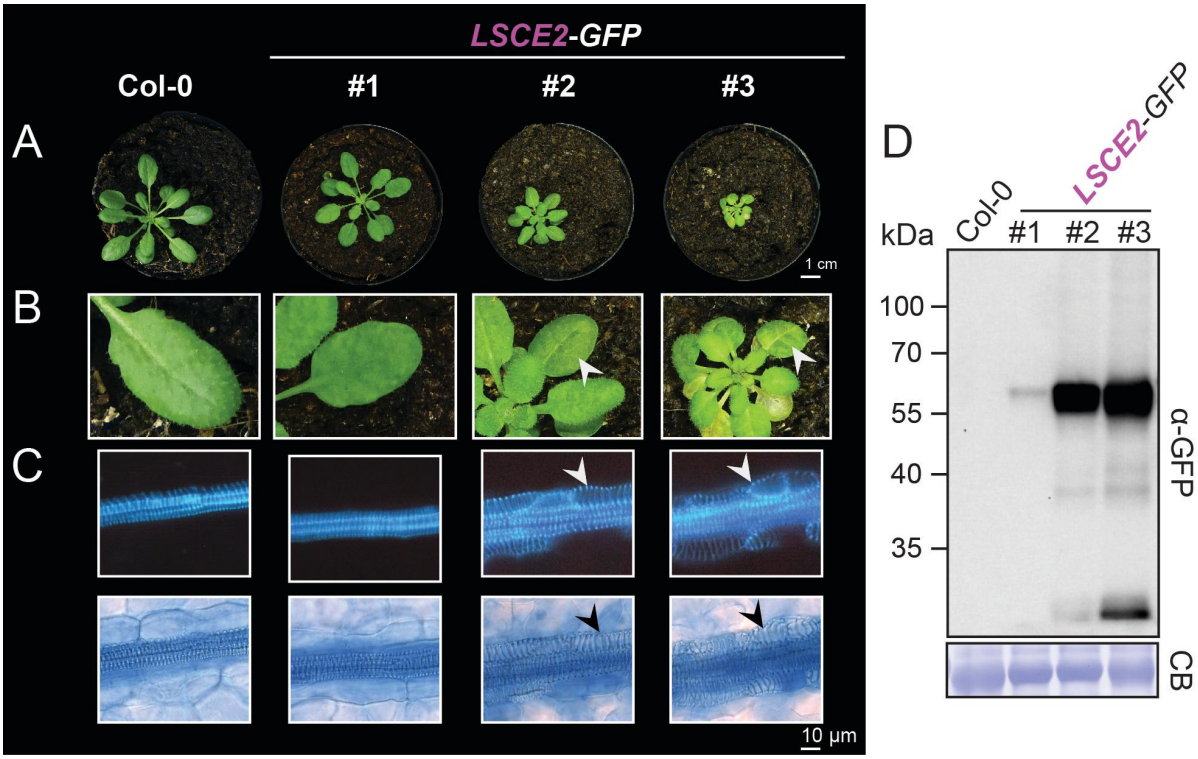

Figure 3.32 LSCE2-GFP plants show chlorosis-class disease-like symptoms. (A) 8 week old wild-type Arabidopsis Col-0 and three independent *LSCE2-GFP* transformants are shown. (B) Enlarged view on mature rosette leaves. White arrowheads mark vein clearing sites. (C) Microscopic images of leaf veins from mature Arabidopsis leaves. Leaves were stained with trypan blue. Top row: epifluorescence microscopy; Bottom row: bright field microscopy. White and black arrowheads mark transdifferentiated bundle sheath cells. (D) Western blot after immunodetection of GFP. Predicted molecular weight of the fusion protein was 51.9 kDa.

3.4.3 Yeast-two-Hybrid assays reveal possible interaction partners of LSCE2

A major advantage in understanding the mechanism of how any effector molecule affects host plants is to know the direct target or targets of the effector in question (Lo Presti et al. 2015). The yeast-two-hybrid system uses the properties of the Gal4 transcription factor to discover protein-protein interactions (Fields and Song 1989). Gal4 consists of two domains called binding and activation domain. In yeast isolates modified for this purpose, the Gal4 binding domain binds to the activating sequence of *HIS3*, a gene which enables yeast to grow on histidine deficient medium. Activation of *HIS3* transcription, however, requires interaction of the Gal4 binding domain with the Gal4 activating domain. The interaction between the Gal4 domains can be initiated by the interaction between proteins fused to the binding (bait protein) and activation (prey protein) domains. This means that transformed yeast colonies growing on histidine deficient medium represent an occurrence of the physical interaction between the expressed fusion proteins. For identifying effector targets out of thousands of expressed proteins, cDNA libraries representing the transcriptome of the organism of interest were established (Chien et al. 1991). This allowed screening of a wide range of potential targets in one assay. In the study presented here, two Arabidopsis cDNA libraries from cell suspension culture (Nemeth et al. 1998) and roots (Klopffleisch et al. 2011), respectively, were used to ideally cover all potential targets of LSCE2 in Arabidopsis. CDNA in both libraries was fused N-terminally with the Gal4 activating domain acted as prey construct in the interaction mating. The *LSCE2*$_{V76}$ coding sequence lacking the N-terminal secretion signal fused N-terminally to the Gal4 binding domain was used as bait (Figure 3.33A).

In total, 192 colonies (96 colonies from each screen) were recovered after the interaction screen with LSCE2 and Arabidopsis cDNA libraries (Figure 3.33B and C). Arabidopsis cDNA from these colonies was successfully amplified and sequenced from 174 colonies. The recovered sequences were matched with Arabidopsis genes in the available databases using the basic local alignment search tool (BLAST). Due to the fact that several genes were found more than once in the screen, the final number of proteins putatively interacting with LSCE2 was reduced from 174 to 80 (Figure 3.33B).

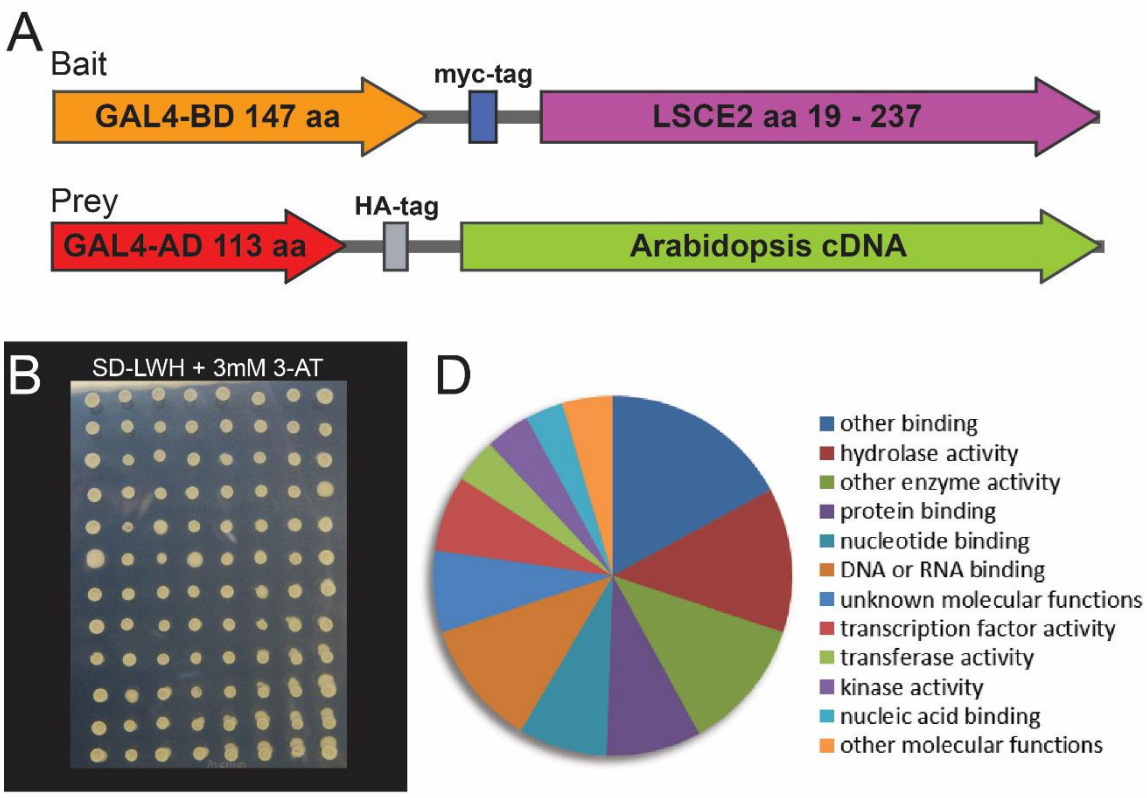

C

Library screen	Colonies selected	Sequencing results	*A. thaliana* accessions per screen	*A. thaliana* accessions found in both screens	Putative *A. thaliana* targets
***A. thaliana* cell suspension**	96	80	34	5	80
***A. thaliana* root**	96	79	51		

Figure 3.33 Yeast-two-Hybrid screen reveals putative Arabidopsis target proteins. (A) *Saccharomyces cerevisiae* (yeast) isolate AH109 was transformed with bait (LSCE2 without signal peptide fused to Gal4 binding domain) and prey (*A. thaliana* Col-0 cDNA libraries). (B) Representative plate with 96 colonies picked from initial yeast-two-hybrid interaction screen between LSCE2 and two Arabidopsis libraries (Arabidopsis cell suspension culture and root library), growing on Synthetic Complete dropout (SD) medium without leucine, tryptophan and histidine, containing 3 mM 3-amino-1,2,4-triazole (SD-L-W-H + 3 mM 3-AT). (C) Results from Yeast-two-hybrid screen. Arabidopsis cDNA was amplified via PCR from yeast colonies growing on SD-L-W-H + 3 mM 3-AT. PCR products were sequenced and identified via homology searches (BLAST) in the databases NCBI (https://www.ncbi.nlm.nih.gov) and TAIR (https://www.arabidopsis.org). *A. thaliana* accessions were assigned to each sequence. Screens were performed once. (D) Distribution of gene ontology (GO) annotations computed with the TAIR GO Annotations tool (Berardini et al. 2004) of 80 putative LSCE2 interaction candidates.

Gene ontology (GO) annotations are a means to sort genes into functional categories and thus uncovering common features of genes from large datasets (Berardini et al. 2004). This could help to identify domains favored for interaction with LSCE2. Therefore, Arabidopsis interaction partners were grouped into functional categories according to their GO annotations. The result of GO annotation showed that Arabidopsis genes with a wide range of associated roles were recovered in the screen (Figure 3.33C). An enrichment of particular GO terms in the putative interaction candidates in comparison with the Arabidopsis genome could reveal a preference of LSCE2 for interacting with particular domains but none of the terms was enriched significantly according to PANTHER Overrepresentation Test (http://pantherdb.org/) (Mi et al. 2019).

Yeast-two-hybrid screens are known to produce large proportions of false-positives due to non-specific interactions between proteins (Brückner et al. 2009). Accordingly, interactions found in the initial screen needed to be confirmed again in individual interaction assays. In order to reduce the number of putative interaction candidates, criteria were established for selecting candidates that were unlikely to be false-positives. The criteria for selecting interaction candidates were first: recovery of the gene more than once in the screens and second: recovery of cDNA that differed in length between individually sequenced colonies. This ensured that interactions between bait and prey occurred more than once, decreasing the chances of selecting a false-positive. Out of 80 genes recovered from the screens, 13 putative interaction candidates were selected for individual interaction assays to confirm interaction with LSCE2 (Supplement Table 6.2). Nine interaction candidates were unable to grow on SD-L-W-H + 3 mM 3-AT after an individual yeast-two-hybrid interaction assay, indicating that the interaction candidates failed to interact with LSCE2 (Table 3.6). Four candidates, on the other hand, did interact with LSCE2 but simultaneously interacted with GFP which was used as negative control. This suggested that the interaction with LSCE2 was not specific but due to an unspecific protein-binding capacity of the interaction candidate. After screening all 13 interaction candidates, none of the specific interactions with LSCE2 were confirmed (Table 3.6).

Table 3.6 Results of individual yeast-two-hybrid interaction assays. Shown are the results of interaction screens using full length coding sequences from putative LSCE2 targets in Arabidopsis. Proteins with predicted signal peptides (PGIP1 and PRXR1) were investigated both with and without the signal peptide. Putative Arabidopsis interaction candidates were fused to Gal4 activation domain (bait). LSCE2 without signal peptide was fused to the Gal4 binding domain (prey). GFP was used as negative control prey. Bait and prey were transformed into yeast isolate AH109. Successful transformation was tested by plating on medium without leucine (Leu) and tryptophan (Trp). Interaction of bait and prey was tested by plating on medium without Leu, Trp and histidine (His). Growth of yeast colonies after 3 days incubation is shown as 'yes' (colonies present) or 'no' (no colonies). More detailed information about the interaction candidates can be found in Supplement Table 6.2.

	Gal4 Activating Domain: Interaction Candidate	**Gal4 Binding Domain: LSCE2**		**Gal4 Binding Domain: GFP**	
Accession	**Description**	**- Leu - Trp**	**- Leu - Trp - His**	**- Leu - Trp**	**- Leu - Trp - His**
AT3G02550	LBD41 LOB domain-containing protein 41	yes	**yes**	yes	**yes**
AT3G09390	MT2A metallothionein 2A	yes	**yes**	yes	**yes**
AT3G19460	Reticulon family protein	yes	**no**	yes	**no**
AT4G04860	DERLIN-2.2	yes	**no**	yes	**no**
AT4G09460	MYB6 myb domain protein 6	yes	**yes**	yes	**yes**
AT4G21960	PRXR1 without signal peptide	yes	**no**	yes	**no**
AT4G21960	PRXR1 Peroxidase superfamily protein	yes	**no**	yes	**no**
AT4G26610	D6 protein kinase like 1	yes	**no**	yes	**no**
AT4G3862	MYB4 myb domain protein 4	yes	**yes**	yes	**yes**
AT5G06860	PGIP1 without signal peptide	yes	**no**	yes	**no**
AT5G06860	PGIP1 polygalacturonase inhibiting protein 1	yes	**no**	yes	**no**
AT5G21990	TPR7 Tetratricopeptide repeat (TPR)-like superfamily protein	yes	**no**	yes	**no**
AT5G52020	Integrase-type DNA-binding superfamily protein	yes	**no**	yes	**no**
AT5G59770	Protein-tyrosine phosphatase-like, PTPLA	yes	**no**	yes	**no**
AT5G67250	SKP1/ASK1-interacting protein 2	yes	**no**	yes	**no**

4 Discussion

Previous studies have described a *Verticillium* infection-associated chlorosis-class disease phenotype on Arabidopsis plants which is accompanied by substantial developmental reprogramming of the host (Reusche et al. 2012; Reusche et al. 2014; Thole 2016). The ability to induce this disease phenotype is shared by a group of *V. longisporum* and *V. dahliae* isolates, whereas most *V. dahliae* isolates induce wilting symptoms on Arabidopsis (Thole 2016). A possible explanation for the different symptom patterns may be the evolution of *Verticillium* lineage-specific effector repertoires (Reusche et al. 2014; Thole 2016). In order to prove or disprove this working hypothesis, this study aimed at the identification and functional characterization of *Verticillium spp.* chlorosis-class specific effector molecules potentially involved in triggering the corresponding developmental reprogramming patterns within the host. Comparative genome and transcriptome analyses identified a lineage-specific genomic region harboring the highly *in planta* expressed *LINEAGE-SPECIFIC CANDIDATE EFFECTOR2* (*LSCE2*). Generation of *LSCE2* knockout and transgenic lines revealed that *LSCE2* is required for establishment of chlorosis-class specific disease symptoms. Moreover, LSCE2 protein heterologously expressed and purified from yeast cultures or transgenically expressed as a GFP fusion protein was sufficient to induce chlorosis-class disease symptoms in the absence of *Verticillium*. In summary, this study provides evidence that a single lineage-specific effector mediates the complex developmental reprogramming patterns associated with chlorosis-inducing *Verticillium* species and isolates.

4.1 Comparative genomics reveal chromosomal rearrangements and lineage-specific candidate effectors

At the starting point of this study, whole-genome assemblies of *V. dahliae* isolates VdLs17 and JR2 were available in public databases (Klosterman et al. 2011; deJonge et al. 2013). However, both VdLs17 and JR2 induce the wilting-class disease phenotype on Arabidopsis (Reusche et al. 2012; Thole 2016). For comparative genomics, it was therefore necessary to establish a chlorosis-class

reference genome. A whole-genome alignment of the *de novo* sequenced chlorosis-class *V. dahliae* V76 and the reference genome of wilting-class reference isolate JR2 (deJonge et al. 2013) revealed extensive structural rearrangements of genomic sequences between the isolates (Figure 3.1). This supports the findings of several studies observing substantial chromosomal rearrangements between *Verticillium spp.* isolates (Klosterman et al. 2011; deJonge et al. 2013; Klimes et al. 2015; Faino et al. 2016; Shi-Kunne et al. 2018) . It has been hypothesized in the literature that the activity of transposable elements in the *Verticillium* genome creates breakpoints between the chromosomes which facilitates structural rearrangements (Klosterman et al. 2011; deJonge et al. 2013; Klimes et al. 2015; Faino et al. 2016) . The instability of these breakpoints may give rise to lineage-specific (LS) regions, i.e. sequences that are shared only by a subset of isolates. LS regions have been reported to be enriched in putative effector genes and to thus contribute to niche adaptation (Klosterman et al. 2011; deJonge et al. 2013; Faino et al. 2016) . Consequently, it has been suggested by Faino et al. (2016) that *Verticillium* does not rely on mutations but on structural variation for generating genome plasticity. In the work presented here, comparative genomics of the reference *V. dahliae* isolates V76 and JR2 revealed 242 V76-specific regions (> 1 kb) with a total size of ~ 1.4 Mb. These regions were mined for putative chlorosis-class specific effectors using bioinformatic analyses including mapping *in planta* RNAseq data and subsequent homology-based searches in the databases. Four *LINEAGE-SPECIFIC CANDIDATE EFFECTORs* (*LSCE*s) that have not yet been described in any other study were discovered (Table 3.2). Of these, *LSCE2* was selected as prime candidate for further in-depth characterization due to its high *in planta* expression levels observed in all chlorosis-class *V. dahliae* isolates (Table 3.2; Figure 3.2). Expression of *LSCE2* was observed at all time points during a 16 day infection experiment with the highest level of expression at 12 dpi (Table 3.3). This indicates that *LSCE2* expression is not restricted to early or late stages of infection. Further analyses are needed to elucidate in detail the expression dynamics of *LSCE2 in planta*.

4.2 Evolution of *LSCE2* and the LSCE region

4.2.1 Transposable elements may have contributed to the formation of the LSCE region

Genome sequence analyses revealed that *LSCE2* is present in two copies in the genome of chlorosis-class reference isolate *V. dahliae* V76 (Table 3.2). This finding is intriguing due to the fact that in haploid organisms such as *V. dahliae,* genes usually are present in single copies. It is especially remarkable when considering that only 4 % of the *V. dahliae* genome are repetitive (Klosterman et al. 2011; deJonge et al. 2013). This is significantly less in comparison to other haploid plant pathogenic fungi such as *Magnaporthe oryzae* (10%), *Fusarium oxysporum* (28%) and *Blumeria graminis* (64 %) (Dean et al. 2005; Ma et al. 2010; Spanu et al. 2010) which suggests that sequence duplications in the *V. dahliae* genome may not be the major driving force in the adaptive evolution of the pathogen. In the work presented here, it was revealed that in all investigated chlorosis-class isolates, *LSCE2* is located in a ~ 20 kb tandem-inverted region (LSCE region) (Figure 3.3; Figure 3.5). In total, six genes were predicted to be encoded within the LSCE region, including putative effector *LSCE1* and two uncharacterized hypothetical proteins (Figure 3.3). Strikingly, a reverse transcriptase and a transposase are located in the LSCE region; both genes are associated with transposable elements. In general, there are two classes of transposable elements. Class I transposable elements (TE) (Retrotransposons) are transcribed from DNA to RNA, then reverse-transcribed by a reverse transcriptase encoded within the TE and last, re-integrated into the genome (Wicker et al. 2007). Transposases, on the other hand, are encoded in Class II TEs (DNA transposons) and mediate the removal of the transposon from its original site and integration into a new site in the genome (Wicker et al. 2007). Interestingly, BLAST homology searches revealed that the reverse transcriptase encoded in the LSCE region is homologous to non-long terminal repeat (LTR) reverse transcriptases (Supplement Figure 6.1). In addition, an endonuclease domain and an RNaseH domain flanking the reverse transcriptase domain were predicted within the putative coding region of the protein. This domain topology is found in long interspersed elements (LINEs) of the Superfamily I, which occurs in plants, animals and fungi (Wicker et al. 2007). In the *V. dahliae* genome, class II transposable elements as well as LINEs have been found (Amyotte et al. 2012). TEs containing both an active reverse transcriptase and transposase have not been described in the literature. It has been reported,

however, that TEs have a tendency to insert themselves into other TEs, which could explain the presence of both a transposase and a reverse transcriptase in the LSCE regions (Fedoroff 2012; Muszewska et al. 2019) . Possibly, the LSCE region originated from two insertion events. First, TE activity mediated assembly of the LSCE region and insertion into another TE which subsequently duplicated and formed the second, inverted copy of the LSCE region.

4.2.2 Sequence conservation in the duplicated LSCE region is due to clonal propagation of *V. dahliae* chlorosis-class isolates

Duplications of single genes or entire regions in fungi have been reported to occur frequently and to contribute to genome plasticity and consequently enhanced adaptation to new hosts (Wapinski et al. 2007; Raffaele and Kamoun 2012; Guyon et al. 2014; Pendleton et al. 2014) . After duplication, mutations or structural changes in the copies give rise to new genetic variation (Raffaele and Kamoun 2012) . The fact that the two copies of the LSCE region and consequently the *LSCE2* copies are identical suggests that either the LSCE regions have been protected from random mutations or that the duplication event has occurred recently. Increased sequence conservation in *Verticillium* LS regions compared to the core genome has been reported recently but why and how LS sequences are conserved has not been demonstrated mechanistically (Depotter et al. 2018). One explanation why LS and consequently the LSCE regions could be more protected from mutations than other regions in the genome may be their epigenetic organization. It has been shown for the human genome that open chromatin had lower mutation rates compared to closed chromatin (Prendergast et al. 2007) . This gave rise to the hypothesis that this was due to higher accessibility of open structures to repair mechanisms such as homologous recombination or proofreading during DNA replication (Prendergast et al. 2007; Branzei and Foiani 2008).

High overall levels of sequence conservation are common for clonally propagating, haploid fungi such as *Verticillium* (deJonge et al. 2013) . Indeed, we found no single nucleotide polymorphisms (SNPs) after sequencing *LSCE2*, *LSCE2-like* and phylogenetic markers of *V. dahliae* chlorosis-class isolates (Table 3.4; Figure 3.9, Supplement Figure 6.9; Figure 6.10). This suggests a common ancestor of those isolates. The first chlorosis-class isolate mentioned in the literature was *V. dahliae* T9 in 1970

when Wiese and DeVay investigated the defoliating disease phenotype on cotton plants upon infection with *V. dahliae*. The link between the chlorosis-class disease phenotype on Arabidopsis and defoliating disease phenotype on cotton and olive has been noted by K. Thole (2016) who found that four out of five characterized chlorosis-class isolates had been isolated from defoliated cotton and olive. The emergence of highly aggressive cotton defoliating *V. dahliae* isolates was first observed in California in the early 1960s (Schnathorst T and Mathre 1966). Fifty years later, population genomics confirmed that the defoliating *V. dahliae* isolates originated from cotton in California and then spread by clonal propagation from there to cotton, olive and woody plants in Europe, Asia and Australia (Milgroom et al. 2016; Chapman et al. 2016). Correspondingly, Milgroom et al. (2016) found only 23 single nucleotide polymorphisms (SNPs) in a collection of 91 defoliating *V. dahliae* isolates collected from various hosts and geographic locations. In comparison, 26 748 SNPs were reported for a collection of 141 *V. dahliae* isolates with diverse disease phenotypes (Milgroom et al. 2014). In summary, the data suggests that *LSCE2* is present in defoliating *V. dahliae* isolates. Clonal expansion of defoliating isolates explains sequence conservation within the LSCE regions and between the chlorosis-class isolates. The question if and how *LSCE2* is involved in the defoliating disease phenotype on cotton and olive is currently being addressed by our collaborators at the University of Wageningen (Netherlands).

4.2.3 LSCE regions in *V. longisporum* originated from hybridization with chlorosis-class *V. dahliae* isolates or horizontal gene transfer

Our experimental data demonstrated that the tandem-inverted LSCE regions and consequently two copies of *LSCE2* are present in the genome of chlorosis-class *V. longisporum* isolate VL43 (A1/D1) (Figure 3.5). *V. longisporum* is a hybrid species that arose from at least three isolated hybridization events (Inderbitzin et al. 2011a; Inderbitzin et al. 2011b; Depotter et al. 2016; Depotter et al. 2017a). All *V. longisporum* lineages share the parental line A1, which has been phylogenetically placed as sister clade to *V. dahliae* and *V. alfalfae*. The second parental line is unique to the lineages and closely related to (D1) or contained within (D2, D3) the *V. dahliae* clade (Inderbitzin et al. 2011b). The fact that two and not four copies of LSCE2 exist in *V. longisporum* suggests either that one parental

line was the donor of the LSCE regions or that the regions were gained independently of hybridization events through horizontal gene transfer.

Here, one A1/D3 and eight A1/D1 isolates were tested and *LSCE2* was found in five A1/D1 isolates, including the reference isolate VL43 but not the in the remaining three A1/D1 isolates and the A1/D3 isolates VL32 (Figure 3.9). The fact that not all members of the A1/D1 lineage possess *LSCE2* confers with the hypothesis that either *LSCE2* was lost in some isolates after hybridization or that A1/D1 isolates with and without *LSCE2* represent two separate hybridization events. Recently, Depotter et al. (2017) discovered that the A1/D1 is subdivided in Europe into an A1/D1 population West and East. Based on whole-genome comparison, they then hypothesized that the two populations did not represent separate hybridization events but segregated from a common ancestor (Depotter et al. 2017b). It is therefore likely that LSCE2 was lost (or gained) after hybridization. If A1/D1 isolates with and without *LSCE2* represent two separate lineages remains to be elucidated.

V. longisporum may have first gained the LSCE regions through hybridization with chlorosis-class *V. dahliae* isolates. To this day, the parental lines of *V. longisporum* have not been isolated as independent, haploid species. It can therefore be hypothesized that chlorosis-class *V. dahliae* isolates presented here gave rise to the D1 parental line but this is not supported by the available data. In 2011, Inderbitzin et al. presented a phylogenetic tree that used genomic sequences from *V. longisporum* lineages and *V. dahliae*. One characterized chlorosis-class *V. dahliae* isolate, V138I, was included in the phylogenetic tree and appeared in a clade separated with significant support from any *V. longisporum* parental lineage (Inderbitzin et al. 2011b). This is supported by the findings presented here demonstrating that sequences from *LSCE2-like*, a homolog of *LSCE2*, clearly separated *V. dahliae* chlorosis-class isolates from *V. longisporum* isolates (Figure 3.5A). The fact that chlorosis-class *V. dahliae* and *V. longisporum* isolates form a paraphyletic group suggests that the *V. dahliae* chlorosis-class isolates presented here are not direct ancestors of the *V. longisporum* chlorosis-class isolates. This of course does not exclude the possibility that yet uncharacterized *V. dahliae* chlorosis-class isolates gave rise to the D1 lineage.

As discussed before, the presence of A1/D1 isolates without *LSCE2* could represent a presence/absence polymorphism of the gene independent of hybridization. This is further supported by the hypothesis that the LSCE regions are associated with transposable elements.

Presence/absence polymorphisms of effector genes, meaning the presence or absence of effectors independent from phylogenetic relationships, are common in plant pathogenic haploid fungi and have been reported to be mediated by transposable elements (Araki et al. 2006; Hartmann et al. 2018; Sánchez-Vallet et al. 2018). Presence/absence polymorphisms contribute to adaptive evolution. In the genome of ascomycete rice pathogen *Magnaporthe oryzae*, for example, presence/absence polymorphisms of effectors were found to be more frequent than nucleotide polymorphisms (Yoshida et al. 2009). It has also been hypothesized that *Verticillium spp.* relies more on the presence and absence of lineage-specific regions than on variation on the nucleotide level in order to adapt to new environmental conditions (deJonge et al. 2013; Faino et al. 2016). An example for a presence/absence polymorphism is the *V. dahliae Avr1* effector which mediates pathogenicity on tomato (deJonge et al. 2012). The current understanding of the evolutionary history of *Avr1* is that it was first acquired through horizontal gene transfer and subsequently lost multiple times in independent *V. dahliae* lineages (Faino et al. 2016). In summary, it can be hypothesized that in the *V. longisporum* A1/D1 lineage the LSCE regions were gained through hybridization from a yet unknown chlorosis-class *V. dahliae* isolate and were subsequently lost in some A1/D1 isolates.

Another possibility of *LSCE2* transfer between *V. dahliae* and *V. longisporum* apart from hybridization is horizontal gene transfer (HGT). HGT means the transmission of genetic material between distinct evolutionary lineages and has been reported contribute to *Verticillium* evolution. Shi-Kunne et al. presented in their study evidence for interkingdom HGT from bacteria to *Verticillium spp.*. Interestingly, they found that several HGT candidates were carbohydrate-active enzymes and suggested that genes acquired from bacteria are involved in host-plant interaction (Shi-Kunne et al. 2019). Other examples for HGT in *Verticillium* are the acquisition of the effector *Ave1* from a yet unidentified plant donor and a glucosyltransferase from bacteria (Klosterman et al. 2011; deJonge et al. 2012). Furthermore, Chen et al. reported in 2017 that a *V. dahliae* isolate highly virulent on cotton has acquired cotton-specific virulence factors through HGT from the vascular plant pathogen *Fusarium oxysporum f. sp. vasinfectum*. Homology searches in the publicly available databases found a homolog of *LSCE2* in the vascular plant pathogen *Fusarium oxysporum f. sp. radicis-cucumerinum* (Supplement Figure 6.6), suggesting that *LSCE2* has been exchanged through HGT between *Verticillium* and *Fusarium*. The function of the *LSCE2* homolog in *Fusarium* has not yet been characterized. It has been reported that transposable elements are frequently involved in HGT and that HGT is more likely between species

inhabiting the same ecological niche (Fortune et al. 2008; Schaack et al. 2010; Venner et al. 2017). The fact that *Fusarium*, *V. dahliae* and *V. longisporum* inhabit the vascular system of overlapping plant hosts and the hypothesis that the LSCE region is associated with transposable elements gives plausibility to the hypothesis that HGT has played a role in the evolution of *LSCE2*.

4.3 The *LSCE2* homolog *LSCE2-like* is a target of pseudogenization in chlorosis-class isolates

Comparative genomics revealed a ~1500 bp region in the core genomes *V. dahliae* reference isolates V76 and JR2 which is homologous to the *LSCE2* encoding gene region (Figure 3.6). The single-copy gene encoded in this region was designated as *LSCE2-like*. Subsequent analyses revealed that *LSCE2-like* is present in the genomes of all 25 *Verticillium spp.* isolates investigated here (Table 3.4). Interestingly, *LSCE2-like* is a pseudogene in all *V. dahliae* chlorosis-class isolates and all *V. longisporum* isolates except VL32 due to single nucleotide polymorphisms (SNPs) or nucleotide deletions (Supplement Figure 6.10). Interestingly, *LSCE2-like* is present as a single-copy gene in the hybrid species *V. longisporum*, suggesting that it was introduced into the genome by only one of the parental lines. Pseudogenes are homologous to functional genes but contain disruptive mutations (Vanin 1985). These disruptive mutations can cause premature stop codons, frameshifts, dysfunctional promoter sequences or defective splicing (Zhang et al. 2010). Pseudogenization usually happens to gene or gene copies that are not required for the survival of the organism and are therefore subject to random genetic mutations. However, pseudogenization can also be driven by selection pressure when, for example, fungal effectors are recognized upon host plant infection and trigger ETI (van der Burgt et al. 2014). How fast pseudogenization can occur was demonstrated by Stergiopoulos et al. (2007) who observed that extensive genetic variation and pseudogenization in the avirulence (*Avr*) genes of the tomato pathogen *Cladosporium fulvum* overcame ETI in tomato in the course of a few years (Stergiopoulos et al. 2007). Interestingly, pseudogenization of *LSCE2-like* is caused by different mutations in the *Verticillium spp.* lineages. The start codon and intron recognition site are mutated and 12 stop codons were introduced by non-synonymous substitutions in all *V. dahliae* chlorosis-class isolates (Figure 6.10, Table 3.4). In *V. longisporum* isolates, on the other hand,

deletion of the 5th and/or 16th nucleotide of *LSCE2-like* coding sequence creates early frame shifts. The deletion is similar between chlorosis-class and asymptomatic *V. longisporum* isolates. *In vitro* data suggests that *LSCE2-like* may be transcriptionally inactive in asymptomatic and wilting-class *V. dahliae* isolates (Figure 3.8). Future expression analyses of *LSCE2-like in planta* are required to reveal if the gene truly is inactive. In addition, experiments focusing on the function of *LSCE2-like* may elucidate why the selective pressure on pseudogenization is stronger in chlorosis-class isolates than in others.

Due to their high sequence homology, it can be assumed that duplication of *LSCE2-like* and subsequent mutations have led to the emergence of *LSCE2*. The hypothesis that *LSCE2-like* is evolutionary older than *LSCE2* is supported by phylogenetic data inferred from *LSCE2-like* sequences. The *LSCE2-like* tree topology was similar compared to the topology generated with a dataset from general phylogenetic markers, which demonstrates that *LSCE2-like* evolved with the core genome (Figure 3.9). Duplication of (effector) genes in the genomes of plant pathogenic fungi is a frequently occurring process that facilitates adaptation (Skamnioti et al. 2008; Möller and Stukenbrock 2017). Through mutations, an effector can gain new functions or lose sites that are recognized by the plant immune system (Sánchez-Vallet et al. 2018). For example, Longya et al. reported that duplication and mutations of the *AVR-Pik* effector in the genome of the rice blast pathogen *Magnaporthe oryzae* led to the emergence of new variants of the effector which evade plant recognition and thus enhance virulence (Longya et al. 2019). Likewise, it was discovered that glutathione synthetases (GS) in plant pathogenic nematodes were subject to neofunctionalization and gave rise to GS-like effectors (Lilley et al. 2018). In summary, it is possible to hypothesize that *LSCE2* arose through duplication and neofunctionalization from *LSCE2-like*.

It was demonstrated here that LSCE2 purified from *P. pastoris* cultures was able to induce transdifferentiation of bundle sheath cells into xylem elements and chlorosis upon infiltration of Arabidopsis leaves (Figure 3.30). In contrast to LSCE2, infiltration of LSCE2-like did not have visible effects on Arabidopsis leaves. Intriguingly, while LSCE2 and LSCE2-like are identical in length, the LSCE2 signal was detected significantly higher than LSCE2-like after SDS-PAGE (Figure 3.7; Figure 3.29). In their study on protein migration during SDS-PAGE, Shi et al. summarized factors that can cause gel shifting of homologous proteins. These potential factors include differences in the secondary

structure of the protein or in their hydrodynamic properties, differences in the intrinsic net charge of the homologous proteins and post-translational modifications (Shi et al. 2012). It will be the subject of future studies to determine which of these effect(s) cause the observed LSCE2/ LSCE2-like band shift and how they influence functionality.

4.4 Deletion of *LSCE2* does not impact vegetative fungal growth

Before the impact of *LSCE2* on pathogenicity and virulence was tested in infection experiments, it was necessary to investigate potential growth defects of the generated *Verticillium spp.* mutant lines. To this end, *in vitro* growth of *Verticillium spp.* single (Δ) as well as double (ΔΔ) *LSCE2* deletion lines and transgenic *V. dahliae* JR2 lines was monitored. No differences between transformants and wild-type isolates were observed (Figure 3.11; Figure 3.12; Figure 3.24). Effectors are defined as molecules that interact with plant targets and modulate immune responses (Selin et al. 2016) and should therefore not affect vegetative fungal growth. There are examples for factors influencing fungal vegetative growth and consequently virulence. It was observed by Tran et al. (2014) that knockout lines of the *V. dahliae* transcription activator of adhesion *Vta2* had aberrant vegetative growth phenotypes and were unable to successfully colonize tomato (Tran et al. 2014). Similar to this, *V. dahliae* knockout lines of the small GTPase *Rac1* and the p21-activated kinase were defective in polarized hyphal growth and microsclerotia formation as well as virulence on cotton (Tian et al. 2015). Our results indicate that *LSCE2* is not involved in vegetative growth. Consequently, none of the effects observed upon Arabidopsis infection with mutant lines were caused by aberrant fungal growth or morphology.

4.5 *LSCE2* mediates establishment of the chlorosis-class disease phenotype which may have different roles in *V. dahliae* and *V. longisporum*

In this study, Arabidopsis infection experiments were conducted with *Verticillium spp.* isolates from all disease classes. No disease symptoms were detected in infections with asymptomatic *V. longisporum* VL32 (Figure 3.14; Figure 3.17; Figure 3.20) whereas wilting-class isolate *V. dahliae* JR2 induced stunting, wilting and enhanced lignification (Figure 3.13; Figure 3.16; Figure 3.19). Chlorosis-class isolates *V. dahliae* V76 and *V. longisporum* VL43 caused stunting, chlorosis, transdifferentiation of bundle sheath cells and xylem hyperplasia (Figure 3.13; Figure 3.14; Figure 3.16; Figure 3.17; Figure 3.19; Figure 3.20). The results confirm previous observations (Reusche et al. 2012; Reusche et al. 2014; Thole 2016). Intriguingly, no changes in the chlorosis-class disease phenotype were observed after infection with *Verticillium spp.* Δ*LSCE2* lines (Figure 3.13; Figure 3.14; Figure 3.16; Figure 3.17; Figure 3.19; Figure 3.20). *In planta* fungal biomass accumulation was also not affected in *Verticillium spp.* Δ*LSCE2* lines when compared to wild-type isolates (Figure 3.21; Figure 3.22). Taken together, the data demonstrates that the deletion of one *LSCE2* copy affects neither pathogenicity nor virulence. This suggests that the *LSCE2* copies are functionally redundant and that expression of one copy compensates deletion of the other.

In contrast to this, the ability to induce chlorosis-class disease symptoms was completely abolished in *Verticillium spp.* ΔΔ*LSCE2* lines. Plants infected with ΔΔ*LSCE2* lines showed neither stunting nor chlorosis, transdifferentiation or xylem hyperplasia (Figure 3.13; Figure 3.14; Figure 3.16; Figure 3.17; Figure 3.19; Figure 3.20). Intriguingly, some wilting leaves were found after infection with *V. dahliae* ΔΔ*LSCE2* lines (Figure 3.13). Furthermore, enhanced lignification was observed in the vascular tissue of the wilting leaves (Figure 3.19). Wilting and enhanced lignification is usually observed after infection with wilting-class *V. dahliae* isolates and has been associated with the occlusion of vascular tissue caused by the fungus and plant defense responses (Fradin and Thomma 2006; Reusche et al. 2014; Thole 2016). This indicates that virulence was not completely abolished in *V. dahliae* ΔΔ*LSCE2* lines. Fungal biomass accumulation was significantly reduced in plants infected with *V. dahliae* V76 ΔΔ*LSCE2* lines (Figure 3.21). This correlated with drastically reduced disease symptoms in these plants. These observations corroborate findings from other studies with *Verticillium* effector deletion

lines. DeJonge et al. (2012) reported decreased disease severity and fungal biomass in susceptible tomato plants infected with Δ*Ave1.* The same was observed for knockout lines of the LysM effector *Vd2LysM* (deJonge et al. 2013; Kombrink et al. 2017). LysM effectors bind chitin and can therefore protect the fungus from recognition through plant receptors (Kombrink and Thomma 2013). The loss of *Vd2LysM* therefore makes *Verticillium* susceptible to plant defense responses limiting fungal *in planta* growth. Thus, it could be the case that with the deletion of *LSCE2*, *V. dahliae* chlorosis-class isolates lose the mechanism that allows them to circumvent plant immune responses.

In marked contrast to V76 ΔΔ*LSCE2* lines, *V. longisporum* VL43 ΔΔ*LSCE2* lines did not induce any disease symptoms on Arabidopsis (Figure 3.14; Figure 3.17; Figure 3.20). However, VL43 ΔΔ*LSCE2* lines were able to proliferate in the plant as rapidly as the wild-type isolate (Figure 3.22). This was also the case for the asymptomatic *V. longisporum* isolate VL32 (Figure 3.22), which indicates that in the absence of *LSCE2*, *V. longisporum* isolates are able to proliferate as endophytes in Arabidopsis. Previously, Depotter et al. (2017a) observed that a *V. longisporum* isolate with high proliferation rates did not cause high losses in rapeseed and cauliflower biomass, supporting our hypothesis that *V. longisporum* can proliferate within the plant without causing detrimental effects (Depotter et al. 2017a). Endophytes are defined as microorganisms that successfully colonize plants without causing disease symptoms. Interestingly, phylogenetic studies demonstrated that endophytism is not an evolutionary stable trait and that lineages can switch between endophytic and necrotrophic lifestyles during evolution or even upon changing environmental conditions (Redman et al. 2001; Delaye et al. 2013). In their review on lifestyles of the plant pathogenic fungus *Botrytis*, van Kan et al. (2014) recognized that signals between fungus, host and environment control the choice of lifestyle of the pathogen. They suggested to abolish the rigid classification of organisms into endophytes, (hemi)-biotrophs, necrotrophs or saprophytes (van Kan et al. 2014). Interestingly, an endophytic lifestyle has been reported for several *Verticillium* isolates in, for example, *Rehmannia glutinosa* (You et al. 2009), cauliflower (Tyvaert et al. 2014) and rotation crops such as pea and peppermint (Wheeler and Johnson 2016). Recently, Wheeler et al. (2019) studied endophytism in *Verticillium* in more detail. They postulated gene flow between endophytic and pathogenic isolates and hypothesized that a single *V. dahliae* isolate can infect and exhibit host adaptation across a variety of hosts, as endophyte or pathogen (Wheeler et al. 2019). The data suggest that under laboratory conditions, *LSCE2* does not act a virulence factor in the *V. longisporum*-Arabidopsis pathosystem. Arguably, *V. longisporum*

reverts to an endophytic lifestyle in the absence of *LSCE2*. It was demonstrated by Reusche et al. that *de novo* xylem formation due to developmental reprogramming enhances drought stress resistance in Arabidopsis (Reusche et al. 2012). Consequently, they argued that the *V. longisporum*–Arabidopsis relationship is conditionally mutualistic, meaning that detrimental and beneficial effects of chlorosis-class infections depend on environmental conditions.

The hypothesis that *LSCE2* does not act exclusively as a virulence factor is supported by the observation that fungal biomass accumulation does not increase in transgenic JR2 [p*LSCE2*:*LSCE2*] lines when compared to wild-type wilting-class isolate JR2 (Figure 3.28). JR2 [p*LSCE2*:*LSCE2*] lines were able to induce chlorosis, transdifferentiation of bundle sheath cells and xylem hyperplasia (Figure 3.25; Figure 3.27; Figure 3.27). Interestingly, wilting-class symptoms were not completely abolished during infection with JR2 [p*LSCE2*:*LSCE2*] lines, as demonstrated by the enhanced lignification of xylem elements observed in leaf midrib transections (Figure 3.27). In addition, chlorosis-class disease symptoms were not as strong as symptoms induced by chlorosis-class *V. dahliae* isolate V76. One reason for this could be a reduced capacity for *LSCE2* expression in JR2 [p*LSCE2*:*LSCE2*] lines due to inhibition of transcription at the insertion site. It may also be taken into consideration that ectopic expression of *LSCE2* introduces a second disease phenotype in addition to the wilting-class disease phenotype inherent to JR2, resulting in interference between the two pathogenicity programs. Notably, infection of Arabidopsis with wilting-class isolate JR2 causes clogging of the vasculature and consequently wilting of rosette leaves (Reusche et al. 2014). Clogging of the vascular stream in plants infected with JR2 [p*LSCE2*:*LSCE2*] lines may therefore limit the distribution of secreted LSCE2.

In summary, our data support the hypothesis that *LSCE2* has different roles in *V. dahliae* and *V. longisporum* chlorosis-class isolates. Arabidopsis as a member of the Brassicaceae family is not a natural host of *V. dahliae*. Therefore, *de novo* xylem formation may enable *V. dahliae* chlorosis-class isolates to evade plant defense responses and successfully colonize the plant. *V. longisporum* isolates, on the other hand, are adapted to Arabidopsis. Here, *LSCE2*-mediated developmental reprogramming may represent a conditionally mutualistic adaptation to drought stress. Transgenic expression of *LSCE2* in wilting-class isolates JR2 furthermore indicates that a single effector mediates developmental reprogramming in host plants.

4.6 A single effector mediates developmental reprogramming in the Arabidopsis-*Verticillium spp.* pathosystem

From the data generated here it is possible to postulate that LSCE2 mediates developmental reprogramming in Arabidopsis after *Verticillium spp.* infection. A prominent example of developmental reprogramming in plant-pathogen interactions is tumorigenic gall formation which usually is triggered through modulation of auxin and/or cytokinin levels by pathogens. Phytohormone production by *Verticillium spp.* isolates has not been described in the literature. Auxin levels measured in mock-treated and *V. dahliae*-infected plants are not significantly different (Fousia et al. 2018). Furthermore, it has been shown that cytokinin levels are decreased in plants infected with chlorosis-class isolate VL43 due to enhanced expression of cytokinin oxidases (Reusche et al. 2013) . This suggests that *Verticillium* modulates phytohormone signaling instead of secreting phytohormones. Intriguingly, putative LSCE2 interaction targets in the yeast-two-hybrid screen encode for a protein involved in auxin signaling (D6PKL1) and another protein upregulated during *Agrobacterium*-induced tumor formation (PGIP1) (Table 3.6, Supplement Table 6.2). *A. tumefaciens* integrates its Transfer (T)-DNA into the genome of plant cells at the infection site (Gelvin 2003). The T-DNA encodes, amongst others, so-called oncogenes (Zhu et al. 2000). Oncogenes are enzymes involved in the biosynthesis of growth hormones responsible for the proliferation of transformed plant cells (Binns and Costantino 1998; Zhu et al. 2000) . The oncogenes *CYT*, *AUX1I* and *AUX2* are essential for tumorigenesis and code for enzymes involved in the biosynthesis of the cytokinin isopentenyl-AMP (*CYT*) and the auxin indole acetic acid (*AUX1, AUX2*) (Garfinkel et al. 1981) . Cytokinin and auxin then mediate tumorigenic cell proliferation (SCHRODER et al. 1984; Akiyoshi et al. 1984; Binns and Costantino 1998) . In addition, another oncogene that is not involved in phytohormone biosynthesis is encoded on the T-DNA. Hooykaas et al. (1988) demonstrated that *oncogene 6b* (*onc 6b*) in absence of *CYT*, *AUX1* and *AUX2* is sufficient to induce small tumors on *Nicotiana glauca*. Functional characterization of *onc 6b* subsequently revealed that it acts as a histone H3 chaperon *in vitro* (Ishibashi et al. 2014). Ishibashi et al. (2014) hypothesized that alterations of the chromatin structure might affect the expression of various genes related to cell division competence and the maintenance of meristematic states. The current understanding is that *onc 6b* reprograms the cells to be more responsive to auxin/cytokinin

signaling (Ishibashi et al. 2014; Ito and Machida 2015). Very interestingly, *Nicotiana tabacum* plants transformed with a dexamethasone-inducible *dex-T-6b* gene shows several striking growth phenomena (Chen and Otten 2016). Ectopic expression of *dex-T-6b* produces ectopic vascular strands in leaf blades, petioles and midveins. These cells, in contrast to *LSCE2*-induced *de novo* xylem formation, constitute a kind of elementary structure without xylem maturation (Chen and Otten 2016). This confirms that substantial developmental reprogramming can be induced by a single factor without direct alteration of phytohormone levels.

4.7 LSCE2 induces xylogenesis in Arabidopsis probably by modulating signaling upstream of VND6 and VND7

LSCE2 purified from *P. pastoris* cultures had the capacity to induce chlorosis and transdifferentiation of bundle sheath cells into xylem elements upon infiltration of Arabidopsis leaves (Figure 3.31). Furthermore, constitutive expression of *LSCE2-GFP* in stably transformed Arabidopsis lines resulted in a strong phenotype exhibiting chlorosis-class disease symptoms (Figure 3.31; Figure 3.33). This demonstrates that developmental reprogramming mediated by chlorosis-class *Verticillium spp.* isolates requires no *Verticillium* factor other than LSCE2. Consequently, it can be postulated that LSCE2 either interacts with several targets in the plant proteome or interacts with a master regulator of xylogenesis to induce *de novo* xylem formation.

Xylogenesis in Arabidopsis is governed by tightly regulated developmental processes (Yang and Wang 2016). An auxin/cytokinin mutually inhibitory feedback loop initiates and mediates the formation of vascular procambium, from which xylem tissues are differentiated (Bishopp et al. 2011). It has been shown that shifting the balance towards cytokinin signaling induces ectopic formation of xylem elements (Katayama et al. 2015). Aside from phytohormone signaling, auxin transport mediated by the PIN1 efflux carrier contributes to procambium development (Yang and Wang 2016). Intriguingly, the PIN1-phosphorylating protein kinase D6pKL1 was recovered from the yeast-two-hybrid interaction screen with LSCE2, indicating a putative role of LSCE2 in this regulatory pathway (Table 3.6; Table 6.2). A factor initiating xylem differentiation in Arabidopsis is the brassinosteroid-responsive

transcription factor *BES1* (Yin et al. 2002). Notably, it has been demonstrated that pharmacological inactivation of the BES1 inhibitor GSK1 initiates ectopic xylem element differentiation in leaf disks (Kondo et al. 2015). Downstream of GSK1, maturation of xylem elements which requires programmed cell death and secondary cell wall deposition are regulated by *VASCULAR-RELATED NAC DOMAIN* (*VND*) transcription factors (Kubo et al. 2005; Yamaguchi et al. 2010). Ectopic expression of *VND6* or *VND7* induces transdifferentiation of mesophyll cells into xylem elements (Kubo et al. 2005; Yamaguchi et al. 2010). Correspondingly, Reusche et al. (2012) reported that expression of *VND6* and *VND7* is induced during *de novo* xylem formation triggered by *V. longisporum* VL43 infection and demonstrated that transdifferentiation is reduced in *VND7* suppressor lines. It therefore seems likely that LSCE2 interacts with Arabidopsis targets upstream of VND6 and VND7 to induce transdifferentiation. In contrast to transdifferentiation initiated by xylogenesis factors discussed above, transdifferentiation remained restricted to bundle sheath cells after infiltration of LSCE2 (Figure 3.31) and expression of *LSCE2* under the control of the ubiquitously active *UBQ10* promoter (Figure 3.33). This could be explained by the fact that *VND6* and *VND7*, like most xylogenesis-related genes, are expressed exclusively in the vascular tissue and bundle sheath of Arabidopsis (Zhong et al. 2008; Yamaguchi et al. 2008; Reusche et al. 2012).

In contrast to transdifferentiation initiated by xylogenesis factors discussed above, transdifferentiation remained restricted to bundle sheath cells after infiltration of LSCE2 (Figure 3.31) and expression of *LSCE2* under the control of the ubiquitously active *UBQ10* promoter (Figure 3.33). In addition, vein clearing as a macroscopic symptom of bundle sheath cell transdifferentiation appeared only in mature leaves and was not present in younger, developing leaves (Figure 3.31; Figure 3.33). This indicates that (1) bundle sheath cells are initially formed in the leaf before they are transdifferentiated and (2) that only specific cells at a specific developmental stage are competent for perceiving LSCE2. A developmental event that coincides with the appearance of vein clearing on LSCE2-GFP leaves is the transition from sink to source organ. Young, developing leaves require nutrients for growth (sink organs) which are provided by photosynthetically active leaves producing an excess of metabolic products (source organs). This means that bundle sheath cells have to transition from mediating nutrient influx (sink) to efflux (source). It remains to be elucidated if transcriptional and/or structural remodeling of bundle sheath cells during the transition from sink to source organ enables these cells to perceive the LSCE2 signal.

4.8 *De novo* xylem formation induced by LSCE2 may trigger early senescence in Arabidopsis

Chlorosis in the *Verticillium*-Arabidopsis pathosystem is a symptom of early senescence induced by the pathogen (Reusche et al. 2012; Thole 2016). Infiltration of purified LSCE2 and transgenic expression of *LSCE2-GFP* induced chlorosis on Arabidopsis leaves (Figure 3.30; Figure 3.31; Figure 3.33). This suggests that early senescence is not induced by toxins or fungal effectors apart from LSCE2 but is a reaction of the plant to LSCE2 function. This is supported by the observation that chlorotic areas appeared on LSCE2-GFP later than transdifferentiation-associated vein clearing (Figure 3.31B; Figure 3.33). Therefore, it can be hypothesized that senescence is induced by a signal generated through the developmental reprogramming of the vasculature rather than direct interaction of LSCE2 with a senescence-triggering target.

One trigger for senescence is the age- or light intensity related decline of photosynthetic activity in (Hensel et al. 1993; Weaver and Amasino 2001). Bundle sheath cells in Arabidopsis constitute ~ 15 % of all chloroplast-containing cells in the leaf (Kinsman and Pyke 1998). Therefore, it is possible that the loss of chlorophyll due to transdifferentiation of bundle sheath cells results in a decline of photosynthetic activity that triggers early senescence. The importance of bundle sheath cells in photosynthesis has been demonstrated by Janacek et al. (2009) who presented Arabidopsis plants with reduced capacities to accumulate chlorophyll in the bundle sheath. Intriguingly, they observed that in these plants growth and flowering were slower and senescence was prolonged (Janacek et al. 2009). Another example for Arabidopsis with reduced photosynthetic activity in the bundle sheath is the *var5-1* mutant (Liang et al. 2017). This mutant has pale green to white leaf veins and green laminas, which is in appearance very similar to the phenotype of *LSCE2-GFP* Arabidopsis plants presented here (Figure 3.31). In contrast to *LSCE2-GFP* plants, neither plant growth nor senescence were affected in the *var5-1* plants (Liang et al. 2017). However, it has to be taken into consideration that in *var5-1* plants, leaves develop with cleared veins whereas in *LSCE2-GFP* leaves, vein clearing appears when the leaf matures. Therefore, the theory that the decline of photosynthetic activity triggers senescence cannot be dismissed.

Senescence can also be activated by the phytohormone ethylene (Lim et al. 2007). Interestingly, enhanced ethylene production in infected plants has been associated with defoliation and defoliating *Verticillium* isolates. As mentioned previously, four out of five *V. dahliae* isolates used here are defoliating isolates and it is likely that the defoliating disease phenotype is linked to *LSCE2*. Wiese and deVay (1970) observed significantly higher ethylene production in cotton plants infected with the defoliating/chlorosis-class isolate *V. dahliae* T9 (there referred to as *V. albo-atrum*, see introduction) compared to non-defoliating isolate SS4. They also demonstrated that cotton plants subjected to exogenous application of ethylene mimic the defoliation disease phenotype (Wiese and Devay 1970). Accumulation of ethylene was also observed in cocoa seedlings infected with defoliating/chlorosis-class isolate *V. dahliae* T9 (RESENDE et al. 1996).

Ethylene production upon infection with *Verticillium spp.* isolates T179 and H93P was also shown in tomato plants by Pegg and Cronshaw (1976) who also demonstrated that *Verticillium* isolates are not able to produce ethylene themselves (Pegg and Cronshaw 1976). A later study investigated the effect of an uncharacterized 'toxin' from *Verticillium albo-atrum* isolate V3 on potato (Mansoori and Smith 2005). Potato seedlings produced ethylene upon toxin treatment. Intriguingly, Mansoori and Smith also demonstrated that toxin-induced chlorosis of potato leaves was inhibited after application of silver ions as an ethylene-signaling inhibitor. Finally, Pantelides et al. investigated disease symptoms of *V. dahliae* infections on Arabidopsis ethylene signaling mutants. They found that disease symptoms were reduced in the *etr1* line but not in *ein2, 3, 4 or 5,* suggesting a differential role of ethylene signaling components upon pathogen-induced ethylene production (Pantelides et al. 2010). The *V. dahliae* isolate used by Pantelides et al. was isolated from *Raphanus sativus* (Brassicaceae) (Tjamos et al. 2005) but from the data presented in the paper, it could not be determined if the isolate belongs to the chlorosis or wilting class. Taken together, the data from the literature suggest that ethylene is an important factor for pathogenicity during *Verticillium spp.* infections. It remains to be determined if ethylene produced by *de novo* xylem formation is sufficient to induce senescence and drought stress and/or defense reaction contribute to the total ethylene production of the host plant.

Intriguingly, ethylene has also been implicated to have a role in xylogenesis. In Arabidopsis, for example, the ethylene biosynthetic gene *1-AMINOCYCLOPROPANE-1-CARBOXYLATE SYNTHASE* (*ACS*) is expressed in developing xylem (Tsuchisaka and Theologis 2004). In poplar, the activity of ethylene biosynthetic gene *AMINOCYCLOPROPANECARBOXYLATE OXIDASE* (*ACC*) has been shown to play a role in tension wood formation in response to gravitational stimulation (Andersson-Gunneras et al. 2003). In 2011, Pesquet and Tuominen investigated ethylene biosynthetic gene expression and ethylene evolution during transdifferentiation of mesophyll cells into xylem elements in the *Zinnia elegans* system. They found that ethylene biosynthesis was substantially induced during transdifferentiation. The highest amount of ethylene was detected upon maturation of xylem elements (Pesquet and Tuominen 2011). Simultaneously they showed that transdifferentiation was inhibited when ethylene production was blocked, suggesting a crucial role of ethylene in the regulation of xylogenesis. The fact that ethylene is produced during transdifferentiation of *Z. elegans* mesophyll cells implies that ethylene is also produced during transdifferentiation of bundle sheath cells triggered by LSCE2. Ethylene could then act as a signal inducing senescence in the leaf. To test this theory, ethylene contents in leaves infiltrated with LSCE2 should be measured in future studies. In addition, it should be investigated whether xylem hyperplasia is also triggered by LSCE2 infiltration or expression in Arabidopsis.

Cytokinin is the antagonist of ethylene in the induction of senescence (Lim et al. 2007). Reusche et al. demonstrated that cytokinin levels are reduced in Arabidopsis plants infected with *V. longisporum* VL43 through enhanced expression of *CYTOKININ OXIDASES/DEHYDROGENASEs* (*CKX*). Correspondingly, they showed that treatment of infected Arabidopsis plants with synthetic cytokinin or pharmacological suppression of CKX activity reduced chlorosis symptoms (Reusche et al. 2013). It is therefore likely that LSCE2 directly or indirectly influences cytokinin levels through *CKX* activation. The influence of cytokinin-deficiency on senescence has been discussed in the literature. Tobacco *AtCKX* overexpressor lines, for example, do not have an early senescence phenotype (Werner et al. 2001). Furthermore, Arabidopsis *CKX* overexpressor lines also do not exhibit an earlier onset of senescence (Werner et al. 2003; Köllmer et al. 2014). The same is the case for cytokinin signaling mutants *cre1* and *ahk2/3* as well as cytokinin deficient plants (Riefler et al. 2006). Consequently, it has been argued that while increasing levels of cytokinin does delay senescence (Zwack and Rashotte 2013), lowering the cytokinin level beyond a threshold is not sufficient to trigger the onset of senescence (Werner et al.

2003). It has furthermore been shown in pea, barley, clover and Arabidopsis that *CKX* expression is induced upon senescence (Conrad et al. 2007; Evans et al. 2012; Klepikova et al. 2016; Ninan et al. 2019). Consequently, it is more plausible that that LSCE2 triggers the onset of senescence through, possibly, increasing ethylene levels. This may then cause enhanced expression of *CKX* to further lower cytokinin levels.

4.9 Outlook

It was demonstrated in this study that the *Verticillium spp.* effector LSCE2 mediates developmental reprogramming in Arabidopsis. Genome sequence analyses revealed that *LSCE2* is located in a ~20 kb tandem-inverted region (LSCE region). Six genes were predicted to be encoded in the LSCE region, including the putative effector *LSCE1* and two uncharacterized genes. It would be interesting to investigate whether these genes contribute to virulence or have other functions.

So far, five *V. dahliae* and five *V. longisporum* isolates containing *LSCE2* have been identified. It should be the aim of future studies to test more *Verticillium* species and isolates for the presence of *LSCE2* and the LSCE region. This could answer the question whether the presence of *LSCE2* coincides with hosts from warm and dry climates and provide insights into the evolutionary history and geographical origin of *LSCE2*. Due to the fact that all *V. dahliae* chlorosis-class isolates were also characterized as defoliating isolates on cotton, it should be tested whether *LSCE2* is linked to the defoliating disease phenotype. Additionally, the ability of *V. longisporum* chlorosis-class isolates to induce defoliation on cotton remains to be investigated. Furthermore, a functionally uncharacterized *LSCE2* homolog was found in publicly available genome sequence data of one *Fusarium* isolate. It should be investigated if there are other *Fusarium* isolates with the *LSCE2* homolog and whether the homolog has a function. This could provide insights into the evolutionary origin of *LSCE2*.

LSCE2-like represents another interesting subject for further analyses. *LSCE2-like* has been subjected to pseudogenization in the genomes of all chlorosis-class *Verticillium spp.* isolates but not in asymptomatic and wilting-class *V. dahliae* isolates. Detailed *in planta* expression studies may reveal if *LSCE2-like* is expressed in in asymptomatic and wilting-class *V. dahliae* isolates upon host plant

infection or not. Furthermore, (over)expression of a functional copy of *LSCE2-like* in *Verticillium spp.* and subsequent infection experiments could elucidate the function of *LSCE2-like*. Likewise, a more in-depth characterization of *LSCE2* should be pursued. Detailed *in planta* expression data will provide insights into the regulation of *LSCE2* expression. Furthermore, expression of GFP-tagged LSCE2 in *Verticillium spp.* and subsequent analyses with confocal laser scanning microscopy during infection may shed light into the distribution of LSCE2 in the plant tissues as well as subcellular localization.

Expression of LSCE2 and LSCE2-like in *P. pastoris* has provided a valuable tool for further characterization of these proteins. It was demonstrated in this study that purified LSCE2-like was not able to induce chlorosis-class disease symptoms. Therefore, LSCE2-like can be used as a negative control in future experiments. From comparisons to LSCE2-like, domains that are crucial for LSCE2 function may be revealed. A first clue in this direction was the observation that LSCE2 and LSCE2-like protein was detected at different positions after SDS-PAGE. Treatment of the proteins with, for example, glycosidases will show if posttranslational modifications cause the observed band shift and if they are important for LSCE2 function. Purified LSCE2 and LSCE2-like can also be used for crystallization and subsequent prediction of the tertiary structure. This may provide insights into the location and presence of enzymatically active regions.

In this study it was shown that purified LSCE2 was able to induce chlorosis-class disease symptoms upon infiltration of Arabidopsis leaves. This provides a fast and easy way to test LSCE2 function on numerous plants from all families. These experiments will show to what extent the pathway targeted by LSCE2 is evolutionary conserved. It was also suggested in this study that the induction of LSCE2-triggered developmental reprogramming depends on endogenous factors of the plant. Infiltration of leaves in different developmental stages can show if age is one of these factors. Furthermore, various mutant plants can be used for infiltration to test, for example, if hormone signaling is required for LSCE2 function.

Another interesting subject for future studies will be the characterization of transgene LSCE2-GFP Arabidopsis plants. It was demonstrated in this study that bundle sheath cells of stably transformed Arabidopsis plants transdifferentiated into xylem elements. Now, it should be investigated through microscopic analyses whether xylem hyperplasia is induced in these plants and how LSCE2 expression affects root tissues. In addition, confocal laser scanning microscopy can help to elucidate

subcellular localization of the construct. Reusche et al. observed increased water storage capacity of plants infected with chlorosis-class *Verticillium spp.* isolates (Reusche et al. 2014) . Drought stress experiments with LSCE2-GFP lines will reveal if these plants also are more resistant to drought. In the future, understanding LSCE2 function and applying it to crop plants might even help generating more drought resistant crops.

Of course, the crucial step to understanding LSCE2 function is to identify its targets in the plant. To this end, GFP-trap protein pulldowns from LSCE2-GFP plants and/or myc-tag pulldowns from leaves infiltrated with purified LSCE2 may be conducted. The recovered Arabidopsis proteins can then be analyzed via chromatography and subsequent mass spectrometry. Alternatively, a reverse genetics approach could be employed. Herein, seeds from LSCE2-GFP lines would be subjected to mutagens. Plants that then loose the phenotype can be screened for mutations in potential target proteins.

Taken together, LSCE2 represents an exciting new tool which may in the future be used to address numerous issues from better understanding developmental processes and xylogenesis up to generating drought stress resistant plants.

5 References

Abadía, Javier; López-Millán, Ana-Flor; Rombolà, Adamo; Abadía, Anunciación (2002): Organic acids and Fe deficiency: a review. In *Plant and Soil* 241 (1), pp. 75–86. DOI: 10.1023/A:1016093317898.

Akiyoshi, D. E.; Klee, H.; Amasino, R. M.; Nester, E. W.; Gordon, M. P. (1984): T-DNA of Agrobacterium tumefaciens encodes an enzyme of cytokinin biosynthesis. In *Proceedings of the National Academy of Sciences* 81 (19), pp. 5994–5998. DOI: 10.1073/pnas.81.19.5994.

Albrecht, V.; Zweiniger, C.; Surendranath, V.; Lang, K.; Schöfl, G.; Dahl, A. et al. (2017): Dual redundant sequencing strategy. Full-length gene characterisation of 1056 novel and confirmatory HLA alleles. In *HLA* 90 (2), pp. 79–87. DOI: 10.1111/tan.13057.

Aloni, Roni; Pradel, Katja S.; Ullrich, Cornelia I. (1995): The three-dimensional structure of vascular tissues in Agrobacterium tumefaciens-induced crown galls and in the host stems of Ricinus communis L. In *Planta* 196 (3), pp. 597–605. DOI: 10.1007/BF00203661.

Altschul, S. F.; Madden, T. L.; Schäffer, A. A.; Zhang, J.; Zhang, Z.; Miller, W.; Lipman, D. J. (1997): Gapped BLAST and PSI-BLAST: a new generation of protein database search programs. In *Nucleic acids research* 25 (17), pp. 3389–3402. DOI: 10.1093/nar/25.17.3389.

Altschul, Stephen F.; Gish, Warren; Miller, Webb; Myers, Eugene W.; Lipman, David J. (1990): Basic local alignment search tool. In *Journal of Molecular Biology* 215 (3), pp. 403–410. DOI: 10.1016/S0022-2836(05)80360-2.

Amey, Richard C.; Mills, Peter R.; Bailey, Andy; Foster, Gary D. (2003): Investigating the role of a Verticillium fungicola β-1,6-glucanase during infection of Agaricus bisporus using targeted gene disruption. In *Fungal Genetics and Biology* 39 (3), pp. 264–275. DOI: 10.1016/S1087-1845(03)00061-6.

Amyotte, Stefan G.; Tan, Xiaoping; Pennerman, Kayla; Jimenez-Gasco, Maria del Mar; Klosterman, Steven J.; Ma, Li-Jun et al. (2012): Transposable elements in phytopathogenic Verticillium spp.: insights into genome evolution and inter- and intra-specific diversification. In *BMC genomics* 13, p. 314. DOI: 10.1186/1471-2164-13-314.

Andersson-Gunneras, Sara; Hellgren, Jenny M.; Bjorklund, Simon; Regan, Sharon; Moritz, Thomas; Sundberg, Bjorn (2003): Asymmetric expression of a poplar ACC oxidase controls ethylene production during gravitational induction of tension wood. In *The Plant Journal* 34 (3), pp. 339–349. DOI: 10.1046/j.1365-313X.2003.01727.x.

Araki, Hitoshi; Tian, Dacheng; Goss, Erica M.; Jakob, Katrin; Halldorsdottir, Solveig S.; Kreitman, Martin; Bergelson, Joy (2006): Presence/absence polymorphism for alternative pathogenicity islands in Pseudomonas viridiflava, a pathogen of Arabidopsis. In *Proceedings of the National Academy of Sciences* 103 (15), pp. 5887–5892. DOI: 10.1073/pnas.0601431103.

Ardui, Simon; Ameur, Adam; Vermeesch, Joris R.; Hestand, Matthew S. (2018): Single molecule real-time (SMRT) sequencing comes of age. Applications and utilities for medical diagnostics. In *Nucleic acids research* 46 (5), pp. 2159–2168. DOI: 10.1093/nar/gky066.

Ashok Kumar, T. (2013): CFSSP. Chou and Fasman Secondary Structure Prediction server.

Baayen, R. P. (1986): Regeneration of vascular tissues in relation to Fusarium wilt resistance of carnation. In *Netherlands Journal of Plant Pathology* 92 (6), pp. 273–285. DOI: 10.1007/BF01977590.

Barros, Jaime; Serk, Henrik; Granlund, Irene; Pesquet, Edouard (2015): The cell biology of lignification in higher plants. In *Annals of Botany* 115 (7), pp. 1053–1074. DOI: 10.1093/aob/mcv046.

Bell, Graham (1993): Pathogen evolution within host individuals as a primary cause of senescence. In *Genetica* 91 (1-3), pp. 21–34. DOI: 10.1007/BF01435985.

Benatti, Matheus; Yookongkaew, Nimnara; Meetam, Metha; Guo, Woei-Jiun; Punyasuk, Napassorn; AbuQamar, Synan; Goldsbrough, Peter (2014): Metallothionein deficiency impacts copper accumulation and redistribution in leaves and seeds of Arabidopsis. In *The New phytologist* 202 (3), pp. 940–951. DOI: 10.1111/nph.12718.

Bender, Carol L. (1999): Chlorosis-inducing Phytotoxins Produced by Pseudomonas syringae. In *European Journal of Plant Pathology* 105 (1), pp. 1–12. DOI: 10.1023/A:1008692227307.

Bendtsen, Jannick Dyrløv; Jensen, Lars Juhl; Blom, Nikolaj; Heijne, Gunnar von; Brunak, Søren (2004): Feature-based prediction of non-classical and leaderless protein secretion. In *Protein engineering, design & selection : PEDS* 17 (4), pp. 349–356. DOI: 10.1093/protein/gzh037.

Benhamou, N. (1995): Ultrastructural and cytochemical aspects of the response of eggplant parenchyma cells in direct contact with Verticillium-infected xylem vessels. In *Physiological and Molecular Plant Pathology* 46 (4), pp. 321–338. DOI: 10.1006/pmpp.1995.1025.

Berardini, Tanya Z.; Mundodi, Suparna; Reiser, Leonore; Huala, Eva; Garcia-Hernandez, Margarita; Zhang, Peifen et al. (2004): Functional annotation of the Arabidopsis genome using controlled vocabularies. In *Plant physiology* 135 (2), pp. 745–755. DOI: 10.1104/pp.104.040071.

Binns, Andrew N.; Costantino, Paolo (1998): The Agrobacterium Oncogenes. In Herman P. Spaink, A. Kondorosi, Paul J. J. Hooykaas (Eds.): The Rhizobiaceae. Molecular Biology of Model Plant-Associated Bacteria, vol. 81. Dordrecht: Springer Netherlands, pp. 251–266.

Bishop, C. D.; Cooper, R. M. (1983): An ultrastructural study of root invasion in three vascular wilt diseases. In *Physiological Plant Pathology* 22 (1), 15-IN13. DOI: 10.1016/S0048-4059(83)81034-0.

Bishopp, Anthony; Help, Hanna; El-Showk, Sedeer; Weijers, Dolf; Scheres, Ben; Friml, Jiří et al. (2011): A mutually inhibitory interaction between auxin and cytokinin specifies vascular pattern in roots. In *Current biology : CB* 21 (11), pp. 917–926. DOI: 10.1016/j.cub.2011.04.017.

Boch, Jens; Bonas, Ulla (2010): Xanthomonas AvrBs3 family-type III effectors: discovery and function. In *Annual review of phytopathology* 48, pp. 419–436. DOI: 10.1146/annurev-phyto-080508-081936.

Bogdanove, Adam J.; Schornack, Sebastian; Lahaye, Thomas (2010): TAL effectors: finding plant genes for disease and defense. In *Current Opinion in Plant Biology* 13 (4), pp. 394–401. DOI: 10.1016/j.pbi.2010.04.010.

Boller, Thomas; He, Sheng Yang (2009): Innate immunity in plants: an arms race between pattern recognition receptors in plants and effectors in microbial pathogens. In *Science (New York, N.Y.)* 324 (5928), pp. 742–744. DOI: 10.1126/science.1171647.

Branzei, Dana; Foiani, Marco (2008): Regulation of DNA repair throughout the cell cycle. In *Nature Reviews Molecular Cell Biology* 9 (4), p. 297. DOI: 10.1038/nrm2351.

Brückner, Anna; Polge, Cécile; Lentze, Nicolas; Auerbach, Daniel; Schlattner, Uwe (2009): Yeast two-hybrid, a powerful tool for systems biology. In *International journal of molecular sciences* 10 (6), pp. 2763–2788. DOI: 10.3390/ijms10062763.

Buchner, Virginia; Nachmias, Abraham; Burstein, Yigal (1982): Isolation and partial characterization of a phytotoxic glycopeptide from a protein—lipopolysaccharide complex produced by a potato isolate of Verticillium dahliae. In *FEBS letters* 138 (2), pp. 261–264. DOI: 10.1016/0014-5793(82)80456-0.

Canonne, Joanne; Froidure-Nicolas, Solène; Rivas, Susana (2011): Phospholipases in action during plant defense signaling. In *Plant signaling & behavior* 6 (1), pp. 13–18. DOI: 10.4161/psb.6.1.14037.

Chapman, Toni A.; Chambers, Grant A.; Kirkby, Karen; Jiménez-Díaz, Rafael M. (2016): First report of the presence of Verticillium dahliae VCG1A in Australia. In *Australasian Plant Dis. Notes* 11 (1), p. 866. DOI: 10.1007/s13314-016-0197-2.

Chatterjee, Srirupa; Chaudhury, Sukanya; McShan, Andrew C.; Kaur, Kawaljit; Guzman, Roberto N. de (2013): Structure and biophysics of type III secretion in bacteria. In *Biochemistry* 52 (15), pp. 2508–2517. DOI: 10.1021/bi400160a.

Chen, Jie-Yin; Liu, Chun; Gui, Yue-Jing; Si, Kai-Wei; Zhang, Dan-Dan; Wang, Jie et al. (2018): Comparative genomics reveals cotton-specific virulence factors in flexible genomic regions in Verticillium dahliae and evidence of horizontal gene transfer from Fusarium. In *The New phytologist* 217 (2), pp. 756–770. DOI: 10.1111/nph.14861.

Chen, Ke; Otten, Léon (2016): Morphological analysis of the 6b oncogene-induced enation syndrome. In *Planta* 243 (1), pp. 131–148. DOI: 10.1007/s00425-015-2387-0.

Chien, C. T.; Bartel, P. L.; Sternglanz, R.; Fields, S. (1991): The two-hybrid system. A method to identify and clone genes for proteins that interact with a protein of interest. In *Proceedings of the National Academy of Sciences* 88 (21), pp. 9578–9582. DOI: 10.1073/pnas.88.21.9578.

Cirulli, Matteo; Bubici, Giovanni; Amenduni, Mario; Armengol, Josep; Berbegal, Mónica; Jiménez-Gasco, María Del Mar; Jiménez-Díaz, Rafael M. (2010): Verticillium Wilt: A Threat to Artichoke Production. In *Plant Dis.* 94 (10), pp. 1176–1187. DOI: 10.1094/PDIS-12-09-0852.

Clough, Steven J.; Bent, Andrew F. (1998): Floral dip: a simplified method forAgrobacterium-mediated transformation ofArabidopsis thaliana. In *The Plant Journal* 16 (6), pp. 735–743. DOI: 10.1046/j.1365-313x.1998.00343.x.

Conrad, Klaus; Motyka, Václav; Schlüter, Torsten (2007): Increase in activity, glycosylation and expression of cytokinin oxidase/dehydrogenase during the senescence of barley leaf segments in the dark. In *Physiol Plant* 130 (4), pp. 572–579. DOI: 10.1111/j.1399-3054.2007.00914.x.

Cook, Melville T. (1923): The Origin and Structure of Plant Galls. In *Science* 57 (1462), pp. 6–14. Available online at http://www.jstor.org/stable/1647141.

Darling, Aaron C. E.; Mau, Bob; Blattner, Frederick R.; Perna, Nicole T. (2004): Mauve. Multiple alignment of conserved genomic sequence with rearrangements. In *Genome research* 14 (7), pp. 1394–1403. DOI: 10.1101/gr.2289704.

Darling, Aaron E.; Mau, Bob; Perna, Nicole T. (2010): progressiveMauve. Multiple genome alignment with gene gain, loss and rearrangement. In *PloS one* 5 (6), e11147. DOI: 10.1371/journal.pone.0011147.

Dean, Ralph A.; Talbot, Nicholas J.; Ebbole, Daniel J.; Farman, Mark L.; Mitchell, Thomas K.; Orbach, Marc J. et al. (2005): The genome sequence of the rice blast fungus Magnaporthe grisea. In *Nature* 434 (7036), p. 980. DOI: 10.1038/nature03449.

Deeken, Rosalia; Engelmann, Julia C.; Efetova, Marina; Czirjak, Tina; Müller, Tobias; Kaiser, Werner M. et al. (2006): An integrated view of gene expression and solute profiles of Arabidopsis tumors: a genome-wide approach. In *Plant Cell* 18 (12), pp. 3617–3634. DOI: 10.1105/tpc.106.044743.

deJonge, Ronnie; van Esse, H. Peter; Maruthachalam, Karunakaran; Bolton, Melvin D.; Santhanam, Parthasarathy; Saber, Mojtaba Keykha et al. (2012): Tomato immune receptor Ve1 recognizes effector of multiple fungal pathogens uncovered by genome and RNA sequencing. In *Proceedings of the National Academy of Sciences of the United States of America* 109 (13), pp. 5110–5115. DOI: 10.1073/pnas.1119623109.

deJonge, Ronnie de; Bolton, Melvin D.; Kombrink, Anja; van den Berg, Grardy C. M.; Yadeta, Koste A.; Thomma, Bart P. H. J. (2013): Extensive chromosomal reshuffling drives evolution of virulence in an asexual pathogen. In *Genome research* 23 (8), pp. 1271–1282. DOI: 10.1101/gr.152660.112.

Delaye, Luis; García-Guzmán, Graciela; Heil, Martin (2013): Endophytes versus biotrophic and necrotrophic pathogens—are fungal lifestyles evolutionarily stable traits? In *Fungal Diversity* 60 (1), pp. 125–135. DOI: 10.1007/s13225-013-0240-y.

Depotter, Jasper; Shi-Kunne, Xiaoqian; Missionnier, Helene; Liu, Tingli; Faino, Luigi; van den Berg, Grardy et al. (2018): Dynamic virulence-related regions of the fungal plant pathogen Verticillium dahliae display remarkably enhanced sequence conservation.

Depotter, Jasper R. L.; Deketelaere, Silke; Inderbitzin, Patrik; Tiedemann, Andreas Von; Höfte, Monica; Subbarao, Krishna V. et al. (2016): Verticillium longisporum, the invisible threat to oilseed rape and other brassicaceous plant hosts. In *Molecular plant pathology* 17 (7), pp. 1004–1016. DOI: 10.1111/mpp.12350.

Depotter, Jasper R. L.; Rodriguez-Moreno, Luis; Thomma, Bart P. H. J.; Wood, Thomas A. (2017a): The Emerging British Verticillium longisporum Population Consists of Aggressive Brassica Pathogens. In *Phytopathology* 107 (11), pp. 1399–1405. DOI: 10.1094/PHYTO-05-17-0184-R.

Depotter, Jasper R. L.; Seidl, Michael F.; van den Berg, Grardy C. M.; Thomma, Bart P. H. J.; Wood, Thomas A. (2017b): A distinct and genetically diverse lineage of the hybrid fungal pathogen Verticillium longisporum population causes stem striping in British oilseed rape. In *Environmental microbiology* 19 (10), pp. 3997–4009. DOI: 10.1111/1462-2920.13801.

Dolzblasz, Alicja; Banasiak, Alicja; Vereecke, Danny (2018): Neovascularization during leafy gall formation on Arabidopsis thaliana upon Rhodococcus fascians infection. In *Planta* 247 (1), pp. 215–228. DOI: 10.1007/s00425-017-2778-5.

Eckert, Maria; Maguire, Kerry; Urban, Martin; Foster, Simon; Fitt, Bruce; Lucas, John; Hammond-Kosack, Kim (2005): Agrobacterium tumefaciens-mediated transformation of Leptosphaeria spp. and Oculimacula spp. with the reef coral gene DsRed and the jellyfish gene gfp. In *FEMS microbiology letters* 253 (1), pp. 67–74. DOI: 10.1016/j.femsle.2005.09.041.

Evans, Thomas; Song, Jiancheng; Jameson, Paula E. (2012): Micro-scale chlorophyll analysis and developmental expression of a cytokinin oxidase/dehydrogenase gene during leaf development and senescence. In *Plant Growth Regul* 66 (1), pp. 95–99. DOI: 10.1007/s10725-011-9627-5.

Faino, Luigi; Seidl, Michael F.; Shi-Kunne, Xiaoqian; Pauper, Marc; van den Berg, Grardy C. M.; Wittenberg, Alexander H. J.; Thomma, Bart P. H. J. (2016): Transposons passively and actively contribute to evolution of the two-speed genome of a fungal pathogen. In *Genome research* 26 (8), pp. 1091–1100. DOI: 10.1101/gr.204974.116.

Farrás, R.; Ferrando, A.; Jásik, J.; Kleinow, T.; Okrész, L.; Tiburcio, A. et al. (2001): SKP1-SnRK protein kinase interactions mediate proteasomal binding of a plant SCF ubiquitin ligase. In *The EMBO Journal* 20 (11), pp. 2742–2756. DOI: 10.1093/emboj/20.11.2742.

Favery, Bruno; Quentin, Michaël; Jaubert-Possamai, Stéphanie; Abad, Pierre (2016): Gall-forming root-knot nematodes hijack key plant cellular functions to induce multinucleate and hypertrophied feeding cells. In *Journal of insect physiology* 84, pp. 60–69. DOI: 10.1016/j.jinsphys.2015.07.013.

Fedoroff, N. v. (2012): Transposable Elements, Epigenetics, and Genome Evolution. In *Science* 338 (6108), pp. 758–767. DOI: 10.1126/science.338.6108.758.

Ferreira, J. F. (1990): First Report of Race 2 of Verticillium dahliae on Tomatoes in South Africa. In *Plant Dis.* 74 (7), p. 530. DOI: 10.1094/PD-74-0530E.

Fields, S.; Song, O. (1989): A novel genetic system to detect protein-protein interactions. In *Nature* 340 (6230), pp. 245–246. DOI: 10.1038/340245a0.

Folger, K. R.; Wong, E. A.; Wahl, G.; Capecchi, M. R. (1982): Patterns of integration of DNA microinjected into cultured mammalian cells: evidence for homologous recombination between

injected plasmid DNA molecules. In *Mol. Cell. Biol.* 2 (11), pp. 1372–1387. DOI: 10.1128/MCB.2.11.1372.

Fortune, Philippe M.; Roulin, Anne; Panaud, Olivier (2008): Horizontal transfer of transposable elements in plants. In *Communicative & Integrative Biology* 1 (1), pp. 74–77.

Fousia, S.; Tsafouros, A.; Roussos, P. A.; Tjamos, S. E. (2018): Increased resistance to Verticillium dahliae in Arabidopsis plants defective in auxin signalling. In *Plant Pathol* 67 (8), pp. 1749–1757. DOI: 10.1111/ppa.12881.

Fradin, Emilie F.; Thomma, Bart P. H. J. (2006): Physiology and molecular aspects of Verticillium wilt diseases caused by V. dahliae and V. albo-atrum. In *Molecular plant pathology* 7 (2), pp. 71–86. DOI: 10.1111/j.1364-3703.2006.00323.x.

Fukuda, H.; Komamine, A. (1980): Establishment of an Experimental System for the Study of Tracheary Element Differentiation from Single Cells Isolated from the Mesophyll of Zinnia elegans. In *Plant physiology* 65 (1), pp. 57–60. DOI: 10.1104/pp.65.1.57.

Fukuda, Hiroo (2004): Signals that control plant vascular cell differentiation. In *Nature Reviews Molecular Cell Biology* 5 (5), p. 379. DOI: 10.1038/nrm1364.

García-Ruiz, R.; García-Carneros, A. B.; Molinero-Ruiz, L. (2014): A New Race of Verticillium dahliae Causing Leaf Mottle of Sunflower in Europe. In *Plant Dis.* 98 (10), p. 1435. DOI: 10.1094/PDIS-04-14-0360-PDN.

Garfinkel, David J.; Simpson, Robert B.; Ream, Lloyd W.; White, Frank F.; Gordon, Milton P.; Nester, Eugene W. (1981): Genetic analysis of crown gall: Fine structure map of the T-DNA by site-directed mutagenesis. In *Cell* 27 (1, Part 2), pp. 143–153. DOI: 10.1016/0092-8674(81)90368-8.

Garibaldi, A.; d. Bertetti; Pensa, P.; Ortega, S. Franco; Gullino, M. L. (2016): First Report of Verticillium Wilt Caused by Verticillium nonalfalfae on Pelargonium grandiflorum in Italy. In *Plant Dis.* 100 (11), p. 2322. DOI: 10.1094/PDIS-03-16-0285-PDN.

Geldner, Niko; Dénervaud-Tendon, Valérie; Hyman, Derek L.; Mayer, Ulrike; Stierhof, York-Dieter; Chory, Joanne (2009): Rapid, combinatorial analysis of membrane compartments in intact plants with a multicolor marker set. In *The Plant journal : for cell and molecular biology* 59 (1), pp. 169–178. DOI: 10.1111/j.1365-313X.2009.03851.x.

Gelvin, Stanton B. (2003): Agrobacterium-mediated plant transformation: the biology behind the "gene-jockeying" tool. In *Microbiology and molecular biology reviews : MMBR* 67 (1), 16-37, table of contents. DOI: 10.1128/mmbr.67.1.16-37.2003.

Groover, Andrew; Jones, Alan M. (1999): Tracheary Element Differentiation Uses a Novel Mechanism Coordinating Programmed Cell Death and Secondary Cell Wall Synthesis. In *Plant physiology* 119 (2), pp. 375–384. DOI: 10.1104/pp.119.2.375.

Guyon, Koanna; Balagué, Claudine; Roby, Dominique; Raffaele, Sylvain (2014): Secretome analysis reveals effector candidates associated with broad host range necrotrophy in the fungal plant pathogen Sclerotinia sclerotiorum. In *BMC genomics* 15, p. 336. DOI: 10.1186/1471-2164-15-336.

Hartmann, Fanny E.; La Rodríguez de Vega, Ricardo C.; Brandenburg, Jean-Tristan; Carpentier, Fantin; Giraud, Tatiana (2018): Gene Presence-Absence Polymorphism in Castrating Anther-Smut Fungi: Recent Gene Gains and Phylogeographic Structure. In *Genome biology and evolution* 10 (5), pp. 1298–1314. DOI: 10.1093/gbe/evy089.

Hellens, R. P.; Edwards, E. A.; Leyland, N. R.; Bean, S.; Mullineaux, P. M. (2000): pGreen. A versatile and flexible binary Ti vector for Agrobacterium-mediated plant transformation. In *Plant molecular biology* 42 (6), pp. 819–832.

Hématy, Kian; Cherk, Candice; Somerville, Shauna (2009): Host–pathogen warfare at the plant cell wall. In *Current Opinion in Plant Biology* 12 (4), pp. 406–413. DOI: 10.1016/j.pbi.2009.06.007.

Hensel, L. L.; Grbić, V.; Baumgarten, D. A.; Bleecker, A. B. (1993): Developmental and age-related processes that influence the longevity and senescence of photosynthetic tissues in arabidopsis. In *Plant Cell* 5 (5), pp. 553–564. DOI: 10.1105/tpc.5.5.553.

Hörtensteiner, S. (2006): Chlorophyll degradation during senescence. In *Annual review of plant biology* 57, pp. 55–77. DOI: 10.1146/annurev.arplant.57.032905.105212.

Hörtensteiner, Stefan; Kräutler, Bernhard (2011): Chlorophyll breakdown in higher plants. In *Biochimica et Biophysica Acta (BBA) - Bioenergetics* 1807 (8), pp. 977–988. DOI: 10.1016/j.bbabio.2010.12.007.

Huisman, O. C. (1982): Interrelations of Root Growth Dynamics to Epidemiology of Root-Invading Fungi. In *Annual review of phytopathology* 20 (1), pp. 303–327. DOI: 10.1146/annurev.py.20.090182.001511.

Iakimova, Elena T.; Woltering, Ernst J. (2017): Xylogenesis in zinnia (Zinnia elegans) cell cultures. Unravelling the regulatory steps in a complex developmental programmed cell death event. In *Planta* 245 (4), pp. 681–705. DOI: 10.1007/s00425-017-2656-1.

Inderbitzin, Patrik; Bostock, Richard M.; Davis, R. Michael; Usami, Toshiyuki; Platt, Harold W.; Subbarao, Krishna V. (2011a): Phylogenetics and taxonomy of the fungal vascular wilt pathogen Verticillium, with the descriptions of five new species. In *PloS one* 6 (12), e28341. DOI: 10.1371/journal.pone.0028341.

Inderbitzin, Patrik; Davis, R. Michael; Bostock, Richard M.; Subbarao, Krishna V. (2011b): The ascomycete Verticillium longisporum is a hybrid and a plant pathogen with an expanded host range. In *PloS one* 6 (3), pp. e18260. DOI: 10.1371/journal.pone.0018260.

Inderbitzin, Patrik; Subbarao, Krishna V. (2014): Verticillium systematics and evolution. How confusion impedes Verticillium wilt management and how to resolve it. In *Phytopathology* 104 (6), pp. 564–574. DOI: 10.1094/PHYTO-11-13-0315-IA.

Irshad, Muhammad; Canut, Hervé; Borderies, Gisèle; Pont-Lezica, Rafael; Jamet, Elisabeth (2008): A new picture of cell wall protein dynamics in elongating cells of Arabidopsis thaliana: confirmed actors and newcomers. In *BMC plant biology* 8, p. 94. DOI: 10.1186/1471-2229-8-94.

Ishibashi, Nanako; Kitakura, Saeko; Terakura, Shinji; Machida, Chiyoko; Machida, Yasunori (2014): Protein encoded by oncogene 6b from Agrobacterium tumefaciens has a reprogramming potential and histone chaperone-like activity. In *Frontiers in plant science* 5. DOI: 10.3389/fpls.2014.00572.

Ito, Masaki; Machida, Yasunori (2015): Reprogramming of plant cells induced by 6b oncoproteins from the plant pathogen Agrobacterium. In *Journal of plant research* 128 (3), pp. 423–435. DOI: 10.1007/s10265-014-0694-3.

Jacobs, Wm. P. (1952): THE ROLE OF AUXIN IN DIFFERENTIATION OF XYLEM AROUND A WOUND. In *American Journal of Botany* 39 (5), pp. 301–309. DOI: 10.1002/j.1537-2197.1952.tb14277.x.

Janacek, Sophie H.; Trenkamp, Sandra; Palmer, Ben; Brown, Naomi J.; Parsley, Kate; Stanley, Susan et al. (2009): Photosynthesis in cells around veins of the C(3) plant Arabidopsis thaliana is important for both the shikimate pathway and leaf senescence as well as contributing to plant fitness. In *The Plant journal : for cell and molecular biology* 59 (2), pp. 329–343. DOI: 10.1111/j.1365-313X.2009.03873.x.

Jensen, T. E.; Valdovinos, J. G. (1967): Fine structure of abscission zones : I. Abscission zones of the pedicels of tobacco and tomato flowers at anthesis. In *Planta* 77 (4), pp. 298–318. DOI: 10.1007/BF00389317.

Jiménez-Díaz, R. M.; Olivares-García, C.; Trapero-Casas, J. L.; Jiménez-Gasco, M. M.; Navas-Cortés, J. A.; Landa, B. B.; Milgroom, M. G. (2017): Variation of pathotypes and races and their correlations

with clonal lineages in Verticillium dahliae. In *Plant Pathol* 66 (4), pp. 651–666. DOI: 10.1111/ppa.12611.

Jiménez-Díaz, Rafael M.; Cirulli, Matteo; Bubici, Giovanni; Del Mar Jiménez-Gasco, María; Antoniou, Polymnia P.; Tjamos, Eleftherios C. (2012): Verticillium Wilt, A Major Threat to Olive Production: Current Status and Future Prospects for its Management. In *Plant Dis.* 96 (3), pp. 304–329. DOI: 10.1094/PDIS-06-11-0496.

Jin, H.; Cominelli, E.; Bailey, P.; Parr, A.; Mehrtens, F.; Jones, J. et al. (2000): Transcriptional repression by AtMYB4 controls production of UV-protecting sunscreens in Arabidopsis. In *The EMBO Journal* 19 (22), pp. 6150–6161. DOI: 10.1093/emboj/19.22.6150.

Johansson, Anna; Staal, Jens; Dixelius, Christina (2006): Early responses in the Arabidopsis-Verticillium longisporum pathosystem are dependent on NDR1, JA- and ET-associated signals via cytosolic NPR1 and RFO1. In *Molecular plant-microbe interactions : MPMI* 19 (9), pp. 958–969. DOI: 10.1094/MPMI-19-0958.

Johnson, Dennis A.; Dung, Jeremiah K. S. (2010): Verticillium wilt of potato – the pathogen, disease and management †. In *Canadian Journal of Plant Pathology* 32 (1), pp. 58–67. DOI: 10.1080/07060661003621134.

Jones, Jonathan D. G.; Dangl, Jeffery L. (2006): The plant immune system. In *Nature* 444 (7117), p. 323. DOI: 10.1038/nature05286.

Jong, M. de; Leyser, O. (2012): Developmental plasticity in plants. In *Cold Spring Harbor symposia on quantitative biology* 77, pp. 63–73. DOI: 10.1101/sqb.2012.77.014720.

Kamoun, Sophien (2006): A catalogue of the effector secretome of plant pathogenic oomycetes. In *Annual review of phytopathology* 44, pp. 41–60. DOI: 10.1146/annurev.phyto.44.070505.143436.

Kang, Julie; Mizukami, Yukiko; Wang, Hong; Fowke, Larry; Dengler, Nancy G. (2007): Modification of cell proliferation patterns alters leaf vein architecture in Arabidopsis thaliana. In *Planta* 226 (5), pp. 1207–1218. DOI: 10.1007/s00425-007-0567-2.

Kasson, M. T.; Short, D. P. G.; O'Neal, E. S.; Subbarao, K. V.; Davis, D. D. (2014): Comparative pathogenicity, biocontrol efficacy, and multilocus sequence typing of Verticillium nonalfalfae from the invasive Ailanthus altissima and other hosts. In *Phytopathology* 104 (3), pp. 282–292. DOI: 10.1094/PHYTO-06-13-0148-R.

Katayama, Hirofumi; Iwamoto, Kuninori; Kariya, Yuka; Asakawa, Tomohiro; Kan, Toshiyuki; Fukuda, Hiroo; Ohashi-Ito, Kyoko (2015): A Negative Feedback Loop Controlling bHLH Complexes Is Involved in Vascular Cell Division and Differentiation in the Root Apical Meristem. In *Current biology : CB* 25 (23), pp. 3144–3150. DOI: 10.1016/j.cub.2015.10.051.

Kazan, Kemal; Lyons, Rebecca (2014): Intervention of Phytohormone Pathways by Pathogen Effectors. In *The Plant cell* 26 (6), pp. 2285–2309. DOI: 10.1105/tpc.114.125419.

Kazazian, Haig H. (2004): Mobile elements. Drivers of genome evolution. In *Science (New York, N.Y.)* 303 (5664), pp. 1626–1632. DOI: 10.1126/science.1089670.

Kearse, Matthew; Moir, Richard; Wilson, Amy; Stones-Havas, Steven; Cheung, Matthew; Sturrock, Shane et al. (2012): Geneious Basic: an integrated and extendable desktop software platform for the organization and analysis of sequence data. In *Bioinformatics (Oxford, England)* 28 (12), pp. 1647–1649. DOI: 10.1093/bioinformatics/bts199.

Keykhasaber, Mojtaba; Thomma, Bart P. H. J.; Hiemstra, Jelle A. (2018): Verticillium wilt caused by Verticillium dahliae in woody plants with emphasis on olive and shade trees. In *European Journal of Plant Pathology* 150 (1), pp. 21–37. DOI: 10.1007/s10658-017-1273-y.

Kim, Sang-Gyu; Kim, Sun-Young; Park, Chung-Mo (2007): A membrane-associated NAC transcription factor regulates salt-responsive flowering via FLOWERING LOCUS T in Arabidopsis. In *Planta* 226 (3), pp. 647–654. DOI: 10.1007/s00425-007-0513-3.

Kinsman, E. A.; Pyke, K. A. (1998): Bundle sheath cells and cell-specific plastid development in Arabidopsis leaves. In *Development* 125 (10), pp. 1815–1822. Available online at http://dev.biologists.org/content/develop/125/10/1815.full.pdf.

Kirst, Mariana E.; Meyer, David J.; Gibbon, Bryan C.; Jung, Rudolf; Boston, Rebecca S. (2005): Identification and characterization of endoplasmic reticulum-associated degradation proteins differentially affected by endoplasmic reticulum stress. In *Plant physiology* 138 (1), pp. 218–231. DOI: 10.1104/pp.105.060087.

Klepikova, Anna V.; Kasianov, Artem S.; Gerasimov, Evgeny S.; Logacheva, Maria D.; Penin, Aleksey A. (2016): A high resolution map of the Arabidopsis thaliana developmental transcriptome based on RNA-seq profiling. In *The Plant journal : for cell and molecular biology* 88 (6), pp. 1058–1070. DOI: 10.1111/tpj.13312.

Klimes, Anna; Dobinson, Katherine F.; Thomma, Bart P. H. J.; Klosterman, Steven J. (2015): Genomics spurs rapid advances in our understanding of the biology of vascular wilt pathogens in the genus Verticillium. In *Annual review of phytopathology* 53, pp. 181–198. DOI: 10.1146/annurev-phyto-080614-120224.

Klopffleisch, Karsten; Phan, Nguyen; Augustin, Kelsey; Bayne, Robert S.; Booker, Katherine S.; Botella, Jose R. et al. (2011): Arabidopsis G-protein interactome reveals connections to cell wall carbohydrates and morphogenesis. In *Molecular systems biology* 7, p. 532. DOI: 10.1038/msb.2011.66.

Klosterman, Steven J.; Subbarao, Krishna V.; Kang, Seogchan; Veronese, Paola; Gold, Scott E.; Thomma, Bart P. H. J. et al. (2011): Comparative genomics yields insights into niche adaptation of plant vascular wilt pathogens. In *PLoS pathogens* 7 (7), e1002137. DOI: 10.1371/journal.ppat.1002137.

Köllmer, Ireen; Novák, Ondřej; Strnad, Miroslav; Schmülling, Thomas; Werner, Tomáš (2014): Overexpression of the cytosolic cytokinin oxidase/dehydrogenase (CKX7) from Arabidopsis causes specific changes in root growth and xylem differentiation. In *The Plant journal : for cell and molecular biology* 78 (3), pp. 359–371. DOI: 10.1111/tpj.12477.

Kombrink, Anja; Rovenich, Hanna; Shi-Kunne, Xiaoqian; Rojas-Padilla, Eduardo; van den Berg, Grardy C. M.; Domazakis, Emmanouil et al. (2017): Verticillium dahliae LysM effectors differentially contribute to virulence on plant hosts. In *Molecular plant pathology* 18 (4), pp. 596–608. DOI: 10.1111/mpp.12520.

Kombrink, Anja; Thomma, Bart P. H. J. (2013): LysM effectors: secreted proteins supporting fungal life. In *PLoS pathogens* 9 (12), e1003769. DOI: 10.1371/journal.ppat.1003769.

Koncz, Csaba; Schell, Jeff (1986): The promoter of TL-DNA gene 5 controls the tissue-specific expression of chimaeric genes carried by a novel type of Agrobacterium binary vector. In *Molec Gen Genet* 204 (3), pp. 383–396. DOI: 10.1007/BF00331014.

Kondo, Yuki; Fujita, Takashi; Sugiyama, Munetaka; Fukuda, Hiroo (2015): A novel system for xylem cell differentiation in Arabidopsis thaliana. In *Molecular plant* 8 (4), pp. 612–621. DOI: 10.1016/j.molp.2014.10.008.

Kranz, Harald d.; Denekamp, Marten; Greco, Raffaella; Jin, Hailing; Leyva, Antonio; Meissner, Ruth C. et al. (1998): Towards functional characterisation of the members of theR2R3-MYBgene family fromArabidopsis thaliana. In *The Plant Journal* 16 (2), pp. 263–276. DOI: 10.1046/j.1365-313x.1998.00278.x.

Krzywinski, Martin; Schein, Jacqueline; Birol, Inanç; Connors, Joseph; Gascoyne, Randy; Horsman, Doug et al. (2009): Circos. An information aesthetic for comparative genomics. In *Genome research* 19 (9), pp. 1639–1645. DOI: 10.1101/gr.092759.109.

Kubicek, Christian P.; Starr, Trevor L.; Glass, N. Louise (2014): Plant cell wall-degrading enzymes and their secretion in plant-pathogenic fungi. In *Annual review of phytopathology* 52, pp. 427–451. DOI: 10.1146/annurev-phyto-102313-045831.

Kubo, Minoru; Udagawa, Makiko; Nishikubo, Nobuyuki; Horiguchi, Gorou; Yamaguchi, Masatoshi; Ito, Jun et al. (2005): Transcription switches for protoxylem and metaxylem vessel formation. In *Genes Dev.* 19 (16), pp. 1855–1860. DOI: 10.1101/gad.1331305.

Kumar, Sudhir; Stecher, Glen; Tamura, Koichiro (2016): MEGA7. Molecular Evolutionary Genetics Analysis Version 7.0 for Bigger Datasets. In *Molecular biology and evolution* 33 (7), pp. 1870–1874. DOI: 10.1093/molbev/msw054.

Land, C. J.; Lawrence, K. S.; Newman, M. (2016): First Report of Verticillium dahliae on Cotton in Alabama. In *Plant Dis.* 100 (3), p. 655. DOI: 10.1094/PDIS-10-15-1143-PDN.

Lazo, G. R.; Stein, P. A.; Ludwig, R. A. (1991): A DNA transformation-competent Arabidopsis genomic library in Agrobacterium. In *Bio/technology (Nature Publishing Company)* 9 (10), pp. 963–967.

Lee, Yuree; Yoon, Taek Han; Lee, Jiyoun; Jeon, So Yeon; Lee, Jae Ho; Lee, Mi Kyoung et al. (2018): A Lignin Molecular Brace Controls Precision Processing of Cell Walls Critical for Surface Integrity in Arabidopsis. In *Cell* 173 (6), 1468-1480.e9. DOI: 10.1016/j.cell.2018.03.060.

Liang, Shuang; Qi, Yafei; Zhao, Jun; Li, Yuanfeng; Wang, Rui; Shao, Jingxia et al. (2017): Mutations in the Arabidopsis AtMRS2-11/AtMGT10/VAR5 Gene Cause Leaf Reticulation. In *Frontiers in plant science* 8, p. 2007. DOI: 10.3389/fpls.2017.02007.

Lilley, Catherine J.; Maqbool, Abbas; Wu, Duqing; Yusup, Hazijah B.; Jones, Laura M.; Birch, Paul R. J. et al. (2018): Effector gene birth in plant parasitic nematodes: Neofunctionalization of a housekeeping glutathione synthetase gene. In *PLoS genetics* 14 (4), e1007310. DOI: 10.1371/journal.pgen.1007310.

Lim, Pyung Ok; Kim, Hyo Jung; Nam, Hong Gil (2007): Leaf senescence. In *Annual review of plant biology* 58, pp. 115–136. DOI: 10.1146/annurev.arplant.57.032905.105316.

Lo Presti, Libera; Lanver, Daniel; Schweizer, Gabriel; Tanaka, Shigeyuki; Liang, Liang; Tollot, Marie et al. (2015): Fungal effectors and plant susceptibility. In *Annual review of plant biology* 66, pp. 513–545. DOI: 10.1146/annurev-arplant-043014-114623.

Longya, Apinya; Chaipanya, Chaivarakun; Franceschetti, Marina; Maidment, Josephine H. R.; Banfield, Mark J.; Jantasuriyarat, Chatchawan (2019): Gene Duplication and Mutation in the Emergence of a Novel Aggressive Allele of the AVR-Pik Effector in the Rice Blast Fungus. In *Molecular plant-microbe interactions : MPMI*, MPMI09180245R. DOI: 10.1094/MPMI-09-18-0245-R.

Lorenzo, G. de; D'Ovidio, R.; Cervone, F. (2001): The role of polygalacturonase-inhibiting proteins (PGIPs) in defense against pathogenic fungi. In *Annual review of phytopathology* 39, pp. 313–335. DOI: 10.1146/annurev.phyto.39.1.313.

Ma, Li-Jun; Does, H. Charlotte van der; Borkovich, Katherine A.; Coleman, Jeffrey J.; Daboussi, Marie-Josée; Di Pietro, Antonio et al. (2010): Comparative genomics reveals mobile pathogenicity chromosomes in *Fusarium*. In *Nature* 464 (7287), p. 367. DOI: 10.1038/nature08850.

Ma, Shisong; Bohnert, Hans J. (2007): Integration of Arabidopsis thaliana stress-related transcript profiles, promoter structures, and cell-specific expression. In *Genome biology* 8 (4), R49. DOI: 10.1186/gb-2007-8-4-r49.

Mansoori, B.; Smith, C. J. (2005): Elicitation of Ethylene by Verticillium albo-atrum Phytotoxins in Potato. In *J Phytopathol* 153 (3), pp. 143–149. DOI: 10.1111/j.1439-0434.2005.00943.x.

Marton, Kristina; Flajšman, Marko; Radišek, Sebastjan; Košmelj, Katarina; Jakše, Jernej; Javornik, Branka; Berne, Sabina (2018): Comprehensive analysis of Verticillium nonalfalfae in silico secretome uncovers putative effector proteins expressed during hop invasion. In *PloS one* 13 (6), e0198971. DOI: 10.1371/journal.pone.0198971.

Mi, Huaiyu; Muruganujan, Anushya; Ebert, Dustin; Huang, Xiaosong; Thomas, Paul D. (2019): PANTHER version 14. More genomes, a new PANTHER GO-slim and improvements in enrichment analysis tools. In *Nucleic acids research* 47 (D1), D419-D426. DOI: 10.1093/nar/gky1038.

Miedes, Eva; Vanholme, Ruben; Boerjan, Wout; Molina, Antonio (2014): The role of the secondary cell wall in plant resistance to pathogens. In *Frontiers in plant science* 5, p. 358. DOI: 10.3389/fpls.2014.00358.

Milgroom, Michael G.; Del Mar Jiménez-Gasco, María; Olivares-García, Concepción; Jiménez-Díaz, Rafael M. (2016): Clonal Expansion and Migration of a Highly Virulent, Defoliating Lineage of Verticillium dahliae. In *Phytopathology* 106 (9), pp. 1038–1046. DOI: 10.1094/PHYTO-11-15-0300-R.

Milgroom, Michael G.; Jiménez-Gasco, María Del Mar; Olivares García, Concepción; Drott, Milton T.; Jiménez-Díaz, Rafael M. (2014): Recombination between clonal lineages of the asexual fungus Verticillium dahliae detected by genotyping by sequencing. In *PloS one* 9 (9), e106740. DOI: 10.1371/journal.pone.0106740.

Milioni, D.; Sado, P. E.; Stacey, N. J.; Domingo, C.; Roberts, K.; McCann, M. C. (2001): Differential expression of cell-wall-related genes during the formation of tracheary elements in the Zinnia mesophyll cell system. In *Plant molecular biology* 47 (1-2), pp. 221–238.

Mishiba, Kei-ichiro; Nishihara, Masahiro; Nakatsuka, Takashi; Abe, Yoshiko; Hirano, Hiroshi; Yokoi, Takahide et al. (2005): Consistent transcriptional silencing of 35S-driven transgenes in gentian. In *The Plant journal : for cell and molecular biology* 44 (4), pp. 541–556. DOI: 10.1111/j.1365-313X.2005.02556.x.

Molinéro-Demilly, V.; Montegano, B.; Julier, B.; Giroult, C.; Baudouin, P.; Chosson, J. F. et al. (2006): Resistance to Verticillium albo-atrum in lucerne (Medicago sativa L.) to distinguish between varieties. In *Euphytica* 153 (1-2), pp. 227–232. DOI: 10.1007/s10681-006-9258-5.

Möller, Mareike; Stukenbrock, Eva H. (2017): Evolution and genome architecture in fungal plant pathogens. In *Nature Reviews Microbiology* 15 (12), p. 756. DOI: 10.1038/nrmicro.2017.76.

Moore, J. K.; Haber, J. E. (1996): Cell cycle and genetic requirements of two pathways of nonhomologous end-joining repair of double-strand breaks in Saccharomyces cerevisiae. In *Molecular and Cellular Biology* 16 (5), pp. 2164–2173.

Morineau, Céline; Gissot, Lionel; Bellec, Yannick; Hematy, Kian; Tellier, Frédérique; Renne, Charlotte et al. (2016): Dual Fatty Acid Elongase Complex Interactions in Arabidopsis. In *PloS one* 11 (9), e0160631. DOI: 10.1371/journal.pone.0160631.

Munné-Bosch, Sergi; Alegre, Leonor (2004): Die and let live: leaf senescence contributes to plant survival under drought stress. In *Functional Plant Biol.* 31 (3), p. 203. DOI: 10.1071/FP03236.

Muszewska, Anna; Steczkiewicz, Kamil; Stepniewska-Dziubinska, Marta; Ginalski, Krzysztof (2019): Transposable elements contribute to fungal genes and impact fungal lifestyle. In *Scientific reports* 9. DOI: 10.1038/s41598-019-40965-0.

Nakano, Toshitsugu; Suzuki, Kaoru; Fujimura, Tatsuhito; Shinshi, Hideaki (2006): Genome-wide analysis of the ERF gene family in Arabidopsis and rice. In *Plant physiology* 140 (2), pp. 411–432. DOI: 10.1104/pp.105.073783.

Nei, M.; Gojobori, T. (1986): Simple methods for estimating the numbers of synonymous and nonsynonymous nucleotide substitutions. In *Molecular biology and evolution* 3 (5), pp. 418–426. DOI: 10.1093/oxfordjournals.molbev.a040410.

Nemeth, K.; Salchert, K.; Putnoky, P.; Bhalerao, R.; Koncz-Kalman, Z.; Stankovic-Stangeland, B. et al. (1998): Pleiotropic control of glucose and hormone responses by PRL1, a nuclear WD protein, in Arabidopsis. In *Genes & Development* 12 (19), pp. 3059–3073. DOI: 10.1101/gad.12.19.3059.

Nguyen, Suong; Mccurdy, David (2016): Transdifferentiation. A Plant Perspective. In, pp. 298–319.

Nielsen, Henrik (2017): Predicting Secretory Proteins with SignalP. In *Methods in molecular biology (Clifton, N.J.)* 1611, pp. 59–73. DOI: 10.1007/978-1-4939-7015-5_6.

Ninan, Annu S.; Grant, Jan; Song, Jiancheng; Jameson, Paula E. (2019): Expression of Genes Related to Sugar and Amino Acid Transport and Cytokinin Metabolism during Leaf Development and Senescence in Pisum sativum L. In *Plants (Basel, Switzerland)* 8 (3). DOI: 10.3390/plants8030076.

Norris, S. R.; Meyer, S. E.; Callis, J. (1993): The intron of Arabidopsis thaliana polyubiquitin genes is conserved in location and is a quantitative determinant of chimeric gene expression. In *Plant molecular biology* 21 (5), pp. 895–906.

Nuruzzaman, Mohammed; Sharoni, Akhter M.; Kikuchi, Shoshi (2013): Roles of NAC transcription factors in the regulation of biotic and abiotic stress responses in plants. In *Frontiers in microbiology* 4, p. 248. DOI: 10.3389/fmicb.2013.00248.

Nziengui, Hugues; Bouhidel, Karim; Pillon, David; Der, Christophe; Marty, Francis; Schoefs, Benoît (2007): Reticulon-like proteins in Arabidopsis thaliana: structural organization and ER localization. In *FEBS letters* 581 (18), pp. 3356–3362. DOI: 10.1016/j.febslet.2007.06.032.

O Manes, C. L. de; van Montagu, M.; Prinsen, E.; Goethals, K.; Holsters, M. (2001): De novo cortical cell division triggered by the phytopathogen Rhodococcus fascians in tobacco. In *Molecular plant-microbe interactions : MPMI* 14 (2), pp. 189–195. DOI: 10.1094/MPMI.2001.14.2.189.

Okada, T. S. (1991): Transdifferentiation. Flexibility in cell differentiation / T.S. Okada. Oxford: Clarendon Press; New York : Oxford University Press.

Pantelides, Iakovos S.; Tjamos, Sotirios E.; Paplomatas, Epaminondas J. (2010): Ethylene perception via ETR1 is required in Arabidopsis infection by Verticillium dahliae. In *Molecular plant pathology* 11 (2), pp. 191–202. DOI: 10.1111/j.1364-3703.2009.00592.x.

Pegg, G. F. (1965): Phytotoxin Production by Verticillium albo-atrum Reinke et Berthold. In *Nature* 208 (5016), pp. 1228–1229. DOI: 10.1038/2081228b0.

Pegg, G. F.; Cronshaw, D. K. (1976): Ethylene production in tomato plants infected with Verticillium albo-atrum. In *Physiological Plant Pathology* 8 (3), pp. 279–295. DOI: 10.1016/0048-4059(76)90022-9.

Pemberton, Clare L.; Salmond, George P. C. (2004): The Nep1-like proteins-a growing family of microbial elicitors of plant necrosis. In *Molecular plant pathology* 5 (4), pp. 353–359. DOI: 10.1111/j.1364-3703.2004.00235.x.

Pendleton, Amanda L.; Smith, Katherine E.; Feau, Nicolas; Martin, Francis M.; Grigoriev, Igor V.; Hamelin, Richard et al. (2014): Duplications and losses in gene families of rust pathogens highlight putative effectors. In *Frontiers in plant science* 5, p. 299. DOI: 10.3389/fpls.2014.00299.

Pérez-Artés, Encarnación; García-Pedrajas, María d.; Bejarano-Alcázar, José; Jiménez-Díaz, Rafael M. (2000). In *European Journal of Plant Pathology* 106 (6), pp. 507–517. DOI: 10.1023/A:1008756307969.

Pesquet, Edouard; Tuominen, Hannele (2011): Ethylene stimulates tracheary element differentiation in Zinnia elegans cell cultures. In *The New phytologist* 190 (1), pp. 138–149. DOI: 10.1111/j.1469-8137.2010.03600.x.

Pfaffl, M. W. (2001): A new mathematical model for relative quantification in real-time RT-PCR. In *Nucleic acids research* 29 (9), e45.

PhyDE® - Phylogenetic Data Editor (2014). Available online at http://www.phyde.de/, updated on 5/4/2014, checked on 2/20/2019.

Prendergast, James G. D.; Campbell, Harry; Gilbert, Nick; Dunlop, Malcolm G.; Bickmore, Wendy A.; Semple, Colin A. M. (2007): Chromatin structure and evolution in the human genome. In *BMC evolutionary biology* 7, p. 72. DOI: 10.1186/1471-2148-7-72.

Radišek, Sebastjan; Jakše, Jernej; Simončič, Andrej; Javornik, Branka (2003): Characterization of Verticillium albo-atrum Field Isolates Using Pathogenicity Data and AFLP Analysis. In *Plant Dis.* 87 (6), pp. 633–638. DOI: 10.1094/PDIS.2003.87.6.633.

Raffaele, Sylvain; Kamoun, Sophien (2012): Genome evolution in filamentous plant pathogens: why bigger can be better. In *Nature reviews. Microbiology* 10 (6), pp. 417–430. DOI: 10.1038/nrmicro2790.

Ramsay, JR; Multani, D. S.; Lyon, B. R. (1996): RAPD-PCR identification of Verticillium dahliae isolates with differential pathogenicity on cotton. In *Aust. J. Agric. Res.* 47 (5), p. 681. DOI: 10.1071/AR9960681.

Rebbeck, J.; Malone, M. A.; Short, D. P. G.; Kasson, M. T.; O'Neal, E. S.; Davis, D. D. (2013): First Report of Verticillium Wilt Caused by Verticillium nonalfalfae on Tree-of-Heaven (Ailanthus altissima) in Ohio. In *Plant Dis.* 97 (7), p. 999. DOI: 10.1094/PDIS-01-13-0062-PDN.

Redman, Regina S.; Dunigan, David d.; Rodriguez, Rusty J. (2001): Fungal symbiosis from mutualism to parasitism: who controls the outcome, host or invader? In *New Phytol* 151 (3), pp. 705–716. DOI: 10.1046/j.0028-646x.2001.00210.x.

RESENDE, M. L. v.; MEPSTED, R.; FLOOD, J.; Cooper, R. M. (1996): Water relations and ethylene production as related to symptom expression in cocoa seedlings infected with defoliating and non-defoliating isolates of Verticillium dahliae. In *Plant Pathology* 45 (5), pp. 964–972. DOI: 10.1111/j.1365-3059.1996.tb02907.x.

Reusche, Michael; Klásková, Jana; Thole, Karin; Truskina, Jekaterina; Novák, Ondřej; Janz, Dennis et al. (2013): Stabilization of cytokinin levels enhances Arabidopsis resistance against Verticillium longisporum. In *Molecular plant-microbe interactions : MPMI* 26 (8), pp. 850–860. DOI: 10.1094/MPMI-12-12-0287-R.

Reusche, Michael; Thole, Karin; Janz, Dennis; Truskina, Jekaterina; Rindfleisch, Sören; Drübert, Christine et al. (2012): Verticillium infection triggers VASCULAR-RELATED NAC DOMAIN7-dependent de novo xylem formation and enhances drought tolerance in Arabidopsis. In *The Plant cell* 24 (9), pp. 3823–3837. DOI: 10.1105/tpc.112.103374.

Reusche, Michael; Truskina, Jekaterina; Thole, Karin; Nagel, Leonhard; Rindfleisch, Sören; van Tran, Tuan et al. (2014): Infections with the vascular pathogens Verticillium longisporum and Verticillium dahliae induce distinct disease symptoms and differentially affect drought stress tolerance of Arabidopsis thaliana. In *Environmental and Experimental Botany* 108, pp. 23–37. DOI: 10.1016/j.envexpbot.2013.12.009.

Riefler, Michael; Novak, Ondrej; Strnad, Miroslav; Schmülling, Thomas (2006): Arabidopsis cytokinin receptor mutants reveal functions in shoot growth, leaf senescence, seed size, germination, root development, and cytokinin metabolism. In *Plant Cell* 18 (1), pp. 40–54. DOI: 10.1105/tpc.105.037796.

Romanos, Mike (1995): Advances in the use of Pichia pastoris for high-level gene expression. In *Current Opinion in Biotechnology* 6 (5), pp. 527–533. DOI: 10.1016/0958-1669(95)80087-5.

Rose, Jocelyn K. C.; Ham, Kyung-Sik; Darvill, Alan G.; Albersheim, Peter (2002): Molecular cloning and characterization of glucanase inhibitor proteins: coevolution of a counterdefense mechanism by plant pathogens. In *Plant Cell* 14 (6), pp. 1329–1345.

Sánchez-Vallet, Andrea; Fouché, Simone; Fudal, Isabelle; Hartmann, Fanny E.; Soyer, Jessica L.; Tellier, Aurélien; Croll, Daniel (2018): The Genome Biology of Effector Gene Evolution in Filamentous

Plant Pathogens. In *Annual review of phytopathology* 56, pp. 21–40. DOI: 10.1146/annurev-phyto-080516-035303.

Schaack, Sarah; Gilbert, Clément; Feschotte, Cédric (2010): Promiscuous DNA: horizontal transfer of transposable elements and why it matters for eukaryotic evolution. In *Trends in ecology & evolution* 25 (9), pp. 537–546. DOI: 10.1016/j.tree.2010.06.001.

Schnathorst, W.; Sibbett, G. (1971): T-1 Verticillium strain …a major factor in cotton and olive wilt. In *California Agriculture* 25 (7), pp. 3–5.

Schnathorst T, W. C.; Mathre, D. E. (1966): Host range and differentiation of a severe form of Verticillium albo-atrum in Cotton. In *Phytopathology* 56 (10), pp. 1155–1161.

SCHRODER, Gudrun; WAFFENSCHMIDT, Sabine; WEILER, Elmar W.; SCHRODER, Joachim (1984): The T-region of Ti plasmids codes for an enzyme synthesizing indole-3-acetic acid. In *Eur J Biochem* 138 (2), pp. 387–391. DOI: 10.1111/j.1432-1033.1984.tb07927.x.

Schweiger, Regina; Schwenkert, Serena (2013): AtTPR7 as part of the Arabidopsis Sec post-translocon. In *Plant signaling & behavior* 8 (8). DOI: 10.4161/psb.25286.

Selin, Carrie; Kievit, Teresa R. de; Belmonte, Mark F.; Fernando, W. G. Dilantha (2016): Elucidating the Role of Effectors in Plant-Fungal Interactions. Progress and Challenges. In *Frontiers in microbiology* 7, p. 600. DOI: 10.3389/fmicb.2016.00600.

Shi, Yunhua; Mowery, Richard A.; Ashley, Jonathan; Hentz, Michelle; Ramirez, Alejandro J.; Bilgicer, Basar et al. (2012): Abnormal SDS-PAGE migration of cytosolic proteins can identify domains and mechanisms that control surfactant binding. In *Protein science : a publication of the Protein Society* 21 (8), pp. 1197–1209. DOI: 10.1002/pro.2107.

Shi-Kunne, Xiaoqian; Faino, Luigi; van den Berg, Grardy C. M.; Thomma, Bart P. H. J.; Seidl, Michael F. (2018): Evolution within the fungal genus Verticillium is characterized by chromosomal rearrangement and gene loss. In *Environmental microbiology* 20 (4), pp. 1362–1373. DOI: 10.1111/1462-2920.14037.

Shi-Kunne, Xiaoqian; van Kooten, Mathijs; Depotter, Jasper R. L.; Thomma, Bart P. H. J.; Seidl, Michael F. (2019): The Genome of the Fungal Pathogen Verticillium dahliae Reveals Extensive Bacterial to Fungal Gene Transfer. In *Genome biology and evolution* 11 (3), pp. 855–868. DOI: 10.1093/gbe/evz040.

Short, Dylan P. G.; Gurung, Suraj; Maruthachalam, Karunakaran; Atallah, Zahi K.; Subbarao, Krishna V. (2014): Verticillium dahliae race 2-specific PCR reveals a high frequency of race 2 strains in commercial spinach seed lots and delineates race structure. In *Phytopathology* 104 (7), pp. 779–785. DOI: 10.1094/PHYTO-09-13-0253-R.

Skamnioti, Pari; Furlong, Rebecca F.; Gurr, Sarah J. (2008): The fate of gene duplicates in the genomes of fungal pathogens. In *Communicative & Integrative Biology* 1 (2), pp. 196–198. DOI: 10.4161/cib.1.2.7144.

Spanu, Pietro D.; Abbott, James C.; Amselem, Joelle; Burgis, Timothy A.; Soanes, Darren M.; Stüber, Kurt et al. (2010): Genome Expansion and Gene Loss in Powdery Mildew Fungi Reveal Tradeoffs in Extreme Parasitism. In *Science* 330 (6010), pp. 1543–1546. DOI: 10.1126/science.1194573.

Stenvik, Grethe-Elisabeth; Butenko, Melinka A.; Urbanowicz, Breeanna Rae; Rose, Jocelyn K. C.; Aalen, Reidunn B. (2006): Overexpression of INFLORESCENCE DEFICIENT IN ABSCISSION activates cell separation in vestigial abscission zones in Arabidopsis. In *Plant Cell* 18 (6), pp. 1467–1476. DOI: 10.1105/tpc.106.042036.

Stepanets, Dimitri (2018): Identification of Arabidopsis genes involved in differential interaction phenotype establishment by distinct Verticillium spp. and isolates. Dissertation. Available online at http://hdl.handle.net/11858/00-1735-0000-002E-E3C0-A.

Stergiopoulos, Ioannis; Kock, Maarten J. D. de; Lindhout, Pim; Wit, Pierre J. G. M. de (2007): Allelic variation in the effector genes of the tomato pathogen Cladosporium fulvum reveals different modes of adaptive evolution. In *Molecular plant-microbe interactions : MPMI* 20 (10), pp. 1271–1283. DOI: 10.1094/MPMI-20-10-1271.

Stes, Elisabeth; Vandeputte, Olivier M.; El Jaziri, Mondher; Holsters, Marcelle; Vereecke, Danny (2011): A successful bacterial coup d'état: how Rhodococcus fascians redirects plant development. In *Annual review of phytopathology* 49, pp. 69–86. DOI: 10.1146/annurev-phyto-072910-095217.

Steventon, L. A.; Okori, P.; Dixelius, C. (2001): An Investigation of the Susceptibility of Arabidopsis thaliana to Isolates of Two Species of Verticillium. In *J Phytopathol* 149 (7-8), pp. 395–401. DOI: 10.1046/j.1439-0434.2001.00643.x.

Stöver, Ben C.; Müller, Kai F. (2010): TreeGraph 2. Combining and visualizing evidence from different phylogenetic analyses. In *BMC bioinformatics* 11, p. 7. DOI: 10.1186/1471-2105-11-7.

Street, P. F. S.; Cooper, R. M. (1984): Quantitative measurement of vascular flow in petioles of healthy and Verticillium-infected tomato. In *Plant Pathol* 33 (4), pp. 483–492. DOI: 10.1111/j.1365-3059.1984.tb02872.x.

Stukenbrock, Eva Holtgrewe (2013): Evolution, selection and isolation: a genomic view of speciation in fungal plant pathogens. In *The New phytologist* 199 (4), pp. 895–907. DOI: 10.1111/nph.12374.

Sugiyama, Munetaka; Komamine, Atsushi (1990): Transdifferentiation of quiescent parenchymatous cells into tracheary elements. In *Cell Differentiation and Development* 31 (2), pp. 77–87. DOI: 10.1016/0922-3371(90)90011-K.

Sultana, Nighat; Florance, Hannah V.; Johns, Alex; Smirnoff, Nicholas (2015): Ascorbate deficiency influences the leaf cell wall glycoproteome in Arabidopsis thaliana. In *Plant, cell & environment* 38 (2), pp. 375–384. DOI: 10.1111/pce.12267.

Talboys, P. W. (1958): Association of tylosis and hyperplasia of the xylem with vascular invasion of the hop by Verticillium albo-atrum. In *Transactions of the British Mycological Society* 41 (2), 249-IN8. DOI: 10.1016/S0007-1536(58)80037-6.

Tan, Tian Tian; Endo, Hitoshi; Sano, Ryosuke; Kurata, Tetsuya; Yamaguchi, Masatoshi; Ohtani, Misato; Demura, Taku (2018): Transcription Factors VND1-VND3 Contribute to Cotyledon Xylem Vessel Formation1OPEN. In *Plant physiology* 176 (1), pp. 773–789. DOI: 10.1104/pp.17.00461.

Tanoi, Keitaro; Kobayashi, Natsuko I. (2015): Leaf Senescence by Magnesium Deficiency. In *Plants (Basel, Switzerland)* 4 (4), pp. 756–772. DOI: 10.3390/plants4040756.

Thatcher, Louise F.; Kazan, Kemal; Manners, John M. (2012): Lateral organ boundaries domain transcription factors: new roles in plant defense. In *Plant signaling & behavior* 7 (12), pp. 1702–1704. DOI: 10.4161/psb.22097.

Thole, Karin (2016): Towards the identification of Verticillium effector molecules involved in host plant developmental reprogramming. Dissertation. Available online at http://hdl.handle.net/11858/00-1735-0000-0028-8762-5.

Tian, Hui; Zhou, Lei; Guo, Wangzhen; Wang, Xinyu (2015): Small GTPase Rac1 and its interaction partner Cla4 regulate polarized growth and pathogenicity in Verticillium dahliae. In *Fungal genetics and biology : FG & B* 74, pp. 21–31. DOI: 10.1016/j.fgb.2014.11.003.

Tjamos, Sotirios E.; Flemetakis, Emmanouil; Paplomatas, Epaminondas J.; Katinakis, Panagiotis (2005): Induction of resistance to Verticillium dahliae in Arabidopsis thaliana by the biocontrol agent K-165 and pathogenesis-related proteins gene expression. In *Molecular plant-microbe interactions : MPMI* 18 (6), pp. 555–561. DOI: 10.1094/MPMI-18-0555.

Tooker, John F.; Moraes, Consuelo M. de (2008): Gall insects and indirect plant defenses: A case of active manipulation? In *Plant signaling & behavior* 3 (7), pp. 503–504.

Torrey, John G. (1975): Tracheary Element Formation from Single Isolated Cells in Culture. In *Physiol Plant* 35 (2), pp. 158–165. DOI: 10.1111/j.1399-3054.1975.tb03886.x.

Tran, Van-Tuan; Braus-Stromeyer, Susanna A.; Kusch, Harald; Reusche, Michael; Kaever, Alexander; Kühn, Anika et al. (2014): Verticillium transcription activator of adhesion Vta2 suppresses microsclerotia formation and is required for systemic infection of plant roots. In *The New phytologist* 202 (2), pp. 565–581. DOI: 10.1111/nph.12671.

Treangen, Todd J.; Salzberg, Steven L. (2011): Repetitive DNA and next-generation sequencing. Computational challenges and solutions. In *Nature reviews. Genetics* 13 (1), pp. 36–46. DOI: 10.1038/nrg3117.

Tsuchisaka, Atsunari; Theologis, Athanasios (2004): Unique and overlapping expression patterns among the Arabidopsis 1-amino-cyclopropane-1-carboxylate synthase gene family members. In *Plant physiology* 136 (2), pp. 2982–3000. DOI: 10.1104/pp.104.049999.

Tyvaert, L.; França, S. C.; Debode, J.; Höfte, M. (2014): The endophyte Verticillium Vt305 protects cauliflower against Verticillium wilt. In *Journal of applied microbiology* 116 (6), pp. 1563–1571. DOI: 10.1111/jam.12481.

Uhrig, Joachim F.; MacFarlane, Stuart A. (2008): Protein-Protein Interactions in Plant Virus Movement and Pathogenicity. In Chandra Shekhar Nautiyal, Patrice Dion (Eds.): Molecular mechanisms of plant and microbe coexistence, vol. 15. Berlin: Springer (Soil Biology, v. 15), pp. 319–338.

Ullrich, C. I.; Aloni, R. (2000): Vascularization is a general requirement for growth of plant and animal tumours. In *Journal of experimental botany* 51 (353), pp. 1951–1960.

Usami, T.; Itoh, M.; Amemiya, Y. (2008): Mating type gene MAT1-2-1 is common among Japanese isolates of Verticillium dahliae. In *Physiological and Molecular Plant Pathology* 73 (6), pp. 133–137. DOI: 10.1016/j.pmpp.2009.04.002.

van der Burgt, Ate; Karimi Jashni, Mansoor; Bahkali, Ali H.; Wit, Pierre J. G. M. de (2014): Pseudogenization in pathogenic fungi with different host plants and lifestyles might reflect their evolutionary past. In *Molecular plant pathology* 15 (2), pp. 133–144. DOI: 10.1111/mpp.12072.

van Kan, Jan A. L.; Shaw, Michael W.; Grant-Downton, Robert T. (2014): Botrytis species: relentless necrotrophic thugs or endophytes gone rogue? In *Molecular plant pathology* 15 (9), pp. 957–961. DOI: 10.1111/mpp.12148.

van Tran, Tuan; Braus-Stromeyer, Susanna A.; Timpner, Christian; Braus, Gerhard H. (2013): Molecular diagnosis to discriminate pathogen and apathogen species of the hybrid Verticillium longisporum on the oilseed crop Brassica napus. In *Applied microbiology and biotechnology* 97 (10), pp. 4467–4483. DOI: 10.1007/s00253-012-4530-1.

Vanin, E. F. (1985): Processed pseudogenes. Characteristics and evolution. In *Annual review of genetics* 19, pp. 253–272. DOI: 10.1146/annurev.ge.19.120185.001345.

Venner, Samuel; Miele, Vincent; Terzian, Christophe; Biémont, Christian; Daubin, Vincent; Feschotte, Cédric; Pontier, Dominique (2017): Ecological networks to unravel the routes to horizontal transposon transfers. In *PLoS Biol* 15 (2), e2001536. DOI: 10.1371/journal.pbio.2001536.

Veronese, Paola; Narasimhan, Meena L.; Stevenson, Rebecca A.; Zhu, Jian-K; Weller, Stephen C.; Subbarao, Krishna V.; Bressan, Ray A. (2003): Identification of a locus controlling Verticillium disease symptom response in Arabidopsis thaliana. In *The Plant journal : for cell and molecular biology* 35 (5), pp. 574–587.

Wang, Dapeng; Zhang, Yubin; Zhang, Zhang; Zhu, Jiang; Yu, Jun (2010): KaKs_Calculator 2.0: A Toolkit Incorporating Gamma-Series Methods and Sliding Window Strategies. In *Genomics, Proteomics & Bioinformatics* 8 (1), pp. 77–80. DOI: 10.1016/S1672-0229(10)60008-3.

Wapinski, Ilan; Pfeffer, Avi; Friedman, Nir; Regev, Aviv (2007): Natural history and evolutionary principles of gene duplication in fungi. In *Nature* 449 (7158), p. 54. DOI: 10.1038/nature06107.

Weaver, L. M.; Amasino, R. M. (2001): Senescence Is Induced in Individually Darkened Arabidopsis Leaves, but Inhibited in Whole Darkened Plants. In *Plant physiology* 127 (3), pp. 876–886. DOI: 10.1104/pp.010312.

Werner, Tomás; Motyka, Václav; Laucou, Valérie; Smets, Rafaël; van Onckelen, Harry; Schmülling, Thomas (2003): Cytokinin-deficient transgenic Arabidopsis plants show multiple developmental alterations indicating opposite functions of cytokinins in the regulation of shoot and root meristem activity. In *Plant Cell* 15 (11), pp. 2532–2550. DOI: 10.1105/tpc.014928.

Werner, Tomáš; Motyka, Václav; Strnad, Miroslav; Schmülling, Thomas (2001): Regulation of plant growth by cytokinin. In *PNAS* 98 (18), pp. 10487–10492. DOI: 10.1073/pnas.171304098.

Wheeler, D. L.; Johnson, D. A. (2016): Verticillium dahliae Infects, Alters Plant Biomass, and Produces Inoculum on Rotation Crops. In *Phytopathology* 106 (6), pp. 602–613. DOI: 10.1094/PHYTO-07-15-0174-R.

Wheeler, David Linnard; Dung, Jeremiah Kam Sung; Johnson, Dennis Allen (2019): From pathogen to endophyte: an endophytic population of Verticillium dahliae evolved from a sympatric pathogenic population. In *The New phytologist* 222 (1), pp. 497–510. DOI: 10.1111/nph.15567.

Wicker, Thomas; Sabot, François; Hua-Van, Aurélie; Bennetzen, Jeffrey L.; Capy, Pierre; Chalhoub, Boulos et al. (2007): A unified classification system for eukaryotic transposable elements. In *Nature reviews. Genetics* 8 (12), pp. 973–982. DOI: 10.1038/nrg2165.

Wiese, M. v.; Devay, J. E. (1970): Growth Regulator Changes in Cotton Associated with Defoliation Caused by Verticillium albo-atrum. In *Plant physiology* 45 (3), pp. 304–309. DOI: 10.1104/pp.45.3.304.

Wilhelm, Stephen (1955): Longevity of the Verticillium wilt fungus in the laboratory and field. In *Phytopath* 45 (3), pp. 180–181.

Willige, Björn C.; Ahlers, Siv; Zourelidou, Melina; Barbosa, Inês C. R.; Demarsy, Emilie; Trevisan, Martine et al. (2013): D6PK AGCVIII kinases are required for auxin transport and phototropic hypocotyl bending in Arabidopsis. In *The Plant cell* 25 (5), pp. 1674–1688. DOI: 10.1105/tpc.113.111484.

Woo, Hye Ryun; Kim, Hyo Jung; Nam, Hong Gil; Lim, Pyung Ok (2013): Plant leaf senescence and death - regulation by multiple layers of control and implications for aging in general. In *Journal of cell science* 126 (Pt 21), pp. 4823–4833. DOI: 10.1242/jcs.109116.

Yamaguchi, Masatoshi; Goué, Nadia; Igarashi, Hisako; Ohtani, Misato; Nakano, Yoshimi; Mortimer, Jennifer C. et al. (2010): VASCULAR-RELATED NAC-DOMAIN6 and VASCULAR-RELATED NAC-DOMAIN7 effectively induce transdifferentiation into xylem vessel elements under control of an induction system. In *Plant physiology* 153 (3), pp. 906–914. DOI: 10.1104/pp.110.154013.

Yamaguchi, Masatoshi; Kubo, Minoru; Fukuda, Hiroo; Demura, Taku (2008): Vascular-related NAC-DOMAIN7 is involved in the differentiation of all types of xylem vessels in Arabidopsis roots and shoots. In *The Plant journal : for cell and molecular biology* 55 (4), pp. 652–664. DOI: 10.1111/j.1365-313X.2008.03533.x.

Yang, Jung Hyun; Wang, Huanzhong (2016): Molecular Mechanisms for Vascular Development and Secondary Cell Wall Formation. In *Frontiers in plant science* 7, p. 356. DOI: 10.3389/fpls.2016.00356.

Yin, Yanhai; Wang, Zhi Yong; Mora-Garcia, Santiago; Li, Jianming; Yoshida, Shigeo; Asami, Tadao; Chory, Joanne (2002): BES1 accumulates in the nucleus in response to brassinosteroids to regulate gene expression and promote stem elongation. In *Cell* 109 (2), pp. 181–191.

Yoshida, Kentaro; Saitoh, Hiromasa; Fujisawa, Shizuko; Kanzaki, Hiroyuki; Matsumura, Hideo; Yoshida, Kakoto et al. (2009): Association genetics reveals three novel avirulence genes from the rice

blast fungal pathogen Magnaporthe oryzae. In *Plant Cell* 21 (5), pp. 1573–1591. DOI: 10.1105/tpc.109.066324.

You, Fei; Han, Ting; Wu, Jing-zhong; Huang, Bao-kang; Qin, Lu-ping (2009): Antifungal secondary metabolites from endophytic Verticillium sp. In *Biochemical Systematics and Ecology* 37 (3), pp. 162–165. DOI: 10.1016/j.bse.2009.03.008.

Zhang, Dan-Dan; Wang, Jie; Wang, Dan; Kong, Zhi-Qiang; Zhou, Lei; Zhang, Geng-Yun et al. (2019): Population genomics demystifies the defoliation phenotype in the plant pathogen Verticillium dahliae. In *The New phytologist* 222 (2), pp. 1012–1029. DOI: 10.1111/nph.15672.

Zhang, Dan-Dan; Wang, Xin-Yan; Chen, Jie-Yin; Kong, Zhi-Qiang; Gui, Yue-Jing; Li, Nan-Yang et al. (2016): Identification and characterization of a pathogenicity-related gene VdCYP1 from Verticillium dahliae. In *Scientific reports* 6, p. 27979. DOI: 10.1038/srep27979.

Zhang, L.; Zhang, G. L.; Qian, X.; Li, G. Y. (2009): First Report of Verticillium Wilt of Grapevine (Vitis vinifera) Caused by Verticillium dahliae in China. In *Plant Dis.* 93 (8), p. 841. DOI: 10.1094/PDIS-93-8-0841C.

Zhang, Zhengdong D.; Frankish, Adam; Hunt, Toby; Harrow, Jennifer; Gerstein, Mark (2010): Identification and analysis of unitary pseudogenes: historic and contemporary gene losses in humans and other primates. In *Genome biology* 11 (3), R26. DOI: 10.1186/gb-2010-11-3-r26.

Zhong, Ruiqin; Lee, Chanhui; Zhou, Jianli; McCarthy, Ryan L.; Ye, Zheng-Hua (2008): A battery of transcription factors involved in the regulation of secondary cell wall biosynthesis in Arabidopsis. In *Plant Cell* 20 (10), pp. 2763–2782. DOI: 10.1105/tpc.108.061325.

Zhou, Jianli; Zhong, Ruiqin; Ye, Zheng-Hua (2014): Arabidopsis NAC Domain Proteins, VND1 to VND5, Are Transcriptional Regulators of Secondary Wall Biosynthesis in Vessels. In *PloS one* 9 (8). DOI: 10.1371/journal.pone.0105726.

Zhu, J.; Oger, P. M.; Schrammeijer, B.; Hooykaas, P. J.; Farrand, S. K.; Winans, S. C. (2000): The bases of crown gall tumorigenesis. In *Journal of bacteriology* 182 (14), pp. 3885–3895. DOI: 10.1128/jb.182.14.3885-3895.2000.

Zwack, Paul J.; Rashotte, Aaron M. (2013): Cytokinin inhibition of leaf senescence. In *Plant signaling & behavior* 8 (7), e24737. DOI: 10.4161/psb.24737.

6 Supplemental material

Table 6.1 *De novo* assembly of *V. dahliae* V76 genome onto 61 scaffolds. Scaffolds that could not be aligned with the *V. dahliae* JR2 reference genome are defined as 'unplaced scaffolds' (see also Figure 3.1). BLAST searches in the publicly available databases were used to characterize unplaced scaffolds.

Scaffold (scf) #	Size [bp]	Comment
1	449661	
2	418518	
3	251192	
4	10469	unplaced scaffold, multiple copy region
5	145789	unplaced scaffold, multiple copy region
6	471093	
7	595870	
8	409546	
9	1103461	
10	4865489	
11	81837	
12	838019	
13	1283329	
14	42347	unplaced scaffold, multiple copy region
15	1536217	
16	48388	unplaced scaffold, multiple copy region
17	1954294	
18	8078	unplaced scaffold, multiple copy region
19	3464283	
20	821895	
21	85631	
22	842370	
23	31991	unplaced scaffold, multiple copy region
24	1289089	
25	1234264	
26	28038	
27	206206	
28	823837	
29	129368	
30	46086	unplaced scaffold, mitochondrial genome
31	567730	
32	1418030	
33	339700	LSCE regions (*LSCE1* and *LSCE2*)
34	96332	

35	213722	
36	934533	
37	46429	unplaced scaffold, ribosomal subunits
38	1040053	
39	27326	
40	726858	
41	935063	*LSCE3*
42	226780	
43	19998	unplaced scaffold, ribosomal subunits
44	18454	unplaced scaffold, multiple copy region
45	208587	
46	2659573	
47	823601	
48	54978	
49	218791	
50	190939	
51	49103	unplaced scaffold, mitochondrial genome
52	198774	
53	449481	
54	55874	unplaced scaffold, multiple copy region
55	149048	unplaced scaffold, multiple copy region
56	78905	unplaced scaffold, multiple copy region
57	710445	
58	90410	*LSCE2-like*
59	160754	*LSCE4*
60	63549	unplaced scaffold, mitochondrial genome
61	120863	unplaced scaffold, mitochondrial genome

A

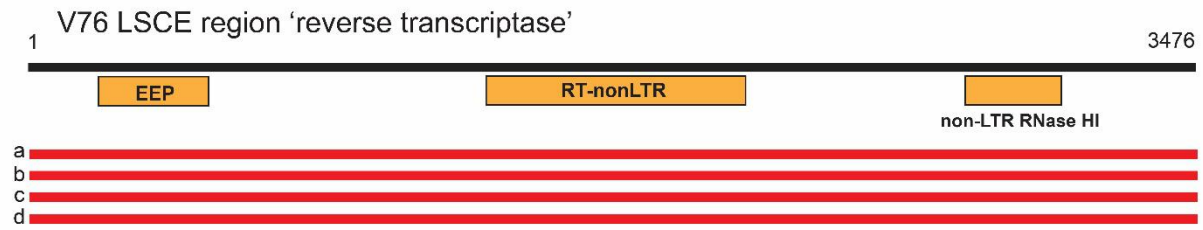

B

	Annotation	Organism	Accession	Query cover (%)	Identities (%)
a	unknown	*V. dahliae VdLs17*	AEB91360.1	98	94.3
b	hypothetical protein	*Fusarium oxysporum* f. sp. *cepae*	RKK21657.1	97	73.1
c	reverse transcriptase	*Purpureocillium lilacinum*	OAQ61371.1	98	70
d	reverse transcriptase, putative	*Talaromyces marneffei* ATCC 18224	XP_002153737.1	98	70

Figure 6.1 Results of BLAST homology search with putative reverse transcriptase from *V. dahliae* V76 LSCE region. 3474 bp putative reverse transcriptase gene sequence was used as query for BLASTx search of protein databases using translated nucleotide query (https://blast.ncbi.nlm.nih.gov/Blast.cgi) (Altschul et al. 1997). (A) Reverse transcriptase sequence with predicted domains in orange boxes. EEP (pfam14529): exonuclease/ endonuclease/ phosphatase domain. This domain represents the endonuclease region of retrotransposons. RT-nonLTR (cd01650): Non-LTR (long terminal repeat) retrotransposon reverse transcriptase (RT) domain. non-LTR RNase HI (cd09276): non-LTR RNase HI domain of reverse transcriptases. Aligned are representative hits of the first four organisms found in the BLASTx search (a-d). Sequence colors correspond to their alignment score: Black < 40, blue 40 – 50, pink 80 – 200, red > 200. (B) Statistics and properties of the BLASTx hits.

A

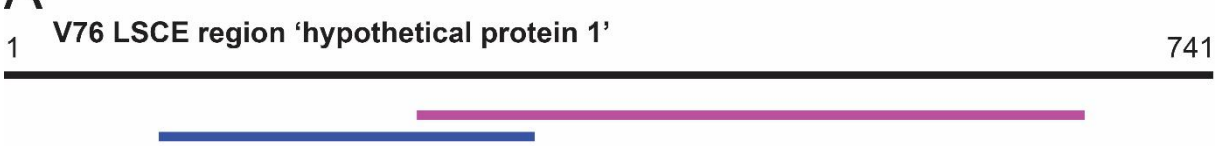

B

Annotation	Organism	Accession	Query cover (%)	Identities (%)
hypothetical protein	*V. longisporum*	CRK21534.1	55	86.1
hypothetical protein	*Ophiostoma piceae* UAMH 11346	EPE03318.1	31	29.9

Figure 6.2 Results of BLAST homology search with hypothetical protein 1 from *V. dahliae* V76 LSCE region. 741 bp *hypothetical protein 1* gene sequence was used as query for BLASTx search of protein databases using translated nucleotide query (https://blast.ncbi.nlm.nih.gov/Blast.cgi) (Altschul et al. 1997). (A) Hypothetical protein 1 aligned to the only two significant (E<0.05) hits found in the BLASTx search. Sequence colors correspond to their alignment score: Black < 40, blue 40 – 50, pink 80 – 200, red > 200. (B) Statistics and properties of the BLASTx hits.

A

B

Annotation	Organism	Accession	Query cover (%)	Identities (%)
hypothetical protein	*V. longisporum*	CRK21532.1	98	86.2
hypothetical protein	*Stachybotrys chartarum* IBT 40288	FA81746.1	93	44.3

Figure 6.3 Results of BLAST homology search with *LSCE1* from *V. dahliae* V76 LSCE region. 195 bp *LSCE1* gene sequence was used as query for BLASTx search of protein databases using translated nucleotide query (https://blast.ncbi.nlm.nih.gov/Blast.cgi) (Altschul et al. 1997). (A) LSCE1 aligned to the only two significant (E<0.05) hits found in the BLASTx search. Sequence colors correspond to their alignment score: Black < 40, blue 40 – 50, pink 80 – 200, red > 200. (B) Statistics and properties of the BLASTx hits.

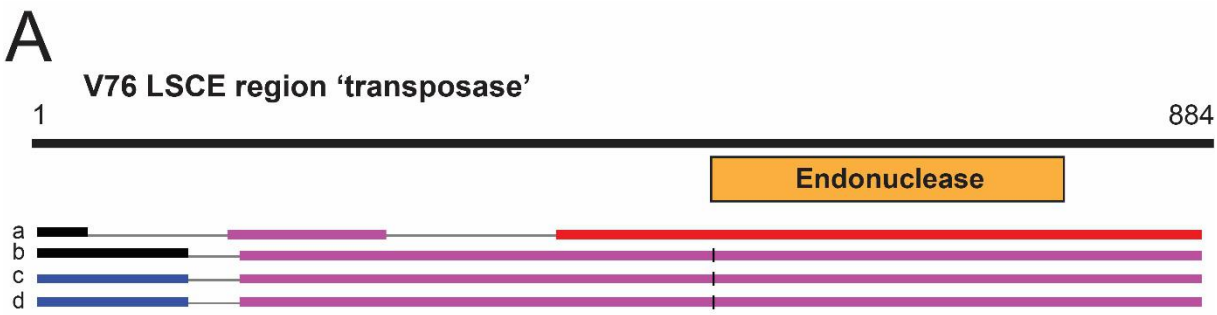

B

	Annotation	Organism	Accession	Query cover (%)	Identities (%)
a	hypothetical protein	*V. alfalfae* VaMs102	XP_002999658.1	73	100
b	hypothetical protein	*Aspergillus tanneri*	THC87446.1	95	66.9
c	hypothetical protein	*Penicillium nalgiovense*	OQE66095.1	95	66.1
d	transposase	*Aspergillus kawachii* IFO 4308	GAA92066.1	95	61.4

Figure 6.4 Results of BLAST homology search with putative transposase from *V. dahliae* V76 LSCE region. 884 bp putative *transposase* gene sequence was used as query for BLASTx search of protein databases using translated nucleotide query (https://blast.ncbi.nlm.nih.gov/Blast.cgi) (Altschul et al. 1997) . (A) Transposase with predicted endonuclease domain (COG3335) in orange boxes. Aligned are representative hits of the first four organisms found in the BLASTx search (a-d). Sequence colors correspond to their alignment score: Black < 40, blue 40 – 50, pink 80 – 200, red > 200. (B) Statistics and properties of the BLASTx hits.

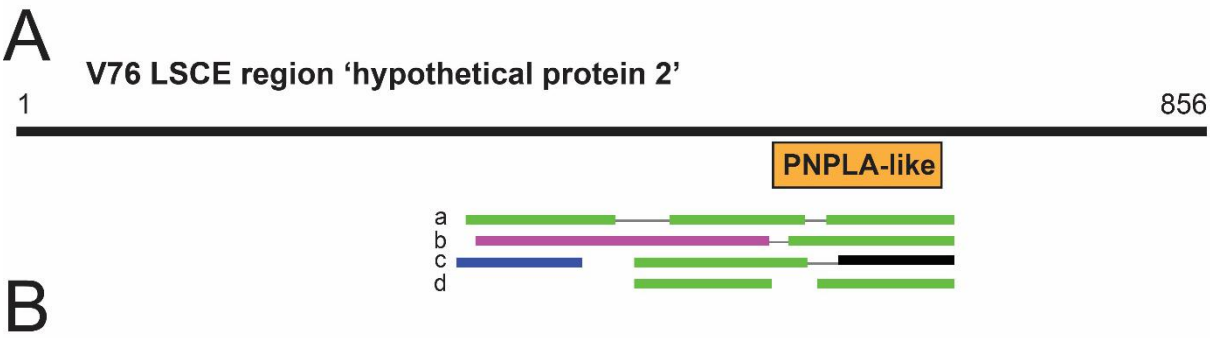

B

	Annotation	Organism	Accession	Query cover (%)	Identities (%)
a	predicted protein	*V. alfalfae* VaMs102	XP_002999657.1	34	100
b	hypothetical protein	*V. longisporum*	CRK21530.1	38	100
c	hypothetical protein	*V. dahliae* VdLs17	RBQ82419.1	25	91
d	FabD/lysophospho-lipase-like protein	*Purpureocillium lilacinum*	OAQ74437.1	25	91

Figure 6.5 Results of BLAST homology search with hypothetical protein *2* from *V. dahliae* V76 LSCE region. 856 bp *hypothetical protein 2* gene sequence was used as query for BLASTx search of protein databases using translated nucleotide query (https://blast.ncbi.nlm.nih.gov/Blast.cgi) (Altschul et al. 1997). (A) Hypothetical protein 2 sequence with predicted Patatin-like phospholipase (PNPLA; cd07216) domain aligned to representative hits of the first four organisms found in the BLASTx search (a-d). Sequence colors correspond to their alignment score: Black < 40, blue 40 – 50, pink 80 – 200, red > 200. (B) Statistics and properties of the BLASTx hits.

B

Annotation	Organism	Accession	Query cover (%)	Identities (%)
hypothetical protein	*Fusarium oxysporum* f. sp. *radicis-cucumerinum*	PCD22147.1	95	79.7

Figure 6.6 Results of BLAST homology search with *LSCE2* from *V. dahliae* V76 LSCE region. 760 bp *LSCE2* gene sequence was used as query for BLASTx search of protein databases using translated nucleotide query (https://blast.ncbi.nlm.nih.gov/Blast.cgi) (Altschul et al. 1997). (A) LSCE2 sequence aligned to the only significant (E<0.05) hit found in the BLASTx search. Sequence colors correspond to their alignment score: Black < 40, blue 40 – 50, pink 80 – 200, red > 200. (B) Statistics and properties of the BLASTx hits.

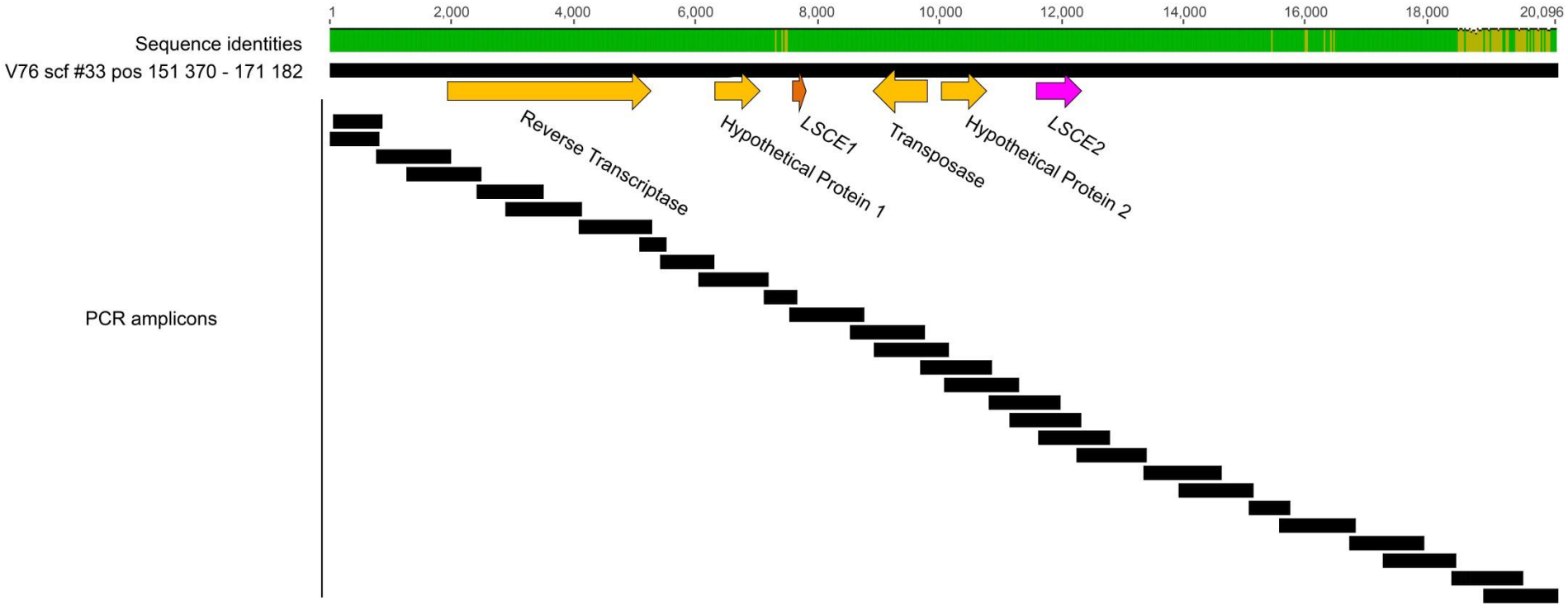

Figure 6.7 Amplification and sequencing of the *V. dahliae* V76 LSCE region on scf #33 with overlapping PCR amplicons. Primers used for PCR amplification can be found in the Materials and Methods section. Sequence identities of the alignment between reference sequence and amplicons are given in colors from green (100 % identity) to green-yellow (30 – 99 % identity). Arrows represent gene models according to their orientation.

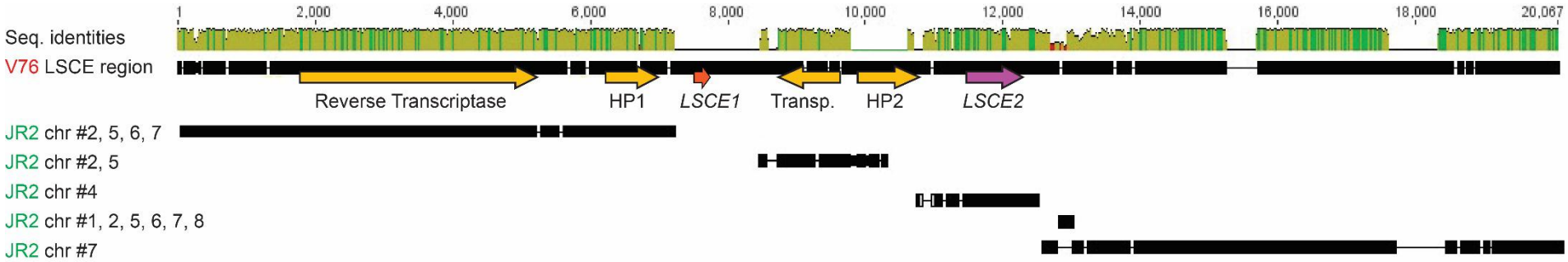

Figure 6.8 Alignment of V76 LSCE region with sequences from wilting-class reference isolate *V. dahliae* JR2. JR2 sequences homologous to LSCE region were searched and aligned using the BLAST plugin in the Geneious v8.1.8 software. First row depicts sequence identities of the alignment between reference sequence and JR2 sequences in colors from green (100 % identity) to green-yellow (30 – 99 % identity). Predicted gene models are shown as arrows on the LSCE region according to their orientation: HP1: Hypothetical Protein 1, Transp.: Transposase, HP2: Hypothetical Protein 2.

Figure 6.9 (p 168) Alignment of 11 *LSCE2* gene sequences from *V. dahliae* and *V. longisporum* isolates. GDNA was isolated from *Verticillium spp.* chlorosis-class isolates. *LSCE2* was amplified and sequenced using primers LW120 and LW121. Sequences were manually aligned using Geneious 8.1.8 software. Polymorphic nucleotide positions are marked in red (adenine), yellow (guanine), green (thymine) and blue (cytosine). First and last nucleotides of the intron are marked with black arrowhead

```
                1         10        20        30        40        50        60        70        80        90       100       110       120       130       140       150
V. dahliae   V76   ATGAAGTTCTCAAGAATCGTTACAGGTGCAGCACTTCTAGCCCGCACATTCGCTATTGCCATCCCGCAATCCGATACCGATCCAACTGAGCAAACGACAGACGCGGCTCCCGACTTGACGCATTTGGTTATTGGACAAACCATAGGGCCTCT
             T9    ATGAAGTTCTCAAGAATCGTTACAGGTGCAGCACTTCTAGCCCGCACATTCGCTATTGCCATCCCGCAATCCGATACCGATCCAACTGAGCAAACGACAGACGCGGCTCCCGACTTGACGCATTTGGTTATTGGACAAACCATAGGGCCTCT
             ST100 ATGAAGTTCTCAAGAATCGTTACAGGTGCAGCACTTCTAGCCCGCACATTCGCTATTGCCATCCCGCAATCCGATACCGATCCAACTGAGCAAACGACAGACGCGGCTCCCGACTTGACGCATTTGGTTATTGGACAAACCATAGGGCCTCT
             V138I ATGAAGTTCTCAAGAATCGTTACAGGTGCAGCACTTCTAGCCCGCACATTCGCTATTGCCATCCCGCAATCCGATACCGATCCAACTGAGCAAACGACAGACGCGGCTCCCGACTTGACGCATTTGGTTATTGGACAAACCATAGGGCCTCT
             V781I ATGAAGTTCTCAAGAATCGTTACAGGTGCAGCACTTCTAGCCCGCACATTCGCTATTGCCATCCCGCAATCCGATACCGATCCAACTGAGCAAACGACAGACGCGGCTCCCGACTTGACGCATTTGGTTATTGGACAAACCATAGGGCCTCT
V. longisporum VL10  ATGAAGTTCTCAAGAATCGTTACAGGTGCAGCACTTCTAGCCCGCACATTCGCTATTGCCATCCCGCAATCCGATACCGATCCAACTGAGCAAACGACAGACGCGGCTCCCGACTTGACGCATTTGGTTATTGGACAAACCATAGGGCCTCT
             VL35  ATGAAGTTCTCAAGAATCGTTACAGGTGCAGCACTTCTAGCCCGCACATTCGCTATTGCCATCCCGCAATCCGATACCGATCCAACTGAGCAAACGACAGACGCGGCTCCCGACTTGACGCATTTGGTTATTGGACAAACCATAGGGCCTCT
             VL43  ATGAAGTTCTCAAGAATCGTTACAGGTGCAGCACTTCTAGCCCGCACATTCGCTATTGCCATCCCGCAATCCGATACCGATCCAACTGAGCAAACGACAGACGCGGCTCCCGACTTGACGCATTTGGTTATTGGACAAACCATAGGGCCTCT
             VL60  ATGAAGTTCTCAAGAATCGTTACAGGTGCAGCACTTCTAGCCCGCACATTCGCTATTGCCATCCCGCAATCCGATACCGATCCAACTGAGCAAACGACAGACGCGGCTCCCGACTTGACGCATTTGGTTATTGGACAAACCATAGGGCCTCT
             VL83  ATGAAGTTCTCAAGAATCGTTACAGGTGCAGCACTTCTAGCCCGCACATTCGCTATTGCCATCCCGCAATCCGATACCGATCCAACTGAGCAAACGACAGACGCGGCTCCCGACTTGACGCATTTGGTTATTGGACAAACCATAGGGCCTCT
             VL334 ATGAAGTTCTCAAGAATCGTTACAGGTGCAGCACTTCTAGCCCGCACATTCGCTATTGCCATCCCGCAATCCGATACCGATCCAACTGAGCAAACGACAGACGCGGCTCCCGACTTGACGCATTTGGTTATTGGACAAACCATAGGGCCTCT

                160       170       180       190       200       210       220       230       240       250       260       270       280       290       300
V. dahliae   V76   CATTGTCGATGTCAGTAGCGTCTTCGAGCTTTACAGGTAAAATCCTAATTATCTAGGCTATCGGCGAACCAATTGCGAGCGAGGTTGAAATCAACGAAGCTTCTGATGAACTCTCGGATGAGAAAGTCGTTCTCAGCCAACCCTCCACCCGC
             T9    CATTGTCGATGTCAGTAGCGTCTTCGAGCTTTACAGGTAAAATCCTAATTATCTAGGCTATCGGCGAACCAATTGCGAGCGAGGTTGAAATCAACGAAGCTTCTGATGAACTCTCGGATGAGAAAGTCGTTCTCAGCCAACCCTCCACCCGC
             ST100 CATTGTCGATGTCAGTAGCGTCTTCGAGCTTTACAGGTAAAATCCTAATTATCTAGGCTATCGGCGAACCAATTGCGAGCGAGGTTGAAATCAACGAAGCTTCTGATGAACTCTCGGATGAGAAAGTCGTTCTCAGCCAACCCTCCACCCGC
             V138I CATTGTCGATGTCAGTAGCGTCTTCGAGCTTTACAGGTAAAATCCTAATTATCTAGGCTATCGGCGAACCAATTGCGAGCGAGGTTGAAATCAACGAAGCTTCTGATGAACTCTCGGATGAGAAAGTCGTTCTCAGCCAACCCTCCACCCGC
             V781I CATTGTCGATGTCAGTAGCGTCTTCGAGCTTTACAGGTAAAATCCTAATTATCTAGGCTATCGGCGAACCAATTGCGAGCGAGGTTGAAATCAACGAAGCTTCTGATGAACTCTCGGATGAGAAAGTCGTTCTCAGCCAACCCTCCACCCGC
V. longisporum VL10  CATTGTCGATGTCAGTAGCGTCTTCGAGCTTTACAGGTAAAATCCTAATTATCTAGGCTATCGGCGAACCAATTGCGAGCGAGGTTGAAATCAACGAAGCTTCTGATGAACTCTCGGATGAGAAAGTCGTTCTCAGCCAACCCTCCACCCGC
             VL35  CATTGTCGATGTCAGTAGCGTCTTCGAGCTTTACAGGTAAAATCCTAATTATCTAGGCTATCGGCGAACCAATTGCGAGCGAGGTTGAAATCAACGAAGCTTCTGATGAACTCTCGGATGAGAAAGTCGTTCTCAGCCAACCCTCCACCCGC
             VL43  CATTGTCGATGTCAGTAGCGTCTTCGAGCTTTACAGGTAAAATCCTAATTATCTAGGCTATCGGCGAACCAATTGCGAGCGAGGTTGAAATCAACGAAGCTTCTGATGAACTCTCGGATGAGAAAGTCGTTCTCAGCCAACCCTCCACCCGC
             VL60  CATTGTCGATGTCAGTAGCGTCTTCGAGCTTTACAGGTAAAATCCTAATTATCTAGGCTATCGGCGAACCAATTGCGAGCGAGGTTGAAATCAACGAAGCTTCTGATGAACTCTCGGATGAGAAAGTCGTTCTCAGCCAACCCTCCACCCGC
             VL83  CATTGTCGATGTCAGTAGCGTCTTCGAGCTTTACAGGTAAAATCCTAATTATCTAGGCTATCGGCGAACCAATTGCGAGCGAGGTTGAAATCAACGAAGCTTCTGATGAACTCTCGGATGAGAAAGTCGTTCTCAGCCAACCCTCCACCCGC
             VL334 CATTGTCGATGTCAGTAGCGTCTTCGAGCTTTACAGGTAAAATCCTAATTATCTAGGCTATCGGCGAACCAATTGCGAGCGAGGTTGAAATCAACGAAGCTTCTGATGAACTCTCGGATGAGAAAGTCGTTCTCAGCCAACCCTCCACCCGC

                310       320       330       340       350       360       370       380       390       400       410       420       430       440       450
V. dahliae   V76   AGAATCTTCAATCTGGTTCTCAAAGATGCATTCGCGAAGTTTGTTCAATGTCCAAAGAATATCAAGTGGGGAGTTATGATGCTTTGGAATCCTTACGAGGAGAATACGGCACACGATGCTCTTCACACGAAAGTCTTGGAAACCAGTCTCAA
             T9    AGAATCTTCAATCTGGTTCTCAAAGATGCATTCGCGAAGTTTGTTCAATGTCCAAAGAATATCAAGTGGGGAGTTATGATGCTTTGGAATCCTTACGAGGAGAATACGGCACACGATGCTCTTCACACGAAAGTCTTGGAAACCAGTCTCAA
             ST100 AGAATCTTCAATCTGGTTCTCAAAGATGCATTCGCGAAGTTTGTTCAATGTCCAAAGAATATCAAGTGGGGAGTTATGATGCTTTGGAATCCTTACGAGGAGAATACGGCACACGATGCTCTTCACACGAAAGTCTTGGAAACCAGTCTCAA
             V138I AGAATCTTCAATCTGGTTCTCAAAGATGCATTCGCGAAGTTTGTTCAATGTCCAAAGAATATCAAGTGGGGAGTTATGATGCTTTGGAATCCTTACGAGGAGAATACGGCACACGATGCTCTTCACACGAAAGTCTTGGAAACCAGTCTCAA
             V781I AGAATCTTCAATCTGGTTCTCAAAGATGCATTCGCGAAGTTTGTTCAATGTCCAAAGAATATCAAGTGGGGAGTTATGATGCTTTGGAATCCTTACGAGGAGAATACGGCACACGATGCTCTTCACACGAAAGTCTTGGAAACCAGTCTCAA
V. longisporum VL10  AGAATCTTCAATCTGGTTCTCAAAGATGCATTCGCGAAGTTTGTTCAATGTCCAAAGAATATCAAGTGGGGAGTTATGATGCTTTGGAATCCTTACGAGGAGAATACGGCACACGATGCTCTTCACACGAGAGTCTTGGAAACCAGTCTCAA
             VL35  AGAATCTTCAATCTGGTTCTCAAAGATGCATTCGCGAAGTTTGTTCAATGTCCAAAGAATATCAAGTGGGGAGTTATGATGCTTTGGAATCCTTACGAGGAGAATACGGCACACGATGCTCTTCACACGAGAGTCTTGGAAACCAGTCTCAA
             VL43  AGAATCTTCAATCTGGTTCTCAAAGATGCATTCGCGAAGTTTGTTCAATGTCCAAAGAATATCAAGTGGGGAGTTATGATGCTTTGGAATCCTTACGAGGAGAATACGGCACACGATGCTCTTCACACGAGAGTCTTGGAAACCAGTCTCAA
             VL60  AGAATCTTCAATCTGGTTCTCAAAGATGCATTCGCGAAGTTTGTTCAATGTCCAAAGAATATCAAGTGGGGAGTTATGATGCTTTGGAATCCTTACGAGGAGAATACGGCACACGATGCTCTTCACACGAGAGTCTTGGAAACCAGTCTCAA
             VL83  AGAATCTTCAATCTGGTTCTCAAAGATGCATTCGCGAAGTTTGTTCAATGTCCAAAGAATATCAAGTGGGGAGTTATGATGCTTTGGAATCCTTACGAGGAGAATACGGCACACGATGCTCTTCACACGAGAGTCTTGGAAACCAGTCTCAA
             VL334 AGAATCTTCAATCTGGTTCTCAAAGATGCATTCGCGAAGTTTGTTCAATGTCCAAAGAATATCAAGTGGGGAGTTATGATGCTTTGGAATCCTTACGAGGAGAATACGGCACACGATGCTCTTCACACGAGAGTCTTGGAAACCAGTCTCAA

                460       470       480       490       500       510       520       530       540       550       560       570       580       590       600
V. dahliae   V76   CTTGGTTAAGAAAAGTGGTACTTTCATCGAAGATCATCTAGGATGGAAGCACGTTGGTGATGGATGGATCGACTTTGCAGCAAACGTCCGGTTACATGCCGATTACTACAACTCATTCAAGGAGTCGACCAGCCACATAAGTGTCTATATGG
             T9    CTTGGTTAAGAAAAGTGGTACTTTCATCGAAGATCATCTAGGATGGAAGCACGTTGGTGATGGATGGATCGACTTTGCAGCAAACGTCCGGTTACATGCCGATTACTACAACTCATTCAAGGAGTCGACCAGCCACATAAGTGTCTATATGG
             ST100 CTTGGTTAAGAAAAGTGGTACTTTCATCGAAGATCATCTAGGATGGAAGCACGTTGGTGATGGATGGATCGACTTTGCAGCAAACGTCCGGTTACATGCCGATTACTACAACTCATTCAAGGAGTCGACCAGCCACATAAGTGTCTATATGG
             V138I CTTGGTTAAGAAAAGTGGTACTTTCATCGAAGATCATCTAGGATGGAAGCACGTTGGTGATGGATGGATCGACTTTGCAGCAAACGTCCGGTTACATGCCGATTACTACAACTCATTCAAGGAGTCGACCAGCCACATAAGTGTCTATATGG
             V781I CTTGGTTAAGAAAAGTGGTACTTTCATCGAAGATCATCTAGGATGGAAGCACGTTGGTGATGGATGGATCGACTTTGCAGCAAACGTCCGGTTACATGCCGATTACTACAACTCATTCAAGGAGTCGACCAGCCACATAAGTGTCTATATGG
V. longisporum VL10  CTTGGTTAAGAAAAGTGGTACTTTCATCGAAGATCATCTAGGATGGAAGCACGTTGGTGATGGATGGATCGACTTTGCAGCAAACGTCCGGTTACATGCCGATTACTACAACTCATTCAAGGAGTCGACCAGCCACATAAGTGTCTATATGG
             VL35  CTTGGTTAAGAAAAGTGGTACTTTCATCGAAGATCATCTAGGATGGAAGCACGTTGGTGATGGATGGATCGACTTTGCAGCAAACGTCCGGTTACATGCCGATTACTACAACTCATTCAAGGAGTCGACCAGCCACATAAGTGTCTATATGG
             VL43  CTTGGTTAAGAAAAGTGGTACTTTCATCGAAGATCATCTAGGATGGAAGCACGTTGGTGATGGATGGATCGACTTTGCAGCAAACGTCCGGTTACATGCCGATTACTACAACTCATTCAAGGAGTCGACCAGCCACATAAGTGTCTATATGG
             VL60  CTTGGTTAAGAAAAGTGGTACTTTCATCGAAGATCATCTAGGATGGAAGCACGTTGGTGATGGATGGATCGACTTTGCAGCAAACGTCCGGTTACATGCCGATTACTACAACTCATTCAAGGAGTCGACCAGCCACATAAGTGTCTATATGG
             VL83  CTTGGTTAAGAAAAGTGGTACTTTCATCGAAGATCATCTAGGATGGAAGCACGTTGGTGATGGATGGATCGACTTTGCAGCAAACGTCCGGTTACATGCCGATTACTACAACTCATTCAAGGAGTCGACCAGCCACATAAGTGTCTATATGG
             VL334 CTTGGTTAAGAAAAGTGGTACTTTCATCGAAGATCATCTAGGATGGAAGCACGTTGGTGATGGATGGATCGACTTTGCAGCAAACGTCCGGTTACATGCCGATTACTACAACTCATTCAAGGAGTCGACCAGCCACATAAGTGTCTATATGG

                610       620       630       640       650       660       670       680       690       700       710       720       730       740       750       760
V. dahliae   V76   GTATTAAAGGGTCGGTGCACGTCGCTACTAACGAGTTCATTATGCGCGGAATTGAGACAGGTCCAGAAGTTTGGTATAACGGGATTCGGTACCAGATGACGGATGGCTCCAGCATTGTCTCGAGTTGGTCTTTTGACGCAGGCCAGCTTTGA
             T9    GTATTAAAGGGTCGGTGCACGTCGCTACTAACGAGTTCATTATGCGCGGAATTGAGACAGGTCCAGAAGTTTGGTATAACGGGATTCGGTACCAGATGACGGATGGCTCCAGCATTGTCTCGAGTTGGTCTTTTGACGCAGGCCAGCTTTGA
             ST100 GTATTAAAGGGTCGGTGCACGTCGCTACTAACGAGTTCATTATGCGCGGAATTGAGACAGGTCCAGAAGTTTGGTATAACGGGATTCGGTACCAGATGACGGATGGCTCCAGCATTGTCTCGAGTTGGTCTTTTGACGCAGGCCAGCTTTGA
             V138I GTATTAAAGGGTCGGTGCACGTCGCTACTAACGAGTTCATTATGCGCGGAATTGAGACAGGTCCAGAAGTTTGGTATAACGGGATTCGGTACCAGATGACGGATGGCTCCAGCATTGTCTCGAGTTGGTCTTTTGACGCAGGCCAGCTTTGA
             V781I GTATTAAAGGGTCGGTGCACGTCGCTACTAACGAGTTCATTATGCGCGGAATTGAGACAGGTCCAGAAGTTTGGTATAACGGGATTCGGTACCAGATGACGGATGGCTCCAGCATTGTCTCGAGTTGGTCTTTTGACGCAGGCCAGCTTTGA
V. longisporum VL10  GTATTAAAGGGTCGGTGCACGTCGCTACTAACGAATTCATTATGCGCGGAATTGAGACAGGTCCAACAAGTTTGGTATAACGGGATTCGGTACCAGATGACGGATGGCTCCAGCATTATCTCGAGTTGGTCTTTTGACGCAGGCCAGCTTTGA
             VL35  GTATTAAAGGGTCGGTGCACGTCGCTACTAACGAATTCATTATGCGCGGAATTGAGACAGGTCCAACAAGTTTGGTATAACGGGATTCGGTACCAGATGACGGATGGCTCCAGCATTATCTCGAGTTGGTCTTTTGACGCAGGCCAGCTTTGA
             VL43  GTATTAAAGGGTCGGTGCACGTCGCTACTAACGAATTCATTATGCGCGGAATTGAGACAGGTCCAACAAGTTTGGTATAACGGGATTCGGTACCAGATGACGGATGGCTCCAGCATTATCTCGAGTTGGTCTTTTGACGCAGGCCAGCTTTGA
             VL60  GTATTAAAGGGTCGGTGCACGTCGCTACTAACGAATTCATTATGCGCGGAATTGAGACAGGTCCAACAAGTTTGGTATAACGGGATTCGGTACCAGATGACGGATGGCTCCAGCATTATCTCGAGTTGGTCTTTTGACGCAGGCCAGCTTTGA
             VL83  GTATTAAAGGGTCGGTGCACGTCGCTACTAACGAATTCATTATGCGCGGAATTGAGACAGGTCCAACAAGTTTGGTATAACGGGATTCGGTACCAGATGACGGATGGCTCCAGCATTATCTCGAGTTGGTCTTTTGACGCAGGCCAGCTTTGA
             VL334 GTATTAAAGGGTCGGTGCACGTCGCTACTAACGAATTCATTATGCGCGGAATTGAGACAGGTCCAACAAGTTTGGTATAACGGGATTCGGTACCAGATGACGGATGGCTCCAGCATTATCTCGAGTTGGTCTTTTGACGCAGGCCAGCTTTGA
```

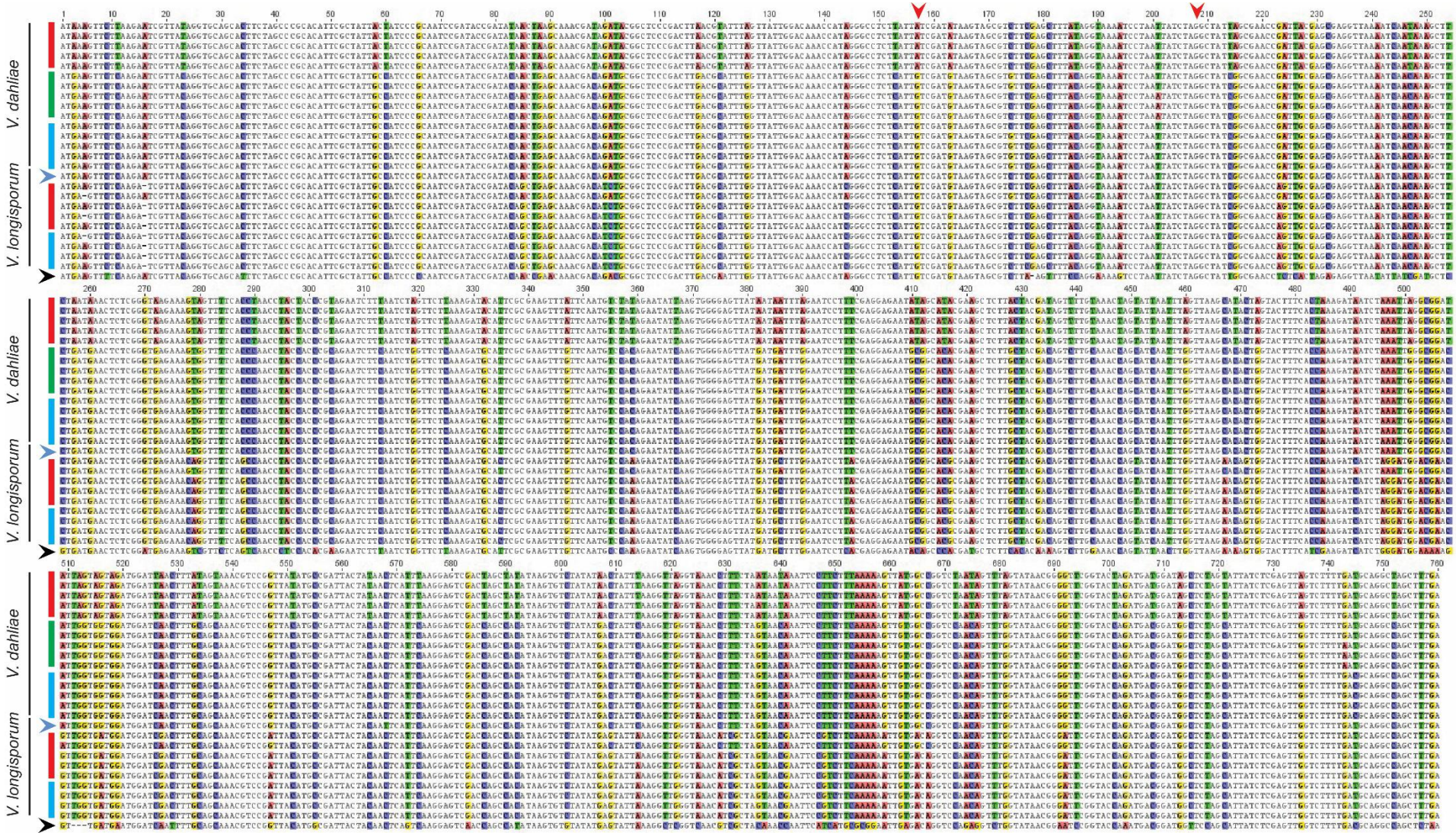
V. dahliae
V. longisporum
V. dahliae
V. longisporum
V. dahliae
V. longisporum

Figure 6.10 Alignment of 25 *LSCE2-like* gene sequences from *V. dahliae* and *V. longisporum* isolates. GDNA was isolated from *Verticillium spp.* chlorosis-class (red), wilting-class (green) and asymptomatic (blue) isolates. *LSCE2-like* was amplified and sequenced using primers LW194 and LW195. *LSCE2-like* homologous sequence from *Fusarium oxysporum* Foc16 was retrieved from NCBI (https://www.ncbi.nlm.nih.gov/) and marked with a black arrowhead. Sequenced isolates (top to bottom): V76, ST100, T9, V138I, V781I, JR2, VdLs17, DVD-S29, DVD-31, V192I, Vd39, Vd42, Vd52, Vd54, Vd152, VL32 (blue arrowhead), VL10, VL35, VL43, VL60, VL83, VL334, VL13, VL18 and VL24. Sequences were manually aligned using Geneious 8.1.8 software. Polymorphic nucleotide positions are marked in red (adenine), yellow (guanine), green (thymine) and blue (cytosine). First and last nucleotides of the intron are marked with red arrowheads.

Table 6.2 Supplemental information for putative LSCE2 interaction candidates recovered from yeast-two-hybrid (Y2H) screen. Putative interactor and accession number were determined after BLASTx homology search. Putative functions of the proteins were researched from the literature. Last column gives information about how often (1 – 4 times) and in which library screen (S: cell suspension culture library; R: root library) sequences were found.

Putative Interactor	Accession	Function (Reference)	Y2H Screen Hits
AGC1-2; D6PKL1	AT4G26610	Protein kinase; Phosphorylation/activation of PIN auxin transporters (Willige et al. 2013)	1R/1S
AtRTNLB11	AT3G19460	ER localized, involved in ER-Golgi trafficking (Nziengui et al. 2007)	2R
DERLIN-2.2	AT4G04860	ER-associated degradation, proteolysis of misfolded proteins in the ER lumen (Kirst et al. 2005)	2R/1S
ERF/AP2 transcription factor	AT5G52020	Transcription factor probably involved in ethylene signaling (defense response/development) (Nakano et al. 2006)	3R
LBD41	AT3G02550	Responsive to leaf necrotroph attack; interacts with the developmental regulator TOPLESS (Thatcher et al. 2012)	2S
MT2A	AT3G09390	Binds to and detoxifies excess copper and other metals, limits oxidative damage, highly expressed during senescence (Benatti et al. 2014)	1R/1S
MYB4	AT4G38620	Transcription factor, balances accumulation of UV-B absorbing compounds (Jin et al. 2000)	3R
MYB6	AT4G09460	Transcription factor with DNA-binding capacity, upregulated after ethylene, ABA and auxin treatment (Kranz et al. 1998)	1S
PGIP1	AT5G06860	Inhibits function of fungal CWDEs (Lorenzo et al. 2001), upregulated in Agrobacterium-induced tumors (Deeken et al. 2006), putatively involved in cell wall organization (Irshad et al. 2008)	4R
PRXR1	AT4G21960	Hydrogen peroxide catabolism, endomembrane-located glycoprotein (Sultana et al. 2015)	1R/1S
PTPLA	AT5G59770	Involved in very long chain fatty acids elongation, synthesis of a regulatory signal modifying suberin production in the endodermis (Morineau et al. 2016)	2S
SKIP2	AT5G67250	Proteasomal protein degradation (Farrás et al. 2001), stress response gene (Ma and Bohnert 2007)	2R
TPR7	AT5G21990	Part of the Arabidopsis Sec translocon, post-translational import of proteins into the ER (Schweiger and Schwenkert 2013)	2R

Deposition of data

Verticillium dahliae V76 and JR2 *in vitro* RNAseq data, *V. dahliae* V76 genome data, lists of lineage-specific regions, expressed gene models and list of Yeast-two-Hybrid candidate interactors will be deposited at the Department of Plant Cell Biology, Georg August University Göttingen, Germany. For access please contact PD Dr. Thomas Teichmann (Thomas.Teichmann@biologie.uni-goettingen.de).

Danksagung

Ich möchte mich hier bei allen bedanken, die mich während meiner Promotion und der Arbeit an meiner Dissertation unterstützt und begleitet haben.

Zunächst möchte ich mich bei Prof. Dr. Volker Lipka bedanken. Er hat mir die Möglichkeit gegeben in seiner Abteilung zu einem wirklich spannenden Thema zu Promovieren. Während meiner Zeit in Göttingen hat er mich stets unterstützt und hatte immer eine offene Tür und ein offenes Ohr für meine Fragen und Probleme. Er hat mich zudem immer dazu animiert mich zu verbessern und durch ihn habe ich unglaublich viel gelernt. Mein Projekt hat er mit vollem Einsatz unterstützt und mir alle Möglichkeiten gegeben, meine Ideen experimentell umzusetzen. Seine fachlichen Beiträge waren unverzichtbar und haben immer dazu beigetragen, mein Projekt weiter voranzubringen. Prof. Dr. Lipka hat in der Abteilung durch Förderung verschiedenster Aktivitäten zu einem kollegialen Gemeinschaftsgefühl beigetragen an das ich mich immer gerne zurückerinnern werde. Ich danke ihm auch für seine Funktion als Erstprüfer und für die Begutachtung meiner Arbeit.

Ich danke auch PD Dr. Thomas Teichmann. Er hat mir nicht nur bei fachlichen sondern auch bei Computerproblemen sehr geholfen und war immer für mich eine Ansprechstelle. Auch ihm danke ich für die Korrektur und Begutachtung meiner Arbeit.

Prof. Dr. Lipka und PD Dr. Teichmann sowie Prof. Dr. Andrea Polle, Prof. Dr. Christiane Gatz, Prof. Dr. Ivo Feußner und Prof. Dr. Gerhard Braus danke ich für die Bereitschaft meine Prüfungskommission zu bilden.

Ein großer Dank geht an Dr. Hassan Ghareeb und Dr. Elena Petutschnig die mir immer mit Rat und Tat zur Seite gestanden haben. Vor allem danke ich Dr. Petutschnig für ihre Hilfe bei der Proteinaufreinigung.

Ebenso möchte ich mich bei allen bedanken die mir außerhalb meiner Abteilung geholfen haben. Dr. Rebekka Harting (AG Braus) hat mir Methoden zur Transformation von Verticillium und Southern Blot beigebracht und Dr. Joachim Uhrig (AG Gatz) hat mich mit seiner Expertise im Yeast-two-Hybrid System unterstützt. Ein großer Dank geht an Dr. Anja Poehlein und Dr. Sascha Dietrich (AG Daniels), die viel Zeit investiert haben um mich bei den vergleichenden Genomanalysen zu unterstützen. Ich möchte mich zudem bei unseren Kollaborateuren an der Universität Wageningen und besonders bei

Prof. Dr. Bart Thomma bedanken. Der gegenseitige und regelmäßige fachliche Austausch mit ihnen hat sehr zum Erfolg meiner Arbeit beigetragen.

Ein besonderer Dank geht an meine Vorgänger auf dem Verticillium-Projekt, Dr. Michael Reusche und Dr. Karin Thole, ohne deren großartige Vorarbeit mein Projekt nicht existieren würde. Danke auch an meinen Verticillium-Mitstreiter Dr. Dimitri Stepanets der mich vor allem am Anfang meiner Arbeit unterstützt hat und dessen Humor im Labor und Büro meine Arbeitszeit immer bereichert haben.

Danke an meine Kolleg*innen die immer für einen fachlichen Rat, ein aufmunterndes Wort oder einen guten Scherz zu haben waren. Hier möchte ich vor allem Sina danken, die sich meine Jammerei immer klaglos angehört hat und deren seelische Unterstützung vor allem am Ende meiner Schreibphase unendlich wertvoll war.

Für ihre Arbeit danke ich den Gärtnerinnen Feli und Susanne, die immer bereit waren mir unter die Arme zu greifen.

Besonders möchte ich denjenigen danken die mich mit ihrer Arbeit im Labor unterstützt haben. Hier geht der Dank vor allem an Melanie Klenke für die unzähligen qRT-PCRs die sie pipettiert und die genauso unzähligen Pflanzen die sie mit mir gemörsert hat. Danke auch an Alexandra Nagel, Jan Teer und Katharina Vaupel die im Rahmen ihres Master- oder Bachelorstudiums einen Teil des Projektes vorangetrieben haben.

Zuletzt möchte ich dann noch meinen Freunden und meiner Familie danken. Meine Eltern haben mir nicht nur mein Studium ermöglicht sondern auch unendlich viel mehr. Danke, dass ihr euch seit meiner Schulzeit angehört habt wie interessant Biologie ist und mir immer das Gefühl gegeben habt alles schaffen zu können. Merci a ma belle-soeur Véro, j'ai toujours profité de les conversations et de les bons moments avec toi. Danke meinem großen Bruder Sebastian. Du bist mein größtes Vorbild.